

Universidade Federal do Rio de Janeiro  
Centro de Ciências da Saúde  
Programa de Pós-Graduação em Biotecnologia Vegetal e Bioprocessos

Desreplicação dos extratos de espécies de *Siparuna* da Amazônia e  
investigação do potencial antiviral

Tese de Doutorado

Carla Monteiro Leal

Rio de Janeiro

Abril de 2022



Universidade Federal do Rio de Janeiro

Centro de Ciências da Saúde

Programa de Pós-Graduação em Biotecnologia Vegetal e Bioprocessos



## Desreplicação dos extratos de espécies de *Siparuna* da Amazônia e investigação do potencial antiviral

Carla Monteiro Leal

Tese de Doutorado apresentada ao Programa de Pós-Graduação em Biotecnologia Vegetal e Bioprocessos da Universidade Federal do Rio de Janeiro, como parte dos requisitos para à obtenção do título de Doutora em Ciências, em Biotecnologia Vegetal e Bioprocessos.

Orientadora: Dr<sup>a</sup>. Suzana Guimarães Leitão

Co-orientadoras: Dr<sup>a</sup>. Gilda Guimarães Leitão  
Dr<sup>a</sup>. Rosineide Costa Simas

Rio de Janeiro

Abril de 2022

## Ficha Catalográfica

## CIP - Catalogação na Publicação

M775d Monteiro Leal, Carla  
Desreplicação dos extratos de espécies de  
Siparuna da Amazônia e investigação do potencial  
antiviral / Carla Monteiro Leal. -- Rio de  
Janeiro, 2022.  
228 f.

Orientadora: Suzana Guimarães Leitão.  
Coorientadora: Gilda Guimarães Leitão e  
Rosineide Costa Simas .  
Tese (doutorado) - Universidade Federal do Rio  
de Janeiro, Decania do Centro de Ciências da Saúde,  
Programa de Pós-Graduação em Biotecnologia Vegetal,  
2022.

1. Siparunaceae. 2. Espectrometria de Massas. 3.  
A(H1N1)pdm09. 4. SARS-CoV-2. 5. Potencial  
antiviral. I. Guimarães Leitão, Suzana, orient. II.  
, Gilda Guimarães Leitão e Rosineide Costa Simas,  
coorient. III. Título.



Universidade Federal do Rio de Janeiro  
Centro de Ciências da Saúde

Coordenação de Pós-Graduação em Biotecnologia Vegetal  
e Bioprocessos

**ATA DA DEFESA DE TESE DE CARLA MONTEIRO LEAL, COMO PARTE DOS REQUISITOS NECESSÁRIOS À OBTENÇÃO DO GRAU DE DOUTOR EM CIÊNCIAS (BIOTECNOLOGIA VEGETAL E BIOPROCESSOS).**

Aos vinte dias do mês de abril do ano de dois mil e vinte e dois, às 09 horas e 30 minutos, reuniu-se via videoconferência, a Banca Examinadora abaixo discriminada, para a defesa de tese de doutorado da aluna **Carla Monteiro Leal**, intitulada: "Desreplicação dos extratos de espécies de *Siparuna* da Amazônia e investigação do potencial antiviral" desenvolvida sob a orientação da **Profª. Drª. Suzana Guimarães Leitão** e co-orientação das **Drª. Gilda Guimarães Leitão** e **Drª. Rosineide Costa Simas**. A apresentação feita pela candidata foi acompanhada da arguição pelos componentes da Banca. Em seguida, esta se reuniu para sua avaliação e a tese foi **aprovada** (inserir letra apropriada).

- A) Aprovado;
- B) Aprovado com pequenas modificações\* a serem combinadas com o Presidente da Banca dentro de um mês;
- C) Não aprovado ainda, é necessária a apresentação das modificações/correções\* em uma nova versão do documento para o Presidente da Banca e uma carta do Presidente com prazo de máximo 3 meses para ser aprovada; se não reprovada
- D) Não aprovado ainda, é necessária uma nova apresentação\*, oral e escrita, para a mesma ou nova banca examinadora dentro de um prazo combinado com a comissão do Programa.
- E) Reprovado, razões da reprovação\* escritas no espaço destinado.

\*As modificações/correções/razões para reprovação precisam ser discriminadas e o Presidente da Banca e o(a) aluno(a) precisam estar cientes.

E, para constar, foi lavrada a presente ata que vai devidamente assinada pelo coordenador, pelos membros da Comissão Examinadora e pelo orientador da aluna. A aluna deve ficar com uma cópia da ata e a outra deve ser entregue para a secretaria do PBV pelo Presidente da Banca.

Rio de Janeiro, 20 de abril de 2022.





Universidade Federal do Rio de Janeiro  
Centro de Ciências da Saúde

Coordenação de Pós-Graduação em Biotecnologia Vegetal  
e Bioprocessos

**ATA DO EXAME DA DEFESA DE TESE DE CARLA MONTEIRO LEAL, COMO PARTE DOS REQUISITOS NECESSÁRIOS À OBTENÇÃO DO GRAU DE DOUTOR EM CIÊNCIAS (BIOTECNOLOGIA VEGETAL E BIOPROCESSOS).**

*Fernanda de Ávila Abreu*

Dr<sup>a</sup>. Fernanda de Ávila Abreu – Coordenadora

*Celso Luiz Salgueiro Lage*

Dr. Celso Luiz Salgueiro Lage – INPI

*Ivana Correa Ramos Leal*

Dr<sup>a</sup>. Ivana Correa Ramos Leal – UFRJ

*Daniel Luiz Reis Simas*

Dr. Daniel Luiz Reis Simas – UFRJ

*Gabriella da Silva Mendes*

Dr<sup>a</sup>. Gabriella da Silva Mendes – UFRJ

*Gabriel Franco dos Santos*

Dr. Gabriel Franco dos Santos – UFG

*Suzana Guimarães Leitão*

Dr<sup>a</sup>. Suzana Guimarães Leitão – UFRJ (Orientadora)

Centro de Ciências da Saúde – Bloco K  
Sala K2-032 – 2º andar – Cidade Universitária  
CEP: 21941-590 – Rio de Janeiro – RJ – Brasil  
Tel: 3938-6676 - E-mail: [pbv@ccsdecania.ufrj.br](mailto:pbv@ccsdecania.ufrj.br)



Universidade Federal do Rio de Janeiro  
Centro de Ciências da Saúde

Coordenação de Pós-Graduação em Biotecnologia Vegetal  
e Bioprocessos

Drª. Gilda Guimarães Leitão – UFRJ (Coorientadora)

Drª. Rosineide Costa Simas – Mackenzie (Coorientadora)

*Carla Monteiro Leal*

Carla Monteiro Leal (Doutoranda)

**LISTA DE MODIFICAÇÕES, CORREÇÕES OU RAZÕES PARA REPROVAÇÕES:**

Ciente,

Presidente da Banca

Ciente,

*Carla Monteiro Leal*

Aluno(a)

## Dedicatória

Aos meus pais, Verônica e Carlos e aos meus irmãos, Gabriela e Gabriel.

## Agradecimentos

A Deus, por ser minha força e meu sustento, pelo dom do estudo, sabedoria e por conceder mais uma vitória em minha vida. Obrigada por tudo meu Deus.

Aos meus pais, Verônica e Carlos, por todo amor, carinho, apoio e incentivo. Mesmo existindo essa distância entre nós, vocês em Goiás e eu em Niterói, estiveram sempre presentes em minha vida e me mostraram que o estudo é a maior herança que podemos ter. A vocês meus pais, minha eterna gratidão por tudo que fizeram e ainda fazem por mim. Amo vocês.

Aos meus irmãos Gabriela e Gabriel, por todo apoio, amor e companheirismo. Amo vocês meus amores.

À professora Dra. Gilda Leitão, pela amizade e incentivo em trilhar a docência. Obrigada por todas as oportunidades, orientações e contribuições em toda a minha jornada científica e acadêmica. A senhora me acompanha desde a iniciação científica e desde então, foram 10 anos de muitos trabalhos e aprendizados. Obrigada por despertar em mim a paixão pela fitoquímica e cromatografia!

À professora Dra. Suzana Leitão, pela amizade e oportunidades. Obrigada por todos os ensinamentos e contribuições ao longo do meu doutorado. A senhora inspira todos nós e nos motiva a trilhar os caminhos da ciência!

À professora Dra. Rosineide Simas, pela amizade, orientações e contribuições ao longo dessa jornada. Foram vários momentos em que tive o privilégio de aprender mais sobre a espectrometria de massas e discutir dados com a senhora. Obrigada por cada oportunidade e principalmente a de aprender com você!

Aos meus queridos Leonardo Mello e Isabel de Castro, por todo auxílio durante os experimentos e pela confiança em mim e em meu trabalho. Obrigada pelo carinho, apoio e amizade. Muito feliz e agradecida por ter vocês em minha vida.

Ao Romain Sausset, pelo companheirismo e amizade. Foi uma grande oportunidade e experiência trabalhar com você durante os seis meses que você permaneceu no Brasil. Thank you for all the moments!

As minhas amigas, Elaine Viana, Simony Mendonça e Searitha Couto, pelo companheirismo, apoio e amizade.

Aos meus amigos, de Goiás, Rio e Niterói, que estiveram comigo em todos os momentos, por cada carinho recebido. Me senti muito acolhida.

Aos colegas do Laboratório de Fitoquímica e Farmacognosia e Laboratório de Fitoquímica e Cromatografia Contracorrente, pelo companheirismo ao longo de todos esses anos.

Aos técnicos da Central Analítica do DPNA, pelas análises realizadas e por sempre estarem dispostos a nos ajudar.

Ao professor Dr. Boniek Vaz, professora Dra. Andréa Chaves, professora Dra. Rosineide Simas, alunos e técnicos do Laboratório de Cromatografia e Espectrometria de Massas da Universidade Federal de Goiás (LaCEM-UFG), pela oportunidade em conhecer o laboratório e realizar as análises das amostras referentes ao meu trabalho. Agradeço por todo o carinho, atenção e suporte que recebi de todos, em especial aos colegas Ayrton Martins e Carla Freitas, pelo auxílio durante as minhas análises.

À Dra. Milene Miranda, Dra. Marilda Siqueira, alunos e pesquisadores do Laboratório de Vírus Respiratórios e do Sarampo (IOC-Fiocruz), pela realização dos ensaios para a avaliação da atividade antiviral e por todas as contribuições em meus trabalhos. Muito obrigada pela parceria ao longo desses 4 anos.

Ao professor Dr. Hector Koolen e seu aluno Carlos Vinicius, da Universidade do Estado do Amazonas (UEA), pelo auxílio na ferramenta *molecular networking* da plataforma GNPS.

À professora Dra. Manuela Leal e seus alunos Maria Eduarda e Caio Cheohen, do NUPEM, UFRJ, pelas análises *in silico*.

À professora Dra. Alane Beatriz Vermelho pela revisão da tese.

A Nova Analítica e Gilson, por disponibilizar o equipamento de cromatografia de partição centrífuga (CPC).

Ao Mario de La Torre, pelo treinamento para o uso do equipamento CPC e o *software* Gilson Glider Prep (GGP).

Ao Instituto Nacional de Pesquisas da Amazônia (INPA), pelas espécies de *Siparuna*.

Aos membros da banca examinadora da minha tese de doutorado, por aceitarem o meu convite e contribuições em meu trabalho.

Aos docentes do Programa de Pós-Graduação em Biotecnologia Vegetal e Bioprocessos (PBV-UFRJ), Instituto de Pesquisas de Produtos Naturais (IPPN-UFRJ) e Faculdade de Farmácia (FF-UFRJ), pelos ensinamentos compartilhados e contribuições para a minha formação científica e acadêmica.

Aos órgãos de fomento CAPES, FAPERJ e CNPq pelo auxílio financeiro e CNPq pela bolsa de estudos concedida.

“Quem ensina aprende ao ensinar e quem aprende, ensina ao aprender.” (Paulo Freire)

“O que vale na vida não é o ponto de partida e sim a caminhada. Caminhando e semeando, no fim terás o que colher.” (Cora Coralina)

“A verdadeira coragem é ir atrás de seu sonho mesmo quando todos dizem que ele é impossível.” (Cora Coralina)

**Lista de Abreviaturas**

<b>AcONa</b>	Acetato de sódio anidro
<b>APCI</b>	<i>Atmospheric Pressure Chemical Ionization</i> /Ionização Química a Pressão Atmosférica
<b>APT</b>	<i>Attached Proton Test</i> /Teste do Hidrogênio Ligado
<b>CDCl<sub>3</sub></b>	Clorofórmio deuterado
<b>CC<sub>50</sub></b>	Concentração citotóxica de 50%
<b>CCC</b>	Cromatografia Contracorrente
<b>CID</b>	<i>Collision Induced Dissociation</i> /Dissociação Induzida por Colisão
<b>3CLpro</b>	Enzima protease 3-quimiotripsina-like
<b>CLQ</b>	Cloroquina
<b>CPC</b>	<i>Centrifugal Partition Chromatography</i> /Cromatografia de Partição Centrífuga
<b>DI-ESI-MS</b>	<i>Direct Infusion-Electrospray Ionization-Mass Spectrometry</i> /Infusão Direta-Ionização por Electrospray-Espectrometria de Massas
<b>DMEM</b>	<i>Dulbecco's Modified Eagle's Medium</i> /Meio de Eagle Modificado por Dulbecco
<b>DMSO</b>	Dimetilsulfóxido
<b>DMSO-d<sub>6</sub></b>	Dimetilsulfóxido deuterado
<b>EC<sub>50</sub></b>	Efeito inibitório de 50% na replicação viral
<b>EIC</b>	<i>Extracted Ion Chromatogram</i> /Cromatograma de Íon Extraído
<b>ESI</b>	<i>Electrospray Ionization</i> /Ionização por Electrospray
<b>GC-MS</b>	<i>Gas Chromatography-Mass Spectrometry</i> /Cromatografia Gasosa-Espectrometria de Massas
<b>HA</b>	Hemaglutinina
<b>HMBC</b>	<i>Heteronuclear Multiple Bond Correlation</i> /Correlação Heteronuclear a Múltiplas Ligações
<b>Hpi</b>	<i>Hours post-infection</i> /Horas pós-infecção

<b>HPLC-DAD</b>	<i>High Performance Liquid Chromatography-Diode Array Detection</i> /Cromatografia Líquida de Alta Eficiência-Detector de Feixe de Diodos
<b>HSCCC</b>	<i>High-Speed Countercurrent Chromatography</i> /Cromatografia Contracorrente de Alta Velocidade
<b>HSQC</b>	<i>Heteronuclear Single Quantum Coherence</i> /Coerência Quântica Única Heteronuclear
<b>K</b>	Coeficiente de Partição
<b>KEEG</b>	<i>Kyoto Encyclopedia of Genes and Genomes</i> /Enciclopédia de Genes e Genomas de Kyoto
<b>LC-HR-MS/MS</b>	<i>Liquid Chromatography-High Resolution Mass/Mass Spectrometry</i> /Cromatografia Líquida-Espectrometria de Massas Sequencial de Alta Resolução
<b>LC-MS</b>	<i>Liquid Chromatography-Mass Spectrometry</i> /Cromatografia Líquida-Espectrometria de Massas
<b>LC-NMR</b>	<i>Liquid Chromatography-Nuclear Magnetic Resonance</i> /Cromatografia Líquida-Ressonância Magnética Nuclear
<b>LC-UV</b>	<i>Liquid Chromatography-Ultraviolet</i> /Cromatografia Líquida-Ultravioleta
<b>LPV/RTV</b>	Lopinavir/ritonavir
<b>MDCK</b>	<i>Madin-Darby Canine Kidney</i> /Rim Canino Madin-Darby
<b>Mpro</b>	Quimiotripsina-like protease
<b>MS/MS ou MS<sup>n</sup></b>	Espectrometria de massas sequencial
<b>MTT</b>	brometo de 3-(4,5-dimetiltiazol-2-il)-2,5- difeniltetrazólio
<b>NA</b>	Neuraminidase
<b>NAIs</b>	Antivirais Inibidores de Neuraminidase
<b>OST-car</b>	Carboxilato de oseltamivir
<b>PLpro</b>	Papaína-like protease
<b>RdRp</b>	RNA-Polimerase-RNA-Dependente
<b>S</b>	<i>Spike</i>
<b>TCID<sub>50</sub></b>	Dose infecciosa para 50% da cultura de tecidos



## Lista de Figuras

<b>Figura 1</b>	Distribuição geográfica da família Siparunaceae no Brasil	19
<b>Figura 2</b>	Espécime de floração da <i>Siparuna cristata</i>	21
<b>Figura 3</b>	Espécime de floração e frutificação da <i>Siparuna decipiens</i>	22
<b>Figura 4</b>	Espécime de frutificação da <i>Siparuna glycyarpa</i>	23
<b>Figura 5</b>	A. Espécime de floração e B. fruto da <i>Siparuna reginae</i>	24
<b>Figura 6</b>	Espécime de floração da <i>Siparuna sarmentosa</i>	24
<b>Figura 7</b>	Subclasses dos flavonoides	25
<b>Figura 8</b>	Biossíntese da chalcona e flavanona	26
<b>Figura 9</b>	Nomenclatura de fragmentos para flavonoides <i>O</i> -glicosídeos	27
<b>Figura 10</b>	Nomenclatura de fragmentos para flavonoides <i>C</i> -glicosídeos	27
<b>Figura 11</b>	Nomenclatura de fragmentos para chalconas e dihidrochalconas	28
<b>Figura 12</b>	Biossíntese dos alcaloides benziltetrahydroisoquinolínicos	29
<b>Figura 13</b>	Biossíntese dos alcaloides aporfínicos	29
<b>Figura 14</b>	Vias de fragmentação propostas para os principais íons produto de alcaloides benzilisoquinolínicos	30
<b>Figura 15</b>	Vias de fragmentação propostas para os principais íons produto de alcaloides aporfínicos	30
<b>Figura 16</b>	Vias de fragmentação propostas para os principais íons produto de alcaloides tetrahydroprotoberberínicos	31
<b>Figura 17</b>	Etapas do processamento de dados LC-MS/MS com o Mzmine	33
<b>Figura 18</b>	Formação de uma rede molecular a partir da inserção dos dados MS <sup>n</sup>	34
<b>Figura 19</b>	A. Coluna do equipamento HSCCC. B. Esquema de distribuição e movimento das duas fases na coluna do HSCCC	35
<b>Figura 20</b>	Coluna do equipamento CPC	36
<b>Figura 21</b>	Representação esquemática do vírus influenza A	39
<b>Figura 22</b>	NAIs (1) Oseltamivir, (2) Zanamivir e (3) Peramivir	39
<b>Figura 23</b>	Representação esquemática das proteínas estruturais do SARS-CoV-2	41

## Resumo

A influenza (gripe) é uma infecção viral aguda do trato respiratório causada pelo *Alphainfluenzavirus* cujos subtipos foram responsáveis por pandemias históricas. Recentemente, o coronavírus SARS-CoV-2 também afetou o mundo, causando a síndrome respiratória aguda. Portanto, a busca por substâncias anti-influenza e anti-SARS-CoV-2 é fundamental para a saúde pública. As espécies de *Siparuna* são utilizadas na medicina popular brasileira para o tratamento e profilaxia de resfriados, febre, cefaleia, distúrbios gastrointestinais e dores reumáticas. Dentre os metabólitos secundários descritos para essas espécies os alcaloides e os flavonoides metilados e glicosilados são conhecidos na literatura por apresentarem atividade antiviral. Assim, espécies de *Siparuna* podem ser fontes de substâncias bioativas com propriedades antivirais. Neste estudo foi investigada a atividade anti-influenza A(H1N1)pdm09 de 25 extratos de folhas de *S. cristata*, *S. decipiens*, *S. glycyarpa*, *S. reginae* e *S. sarmentosa*. Os perfis químicos (*metabolic fingerprinting*) por DI-ESI-MS nos modos de ionização positivo e negativo destes extratos foram analisados. Os extratos em *n*-butanol de *S. glycyarpa* e *S. sarmentosa* foram os mais ativos, inibindo  $96,0 \pm 1,3$  % e  $89,5 \pm 0,8$  % da replicação do vírus influenza A(H1N1)pdm09 *in vitro* respectivamente, na concentração de  $100 \mu\text{g}\cdot\text{mL}^{-1}$  24 h após a infecção sendo mantidos até 72 hpi. A partir da desreplicação desses extratos promissores por LC-HR-MS/MS e a utilização do *software* MZmine 2, alcaloides, flavonoides *O*- e *C*-glicosilados, dihidrochalconas e um dímero de procianidina foram anotados. Posteriormente, o extrato em *n*-butanol de *S. glycyarpa* foi fracionado por cromatografia de partição centrífuga (CPC) em modo descendente, com o sistema de solventes polar BuOH-MeOH-H<sub>2</sub>O (9:1:10, v/v). Dentre as frações coletadas, SGA, SGC, SGD e SGO apresentaram a maior inibição da replicação viral (acima de 74 %) na concentração de  $100 \mu\text{g}\cdot\text{mL}^{-1}$  após 24 hpi. Os dados de LC-HR-MS/MS dessas frações foram investigados através da construção de redes moleculares na plataforma GNPS. Alcaloides benzilisoquinolínicos foram anotados em SGA, SGC e SGD, e alcaloides aporfínicos, flavonoides *O*-glicosilados e dihidrochalconas em SGO. Devido a situação emergencial da COVID-19, o extrato em diclorometano da *S. cristata*, com flavonoides metilados e efeito inibitório para a replicação do vírus SARS-CoV-2 *in vitro* em células Vero E6 e Calu-3, foi fracionado por cromatografia contracorrente de alta velocidade (HSCCC) com o sistema de solventes hexano-acetato de etila-metanol-água (1:1:1:1, v/v). Os flavonoides retusina e kumatakenina isolados a partir desta técnica, foram capazes de inibir a replicação do SARS-CoV-2 com os valores de EC<sub>50</sub>  $0,4 \pm 0,05$  (Vero E6) e  $0,6 \pm 0,06$  (Calu-3), EC<sub>50</sub>  $10 \pm 0,7$  (Vero E6) e  $0,3 \pm 0,02$  (Calu-3) respectivamente, e índices de seletividade maiores que os controles lopinavir/ritonavir e cloroquina. Os resultados *in silico* demonstraram a potencial interação entre os flavonoides e as proteases 3CLpro e PLpro do vírus.

Palavras-chave: Siparunaceae, espectrometria de massas, A(H1N1)pdm09, SARS-CoV-2, potencial antiviral.

## Abstract

Influenza (flu) is an acute viral infection of the respiratory tract caused by the *Alphainfluenzavirus* which subtypes were responsible for historical pandemics. Recently, the coronavirus SARS-CoV-2 has also affected the world, causing acute respiratory syndrome. Therefore, the search for anti-influenza and anti-SARS-CoV-2 compounds is pivotal for public health. *Siparuna* species are used in Brazilian folk medicine for the treatment and prophylaxis of colds, fever, headache, gastrointestinal disorders, and rheumatic pain. Among the secondary metabolites described for these species, alkaloids and methylated and glycosylated flavonoids are well described in literature for their antiviral activity. Thus, *Siparuna* species may be sources of bioactive compounds with antiviral properties. In this study, the anti-influenza A(H1N1)pdm09 activity of 25 extracts from leaves of *S. cristata*, *S. decipiens*, *S. glycyarpa*, *S. reginae* and *S. sarmentosa* were investigated. The chemical profiles (metabolic fingerprinting) obtained by DI-ESI-MS in positive and negative ionization modes of these extracts were analyzed. The *n*-butanol extracts of *S. glycyarpa* and *S. sarmentosa* were the most active, inhibiting  $96.0 \pm 1.3\%$  and  $89.5 \pm 0.8\%$  of influenza A(H1N1)pdm09 virus replication in vitro respectively, in the concentration of  $100 \mu\text{g}\cdot\text{mL}^{-1}$  24 h post-infection, being maintained up to 72 hpi. Through the dereplication of these promising extracts by LC-HR-MS/MS and the MZmine 2 software, alkaloids, *O*- and *C*-glycosylated flavonoids, dihydrochalcones and a procyanidin dimer were annotated. After, *S. glycyarpa* *n*-butanol extract was fractionated by centrifugal partition chromatography (CPC) in descending mode, with the polar solvent system BuOH-MeOH-H<sub>2</sub>O (9:1:10, v/v). Among the collected fractions, SGA, SGC, SGD, and SGO showed the highest inhibition of viral replication (above 74%) at the concentration of  $100 \mu\text{g}\cdot\text{mL}^{-1}$  after 24 hpi. The LC-HR-MS/MS data of these fractions were investigated through the construction of molecular network in the GNPS platform. Benzylisoquinoline alkaloids were annotated in SGA, SGC, and SGD, and aporphine alkaloids, *O*-glycosylated flavonoids, and dihydrochalcones in SGO. Due to COVID-19 emergency, the dichloromethane extract from the *S. cristata*, with methylated flavonoids and inhibitory effect for the SARS-CoV-2 virus replication in vitro in Vero-E6 and Calu-3 cells, was fractionated by high-speed countercurrent chromatography (HSCCC) with solvent system hexane-ethyl acetate-methanol-water (1:1:1:1, v/v). The flavonoids retusin and kumatakenin isolated from this technique were able to inhibit viral replication of SARS-CoV-2 with EC<sub>50</sub> values  $0,4 \pm 0,05$  (Vero E6) and  $0,6 \pm 0,06$  (Calu-3), EC<sub>50</sub>  $10 \pm 0,7$  (Vero E6) and  $0,3 \pm 0,02$  (Calu-3) respectively, and a higher selectivity index than lopinavir/ritonavir and chloroquine controls. The in silico results demonstrated the potential interaction between flavonoids and the virus proteases 3CLpro and PLpro.

**Keywords:** Siparunaceae, mass spectrometry, A(H1N1)pdm09, SARS-CoV-2, antiviral potential.

## Sumário

<b>1</b>	<b>INTRODUÇÃO</b>	19
<b>1.1</b>	<b>Família Siparunaceae</b>	19
1.1.1	Gênero <i>Siparuna</i>	19
1.1.2	<i>Siparuna cristata</i>	21
1.1.3	<i>Siparuna decipiens</i>	21
1.1.4	<i>Siparuna glycyarpa</i>	22
1.1.5	<i>Siparuna reginae</i>	23
1.1.6	<i>Siparuna sarmentosa</i>	24
<b>1.2</b>	<b>Flavonoides</b>	25
<b>1.3</b>	<b>Alcaloides</b>	28
<b>1.4</b>	<b>Desreplicação</b>	31
<b>1.5</b>	<b>Cromatografia Contracorrente (CCC)</b>	34
1.5.1	Tipos de equipamentos	35
1.5.2	Escolha do sistema de solventes	36
<b>1.6</b>	<b>Produtos naturais como fonte de agentes antivirais</b>	37
<b>1.7</b>	<b>Vírus influenza e fármacos antivirais</b>	38
<b>1.8</b>	<b>Vírus SARS-CoV-2</b>	40
<b>2</b>	<b>OBJETIVOS</b>	42
<b>2.1</b>	<b>Objetivo geral</b>	42

<b>2.2</b>	<b>Objetivos específicos</b>	42
<b>3</b>	<b>MATERIAL E MÉTODOS</b>	43
<b>3.1</b>	<b>Pesquisa bibliográfica</b>	43
<b>3.2</b>	<b>Coleta do material botânico</b>	43
<b>3.3</b>	<b>Preparo dos extratos</b>	44
<b>3.4</b>	<b>Análises em espectrômetro de massas</b>	44
<b>3.5</b>	<b>Análises por LC-HR-MS/MS</b>	44
<b>3.6</b>	<b>Análises por HPLC-DAD</b>	45
<b>3.7</b>	<b>Fracionamento por cromatografia contracorrente</b>	45
3.7.1	Fracionamento por CPC	45
3.7.2	Fracionamento por HSCCC	46
<b>3.8</b>	<b>Ferramentas para desreplicação</b>	46
3.8.1	<i>Software</i> MZmine 2	46
3.8.2	GNPS	46
<b>3.9</b>	<b>Identificação das substâncias isoladas</b>	47
<b>3.10</b>	<b>Avaliação antiviral <i>in vitro</i></b>	47
3.10.1	Preparo das soluções estoque	47
3.10.2	Células	48
3.10.3	Ensaio para avaliação da citotoxicidade	48
3.10.4	Ensaio anti-influenza	48

3.10.4.1	<i>Screening</i> anti-influenza	48
3.10.4.2	Determinação do EC <sub>50</sub>	49
3.10.4.3	Titulação viral	49
3.10.5	Ensaio anti SARS-CoV-2	50
3.10.5.1	Determinação do EC <sub>50</sub>	50
3.10.5.2	Titulação viral	50
3.10.6	Análise estatística	50
<b>3.11</b>	<b>Avaliação antiviral <i>in silico</i></b>	<b>51</b>
3.11.1	Preparação dos receptores e ligantes	51
3.11.2	<i>Docking molecular</i>	51
<b>4</b>	<b>RESULTADOS E DISCUSSÃO</b>	<b>53</b>
4.1	Capítulo I. Amazonian <i>Siparuna</i> extracts as potential anti-influenza agents: Metabolic fingerprinting	53
4.2	Capítulo II. Bioassay-Guided Fractionation of <i>Siparuna glycyarpa</i> <i>n</i> -Butanol extract with Inhibitory Activity against Influenza A(H1N1)pdm09 Virus by Centrifugal Partition Chromatography (CPC)	90
4.3	Capítulo III. Flavonoids from <i>Siparuna cristata</i> as Potential Inhibitors of SARS-CoV-2 Replication	136
<b>5</b>	<b>CONCLUSÕES</b>	<b>198</b>
<b>6</b>	<b>REFERÊNCIAS BIBLIOGRÁFICAS</b>	<b>199</b>
	<b>ANEXOS</b>	<b>210</b>

## 1. Introdução

### 1.1 Família Siparunaceae

A família Siparunaceae compreende os gêneros *Glossocalyx* e *Siparuna*. No Brasil, esta família está distribuída nas cinco regiões geográficas e presente nos biomas Amazônia, Caatinga, Pantanal, Mata Atlântica e Cerrado (**Figura 1**). O gênero *Glossocalyx* é distribuído na África Ocidental e ocorre em florestas primárias sombrias e ao longo de estradas. Apresenta uma única espécie, a *Glossocalyx longicuspis* (sinonímias: *Glossocalyx brevipes*, *Glossocalyx staudtii* e *Glossocalyx zenkeri*), distribuída na Nigéria, Camarões, Gabão, Congo e ilha de Bioko (RENNER & HAUSNER, 2005). Além disso, o gênero *Siparuna* neotropical apresenta 53-60 espécies de arbustos e árvores que se distribuem do México ao Paraguai e são reconhecidas no campo pelo cheiro cítrico. Em geral, os arbustos são plantas dióicas que ocorrem na América Central e nos Andes, enquanto as plantas monóicas são árvores de grande porte (cerca de 15 espécies) que ocorrem na bacia amazônica (RENNER & HAUSNER, 2005).



Figura 1. Distribuição geográfica da família Siparunaceae no Brasil.

(Fonte: PEIXOTO *et al.*, 2020, disponível em <http://floradobrasil.jbrj.gov.br/reflora/floradobrasil/FB223>)

#### 1.1.1 Gênero *Siparuna*

Em geral, as espécies de *Siparuna* são utilizadas em rituais religiosos e na medicina popular brasileira no tratamento e profilaxia de resfriados, febre, cefaleia, dores reumáticas e distúrbios gastrointestinais (LEITÃO *et al.*, 1999; LEITÃO *et al.*, 2000; RENNER & HAUSNER, 2005). Dentre essas espécies, a *Siparuna brasiliensis* (sinonímia: *Siparuna apiosyce*), conhecida popularmente como “limão bravo” e “negramina” está descrita na

primeira Farmacopéia Brasileira (1926), sendo conhecida, no Brasil, por originar o primeiro medicamento popular vendido, no passado, por empresas farmacêuticas na forma de pastilhas e xarope para tosse (LEITÃO *et al.*, 1999). Apresentam importância etnobotânica e etnofarmacológica, como por exemplo, a *Siparuna guianensis*, utilizada pela tribo Jamamadi na Amazônia no preparo do chá para dores reumáticas (LEITÃO *et al.*, 1999). Curandeiros tradicionais utilizam cataplasmas, feitos a partir das folhas e cascas das espécies de *Siparuna* para o tratamento de pequenas feridas e picadas de cobra. Além disso, a casca aquecida de *Siparuna sessiliflora* e *Siparuna thecaphora* são utilizadas para acelerar a cicatrização de feridas de herpes, assim como as folhas de *Siparuna guajalensis* e *Siparuna schimpffii* são utilizadas no preparo de chá para auxiliar na fadiga (RENNER & HAUSNER, 2005). Dentre as espécies mais utilizadas medicinalmente estão: *Siparuna aspera*, *Siparuna brasiliensis*, *Siparuna cervicornis*, *Siparuna echinata*, *Siparuna eggersii*, *Siparuna guianensis*, *Siparuna lepidota*, *Siparuna macrotapala*, *Siparuna pilosolepidota*, *Siparuna schimpffii*, *Siparuna sessiliflora* e *Siparuna thecaphora* (RENNER & HAUSNER, 2005).

Além do uso tradicional, são encontrados na literatura estudos que descrevem atividades biológicas para algumas espécies desse gênero. Os extratos brutos provenientes das folhas de *Siparuna grandiflora*, *Siparuna pauciflora* e *Siparuna thecaphora* apresentaram atividade antiplasmódica e extratos de *Siparuna decipiens* demonstraram efeitos citotóxicos (antitumorais) (RENNER & HAUSNER, 2005). Em outro trabalho foi possível confirmar que os extratos de *Siparuna thecaphora* apresentaram capacidade neutralizante moderada frente aos efeitos hemorrágicos do veneno de *Bothrops atrox* (RENNER & HAUSNER, 2005). Ademais, os óleos essenciais provenientes das folhas de *Siparuna guianensis* também são alvos de pesquisas. De acordo com resultados descritos, apresentaram atividade repelente para a fase adulta do *Aedes aegypti* e *Culex quinquefasciatus* (AGUIAR *et al.*, 2015), alta atividade inseticida, controlando cepas de lepidópteros resistentes a toxinas Bt (LOURENÇO *et al.*, 2018), atividades anticariogênicas frente ao *Streptococcus mutans* e antimicobacterianas para *Mycobacterium avium*, *M. tuberculosis* e *M. kansasii* (MELO *et al.*, 2017). Recentemente, um estudo *in vitro* mostrou que os extratos em etanol e acetato de etila e o óleo essencial de *Siparuna guianensis* controlaram a infecção por *Toxoplasma gondii* (SOUZA *et al.*, 2021).

Dentre as classes de metabólitos secundários presentes na natureza, flavonoides livres e glicosilados com agliconas de kaempferol e quercetina, alcaloides aporfínicos, e benzilisoquinolínicos, e terpenoides já foram previamente relatados no gênero *Siparuna* (LEITÃO *et al.*, 1999; LEITÃO *et al.*, 2000; RENNER & HAUSNER, 2005). O flavonoide 3,7,4'-



tri-*O*-metil-kaempferol presente nas folhas e cascas de *Siparuna apiosyce*, foi o primeiro relato de isolamento de flavonoides metilados no gênero *Siparuna* (LEITÃO *et al.*, 1999). A liriodenina, um alcaloide oxoaporfínico, foi encontrado em diferentes espécies de *Siparuna*, e a presença deste alcaloide nas folhas de *Siparuna brasiliensis* pode ser responsável pelo seu uso como medicamento antitussígeno (RENNER & HAUSNER, 2005).

### 1.1.2 *Siparuna cristata*

Árvore monóica com 8-22 m de altura, apresenta tronco reto e redondo com casca amarelada ou marrom clara e lisa. Folhas opostas, grandes, coriáceas e glabras, com nervuras secundárias e terciárias. Pecíolos com 1,5-5 cm de comprimento e receptáculo de frutificação piriforme a oblongo com 2-3,5 cm de diâmetro. Flores brancas ou amarelas. As flores masculinas apresentam 1,8-4 mm de diâmetro e 1,7-3 mm de altura, enquanto as flores femininas são subglobosas com 2-4 mm de diâmetro e 3-4 mm de altura (**Figura 2**). Essa espécie ocorre em floresta tropical não inundada em 100 a 750 m de altitude, do Panamá a Colômbia, Venezuela, Equador, Peru e Brasil até as Guianas (RENNER & HAUSNER, 2005).



Figura 2. Espécime de floração da *Siparuna cristata*. (Fonte: RENNER & HAUSNER, 2005)

### 1.1.3 *Siparuna decipens*

Árvore monóica com 10-20 m de altura, casca cinza ou marrom clara e casca interna amarelada. Folhas opostas e glabras e pecíolos de 2-3 cm de comprimento. Flores com coloração creme ou verde esbranquiçadas, tornando-se amarelas com a idade. As flores masculinas apresentam 2,2 mm de diâmetro e 3-3,5 mm de altura, enquanto as flores femininas

possuem 2-3 mm de diâmetro e 3-7 mm de altura (**Figura 3**). A *Siparuna decipiens* ocorre em floresta de várzea, até 800 m de altitude e em toda a bacia Amazônica desde a Colômbia, Equador, Peru e Bolívia até o Brasil, Venezuela e as três Guianas. No Brasil essa espécie é conhecida como amarelinho, quariquara de igapó e na bacia Amazônica é chamada de quariquara branca (RENNER & HAUSNER, 2005).



Figura 3. Espécime de floração e frutificação da *Siparuna decipiens*.  
(Fonte: RENNER & HAUSNER, 2005)

#### 1.1.4 *Siparuna glycyarpa*

Essa espécie é encontrada na bacia Amazônica Brasileira abaixo de 600 m de altitude sendo conhecida como itaúba preta, aquariquara de igapó, quá pitiú e erva de rato. É uma árvore monóica de 8-30 m de altura, com folhas opostas e pecíolos de 1,5-3 cm de comprimento. As flores são esverdeadas, sendo as flores masculinas obcônicas ou urceoladas com 1,5-2,5 mm de diâmetro e 2,5-4 mm de altura, enquanto as flores femininas são ovóides de 3-3,5 mm de diâmetro e 3,5-4,5 mm de altura. Os receptáculos de frutificação são globosos e quando estão frescos apresentam cor amarela e polpa doce. O exocarpo e mesocarpo são carnosos e o endocarpo pedregoso (**Figura 4**) (RENNER & HAUSNER, 2005).



Figura 4. Espécime de frutificação da *Siparuna glycyarpa*. (Fonte: RENNER & HAUSNER, 2005)

### 1.1.5 *Siparuna reginae*

Essa espécie é encontrada como árvore monóica, com 5-22 m de altura em florestas primárias e secundárias da Amazônia, em solos arenosos próximo a córregos e em áreas de areia branca. Apresenta folhas opostas e pecíolos com 0,5-2,2 cm de comprimento. As flores são amareladas sendo as flores masculinas subglobosas, ovadas ou urceoladas com 1,2-3,3 mm de diâmetro e 1-2,8 mm de altura, cobertas por tubérculos minúsculos. As flores femininas são ovaladas a subglobosas, com 1,5-3,5 mm de diâmetro e 2-2,8 mm de altura, tomentosas e com tubérculos. O receptáculo de frutificação é globoso, com aproximadamente 1,5 cm de diâmetro, apresenta espinhos ou tubérculos carnosos, glabros ou tomentosos e quando estão maduros apresentam coloração rosa a vermelho e odor adstringente (**Figura 5**). Esta planta está distribuída na Colômbia, Venezuela, Guiana, Suriname, Equador, Peru e no Brasil, na região Amazônica e costeira (RENNER & HAUSNER, 2005).

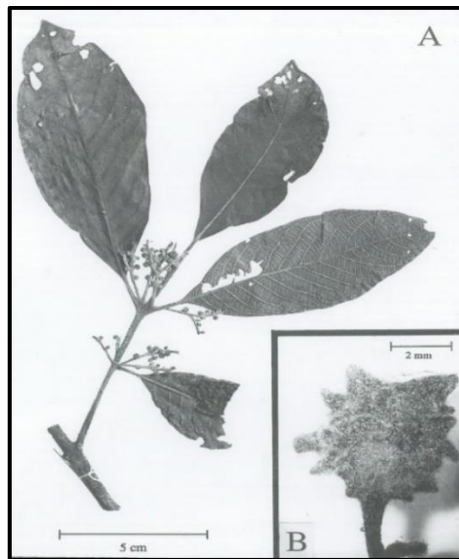


Figura 5. A. Espécime de floração e B. fruto da *Siparuna reginae*.  
(Fonte: RENNER & HAUSNER, 2005)

### 1.1.6 *Siparuna sarmentosa*

Árvore monóica com 5-20 m de altura, distribuída no oeste da bacia Amazônica abaixo de 500 m de altitude. É reconhecida por apresentar folhas opostas, glabras e com aspecto envelhecido. Pecíolos com 1-2 cm de comprimento e flores com coloração amarelo esverdeado, amarelo ou laranja. As flores masculinas são subglobosas, com 2,5-3,1 mm de diâmetro e 2,2-2,5 mm de altura, enquanto as flores femininas são subglobosas, com 2,2-2,5 mm de diâmetro e 2,3-2,5 mm de altura. O receptáculo de frutificação é globoso, com aproximadamente 1,2 cm de diâmetro e apresenta coloração verde (imaturo) e laranja (maduro) (**Figura 6**) (RENNER & HAUSNER, 2005).



Figura 6. Espécime de floração da *Siparuna sarmentosa*. (Fonte: RENNER & HAUSNER, 2005)

## 1.2 Flavonoides

Os flavonoides são substâncias fenólicas que apresentam um núcleo fundamental com esqueleto C<sub>6</sub>-C<sub>3</sub>-C<sub>6</sub>, sendo dois anéis aromáticos (A e B) e um anel pirano (C). Dentre as subclasses, as principais são flavona, isoflavona, flavanona, flavanonol, flavan-3-ol, flavonol, isoflavanona, isoflavana e antocianidina (**Figura 7**) (HEJAZI *et al.*, 2020). Como descrito na literatura, apresentam propriedades antivirais, antioxidantes, anti-inflamatórias, antimutagênicas, anticancerígenas e podem promover efeitos benéficos a saúde humana (HEJAZI *et al.*, 2020; HOFER, 2016; KOIRALA *et al.*, 2016; PANCHE *et al.*, 2016).

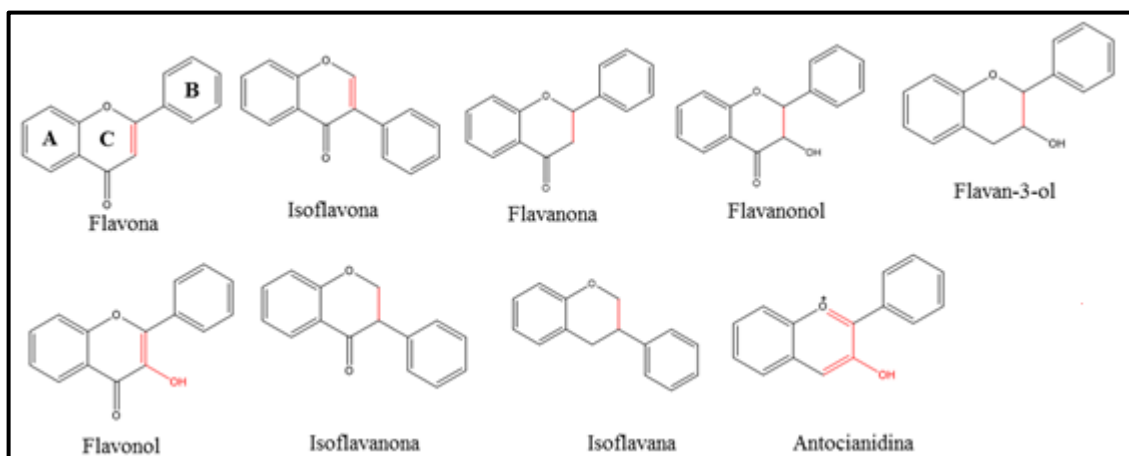


Figura 7. Subclasses dos flavonoides. (Adaptada de HOFER, 2016)

Na biossíntese dos flavonoides, os anéis B e C (porção fenilpropanoídica) são formados a partir de uma unidade iniciadora 4-hidroxycinamoil-CoA, precursor da via do chiquimato. Através de reações de condensação do tipo Claisen são adicionadas três unidades de malonil-CoA, precursor da via do acetato, ao 4-hidroxycinamoil-CoA, ocorrendo uma extensão de cadeia originando o anel A. A partir do ataque nucleofílico intramolecular do tipo Michael na ligação dupla ( $\alpha$ ,  $\beta$ ) da chalcona, precursora dos flavonoides, ocorre uma ciclização em  $\beta$ , originando a flavanona (**Figura 8**). A partir das flavanonas podem ser originadas as flavonas, flavonóis, isoflavonoides, antocianidinas e catequinas (DEWICK, 2009).

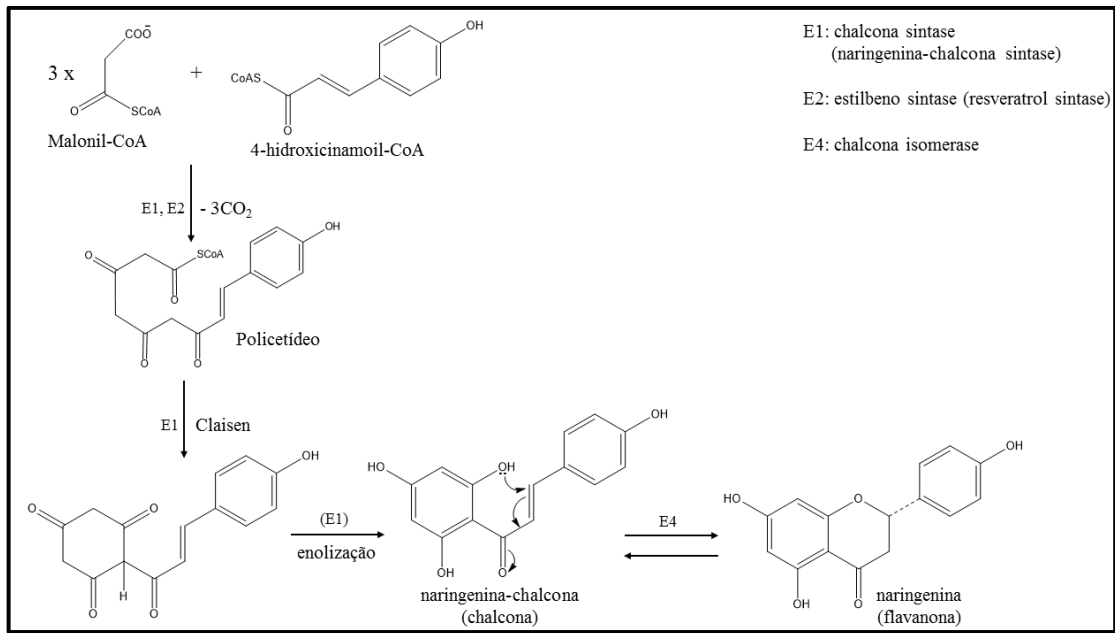


Figura 8. Biossíntese da chalcona e flavanona. (Adaptada de DEWICK, 2009)

Dentre as diferentes formas que os flavonoides podem ser encontrados estão a glicosilada e metilada. A glicosilação e metilação podem ocorrer via oxigênio ou átomo de carbono, formando os flavonoides *O*- ou *C*-glicosídeos, assim como os *O*- ou *C*-metilados, respectivamente (HOFER, 2016; KOIRALA *et al.*, 2016). Em flavonoides *O*-glicosídeos as posições O3 no anel C e O7 no anel A são comumente glicosiladas enquanto em *O*-metilados, 3-OH (anel C), 7-OH (anel A), 3' e 4'-OH (anel B) (HOFER, 2016; KOIRALA *et al.*, 2016). Para os *C*-glicosídeos, é comum a glicosilação em C6 e C8 no anel A (CAVALIERE *et al.*, 2005; KACHLICKI *et al.*, 2016). Dentre os carboidratos, glicose, galactose, rhamnose, xilose, arabinose e rutinose são comumente ligados aos flavonoides (CAVALIERE *et al.*, 2005; HOFER, 2016; KACHLICKI *et al.*, 2016).

A partir da fragmentação dos flavonoides glicosilados por espectrometria de massas é possível adquirir informações sobre as massas de agliconas, unidades de carboidrato e o tipo de ligação interglicosídica (*O*-glicosídeo e *C*-glicosídeo) (KACHLICKI *et al.*, 2016; VILLIERS *et al.*, 2016). Pode ser observado na nomenclatura de fragmentos para flavonoides glicosilados, proposta por Domon & Costello (**Figura 9**), os íons  $^{kl}X_j$ ,  $Y_j$  e  $Z_j$  tanto em modo de ionização positivo quanto negativo (KACHLICKI *et al.*, 2016). O  $j$  refere-se ao número de ligações interglicosídicas quebradas sendo contadas a partir da aglicona e  $k$  e  $l$  indicam as ligações que são quebradas no interior dos anéis do carboidrato (KACHLICKI *et al.*, 2016; VILLIERS *et al.*, 2016). Em flavonoides *O*-glicosídeos, as perdas mais comuns referentes as unidades de

carboidratos são 146 (desoxihexoses), 162 (hexoses) e 132 (pentoses) (KACHLICKI *et al.*, 2016; VILLIERS *et al.*, 2016).

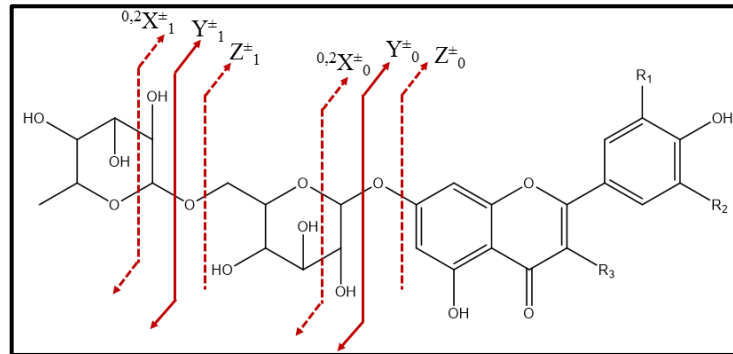


Figura 9. Nomenclatura de fragmentos para flavonoides *O*-glicosídeos. (Adaptada de VILLIERS *et al.*, 2016)

Nos flavonoides *C*-glicosídeos as quebras ocorrem no interior do anel do carboidrato. Como pode ser observado na **Figura 10**, os principais fragmentos são  $^{0,1}X_0$ ,  $^{0,2}X_0$ ,  $^{0,3}X_0$  e  $^{0,4}X_0$  (VILLIERS *et al.*, 2016). Na presença de hexoses, as nomenclaturas  $^{0,1}X_0$ ,  $^{0,2}X_0$ ,  $^{0,3}X_0$  correspondem as perdas de 150, 120 e 90 Da (*Daltons*) (**Figura 10**) e na presença de pentoses,  $^{0,1}X_0$ ,  $^{0,2}X_0$ ,  $^{0,3}X_0$  correspondem as perdas de 120, 90 e 60 Da (*Daltons*) (CUYCKENS & CLAEYS, 2004).

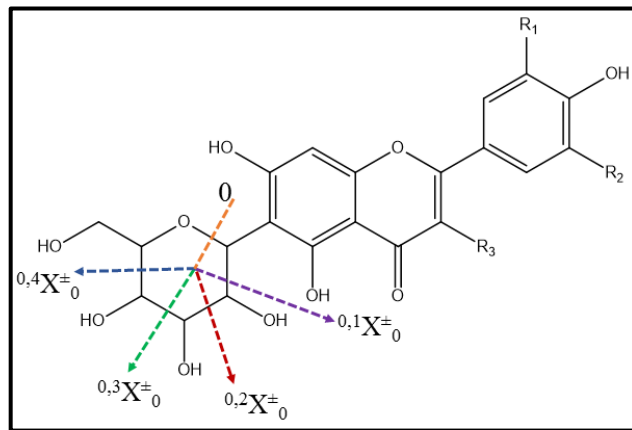


Figura 10. Nomenclatura de fragmentos para flavonoides *C*-glicosídeos. (Adaptada de VILLIERS *et al.*, 2016)

Segundo a nomenclatura de fragmentos para chalconas e dihidrochalconas (**Figura 11**), os fragmentos do tipo A ou B correspondem a presença da porção do anel A ou B enquanto ocorre a perda do segundo anel (PORTET *et al.*, 2008).

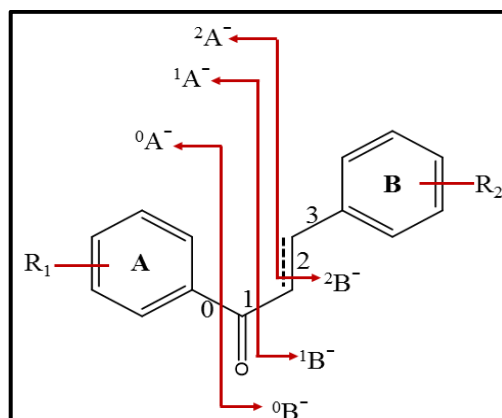


Figura 11. Nomenclatura de fragmentos para chalconas e dihidrochalconas.  
(Adaptada de PORTET *et al.*, 2008)

### 1.3 Alcaloides

Os alcaloides são substâncias com um ou mais átomos de nitrogênio sendo encontrados em plantas, animais, microrganismos e apresentam amplo espectro de atividades biológicas dentre elas, antivirais, antibacterianas, anticancerígenas e anti-inflamatórias (ADAMSKI *et al.*, 2020; DEBNATH *et al.*, 2018; DEWICK, 2009; KOLEVA *et al.*, 2012).

Os átomos de nitrogênio são provenientes de um aminoácido e o esqueleto de carbono do aminoácido precursor é mantido na estrutura química do alcaloide (DEWICK, 2009). Os principais aminoácidos precursores são ornitina, lisina, tirosina, histidina, ácido nicotínico, triptofano e ácido antranílico. A partir do anel heterocíclico típico, é possível classificar essas substâncias em pirrolidina, piperidina, piridina, quinolina, isoquinolina e indol (DEWICK, 2009; LEITÃO *et al.*, 2021).

Duas unidades de L-tirosina são utilizadas na via biossintética dos alcaloides benziltetrahydroisoquinolínicos. Entretanto, esses alcaloides apresentam *orto* dioxigenação no anel aromático, um padrão derivável da utilização de unidade de DOPA. Portanto, o fragmento feniletilamina do sistema de anéis tetrahydroisoquinolina é formado via DOPA. Assim, a dopamina é formada através da descarboxilação da L-DOPA e a partir da transaminação da segunda unidade de tirosina, ocorre a formação do ácido 4-hidroxifenilpirúvico que, após a descarboxilação, será transformado em 4-hidroxifenilacetaldeído. Posteriormente, a (*S*)-norcoclaurina é formada a partir da condensação da dopamina e o 4-hidroxifenilacetaldeído, na presença da norcoclaurina sintase, através da reação do tipo Mannich. A *O*-metilação na posição 6 da (*S*)-norcoclaurina produz a (*S*)-coclaurina, que após *N*-metilação, origina a (*S*)-*N*-metilcoclaurina. Em seguida, a hidroxilação em 3'na (*S*)-*N*-metilcoclaurina forma a (*S*)-



3'-hidroxi-*N*-metilcoclaurina, que durante a etapa de 4'-*O*-metilação, formará a (*S*)-reticulina, um intermediário fundamental para outros alcaloides, como os aporfínicos (**Figura 12**) (DEWICK, 2009).

Os alcaloides aporfínicos são formados a partir do acoplamento oxidativo intramolecular *orto-orto* ou *orto-para* da (*S*)-reticulina. Assim, a partir do acoplamento oxidativo *orto-orto* da (*S*)-reticulina é formada a (*S*)-corituberina enquanto a (*S*)-isoboldina é proveniente do acoplamento *orto-para* da (*S*)-reticulina (**Figura 13**) (DEWICK, 2009; STÉVIGNY *et al.*, 2005).

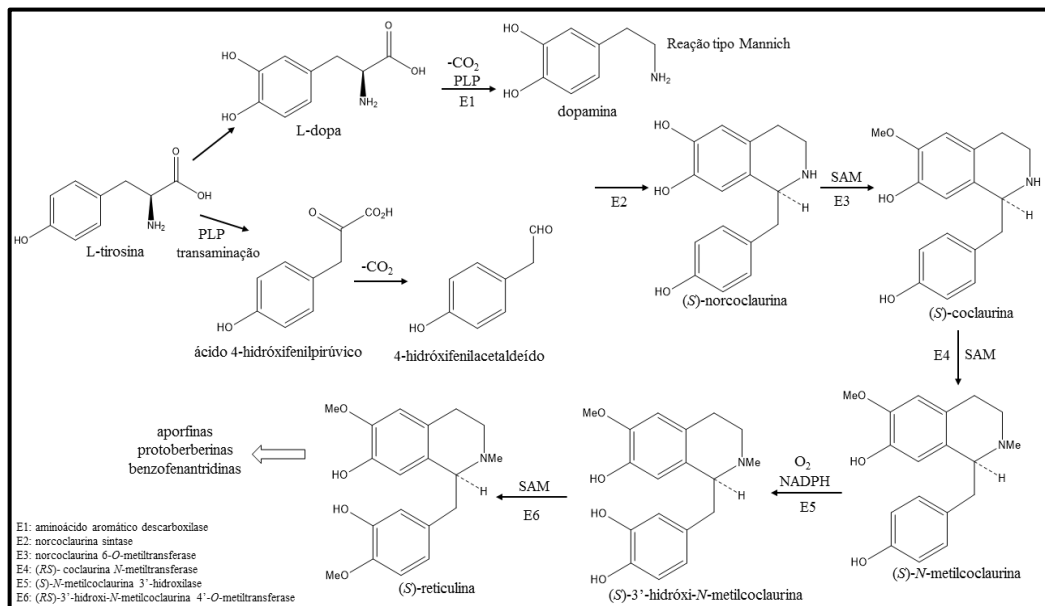


Figura 12. Biossíntese dos alcaloides benziltetrahydroisoquinolínicos. (Adaptada de DEWICK, 2009)

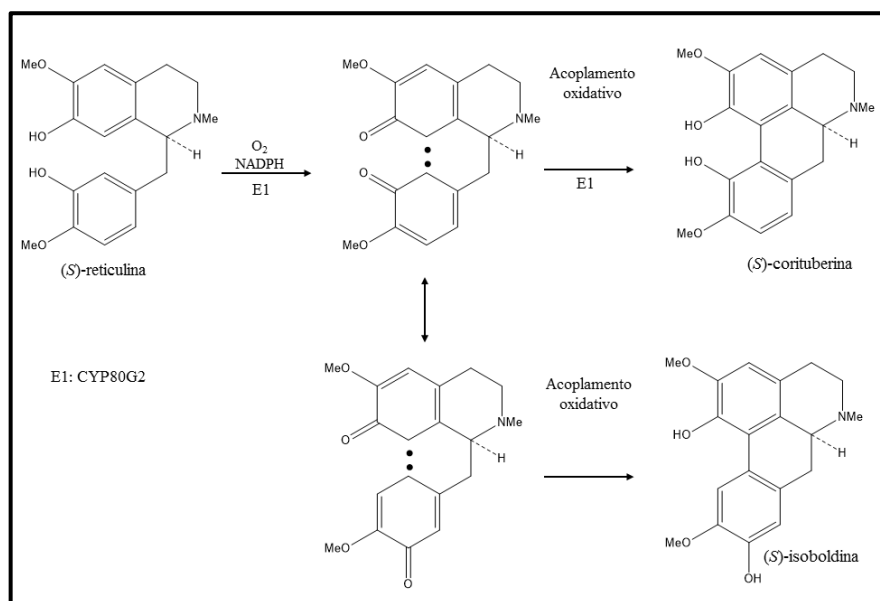


Figura 13. Biossíntese dos alcaloides aporfínicos. (Adaptada de DEWICK, 2009)

Os espectros de fragmentação dos alcaloides apresentam íons que indicam a presença desses metabólitos e informações importantes sobre as respectivas estruturas químicas. Para os alcaloides benzilisoquinolínicos, é comum observar nos espectros MS/MS as perdas referentes aos grupos  $\text{NH}_3$  ou  $\text{CH}_3\text{NH}_2$ ,  $\text{H}_2\text{O}$ ,  $\text{CO}$ ,  $\text{CH}_3\text{OH}$ , e os íons produto com  $m/z$  192 e  $m/z$  107 (**Figura 14**) (LIMA *et al.*, 2020).

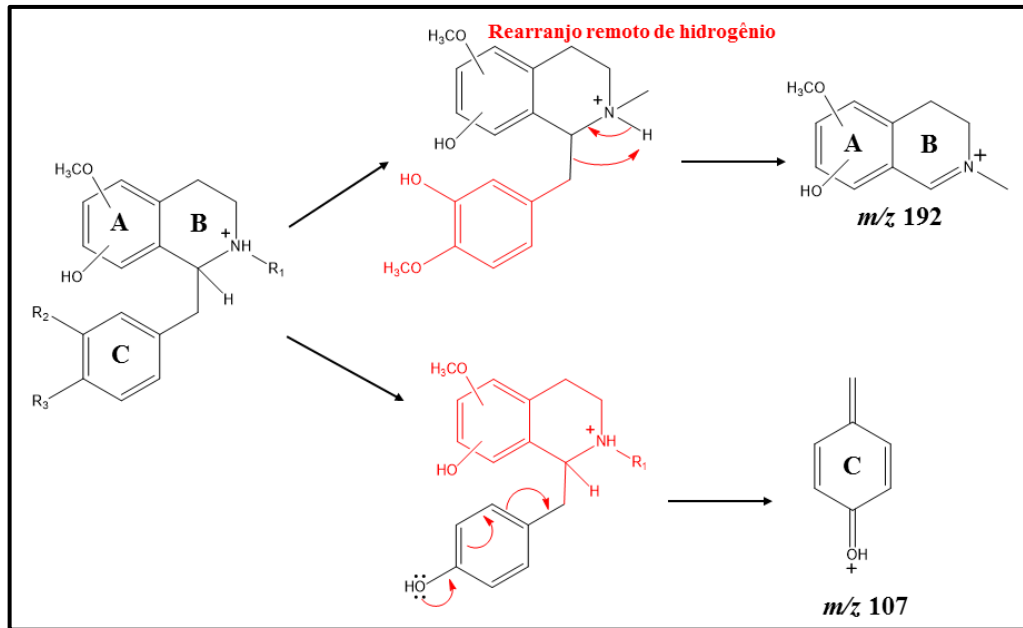


Figura 14. Vias de fragmentação propostas para os principais íons produto de alcaloides benzilisoquinolínicos. (Adaptada de LIMA *et al.*, 2020)

Para os alcaloides aporfínicos observa-se, inicialmente, a perda de um grupo amino e seu substituinte (**Figura 15**). Além disso, na presença de grupos OH e  $\text{OCH}_3$  vicinais no anel aromático, o espectro MS/MS exibe a perda de  $\text{CH}_3\text{OH}$  seguida de  $\text{CO}$ , e na presença de grupo metilendioxi, a perda de  $\text{CH}_2\text{O}$  seguida de  $\text{CO}$  (LIMA *et al.*, 2020; STÉVIGNY *et al.*, 2004).

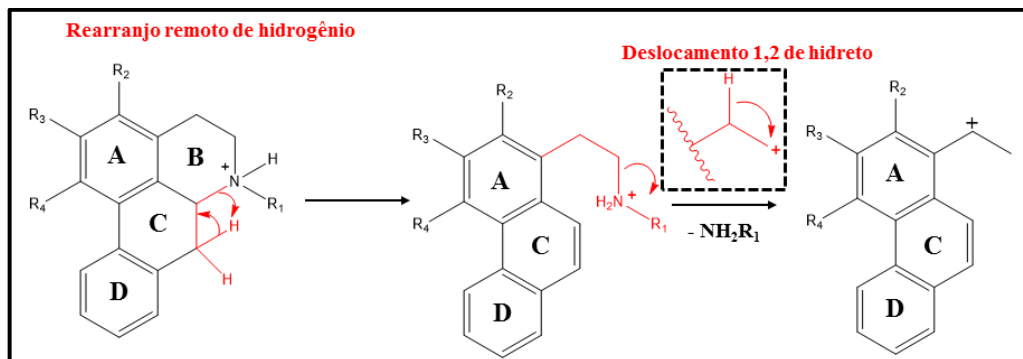


Figura 15. Vias de fragmentação propostas para os principais íons produto de alcaloides aporfínicos. (Adaptada de LIMA *et al.*, 2020)

Os espectros de MS/MS dos alcaloides tetrahidroprotoberberínicos apresentam o íon produto com  $m/z$  178, formado a partir da abertura do anel C através da reação *Retro-Diels-Alder* (**Figura 16**) (LIMA *et al.*, 2020).

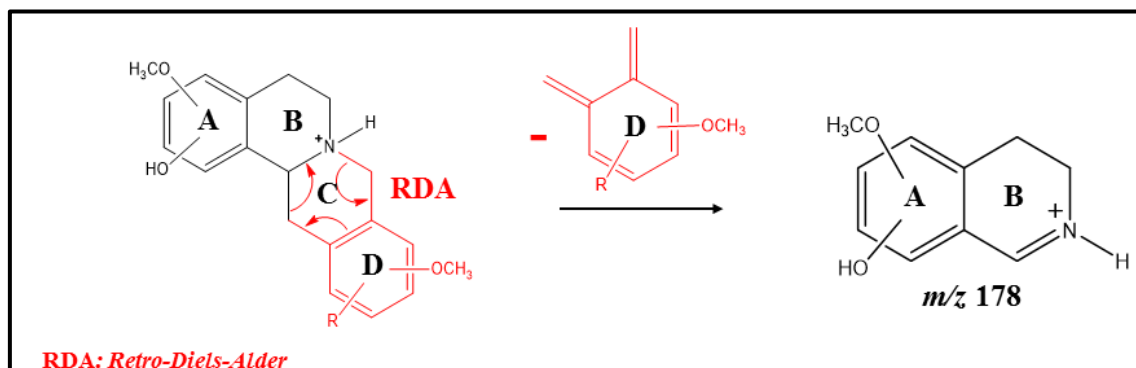


Figura 16. Vias de fragmentação propostas para os principais íons produto de alcaloides tetrahidroprotoberberínicos. (Adaptada de LIMA *et al.*, 2020)

#### 1.4 Desrepliação

Em 1978, o conceito desrepliação, do inglês *dereplication*, foi introduzido na literatura, quando se pretendia realizar a descoberta de novas substâncias anticancerígenas (ZANI *et al.*, 2017). Desde então, essa metodologia definida como a identificação de substâncias conhecidas em matrizes biológicas complexas, tem sido aplicada em diferentes áreas, como a de produtos naturais. Além disso, tornou-se crucial no processo de *screening* de extratos, frações, objetivando-se conhecer as substâncias presentes no material de interesse com foco nas inéditas, minimizando tempo e custo em análises (ALLARD *et al.*, 2016; ARORA *et al.*, 2019; YANG *et al.*, 2013).

Dentre as estratégias de desrepliação estão incluídas as técnicas hifenadas como as cromatografias com fase líquida e gasosa acopladas à espectrometria de massas (LC-MS e GC-MS), cromatografia com fase líquida acoplada à ressonância magnética nuclear (LC-NMR), cromatografia com fase líquida acoplada ao ultravioleta (LC-UV) e entre outras (ARORA *et al.*, 2019; EL-ELIMAT *et al.*, 2013; FRAIGE *et al.*, 2018; NIELSEN *et al.*, 2011; YANG *et al.*, 2013).

A partir da espectrometria de massas de alta resolução é possível adquirir um grande conjunto de dados com medições de massa com alta resolução e precisão, possibilitando a análise de misturas complexas. Centenas e milhares de metabólitos podem ser detectados e a identificação dessas substâncias está relacionada com a qualidade dos dados analíticos, e

eficiência das ferramentas para processamento e análise de dados (RATHAHAO-PARIS *et al.*, 2016). A massa exata, tempo de retenção e padrão de fragmentação que podem ser adquiridos a partir das análises por LC-MS, são critérios utilizados para a anotação (CHALECKIS *et al.*, 2019). Além disso, a comunidade *Metabolites Standard Initiaves* (MSI) considera diferentes níveis de confiabilidade para a anotação e/ou identificação de substâncias, classificando-os em cinco níveis (BLAZENOVIC *et al.*, 2018; CHALECKIS *et al.*, 2019; PILON *et al.*, 2020). O nível 0, apresenta maior confiança e corresponde a identificação completa, incluindo a elucidação estrutural que é realizada a partir do isolamento da substância de interesse. No nível 1 ocorre a comparação das análises espectrométricas e espectroscópicas com um padrão. Para esta finalidade requer, além do uso de padrão, métodos analíticos em pelo menos duas dimensões ortogonais, envolvendo a etapa de separação cromatográfica para a aquisição do tempo de retenção seguida de uma etapa de detecção espectral, que pode ser realizada a partir da espectrometria de massas em *tandem* (MS/MS). No nível 2, os dados são obtidos em duas dimensões ortogonais para a comparação da substância de interesse com dados da literatura e bancos de dados. Em nível 3, não há possibilidades de diferenciar isômeros, sendo possível determinar ao menos a classe da substância e o nível 4, não apresenta informações completas sobre o metabólito, sendo conhecido por ser o nível sem anotação (BLAZENOVIC *et al.*, 2018; CHALECKIS *et al.*, 2019; PILON *et al.*, 2020).

Para diminuir a complexidade dos dados gerados por espectrometria de massas, o processamento dos dados é uma etapa crucial para sua simplificação e redução da variação experimental dentro do conjunto de dados, o que possibilita extrair as informações relevantes facilitando sua interpretação (RATHAHAO-PARIS *et al.*, 2016). *Softwares* como os de código aberto MZmine, XCMS, MS-Dial, MetAlign e os comerciais MarkerView, Compound Discoverer e MarkerLynx podem ser utilizados para o processamento, visualização e análise dos dados (BORGES *et al.*, 2018; LI *et al.*, 2018; ZHOU *et al.*, 2012).

No MZmine as etapas necessárias para o processamento dos dados de espectrometria de massas de resolução unitária e alta resolução, incluindo os espectros de fragmentação ( $MS^n$ ), são: importação dos arquivos de dados brutos, listagem dos sinais a partir da detecção das massas dos dados brutos, construção dos cromatogramas para cada massa detectada (*Extracted Ion Chromatogram*-EIC), deconvolução, agrupamento dos sinais de isótopos, alinhamento dos dados e exportação (**Figura 17**) (PILON *et al.*, 2020; PILON *et al.*, 2021; PLUSKAL *et al.*, 2010). Além disso, a identificação dos picos pode ser realizada através da busca em bancos de

dados personalizados ou bases de dados *online* como *Kyoto Encyclopedia of Genes and Genomes* (KEGG) e PubChem (PLUSKAL *et al.*, 2010).

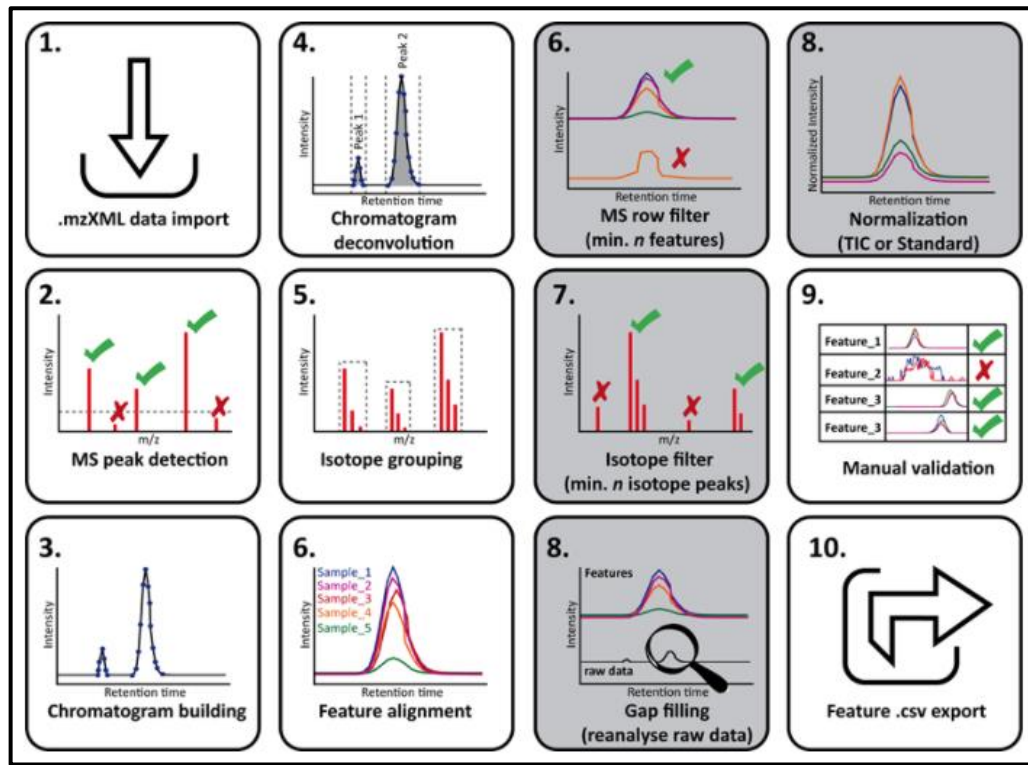


Figura 17. Etapas do processamento de dados LC-MS/MS com o MZmine. (Fonte: GNPS Documentation, disponível em <https://ccms-ucsd.github.io/GNPSDocumentation/featurebasedmolecularnetworking-with-mzmine2/>)

A plataforma *Global Natural Products Social Molecular Networking* (GNPS), permite organizar, visualizar e analisar um grande conjunto de dados de espectrometria de massas, a partir de íons fragmento (ARON *et al.*, 2020; PILON *et al.*, 2021; WANG *et al.*, 2016). Dentre as ferramentas de análise utilizadas nesta plataforma, as redes moleculares (*Molecular Networking*) agrupam os íons de acordo com a similaridade estrutural, possibilitando buscar substâncias conhecidas e análogos estruturais (ALLARD *et al.*, 2016; YANG *et al.*, 2013). Nesta ferramenta, os espectros MS/MS são organizados e classificados a partir de um valor de similaridade, calculado pelo valor de cosseno entre os espectros que estão nas amostras e os espectros de referência que estão disponíveis nos bancos de dados. Assim, os espectros serão agrupados a partir do valor de cosseno, ou seja, se entre dois espectros que estão pareados houver similaridade de cosseno maior ou igual ao valor limite, atribuído pelo usuário, esses espectros serão conectados. Este valor pode variar de 0 a 1, onde 0 indica que são totalmente diferentes e 1, 100 % de similaridade. Cada substância pode apresentar um conjunto de espectros, portanto é necessário a formação do espectro de consenso, que corresponde ao

agrupamento de espectros de MS/MS considerados idênticos com base no MSCluster. Esse espectro é representado por um nodo (*node*), ou seja, os espectros de MS/MS de uma mesma substância ficam agrupados em um nodo que pode estar conectado com outros (**Figura 18**). Ao final, os nodos da rede podem ser anotados utilizando as bibliotecas da plataforma e podem ser visualizadas no *software* livre Cytoscape em forma de um mapa de rede molecular, constituído por nodos unidos por arestas (*edge*), formando grupos conhecidos como *clusters*, que apresentam substâncias análogas e com padrões de fragmentação semelhantes (ARON *et al.*, 2020; OLIVEIRA *et al.*, 2017; PILON *et al.*, 2021; WANG *et al.*, 2016).

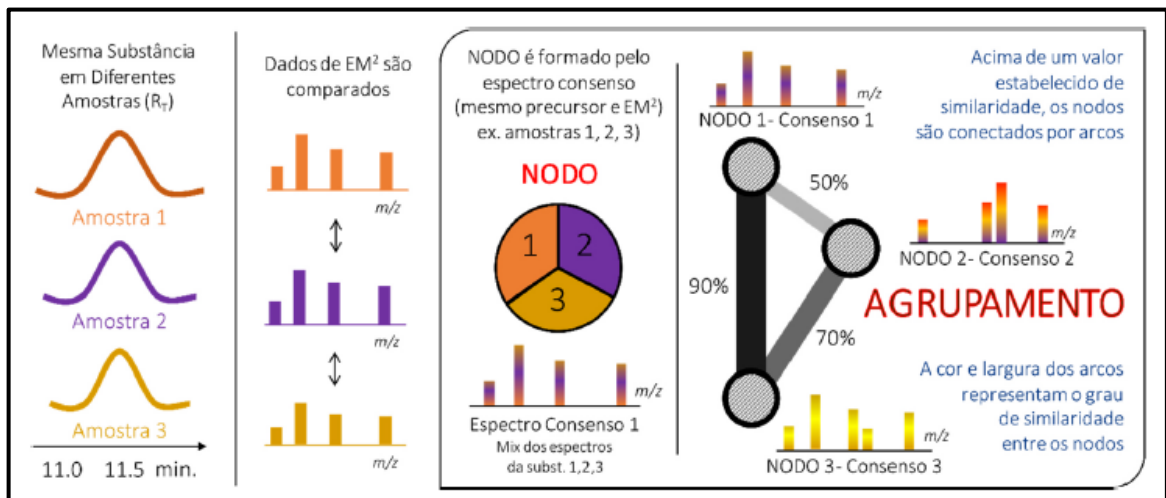


Figura 18. Formação de uma rede molecular a partir da inserção dos dados MS<sup>n</sup>. (PILON *et al.*, 2021)

### 1.5 Cromatografia contracorrente (CCC)

A cromatografia contracorrente, criada no final de 1960, por Yoichiro Ito (ITO, 2005, a), é uma técnica cromatográfica de partição líquido-líquido, principalmente preparativa, amplamente utilizada no isolamento e purificação de produtos naturais (PAULI *et al.*, 2008; BERTHOD *et al.*, 2009). Além disso, tem sido aplicada em trabalhos envolvendo a separação de proteínas, separações quirais, misturas sintéticas, fracionamentos guiados por atividade biológica e transformações microbianas (FRIESEN *et al.*, 2015). Sua principal diferença em relação às demais técnicas cromatográficas é a ausência de suporte sólido no interior da coluna, o que gera vantagens como a ausência de adsorção irreversível. O princípio fundamental da técnica é a partição do analito entre as duas fases líquidas imiscíveis, onde a proporção relativa do analito que passa para cada uma das fases (móvel e estacionária) é determinada pelo seu coeficiente de partição ( $K$ ). A fase estacionária permanece retida no interior da coluna enquanto a fase móvel é bombeada, passando pela fase estacionária (PAULI *et al.*, 2008; BERTHOD *et*

*al.*, 2009; FRIESEN *et al.*, 2015). As principais vantagens da cromatografia contracorrente são: (I) versatilidade em relação ao sistema de solventes (qualquer uma das fases, superior ou inferior podem ser utilizadas como fase móvel); (II) eficiência e rapidez do método; (III) boa resolução; (IV) previsibilidade e reprodutibilidade; (V) recuperação total da amostra sem modificações químicas ou perda da atividade biológica em fracionamentos guiados por ensaios biológicos (CONWAY, 1990; MARSTON & HOSTETTMANN, 2006).

### 1.5.1 Tipos de equipamentos

Na CCC moderna, a retenção da fase líquida estacionária nos equipamentos ocorre através de um campo de força centrífuga e o equilíbrio entre as duas fases líquidas no interior da coluna pode ser hidrostático ou hidrodinâmico. Entre os equipamentos disponíveis no mercado estão o HSCCC hidrodinâmico e o CPC hidrostático (BERTHOD *et al.*, 2009; BOJCZUK *et al.*, 2017).

A cromatografia contracorrente de alta velocidade (*high-speed countercurrent chromatography* - HSCCC) dispõe de um equilíbrio hidrodinâmico entre as duas fases líquidas imiscíveis no interior da coluna. Os equipamentos apresentam colunas enroladas em uma bobina que gira em torno do seu próprio eixo de rotação (periférico) e em torno do eixo central do equipamento, mimetizando o movimento planetário, fazendo com que o campo de força centrífuga seja variável ao longo da coluna, formando as zonas de mistura e separação (**Figura 19**) (BERTHOD *et al.*, 2009; KHAN & LIU, 2018; WANG *et al.*, 2019).

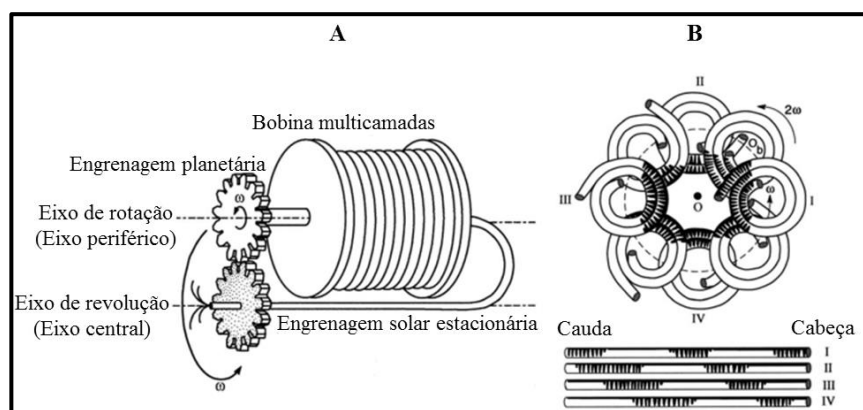


Figura 19. A. Coluna do equipamento HSCCC. B. Esquema da distribuição e movimento das duas fases na coluna do HSCCC. (Adaptada de WANG *et al.*, 2019)

Na cromatografia de partição centrífuga (*centrifugal partition chromatography*- CPC), ocorre o equilíbrio hidrostático entre as duas fases líquidas imiscíveis no interior dos compartimentos da coluna, onde a fase estacionária encontra-se retida. A coluna do CPC

consiste em vários discos quase idênticos, montados um sobre o outro. Cada disco apresenta uma série de células (câmaras ou canais) conectadas por dutos em cascata e dispostos em uma centrífuga com um eixo de rotação (**Figura 20**). O campo de força centrífuga constante e uniforme presente no sistema hidrostático é responsável pela retenção da fase estacionária nos canais e a dispersão da fase móvel pela coluna (BOJCZUK *et al.*, 2017).

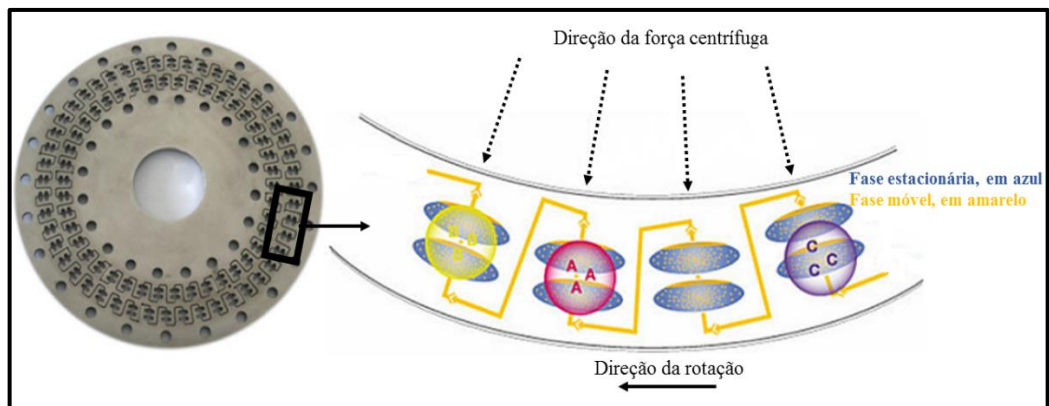


Figura 20. Coluna do equipamento CPC. (Adaptada de BOJCZUK *et al.*, 2017)

### 1.5.2 Escolha do sistema de solventes

A seleção do sistema de solventes é uma das etapas mais importantes e que está associada ao sucesso da separação cromatográfica por cromatografia contracorrente. Algumas condições importantes para um sistema de solventes adequado incluem: (I) o sistema de solventes precisa ser bifásico; (II) apresentar retenção na coluna do equipamento; (III) o sistema bifásico deve apresentar volumes semelhantes para cada fase; (IV) a amostra deve ser solúvel no sistema de solventes; (V) o sistema não deve formar emulsão; (VI) tempo de decantação inferior a 30 segundos para garantir a retenção satisfatória da fase estacionária; (VII) o coeficiente de partição ( $K$ ) das substâncias alvo deve permanecer no intervalo de  $0,5 < K < 2,0$  (CONWAY, 1990).

Na literatura estão descritas algumas estratégias adotadas para a seleção do sistema de solventes como (HOSTETTMANN *et al.*, 1984; FOCAULT & CHEVOLOT, 1998; ITO, 2005, b; COSTA & LEITÃO, 2010; LIU *et al.*, 2015):

- (1) **Literatura:** realizar um levantamento bibliográfico referente a sistemas de solventes utilizados no isolamento e purificação de substâncias semelhantes às de interesse;
- (2) **Tabelas de famílias de sistemas de solventes:** em CCC, os sistemas de solventes encontram-se organizados em famílias onde a polaridade do sistema varia alterando-se as proporções dos solventes;



(3) **Diagrama de fases:** através do estudo dos diagramas de fase, é possível obter conhecimento da composição de ambas as fases, móvel e estacionária;

(4) **Uso de solvente auxiliar:** a partir de um sistema binário é adicionado um terceiro solvente que auxiliará na distribuição do analito entre as fases.

## 1.6 Produtos naturais como fonte de agentes antivirais

O Brasil é considerado o país com a maior biodiversidade do mundo, sendo constituído por seis biomas terrestres dentre eles a Amazônia, Cerrado, Caatinga, Mata Atlântica, Pampa e Pantanal. Mediante este cenário, os biomas Brasileiros apresentam uma grande diversidade química e um reservatório de substâncias naturais bioativas (VALLI *et al.*, 2018; EKIERT *et al.*, 2020). Os produtos naturais são fontes de substâncias promissoras e desde a antiguidade têm sido empregados para fins medicinais (NEWMAN *et al.*, 2020). Além disso, são conhecidos por apresentarem atividades anticancerígena, imunomoduladora, anti-inflamatória, antiviral, antioxidante, neuroprotetora, hepatoprotetora e antibacteriana, sendo alvos de pesquisas para o desenvolvimento de medicamentos, cosméticos, suplementos alimentares, defensivos agrícolas (DENARO *et al.*, 2019; BEN-SHABAT *et al.*, 2020; EKIERT *et al.*, 2020). Dentre os metabólitos secundários encontrados no reino vegetal, flavonoides, terpenoides, saponinas, lignanas e cumarinas são conhecidos na literatura por influenciarem as funções celulares, a permeabilidade da membrana e a replicação viral (MUSARRA-PIZZO *et al.*, 2021). Assim, a busca por produtos naturais pode ser uma alternativa para o tratamento de doenças virais.

Os vírus podem infectar humanos e animais, o que leva ao surgimento de doenças virais crônicas e agudas como, por exemplo, as síndromes respiratórias que estão associadas a altas taxas de morbidade e mortalidade humana (MUSARRA-PIZZO *et al.*, 2021). As doenças infecciosas virais provocam ameaças à saúde da população, como as pandemias históricas causadas pelo vírus influenza e atualmente, a COVID-19. Diante disso, a busca por substâncias com potencial antiviral é fundamental para a saúde pública.

## 1.7 Vírus influenza e fármacos antivirais

Influenza, comumente chamada de gripe, é uma infecção viral aguda do trato respiratório causada pelo *Alphainfluenzavirus*, ocasionando febre, tosse geralmente seca, dores musculares e articulares, cefaleia, dor de garganta e coriza (WHO 2018; AI *et al.*, 2020). Existem quatro tipos de vírus influenza sazonal, tipos *alphainfluenzavirus*, *betainfluenzavirus*, *deltainfluenzavirus* e *gammainfluenzavirus* e o que os difere são as composições de suas proteínas nucleares e de matriz (WHO 2018; AI *et al.*, 2020; ICTV, 2021). Os *alphainfluenzavirus* e *betainfluenzavirus* causam epidemias sazonais da doença sendo o tipo *alpha*- (influenzavirus A), encontrado em espécies de mamíferos (incluindo seres humanos) e aves e o mais significativo em morbidade e mortalidade humana (WHO 2018). Os subtipos do influenzavirus A (H1N1, H2N2, H3N2, H5N1) foram responsáveis por pandemias globais da gripe que marcaram a história. O H1N1 foi o agente etiológico da gripe espanhola em 1918 com 40-50 milhões de mortes no mundo e da gripe suína em 2009. O H2N2 causou em 1957 a gripe asiática, ocasionando mais de um milhão de mortes no mundo. Em 2004, o H5N1 causou a gripe aviária e o vírus H3N2 foi responsável pela gripe de Hong Kong em 1968 (SETZER *et al.*, 2016). Atualmente, o H3N2 também foi responsável por surtos de influenza que iniciaram em julho de 2020, no Reino do Camboja, durante a pandemia de COVID-19, se estendendo para diferentes estados do Brasil, aumentando o número de casos de infecção (SOVANN *et al.*, 2021).

O *alphainfluenzavirus* (**Figura 21**) é pleomórfico (100 nm de diâmetro), constituído por RNA fita simples, octa-segmentado, com polaridade negativa, revestido por um nucleocapsídeo com simetria helicoidal e, externamente, por um envelope lipídico, onde se encontram inseridas as glicoproteínas hemaglutinina (HA) e neuraminidase (NA) (VRIES *et al.*, 2020; AI *et al.*, 2020). A NA é um alvo terapêutico para o desenvolvimento de medicamentos antigripais devido ao seu papel crucial para a dispersão viral (AI *et al.*, 2020). Dezoito subtipos de HA (H1 a H18) e onze NA (N1 a N11) foram identificados para este tipo de vírus e atualmente, os subtipos A(H1N1) e A(H3N2) circulam em humanos e causam as epidemias sazonais (WHO 2018; VRIES *et al.*, 2020; AI *et al.*, 2020).

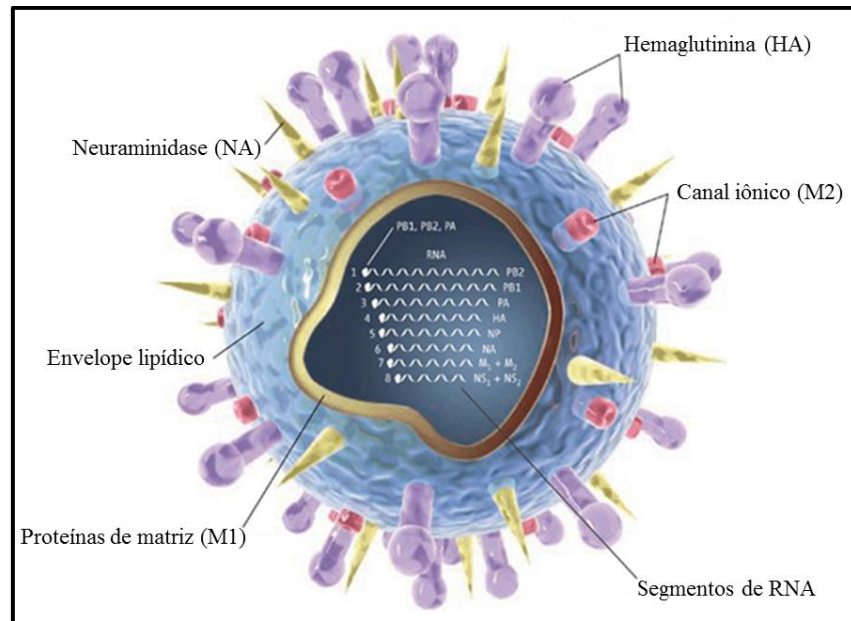


Figura 21. Representação esquemática do *alpha*influenzavirus. (Adaptado de KAISER *et al.*, 2006)

Dentre as classes de antivirais principais utilizadas para o tratamento das infecções por Influenza, estão disponíveis os antivirais inibidores de neuraminidase (NAIs) Zanamivir (Relenza®), Oseltamivir (Tamiflu®) e Peramivir (Rapiacta®), aprovados pelo *Food and Drug Administration* (FDA) (Figura 22), que são ativos contra o vírus influenza tipo *alpha*- e *beta*- (AI *et al.*, 2020). Os NAIs ligam-se ao sítio ativo da neuraminidase (NA), impedindo a clivagem do ácido siálico e conseqüentemente a liberação do vírus influenza no trato respiratório, sendo indicados no Brasil para os pacientes que apresentam Síndrome Respiratória Aguda Grave (DAS *et al.*, 2010; WANG & ZHANG *et al.*, 2010).

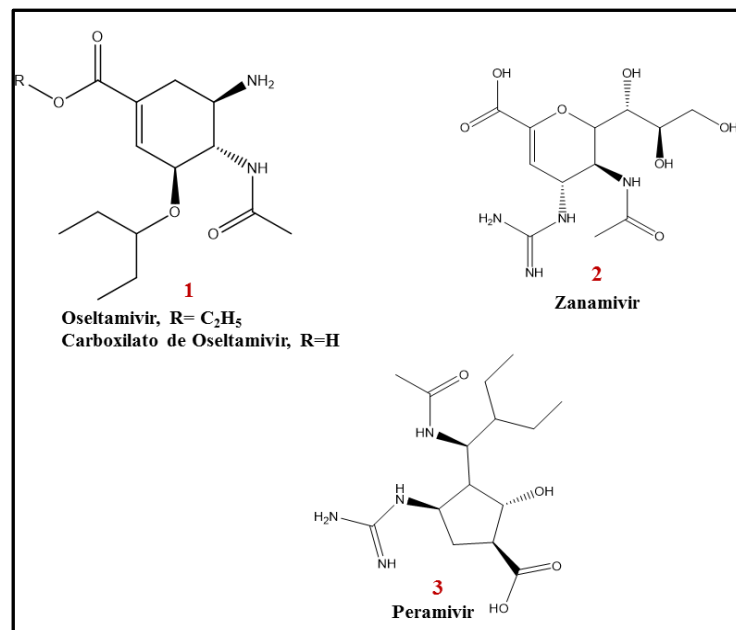


Figura 22. NAIs (1) Oseltamivir, (2) Zanamivir e (3) Peramivir. (Adaptado de AI *et al.*, 2020)

Os produtos naturais podem ser fontes de substâncias com potencial antiviral (DENARO *et al.*, 2019; BEM-SHABAT *et al.*, 2020; NEWMAN AND CRAGG, 2020), como exemplo, o Oseltamivir, semi-sintetizado a partir do ácido chiquímico encontrado em *Illicium verum* (GRIENKE *et al.*, 2012). Além disso, extratos etanólicos de própolis apresentaram atividade contra o vírus influenza A (H1N1) *in vitro* e diarilheptanoides isolados da *Alpinia officinarum* Hance também exibiram um potencial contra o vírus influenza *in vitro* (KUROKAWA *et al.*, 2010).

Dentre as classes de metabólitos secundários produzidos pelas plantas, os flavonoides são proeminentes para a inibição do vírus influenza, podendo ser utilizados como antivirais inibidores de neuraminidase (GRIENKE *et al.*, 2012). Os substituintes do esqueleto flavonoidico como por exemplo, a presença de glicosídeos, grupos hidroxila e metila podem estar relacionados com a atividade antiviral assim como a presença da ligação dupla  $C_2=C_3$  (WANG *et al.*, 2018). Flavonoides com C-metilação isolados a partir de *Cleistocalyx operculatus* (GRIENKE *et al.*, 2012), isorhamnetina, que apresenta grupo metila no anel B (DAYEM *et al.*, 2015), (2S)-6,8-dimetil-4'-metoxi-5,3',5'-trihidroxi-flavanona-7-O- $\beta$ -D-glicopiranosídeo isolado dos rizomas de *Matteuccia struthiopteris* (LI *et al.*, 2015), são exemplos de flavonoides que apresentaram atividade contra o vírus influenza H1N1. Outras substâncias, como alguns alcaloides, cumarinas, ácido gálico e taninos também inibiram a replicação deste vírus (GRIENKE *et al.*, 2012; THEISEN *et al.*, 2014; MORADI *et al.*, 2017).

## 1.8 Vírus SARS-CoV-2

Em 2019, foram relatados em Wuhan, na China, os primeiros casos de COVID-19, causados pelo novo coronavírus SARS-CoV-2 (betacoronavírus), que ocasionou a pandemia (MANI *et al.*, 2020). Atualmente, já foram registrados no mundo mais de 6 milhões de óbitos e somente no Brasil, mais de 650.000 (JHU CSSE COVID-19, 2022). Manifestações clínicas nos pulmões, rins, coração, sistema nervoso central, sistema gastrointestinal, anormalidades da coagulação sanguínea e pele têm sido relatadas em pacientes infectados com este vírus (KASAL *et al.*, 2020). Diante desse cenário emergencial, pesquisadores do mundo inteiro têm se mobilizado em busca de alternativas para combater o vírus. As proteínas não estruturais 3CLpro (também conhecida como Mpro), PLpro e RNA-Polimerase RNA-Dependente (RdRp), assim como a proteína estrutural *spike* (S) pertencentes ao SARS-CoV-2 (**Figure 23**) têm sido alvos em estudos científicos (MANI *et al.*, 2020; ULLRICH & NITSCHKE, 2020; KOUZNETSOVA *et al.*, 2021; MOLAVI *et al.*, 2021). A protease 3CLpro é responsável pelo controle da

replicação do coronavírus enquanto a PLpro desempenha as atividades protease, ubiquitinase e deslSGilase apresentando um papel na disseminação e resposta imune inata contra o vírus (LINDNER *et al.*, 2007; QAMAR *et al.*, 2020; XU *et al.*, 2021). Portanto, são importantes alvos na busca por terapias anti-SARS-CoV-2.

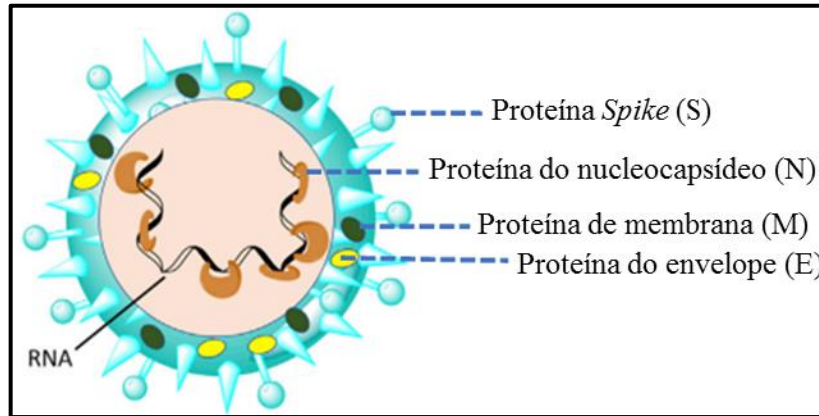


Figura 23. Representação esquemática das proteínas estruturais do SARS-CoV-2. (Adaptado de DOMLING & GAO *et al.*, 2020)

O remdesivir foi o primeiro medicamento aprovado pelo *Food and Drug Administration* (FDA) para o tratamento da COVID-19 e recentemente, foi aprovado pela Agência Nacional de Vigilância Sanitária (ANVISA) o uso emergencial de um novo medicamento, o paxlovid, uma combinação de nirmatrelvir e ritonavir, fabricado pela Pfizer (MAHASE, 2021; MARTIN *et al.*, 2021). Além disso, trabalhos científicos envolvendo diferentes tipos de produtos naturais mostraram o potencial antiviral contra SARS-CoV-2 como por exemplo, a inibição pelos triterpenos de *Tritergium regelii* em 3CLpro (MUSARRA-PIZZO *et al.*, 2021). Outros triterpenos como o ácido betulínico e o lignoide savinina formaram ligações de hidrogênio simples e duplas com resíduos de aminoácidos específicos, o que favoreceu a ligação com a 3CLpro inativando-a (MUSARRA-PIZZO *et al.*, 2021). Além desses triterpenos, foi avaliado que a quercetina extraída de *Ginkgo biloba* liga-se ao sítio ativo da 3CLpro, o que interfere na estabilidade do vírus (MUSARRA-PIZZO *et al.*, 2021). Os polifenóis 3-isoteaflavina-3-galato e a teaflavina-3,3'-dígalo presentes no chá preto também podem ser responsáveis pela inibição da 3CLpro (MUSARRA-PIZZO *et al.*, 2021). Além da inibição da replicação viral, estudos mostram que alguns produtos naturais, como a curcumina, podem inibir a expressão de citocinas pró-inflamatórias (MUSARRA-PIZZO *et al.*, 2021). Por outro lado, alguns diterpenos com esqueleto abietano isolados de *Salvia miltiorrhiza*, flavonoides prenilados de *Paulownia tomentosa* e chalconas de *Angelica keiskei*, inibiram a PLpro de SARS-CoV-2 (BOOZARI & HOSSEINZADEH, 2021).

## 2. Objetivos

### 2.1 Objetivo geral

Investigar o perfil químico por espectrometria de massas e atividade anti-influenza A(H1N1)pdm09 dos extratos de *Siparuna cristata*, *Siparuna decipiens*, *Siparuna glycyarpa*, *Siparuna reginae* e *Siparuna sarmentosa*. Além disso, utilizar a cromatografia contracorrente para adquirir frações e substâncias isoladas com potencial atividade anti-influenza A(H1N1)pdm09 e anti-SARS-CoV-2.

### 2.2 Objetivos específicos

- Analisar o perfil químico (*metabolic fingerprinting*) por DI-ESI-MS dos 25 extratos provenientes das folhas de *Siparuna cristata*, *Siparuna decipiens*, *Siparuna glycyarpa*, *Siparuna reginae* e *Siparuna sarmentosa*, assim como a atividade anti-influenza A(H1N1)pdm09.
- Realizar a desreplicação dos extratos brutos em etanol das cinco espécies de *Siparuna*, assim como, os extratos em *n*-butanol de *Siparuna glycyarpa* e *Siparuna sarmentosa*, a partir dos dados de LC-HR-MS/MS e da utilização do *software* MZmine 2, juntamente com bancos de dados online.
- Realizar o fracionamento bioguiado do extrato em *n*-butanol de *Siparuna glycyarpa* por CPC.
- Avaliar a atividade anti-influenza A(H1N1)pdm09 das frações provenientes do fracionamento do extrato em *n*-butanol por CPC e investigar os perfis químicos das frações bioativas por LC-HR-MS/MS, explorando a plataforma GNPS.
- Avaliar o potencial anti-SARS-CoV-2 *in vitro* e *in silico* dos flavonoides metilados isolados do extrato em diclorometano de *Siparuna cristata* por HSCCC.

### 3. Material e Métodos

#### 3.1 Pesquisa bibliográfica

A pesquisa bibliográfica consistiu em listar as substâncias que foram isoladas e/ou anotadas das espécies do gênero *Siparuna* (**Anexos, Tabela 1**). Ao total, 21 espécies foram incluídas dentre elas, *Siparuna aspera* (Ruiz & Pav.) A.DC., *Siparuna brasiliensis* (Spreng.) A. DC., *Siparuna cristata* (Poepp. & Endl.) A.DC., *Siparuna decipiens* (Tul.) A.DC., *Siparuna dresslerana* T. M. Antonio, *Siparuna echinata* (Kunth) A. DC., *Siparuna eggersii* Hieron, *Siparuna gesnerioides* (Kunth) A.DC., *Siparuna gigantotepala* S.S. Renner & Hausner, *Siparuna glycyarpa* (Ducke) S.S. Renner & Hausner, *Siparuna grandiflora* (Kunth) Perkins, *Siparuna guianensis* Aubl., *Siparuna macrotepala* Perkins, *Siparuna pachyantha* A.C. Sm., *Siparuna pauciflora* (Beurl.) A. D.C., *Siparuna poeppigii* (Tul.) A. DC., *Siparuna reginae* (Tul.) A. DC., *Siparuna sarmentosa* Perkins, *Siparuna schimpffii* Diels, *Siparuna sessiliflora* (Kunth) A.DC. e *Siparuna thecaphora* (Poepp. & Endl.) A.DC..

A pesquisa foi realizada utilizando as palavras-chave: Siparunaceae, *Siparuna*, *Siparuna compounds* nas bases de dados: Google Acadêmico, SciELO, ScienceDirect (Elsevier) e SciFinder. Através da base *The Plant List* foi possível consultar e confirmar o nome aceito das espécies do gênero *Siparuna* e as sinônimas. As espécies do gênero *Siparuna*, os nomes das substâncias, fórmula molecular e massa monoisotópica (Da) podem ser consultadas em **Anexos, Tabela 1**. A massa monoisotópica foi calculada a partir da fórmula molecular no *ChemCalc: molecular formula information*, disponível em <https://www.chemcalc.org>.

#### 3.2 Coleta do material botânico

As folhas de *Siparuna cristata* (Poepp & Endl.) A.DC., *S. decipiens* (Tul.) A.DC., *S. glycyarpa* (Ducke) S.S. Renner & Hausner, *S. reginae* (Tul.) A.DC. e *S. sarmentosa* Perkins foram coletadas na Reserva Adolpho Ducke, Manaus, Brasil, em Agosto de 2015. Os espécimes foram depositados no herbário do Instituto Nacional de Pesquisas da Amazônia (INPA) (Manaus, Brasil) sob os números de registro INPA 269731 (*S. cristata*), INPA 269734 (*S. decipiens*), INPA 269732 (*S. glycyarpa*), INPA 269735 (*S. reginae*) e INPA 269733 (*S. sarmentosa*). Este trabalho foi autorizado pelo Conselho de Gestão do Patrimônio Genético (CGEN) através da autorização A3C04CB.

### 3.3 Preparo dos extratos

As folhas secas e trituradas de *S. cristata* (SC, 1325,72 g), *S. decipiens* (SD, 100,12 g), *S. glycyarpa* (SG, 101,97 g), *S. reginae* (SR, 102,32 g) e *S. sarmentosa* (SS, 1226,80 g) foram extraídas por percolação com etanol 96° GL. Parte dos extratos brutos em etanol (EtOH) (151 g, 11,4 % p/p – SC), (12,5 g, 12,5 % p/p – SD), (14,1 g, 13,8 % p/p - SG), (22,55 g, 22 % p/p – SR), (155 g, 12,6 % p/p – SS) foram submetidos a partição entre água-metanol 7:3 (v/v) e *n*-hexano (Hex), diclorometano (DCM), acetato de etila (AcOEt) e *n*-butanol (BuOH), proporcionando os extratos em Hex (23,72 g SC; 2,38 g SD; 2,80 g SG; 3,74 g SR; 31,20 g SS); DCM (20,11 g SC; 2,21 g SD; 2,20 g SG; 4,40 g SR; 15,69 g SS); AcOEt (25,46 g SC; 3,53 g SD; 2,33 g SG; 4,85 g SR; 22,74 g SS) e BuOH (35,43 g SC; 2,47 g SD; 2,18 g SG; 5,98 g SR; 14,29 g SS).

### 3.4 Análises em espectrômetro de massas

As análises foram realizadas por infusão direta (15 µL) em um espectrômetro de massas LCQ Fleet (Thermo Fisher Scientific, Waltham, Massachusetts, EUA), com resolução unitária e fluxo de 0,1 mL.min<sup>-1</sup>. Para as análises dos 25 extratos das espécies de *Siparuna*, foi utilizada a fonte de ionização por *electrospray* (ESI) em modo de ionização positivo e negativo, e *atmospheric-pressure chemical ionization* (APCI) em modo positivo para as análises das frações adquiridas por HSCCC. As amostras foram diluídas em MeOH:H<sub>2</sub>O (9:1) com 0,1 % de ácido fórmico como modificador para o modo de ionização positivo ou 0,1% de NH<sub>4</sub>OH para o modo negativo. A aquisição dos dados foi realizada na faixa de massas *m/z* 50-1000 e *collision-induced dissociation* (CID) de 35 eV. Os espectros foram processados através do *software* XCALIBUR versão 2.2 SP1 (Thermo Scientific).

### 3.5 Análises por LC-HR-MS/MS

O equipamento de cromatografia líquida de ultra eficiência (Shimadzu), acoplado a um espectrômetro de massas MicrOTOF-QIII-MS (Bruker Daltonics, Inc., Billerica, MA, EUA), de alta resolução (50.000 FWHM) e com fonte de ionização ESI, foi utilizado para as análises dos extratos em etanol das cinco espécies de *Siparuna*, os extratos em *n*-butanol das espécies *S. glycyarpa* e *S. sarmentosa* e as frações adquiridas por CPC. As amostras (0,5 mg) foram dissolvidas em 2 mL de metanol e 3 µL foram injetados em uma coluna Acquity UPLC® BEH C18 (2,1 x 150 mm de diâmetro interno (d.i.); tamanho de partícula de 1,7 µm; Waters, Dublin,



Irlanda) aquecida a 40 °C. A fase móvel foi constituída por água – 5 mM de formiato de amônio – 0,1 % de ácido fórmico (A) e metanol (B). As condições de gradiente foram definidas como B = 50 % em 0 min, B = 99 % em 10 min, B = 100 % em 30 min e permanece em 100 % até 32 min, B = 50 % em 35 min e permanece em 50 % até 45 min a uma taxa de fluxo de 0,2 mL.min<sup>-1</sup>. Os dados foram adquiridos em modo de ionização positivo e negativo na faixa de massas  $m/z$  50-1200 e CID de 20 eV. Os espectros foram processados através do *software* Bruker Daltonics ESI Compass Data Analysis versão 5.0 SR1 (Bruker Daltonics, Inc., Billerica, MA, EUA).

### 3.6 Análises por HPLC-DAD

As análises das frações adquiridas por HSCCC foram realizadas em HPLC-DAD (280 nm) utilizando o equipamento Agilent 1260 Infinity Series com uma coluna Poroshell 120 EC-C18 (2,1 × 100 mm d.i.; 2,7 µm de tamanho de partícula; Agilent) a 30 °C. As condições de gradiente foram: solvente A = água – 0,01 % de ácido fórmico, solvente B = acetonitrila, B = 60 % em 40 min e B = 100 % em 45 min.

### 3.7 Fracionamentos por cromatografia contracorrente

#### 3.7.1 Fracionamento por CPC

Para o fracionamento do extrato em *n*-butanol de *S. glycyarpa* foi utilizado o CPC Lab System (Gilson, Middleton, WI, EUA) que combina um sistema de purificação PLC (modelo 2050) com um CPC 250, que apresenta uma coluna com volume total de 250 mL. O sistema de solventes selecionado foi *n*-butanol-metanol-água (9:1:10, v/v). A fase orgânica superior foi utilizada como fase estacionária e a fase aquosa inferior como fase móvel (modo descendente) com fluxo de 6 mL.min<sup>-1</sup>. A amostra (500 mg do extrato) foi dissolvida em 10 mL do sistema de solventes (1:1, v/v) e introduzida na coluna através de um loop de amostra de 10 mL. Foram realizados três fracionamentos com diferentes velocidades de rotação: 1000 e 1300 rpm e o monitoramento em ultravioleta em diferentes comprimentos de onda (254 nm, 365 nm e 200-400 nm- varredura completa). No primeiro e no segundo fracionamento, foram coletados 22 tubos de 12 mL durante a etapa de eluição e 25 tubos de 12 mL na etapa de extrusão. Para o último fracionamento, a função *local minimum* foi aplicada para a etapa de coleta das frações, sendo coletados 94 tubos na etapa de eluição, correspondendo a 250 mL de fase móvel (1,0

volume da coluna) e 73 tubos na etapa de extrusão, correspondendo a 302,2 mL (1,2 volume da coluna) de fase superior bombeada.

### 3.7.2 Fracionamento por HSCCC

Parte do extrato em diclorometano (600 mg) das folhas de *S. cristata* foi submetido ao fracionamento por HSCCC no equipamento Quattro HTPrep com duas bobinas contendo duas colunas cada (26 mL, 1,0 mm d.i., + 224 mL, 3,2 mm d.i. e 95 mL, 2,0 mm d.i., + 98 mL, 2,0 mm d.i.). A coluna de 98 mL foi utilizada e o sistema de solventes escolhido foi *n*-hexano–acetato de etila–metanol–água 1:1:1:1 (v/v). A fase orgânica superior foi utilizada como fase estacionária (modo de eluição de fase reversa), e a fase aquosa como fase móvel com fluxo de 2 mL.min<sup>-1</sup>. A amostra foi dissolvida em 5 mL do sistema solvente (1:1, v/v) e introduzida na coluna através de um loop de amostra de 5 mL. Foram recolhidas 30 frações de 4 mL durante a eluição com rotação de 860 rpm e outras 30 frações de 4 mL durante a extrusão.

## 3.8 Ferramentas para a desreplicação

### 3.8.1 Software Mzmine 2

Os dados de LC-HR-MS/MS, inicialmente, foram convertidos para .mzXML no software MSConvertGUI (64-bit) disponível em (ProteoWizard; proteowizard.sourceforge.net/tools.shtml). Em seguida, esses arquivos foram inseridos no software MZmine 2 versão 2.10, o qual foi utilizado para o processamento, visualização e análise dos dados de espectrometria de massas (**Tabela S1, material suplementar do capítulo I**). Além disso, foram realizadas neste software, pesquisas no banco de dados *on-line* KEGG e em banco de dados personalizado (revisão das substâncias isoladas das espécies do gênero *Siparuna*, **Anexos, Tabela 1**).

### 3.8.2 GNPS

Os dados provenientes das análises por LC-HR-MS/MS do extrato em *n*-butanol de *S. glycyarpa* e das frações adquiridas por CPC, foram analisados e organizados em redes moleculares usando a plataforma GNPS (<http://gnps.ucsd.edu>) (ARON *et al.*, 2020). Os dados foram convertidos para o formato .mzXML através do MS Convert (HOLMAN *et al.*, 2014) e inseridos na plataforma. Os parâmetros utilizados para a geração das redes moleculares foram:

*precursor ion mass tolerance* 0,05 Da, *product ion (fragment ion) tolerance* 0,5 Da, *minimum matched fragment ions* 6, *matched peaks* 4 e *cosine score* 0,65. As redes foram visualizadas no *software* Cytoscape 3.7.0 e a anotação das substâncias foi realizada a partir da interpretação dos espectros MS/MS em comparação com os bancos de dados do GNPS. As redes moleculares estão disponíveis nos seguintes links: <https://gnps.ucsd.edu/ProteoSAFe/status.jsp?task=daf5b5b0355e4862b3f163d3d62052cc>, e <https://gnps.ucsd.edu/ProteoSAFe/status.jsp?task=9dc29a10767344f5902b709fdb440722>.

### 3.9 Identificação das substâncias isoladas

Os flavonoides isolados por HSCCC foram identificados por ressonância magnética nuclear. Os espectros de  $^1\text{H}$ ,  $^{13}\text{C}$ , APT, HMBC e HSQC foram adquiridos em dimetilsulfóxido deuterado (DMSO- $d_6$ ) e clorofórmio deuterado ( $\text{CDCl}_3$ ) através de um espectrômetro Varian VNMRS a 25 °C, operando a 500 MHz para  $^1\text{H}$  e 125 MHz para  $^{13}\text{C}$ . Essas substâncias também foram analisadas no espectrômetro ultravioleta UV 1240 (Shimadzu, Japão) e o metanol e acetato de sódio anidro (AcONa) P.A. foram utilizados como reagentes de deslocamento.

### 3.10 Avaliação antiviral *in vitro*

As metodologias descritas neste tópico foram desenvolvidas no Laboratório de Vírus Respiratórios e do Sarampo (LVRS), localizado no Pavilhão Hélio e Peggy Pereira (HPP), e no Laboratório de Biossegurança Nível 3 (BSL3), localizado no Pavilhão Leonidas Deane, ambos pertencem ao Instituto Oswaldo Cruz, Fiocruz-RJ. Estes estudos antivirais *in vitro* foram realizados em colaboração com o grupo de pesquisa coordenado pela Dra. Milene Dias Miranda.

#### 3.10.1 Preparo das soluções estoque

Os extratos, frações e substâncias isoladas avaliados neste estudo foram diluídos em 100 % de dimetilsulfóxido (DMSO) na concentração final de 100 mg.mL $^{-1}$  (solução estoque), divididos em alíquotas e armazenados a -20 °C. Foram realizados no máximo 3 ciclos de congelamento e descongelamento para evitar a degradação dos materiais (KOZIKOWSKI *et al.*, 2003). As concentrações de DMSO resultantes durante os ensaios foram inferiores a 1 % (v/v), nível que é considerado não significativamente citotóxico (DLUDLA *et al.*, 2018; NGUYEN *et al.*, 2020).

### 3.10.2 Células

Foram utilizadas células de linhagem MDCK (*Madin-Darby Canine Kidney*), Vero E6 (rim de macaco verde africano) e Calu-3 (epitélio pulmonar humano), cultivadas em meio *Dulbecco's modified Eagle's médium* (DMEM-Gibco). As células foram mantidas em estufa a 37 °C e atmosfera de 5 % de CO<sub>2</sub> (LEAL *et al.*, 2021(a); LEAL *et al.*, 2021(b); LEAL *et al.*, 2022).

### 3.10.3 Ensaio para avaliação da citotoxicidade

Para a avaliação da citotoxicidade dos 25 extratos de espécies de *Siparuna* e das 18 frações adquiridas por CPC, monocamadas de MDCK (2x10<sup>4</sup> células por poço em microplaca de 96 poços) foram tratadas por 72 h, com 1000, 750 ou 500 µg.mL<sup>-1</sup> dos extratos ou 100 µg.mL<sup>-1</sup> das frações. O carboxilato de oseltamivir (OST-car) a 0,05 µM foi utilizado como controle.

Para a avaliação dos flavonoides isolados por HSCCC, monocamadas de Vero E6 (10<sup>4</sup> células por poço) e Calu-3 (10<sup>5</sup> células por poço) foram tratadas por 72 h com diluições semi-log (de 6000 a 50 µM) de todas as substâncias isoladas. A combinação de lopinavir/ritonavir (LPV/RTV) e cloroquina (CLQ) foram utilizadas como controle.

Nos diferentes ensaios, após o período de incubação das células e a remoção do meio de cultura, foi adicionada uma solução de brometo de 3-(4,5-dimetiltiazol-2-il)-2,5-difeniltetrazólio – MTT. Após 2 h foi adicionada a solução de SDS (10 %) e após mais 2 h de incubação, a leitura das placas foi realizada em espectrofotômetro a 570 nm. O cálculo para verificar a viabilidade celular foi realizado pela comparação entre a absorbância das células tratadas (A) e não tratadas (B) utilizando a fórmula  $A/B \times 100$ . A concentração citotóxica de 50 % (CC<sub>50</sub>) foi calculada por uma análise de regressão não linear das curvas de dose-resposta.

### 3.10.4 Ensaio anti-influenza

Os ensaios de infecção celular foram realizados com a cepa A/Michigan/45/2015, um vírus influenza A(H1N1)pdm09. O vírus foi cultivado e titulado de acordo com o manual da Organização Mundial de Saúde (OMS) para o diagnóstico laboratorial e vigilância virológica da influenza (WHO, 2011). Os estoques virais foram armazenados a -70 °C.

#### 3.10.4.1 *Screening* anti-influenza

Para a avaliação do efeito inibitório dos 25 extratos das espécies de *Siparuna* e das 11 frações adquiridas por CPC, as monocamadas das células MDCK foram infectadas por 1 h a 37 °C e 5 % de CO<sub>2</sub>. Em seguida, a suspensão viral foi removida e as monocamadas foram tratadas com 100 µg.mL<sup>-1</sup> de cada extrato e 25 ou 100 µg.mL<sup>-1</sup> do extrato em *n*-butanol da *S. glycyarpa* e frações. OST-car, a diferentes concentrações dependendo do objetivo do ensaio, foi utilizado como controle positivo para inibição da replicação viral. Após 24, 48 e 72 horas de infecção (hpi), os sobrenadantes foram coletados para a titulação viral pelo método de quantificação da atividade neuraminidase viral.

#### 3.10.4.2 Determinação do EC<sub>50</sub>

Com os extratos e frações que inibiram de forma significativa a replicação viral (acima de 85 %), estabelecemos os valores de EC<sub>50</sub>. Esse valor indica a concentração de produto testado capaz de inibir em 50 % a replicação viral. Para tal, células MDCK em placas com 24 poços foram infectadas com 400 TCID. Após 1 hpi, a suspensão viral foi removida e as monocamadas foram tratadas com diferentes concentrações dos produtos (12,5–400 µg.mL<sup>-1</sup>). O OST-car (0,001-1,0 µM) foi utilizado como controle positivo. Após 24 h, os sobrenadantes foram coletados para a realização da titulação viral através do método de Reed e Muench (REED, J. & MOUNCH, 1938).

#### 3.10.4.3 Titulação viral

A titulação do vírus influenza nos sobrenadantes das células infectadas com e sem tratamento foi realizado por dois métodos: 50 % *tissue culture infectious dose* (TCID<sub>50.mL<sup>-1</sup></sub>) e atividade neuraminidase.

Para o TCID, diluições logarítmicas dos sobrenadantes foram feitas em placas de 96 poços com 10 réplicas. 72 hpi, os efeitos citopáticos são avaliados ao microscópio eletrônico por pelo menos 2 operadores diferentes e contabilizados. O cálculo foi realizado através do método proposto por Reed e Mounch (REED, J. & MOUNCH, 1938).

A atividade da neuraminidase viral nos sobrenadantes coletados durante os ensaios de inibição da replicação do vírus influenza foi realizada através do kit NA-Star<sup>TM</sup> (Life Technologies). Os sobrenadantes da cultura foram incubados por 30 minutos com um substrato de neuraminidase quimioluminescente à temperatura ambiente e, em seguida, uma solução aceleradora foi adicionada para desencadear a emissão de luz do substrato clivado. A leitura do

sinal quimioluminescente foi realizada em um luminômetro (FLUOstar OPTIMA), seguindo as instruções do fabricante.

### 3.10.5 Ensaios anti-SARS-CoV-2

O isolado de SARS-CoV-2 foi propagado em célula Vero E6, sequenciado e seu genoma depositado (GISAID#414045, SisGen ACCF49F). Os estoques virais foram armazenados a -70 °C.

#### 3.10.5.1 Determinação do EC<sub>50</sub>

As células Vero E6 e Calu-3 foram infectadas com o SARS-CoV-2 isolado em multiplicidade de infecção (MOI) 0,01 e 0,1, respectivamente. Após 1 h, os sobrenadantes foram coletados e as células foram incubadas com os flavonoides 3,3',4'-tri-*O*-metil-quercetina, retusina e kumatakenina em concentrações log e semi-log (de 10 a 0,01 µM) e o extrato em diclorometano das folhas da *S. cristata* (de 250 a 31,25 µg/ml). A combinação de LPV/RTV e a CLQ foram utilizados como controle para inibição da replicação viral. Após 24 h de infecção em células Vero E6 ou 48 h de infecção em células Calu-3, os sobrenadantes foram recolhidos e os vírus titulados por unidades formadoras de placa (PFU/ml).

#### 3.10.5.2 Titulação viral

Para o ensaio de PFU, monocamadas de Vero E6 (10<sup>5</sup> células/poço) em placas de 24 poços foram infectadas com 300 µl de logarítmicas diluições do sobrenadante (10<sup>-3</sup>, 10<sup>-4</sup> ou 10<sup>-5</sup>). Após 1 h a 37 °C em 5 % de CO<sub>2</sub>, o meio foi substituído por 500 µl de solução de carboximetilcelulose (DMEM-HG 10 ×, 1,8 % de carboximetilcelulose e 2 % de soro fetal bovino). Após 72 h de infecção, o efeito citopático (CPE) foi analisado em microscópio óptico e 500 µl de formol a 10 % foram adicionados para fixar as células. Após 3 h, esta solução foi coletada e as placas foram coradas por azul de bromofenol 0,4 % e foi realizada a contagem por PFU.

### 3.10.6 Análise estatística

O *software* Excel 2010 do Windows (Microsoft) foi utilizado para gerar as curvas dose-resposta para calcular os valores dos parâmetros farmacológicos. Todos os experimentos foram

realizados em triplicatas e os resultados são apresentados como média ou média  $\pm$  desvio padrão.

### 3.11 Avaliação antiviral *in silico*

Esta etapa do trabalho foi realizada em colaboração com o grupo de pesquisa da professora Dra. Manuela Leal da Silva, do programa de pós-graduação Multicêntrico em Ciências Fisiológicas, no Centro de Ciências da Saúde, do Instituto de Biodiversidade e Sustentabilidade, NUPEM, UFRJ, campus Macaé.

#### 3.11.1 Preparação dos receptores e ligantes

As estruturas cristalinas selecionadas para 3CLpro (PDBid 6XQT) e PLpro (PDBid 7JRN) foram obtidas do *Protein Data Bank*. Através do *software* Pymol foram retirados os ligantes de ambos os cristais e, com o UCSF Chimera foi retirada a segunda cadeia da PLpro enquanto para a 3CLpro, as simulações seguiram com a estrutura em homodímero (DE LANO 2002; PETTERSEN *et al.*, 2004). Os arquivos das proteínas foram processados no PDB2PQR (<http://server.poissonboltzmann.org/pdb2pqr>) (DOLINSKY *et al.*, 2007) com o campo de força AMBER para avaliar a predição do *pKa* dos resíduos de aminoácidos ionizáveis em pH 7,4. Para 3CLpro, a seleção do provável estado de protonação da estrutura 3D foi realizada através do módulo *pdb2gmx* do pacote computacional GROMACS com a força de campo da proteína AMBER99SB-ILDN, nucléico AMBER94 (ABRAHAN *et al.*, 2015). A conversão da estrutura e do ligante para o formato *pdbqt* foi realizada com ferramentas AutoDock (MORRIS *et al.*, 2009), enquanto a saída PLpro PDB2PQR foi convertida usando UCSF Chimera.

#### 3.11.2 *Docking molecular*

Através da função *Zone*, que está disponível no *software* Chimera (PETTERSEN *et al.*, 2004), foram selecionados os resíduos de aminoácidos a 5 Å dos ligantes para ambas as proteases. Com este perímetro selecionado, foi construído o *grid* com coordenadas de centro  $x = -11$ , centro  $y = 1$ , e centro  $z = 45$ , e tamanho  $x = 32$ , tamanho  $y = 35$ , e tamanho  $z = 33$  para 3CLpro, e centro  $x = 13$ , centro  $y = -9$  e centro  $z = 30$ , e tamanho  $x = 30$ , tamanho  $y = 30$  e tamanho  $z = 30$  para PLpro. As simulações de *redocking* foram realizadas utilizando o *software* AutoDock Vina (TROTT *et al.*, 2009). A partir dos parâmetros obtidos com as simulações do

*redocking*, foram realizados seis *dockings* diferentes para ambos os receptores utilizando as seguintes substâncias: lopinavir, ritonavir, cloroquina, 3,3',4'-tri-*O*-metil-quercetina, retusina e kumatakenina. Os resultados foram reclassificados com base nas distâncias em Å das ligações de hidrogênio entre os resíduos His41, Cys145 e Glu166 para 3CLpro, e do resíduo Tyr268, descrito com impacto na atividade catalítica desta enzima.



## **4. Resultados e Discussão**

### **4.1 Capítulo I.** Amazonian *Siparuna* extracts as potential anti-influenza agents: Metabolic fingerprinting

Trabalho publicado em *Journal of Ethnopharmacology*

(doi: 10.1016/j.jep.2021.113788)



Contents lists available at ScienceDirect

Journal of Ethnopharmacology

journal homepage: [www.elsevier.com/locate/jethpharm](http://www.elsevier.com/locate/jethpharm)

## Amazonian *Siparuna* extracts as potential anti-influenza agents: Metabolic fingerprinting

Carla Monteiro Leal<sup>a,b</sup>, Rosineide Costa Simas<sup>c</sup>, Milene Miranda<sup>d</sup>, Mariana Freire Campos<sup>a,e</sup>, Brendo Araujo Gomes<sup>a,e</sup>, Marilda M. Siqueira<sup>d</sup>, Gabrielle do Vale<sup>d</sup>, Carlos Vitor Gomes de Almeida<sup>d</sup>, Suzana Guimarães Leitão<sup>a,e</sup>, Gilda Guimarães Leitão<sup>b,\*</sup>

<sup>a</sup> Programa de Biotecnologia Vegetal e Bioprocessos (PBV), Universidade Federal do Rio de Janeiro, Rio de Janeiro, 21.941-902, Brazil

<sup>b</sup> Instituto de Pesquisas de Produtos Naturais (IPP), Universidade Federal do Rio de Janeiro, Rio de Janeiro, 21.941-902, Brazil

<sup>c</sup> Laboratório de Cromatografia e Espectrometria de Massas (LaCEM), Universidade Federal de Goiás, Goiânia, 74.690-900, Brazil

<sup>d</sup> Laboratório de Vírus Respiratórios e do Sarampo, Instituto Oswaldo Cruz, Fundação Oswaldo Cruz, Rio de Janeiro, 21.041-210, Brazil

<sup>e</sup> Faculdade de Farmácia, Departamento de Produtos Naturais e Alimentos, Universidade Federal do Rio de Janeiro, Rio de Janeiro, 21.941-902, Brazil

### ARTICLE INFO

#### Keywords:

Chemical fingerprint  
Liquid chromatography-high resolution tandem mass spectrometry  
Flavonoids  
Alkaloids  
Dihydrochalcones  
Anti-Influenza activity

### ABSTRACT

**Ethnopharmacological relevance:** *Siparuna* species are used in Brazilian Folk Medicine for the treatment and prophylaxis of colds, fever, headache, gastrointestinal disorders and rheumatic pain.

**Aim of the study:** This study aimed to investigate a possible anti-influenza activity of 25 extracts from leaves of Amazonian *S. cristata*, *S. decipiens*, *S. glycyarpa*, *S. reginae* and *S. sarmentosa* based on their folk medicinal uses as well as to investigate their metabolic fingerprinting. The chemical composition of the active extracts was further dereplicated.

**Material and methods:** The chemical composition of the crude EtOH extracts from five *Siparuna* species were investigated by ESI ( $\pm$ ) LC-QTOF-MS<sup>2</sup>. Organic extracts were obtained by liquid-liquid partition with solvents of increasing polarity, generating 25 extracts which were subjected to a quick DI-ESI ( $\pm$ ) IT-MS fingerprint analysis. These extracts were tested against influenza virus replication and cellular toxicity using MDCK cells and influenza A/Michigan/45/2015 (H1N1)pdm09 virus. The compounds in the active BuOH extracts from *S. glycyarpa* and *S. sarmentosa* were annotated by ESI ( $\pm$ ) LC-QTOF-MS<sup>2</sup>.

**Results:** Analysis of the EtOH extracts revealed the presence of alkaloids and flavonoids, in the positive and negative ionization modes. Out of the 25 organic extracts screened for their antiviral activity, the BuOH extracts from *S. glycyarpa* and *S. sarmentosa* were the most active, inhibiting  $96.0 \pm 1.3\%$  and  $89.5 \pm 0.8\%$  of influenza virus replication 24 h post-infection. These inhibitory effects were maintained until 72 hpi. Alkaloids, O- and C-flavonoid glycosides, dihydrochalcones and a procyanidin dimer were annotated in these extracts.

**Conclusions:** The inhibitory effect against influenza A(H1N1)pdm09 virus replication shown by Amazonian *Siparuna* species corroborates the use of these plants in Brazilian Folk Medicine, showing their potential as anti-influenza agents. These promising results stimulate the continuation of this study with the aim of isolating the

**Abbreviations:** BuOH, butanol; CC<sub>50</sub>, concentration required to reduce normal non-infected cell viability by 50%; CDC, Centers for Disease Control and Prevention; CGEN, Conselho de Gestão do Patrimônio Genético; CID, collision-induced dissociation; DCM, dichloromethane; DI-ESI( $\pm$ )-MS, direct infusion-electrospray ionization-mass spectrometry; DI-ESI ( $\pm$ ) IT-MS, direct infusion-electrospray ionization-ion trap-mass spectrometry; DI-MS, direct infusion-mass spectrometry; DMEM, Dulbecco's modified Eagle's medium; DMSO, dimethyl sulfoxide; EC<sub>50</sub>, the concentration required to reduce inhibition of viral infection-induced cytopathogenicity by 50%; ESI, electrospray ionization source; ESI ( $\pm$ ) LC-QTOF-MS<sup>2</sup>, liquid chromatography-quadrupole time-of-flight-tandem mass spectrometry; EtOAc, ethyl acetate; EtOH, ethanol; FBS, fetal bovine serum; FWHM, full width half maximum; Hex, hexane; hpi, hours post-infection; HPLC, High Performance Liquid Chromatography; INPA, Instituto Nacional de Pesquisas da Amazônia; IRR, Influenza Reagent Resources; KEGG, Kyoto Encyclopedia Genes and Genomes; LC-MS, liquid chromatography-mass spectrometry; MDCK cells, Madin-Darby canine kidney cells; MeOH, methanol; MS, mass spectrometry; MS/MS, tandem mass spectrometry; MS<sup>n</sup>, multi-stage mass spectrometry; MTT, 3-(4,5-dimethylthiazol-2-yl)-2,5-diphenyltetrazolium bromide; NAIs, Neuraminidase Inhibitors; NH<sub>4</sub>OH, Ammonium hydroxide; OST-car, OSTcarboxylate; pdm09, pandemic A(H1N1)09 virus; SC, *Siparuna cristata*; SD, *Siparuna decipiens*; SG, *Siparuna glycyarpa*; SI, selective index is determined by the ratio between CC<sub>50</sub> and EC<sub>50</sub>; SR, *Siparuna reginae*; SS, *S. sarmentosa*; TCID<sub>50</sub>, 50% tissue culture infectious dose; TOF, time-of-flight; UFLC, ultra fast liquid chromatography; UPLC, Ultra Performance Liquid Chromatography.

\* Corresponding author.

E-mail addresses: [ggleitao@ippn.ufrj.br](mailto:ggleitao@ippn.ufrj.br), [ggleitao@yahoo.com.br](mailto:ggleitao@yahoo.com.br) (G.G. Leitão).

<https://doi.org/10.1016/j.jep.2021.113788>

Received 6 November 2020; Received in revised form 28 December 2020; Accepted 4 January 2021

Available online 8 January 2021

0378-8741/© 2021 Elsevier B.V. All rights reserved.



compound(s) responsible for this bioactivity, thus contributing to a better knowledge of those species and to the research of natural products with potential anti-influenza activity.

## 1. Introduction

The flu is an acute viral infection of the respiratory tract caused by Orthomyxovirus influenza. Influenza A and B circulate and cause seasonal epidemic disease. Influenza B only infects humans and influenza A humans and animals, having great significance in human morbidity and mortality. Subtypes of the influenza A virus (H1N1, H2N2, H3N2, H5N1) were responsible for global influenza historical pandemics (Setzer, 2016; WHO 2018). Oseltamivir (OST - Tamiflu®) and Zanamivir (Relenza®) belong to the class of antiviral Neuraminidase Inhibitors (NAIs) for the treatment and prophylaxis of influenza virus and are active against all influenza A and B (Setzer, 2016). Although most seasonality influenza viruses are NAIs susceptible, the appearance of resistance or compensatory mutations at independent fashion have led to the selection of OST-resistant strains, with a prevalence of 1–2% in different countries (Dixit et al., 2013; Lopes e Souza et al., 2015). Therefore, studies search for new anti-influenza compounds is pivotal for public health.

Natural products are sources of promising compounds and have been used for medicinal purposes since antiquity and the plant kingdom has proved to be still a source of potential new antiviral drugs (Denaro, 2019; Ben-Shabat, 2020; Newman and Cragg, 2020). One good example is Oseltamivir, semi-synthesized from shikimic acid, found in *Illicium verum* (Grienke et al., 2012). Among the classes of secondary metabolites produced from plants, alkaloids, coumarins, diarylheptanoids, flavonoids, gallic acid, and tannins are prominent for inhibiting the influenza virus and can be used as antiviral inhibitors (Grienke et al., 2012; Theisen et al., 2014; Moradi et al., 2017).

In previous works on the genus *Siparuna* (Siparunaceae) we have reported the occurrence of flavonoids, alkaloids, and terpenoids as a common feature on this genus (Leitão et al., 1999). *Siparuna* species are distributed in the Central and South America as shrubs or trees (Renner et al., 2005) and are used in Brazilian Folk Medicine for the treatment and prophylaxis of colds, fever, headache, gastrointestinal disorders and rheumatic pain (Leitão et al., 2000). Given the fact that *Siparuna apiosyce* ("Limão Bravo", "Negramina") is a popular medicine in Brazil, included in the first Brazilian Pharmacopoeia, and being sold in the past by pharmaceutical companies in the form of a syrup (Leitão et al., 2000), *Siparuna* species may be a source of antiviral compounds.

In natural products research, among the classifications of metabolomic approaches, the metabolic fingerprint is a rapid screening of all analytes in a complex sample, where the identification of compounds isn't mandatory and can be obtained by spectrometric, spectroscopic and chromatographic techniques (Ernst et al., 2014; Comejo-Báez et al., 2019).

Analytical techniques such as mass spectrometry coupled to liquid chromatography (LC-MS) and direct infusion mass spectrometry (DI-MS) are applied in chemical profiling studies of plant extracts. Mass spectrometry (MS) can be applied for the identification of compounds and provides data with high selectivity and sensitivity. The understanding of fragmentation mechanism aids the interpretation of the MS/MS and MS<sup>n</sup> fragmentation spectra, enabling structural elucidation (Ernst et al., 2014; Demarque et al., 2016).

In this study, the chemical composition of crude EtOH extracts from leaves of *Siparuna cristata*, *S. decipiens*, *S. glycyarpa*, *S. reginae* and *S. sarmentosa* were investigated. These extracts were submitted to liquid-liquid partition with solvents of increasing polarity (Hex, DCM, EtOAc and BuOH) for the investigation of inhibitory effects against influenza A (H1N1)pdm09 virus replication, cellular toxicity and metabolic fingerprinting. The active BuOH extracts from *S. glycyarpa* and *S. sarmentosa* were further dereplicated.

## 2. Materials and methods

### 2.1. Reagents

Organic solvents used were HPLC grade from Tedia (Tedia Brazil, Rio de Janeiro, Brazil) and ultrapure water (18.2MΩ-cm) was prepared with a PURELAB® Classic system (ELGA, USA). Ammonium formate (CAS number: 540-69-2) was purchased from Sigma-Aldrich® and formic acid from Vetec Química Fina®, LTDA (Rio de Janeiro, Brazil).

### 2.2. Plant material

Leaves of *Siparuna cristata* (Poepp. & Endl.) A.D.C., *S. decipiens* (Tul.) A.D.C., *S. glycyarpa* (Ducke) S.S. Renner & Hausner, *S. reginae* (Tul.) A. DC. and *S. sarmentosa* Perkins were collected at Reserva Adolpho Ducke, Manaus, Brazil, in August 2015. Voucher specimens are deposited at Instituto Nacional de Pesquisas da Amazônia (INPA) herbarium (Manaus, Brazil) under the registration numbers INPA 269731 (*S. cristata*), INPA 269734 (*S. decipiens*), INPA 269732 (*S. glycyarpa*), INPA 269735 (*S. reginae*) and INPA 269733 (*S. sarmentosa*). This work was authorized by the Directing Council of Genetic Heritage (Conselho de Gestão do Patrimônio Genético, CGEN) by the authorization A3C04CB.

### 2.3. Preparation of extracts

Dried and ground leaves of *S. cristata* (SC, 1325.72 g), *S. decipiens* (SD, 100.12 g), *S. glycyarpa* (SG, 101.97 g), *S. reginae* (SR, 102.32 g) and *S. sarmentosa* (SS, 1226.80 g) were extracted by percolation with ethanol 96° GL. Part of the crude ethanol (EtOH) extracts (151 g, 11.4% w/w - SC), (12.5 g, 12.5% w/w - SD), (14.1 g, 13.8% w/w - SG), (22.55 g, 22.0% w/w - SR), (155 g, 12.6% w/w - SS) were partitioned between water-methanol 7:3 (v/v) and hexane (Hex), dichloromethane (DCM), ethyl acetate (EtOAc) and butanol (BuOH), affording Hex (23.72 g SC; 2.38 g SD; 2.80 g SG; 3.74 g SR; 31.20 g SS); DCM (20.11 g SC; 2.21 g SD; 2.20 g SG; 4.40 g SR; 15.69 g SS); EtOAc (25.46 g SC; 3.53 g SD; 2.33 g SG; 4.85 g SR; 22.74 g SS) and BuOH (35.43 g SC; 2.47 g SD; 2.18 g SG; 5.98 g SR; 14.29 g SS) extracts. Dried extracts were resuspended in dimethyl sulfoxide (DMSO) in a final concentration of 100 mg.mL<sup>-1</sup> (stock solution). For *in vitro* tests, the stock solutions were diluted in cell culture medium to obtain the different crude extracts concentrations. For all assays, DMSO did not exceed 1% (v/v).

### 2.4. DI-ESI (±) IT-MS extracts analysis

All *Siparuna* extracts were analyzed through direct infusion (15 µL) on a LCQ Fleet (Thermo Fisher Scientific, Waltham, Massachusetts, USA) unit resolution mass spectrometer, equipped with electrospray ionization (ESI) source, operated in negative (-) and positive (+) mode. Extracts were diluted in MeOH:H<sub>2</sub>O (9:1) with 0.1% formic acid as modifier (positive ionization mode) or 0.1% NH<sub>4</sub>OH (negative ionization mode); flow rate of 0.1 mL.min<sup>-1</sup> (5 min for each sample). Nitrogen (N<sub>2</sub>) was used as sheath gas (25 arbitrary units) and Helium (He), as collision gas. Mass spectrometer parameters were 6.0 kV source voltage, 43 V capillary voltage, 100 V tube lens voltage and 400 °C capillary temperature. The full scan data acquisition was mass range *m/z* 50–1000, collision-induced dissociation (CID) cell was 35 eV and the spectra were processed in the XCALIBUR software version 2.2 SP1.

### 2.5. ESI (±) LC-QTOF-MS<sup>2</sup> analysis

EtOH extracts from five *Siparuna* species and BuOH extracts from SG



and SS were analyzed on an Ultra Fast Liquid Chromatography (UFLC) equipment (Shimadzu), coupled to a MicrOTOF-QIII-MS (Bruker Daltonics, Inc., MA, USA), a high resolution Quadrupole - TOF hybrid mass spectrometer, with 50,000 (FWHM) resolution, equipped with ESI ( $\pm$ ) source using a column Acquity UPLC<sup>®</sup> BEH C18 (2.1  $\times$  150 mm internal diameter (i.d.); 1.7  $\mu$ m particle size; Waters, Dublin, Ireland) heated at 40 °C. Extracts (0.5 mg) were dissolved in 2 mL of methanol and 3  $\mu$ L were injected under gradient conditions with water - 5 mM ammonium formate - 0.1% formic acid (A) and methanol (B) as mobile phases, started with a flow rate of 0.2 mL.min<sup>-1</sup> and begins with 50% B gradient from 0 to 10 min 99% gradually increased B, 10–30 min increased 100% B, 30–32 min remains at 100% B, 32–35 min gradually decreased 50% B, and 35–45 min remains at 50%. Mass spectrometer parameters: 200 °C source temperature, 8.0 L.min<sup>-1</sup> dry gas flow rate (nitrogen), 4.0 bar nebulizer gas pressure (nitrogen), full scan data acquisition in mass range  $m/z$  50–1200 and collision-induced dissociation (CID) cell was 20 eV. The spectra and chromatograms were processed using Bruker Daltonics ESI Compass Data Analysis software version 5.0 SR1 (Bruker Daltonics, Inc., MA, USA).

## 2.6. Cells

Madin-Darby canine kidney (MDCK) cells (London line), kindly donated by the Centers for Disease Control and Prevention (CDC), were cultured in Dulbecco's modified Eagle's medium (DMEM; Gibco, Waltham, MA, USA), followed by supplemented with 10% of fetal bovine serum (FBS; Gibco), 100 U/mL penicillin and 100 mg/mL streptomycin (Sigma-Aldrich St. Louis, MO, USA) at 37 °C in 5% CO<sub>2</sub> atmosphere.

## 2.7. Influenza virus

Influenza virus A/Michigan/45/2015, an A(H1N1)pdm09 virus, kindly donated by the Influenza Reagent Resources (IRR), was used in antiviral assays. The virus was grown and titrated according to WHO manual for the laboratory diagnosis and virological surveillance of influenza (WHO, 2011) and, the 50% Tissue Culture Infectious Dose (TCID<sub>50</sub>) assay was applied for virus titration.

## 2.8. Cytotoxicity assay

$2.0 \times 10^4$  MDCK cells were seeded in 96-well culture plates. After 24 h, the extracts were diluted in DMEM with a final concentration of 1000, 750 or 500  $\mu$ g.mL<sup>-1</sup>. The DMSO final concentration in extracts treated and control cells was not more than 1.0% (v/v), not affecting the growth of the cells. After 72 h of cells incubation with extracts or vehicle (DMSO), a freshly prepared 3-(4,5-dimethylthiazol-2-yl)-2,5-diphenyltetrazolium bromide - MTT (Sigma) solution was added, according to manufacturer's instructions. Actively respiring cells convert the water-soluble MTT to an insoluble purple formazan by the action of mitochondrial reductase, and its concentration determined by optical density. The calculation for verifying cell viability was made by the comparison between absorbance (A570 nm) from treated (A) and untreated (B) cells using A/B  $\times$  100 formula.

## 2.9. Anti-influenza screening

The inhibitory effect of the 25 *Siparuna* extracts was screened in 24-well tissue culture plates. Monolayers of MDCK cells ( $2.0 \times 10^5$  cells/well) were infected with 400 TCID per well of A(H1N1)pdm09 during 1 h at 37 °C and 5% CO<sub>2</sub>. After that, the viral suspension was removed and the monolayers were treated with 100  $\mu$ g.mL<sup>-1</sup> of each extract. Oseltamivir carboxylate (OST-car; donated by Hoffman-La Roche Inc., Basel, Switzerland) at 1.0  $\mu$ M was used as a positive control for influenza inhibition. At 24 and 72 h post-infection (hpi), the supernatant was harvested to quantify the influenza growth in the presence of extracts through neuraminidase activity by NA-Star<sup>™</sup> assay kit (Life

Technologies, Carlsbad, CA, USA), according to the manufacturer's instructions. The extracts antiviral activity was analyzed in triplicate and calculated related to the untreated virus control.

## 2.10. Infectivity assay

According to screening results, the extracts that inhibited influenza growth more than 85% up to 72 hpi were selected and virus infectivity in supernatant harvested from treated and non treated cells measured by 50% tissue culture infectious dose (TCID<sub>50</sub>) (Reed, J. & Mouch, 1938).

## 2.11. EC<sub>50</sub> determination

For the BuOH extracts from *S. glycyarpa* (SG) and *S. sarmentosa* (SS) that inhibited influenza replication in more than 85% up to 72 hpi, the 50% inhibitory effect on viral replication (EC<sub>50</sub>) was determined. MDCK cells seeded in 24-well plates were infected with 400 TCID. After 1 hpi, the viral suspension was removed and the monolayers were treated with different extracts concentrations (12.5–400  $\mu$ g.mL<sup>-1</sup>). OST-car was used as a positive control for influenza inhibition (0.001–1.0  $\mu$ M). After 24 hpi, the supernatants were harvested and the influenza titer determined by Reed and Muench method (Reed, J. & Mouch, 1938). For determining the EC<sub>50</sub> for the extracts and OST-car, the non-linear regression of the dose response curves was performed.

## 2.12. Statistical analysis

Excel 2010 for Windows software (Microsoft) was used to generate the dose-response curves to calculate the pharmacological parameter values. All the experiments were performed at least three times and, the results are displayed as the mean or the mean  $\pm$  standard error.

## 2.13. MZmine parameters

The ESI ( $\pm$ ) LC-QTOF-MS<sup>2</sup> files were converted to mzXML in the MSConvert software (ProteoWizard; proteowizard.sourceforge.net/tools.shtml) after which, the MZmine software version 2.10 was used for processing, visualizing, and analyzing mass spectrometry profile data. Kyoto Encyclopedia Genes and Genomes (KEGG Compound Database) online database and custom database search (chemical compounds review of *Siparuna* species) were used in this software for compound annotation (Table S1).

## 3. Results and discussion

Five *Siparuna* species, *S. cristata* (SC), *S. decipiens* (SD), *S. glycyarpa* (SG), *S. reginae* (SR) and *S. sarmentosa* (SS) were collected based on the popular use of plants of this genus in the treatment and prophylaxis of colds as well as the commercialization (in Brazil), in the 1990's, of a syrup and caught drops constituted by extracts of *S. apyosice*. The ethanol extracts of these five species were prepared and initially screened by ESI ( $\pm$ ) LC-QTOF-MS<sup>2</sup> to investigate their chemical composition, which has not yet been described in the literature, with the exception of SG ethyl acetate extract (Costa et al., 2013).

### 3.1. ESI ( $\pm$ ) LC-QTOF-MS<sup>2</sup> fingerprints of the crude EtOH extracts from *Siparuna* species

Some of the compounds in the crude EtOH extracts of the five *Siparuna* species were annotated from the fragments in their MS<sup>2</sup> spectra obtained by ESI ( $\pm$ ) LC-QTOF-MS<sup>2</sup> and based in previous literature data for the occurrence of secondary metabolites in this genus. Data obtained in the positive ionization mode were effective in pointing out alkaloids in the samples, whereas at the negative ionization mode, flavonoids were better observed. In the positive mode analysis (Fig. S1; Table S2),



the peaks in the time range 10.1–13.6 min showed characteristic fragments suggestive of the alkaloids reticuline, boldine, coclaurine, actinodaphnine, lauroilsine, norneolitsine, N-methyl-laurotetanine, nantenine or dicentrine and xylopine, according to the literature data (Stévigny et al., 2004; Wang et al., 2017; Neto et al., 2019; Torres-Vega et al., 2020). In the negative mode, the ion fragments for compounds at 17.0 min (SC), 14.3 min (SS), 17.0 min (SG) and 17.3 min (SG) (Fig. S2; Table S2) are characteristic of kaempferol 3,7 dimethyl ether, quercetin 3-O-rutinoside (rutin), 2',6'-dihydroxy-4'-methoxydihydrochalcone and 2',6'-dihydroxy-4,4'-dimethoxydihydrochalcone respectively (Table S3) (Portet et al., 2008; Facundo et al., 2012; Costa et al., 2013).

These results showed the complex chemical profiles of the *Siparuna* crude EtOH extracts. Therefore, they were submitted to liquid-liquid extraction between water-methanol and organic solvents of increasing polarity, to obtain 25 extracts (crude EtOH extracts included), which were assayed towards cell viability and anti-influenza activity (Table 1) and quickly analyzed by DI-ESI(±) IT-MS (Figs. S26–S35).

### 3.2. In vitro anti-influenza effects of the *Siparuna* extracts and DI-ESI (±) IT-MS fingerprint analysis

The anti-influenza activity screening and cellular toxicity of the 25 extracts produced are shown in Table 1. Except for SC and SD, all EtOH extracts showed good cell viability (above 50%). Nevertheless, the BuOH extracts of these two species showed no cytotoxicity at all. In fact, all BuOH extracts showed high cell viability, whereas for DCM extracts, SG was the only one showing good cell viability. As for the EtOAc extracts, three out of the five showed cell viability over 50% (SG, SR, SS).

The anti-viral screening showed that at 24 hpi nineteen extracts inhibited influenza replication above 50%. When evaluating the inhibitory effect of these extracts, cell viability results must be considered. In this sense, EtOH (SD), Hex (SD, SG), DCM (SC, SD) and EtOAc (SC, SD) extracts showed high virus replication inhibition, above 50%, but low cell viability. On the other hand, EtOH (SG, SR, SS), DCM (SG), EtOAc (SG, SR, SS) and BuOH (SC, SD, SG, SR, SS) extracts showed high cell viability and virus replication inhibition at 24 hpi. Among those, the BuOH extracts from SG and SS were able to keep the inhibition above 85% at 72 hpi. In screening assay, OST-car was used as a control for influenza inhibition about 95% at 24 hpi, however this effect was not maintained until 72 hpi.

DI-ESI (±) IT-MS analyses showed the influence of the polarity of the extracting solvents on the nature of the possible compounds. Based on previous studies with *Siparuna* species, the ions at  $m/z$  203 [M+H]<sup>+</sup>,  $m/z$  326 [M+H]<sup>+</sup>,  $m/z$  313 [M-H]<sup>-</sup> in the Hex and DCM extracts (Figs. S27, S28, S32, S33) can be assigned to calamenene terpenoid, nornantenine and kaempferol 3,7-dimethyl ether respectively, whereas in the EtOAc and BuOH extracts (Figs. S29, S30, S34, S35) the ions at  $m/z$  577 [M-H]<sup>-</sup>,  $m/z$  593 [M-H]<sup>-</sup> and  $m/z$  609 [M-H]<sup>-</sup> may be ascribed to kaempferol 3,7-di-O-rhamnoside or procyanidin dimmer; quercetin 3,7-di-O-rhamnoside, tiliroside or vicenin-2; rutin, lucenin-2 or quercetin 7-O-rutinoside, respectively (Leitão et al., 1999; Facundo et al., 2012; Negri et al., 2013; Costa et al., 2013).

### 3.3. Infectivity assay, EC<sub>50</sub> values for influenza inhibition and chemical profiling of *Siparuna glycyarpa* and *Siparuna sarmentosa* BuOH extracts

Since SG and SS BuOH extracts maintained their high antiviral inhibition at 72 hpi, the infectivity assay and chemical profiling analysis were developed for these extracts. In the infectivity assay, the infected MDCK cells, treated with the SG and SS BuOH extracts were compared to non-treated control ( $7.6 \times 10^6$  TCID<sub>50</sub>.mL<sup>-1</sup>). In the treated ones, virus titres decreased to  $1.0 \times 10^6$  TCID<sub>50</sub>.mL<sup>-1</sup> (SG) and  $2.0 \times 10^6$  TCID<sub>50</sub>.mL<sup>-1</sup> (SS), showing 87% and 72.6% of virus inhibition for SG and SS, respectively (Table S4). The SG and SS extracts inhibited influenza replication in a dose-dependent manner (Fig. 1).

The EC<sub>50</sub> values calculated from the dose-response curves were  $25 \pm$

**Table 1**

Cell viability and anti-influenza activity of *Siparuna* species extracts.

<i>Siparuna</i> species	Extract Solvent	Cell viability (%)			Anti-influenza Screening (%)		
		1000 µg. mL <sup>-1</sup>	750 µg. mL <sup>-1</sup>	500 µg. mL <sup>-1</sup>	24 hpi	72 hpi	
<i>S. cristata</i>	EtOH	27.5 ± 3.5	26.7 ± 4.9	24.5 ± 3.2	36.0 ± 3.0	6.3 ± 1.3	
		25.1 ± 4.2	25.9 ± 4.8	25.4 ± 3.5	41.0 ± 2.0	20.2 ± 1.5	
	Hex	25.9 ± 3.3	25.2 ± 2.4	27.8 ± 2.0	75.4 ± 1.3	63.9 ± 1.5	
		40.3 ± 2.3	49.3 ± 1.5	50.4 ± 9.8	51.5 ± 2.7	36.9 ± 0.5	
	DCM	100.0	100.0	100.0	53.0 ± 2.2	17.5 ± 2.6	
		EtOAc	40.3 ± 2.3	49.3 ± 1.5	50.4 ± 9.8	51.5 ± 2.7	36.9 ± 0.5
	BuOH	100.0	100.0	100.0	53.0 ± 2.2	17.5 ± 2.6	
		EtOH	52.8 ± 3.3	69.1 ± 6.3	100.0	94.4 ± 3.5	74.8 ± 3.4
	<i>S. glycyarpa</i>	EtOH	30.9 ± 2.1	43.3 ± 1.1	41.5 ± 6.1	66.2 ± 2.4	63.9 ± 4.5
			94.8 ± 0.2	100.0	100.0	93.5 ± 1.3	54.1 ± 1.5
Hex		59.9 ± 3.6	62.4 ± 4.6	84.7 ± 2.6	91.1 ± 2.0	17.5 ± 2.8	
		50.7 ± 1.3	71.3 ± 3.1	94.3 ± 7.1	96.0 ± 1.3	94.8 ± 1.1	
DCM		80.4 ± 3.4	93.8 ± 9.6	100.0	84.6 ± 2.3	77.2 ± 3.4	
		32.9 ± 3.4	36.6 ± 5.2	43.7 ± 5.9	7.4 ± 5.3	42.6 ± 2.2	
EtOAc		45.0 ± 5.3	49.3 ± 1.9	44.9 ± 6.4	33.6 ± 2.5	24.6 ± 1.8	
		61.6 ± 6.4	61.2 ± 1.3	88.3 ± 2.4	85.7 ± 1.8	79.2 ± 5.6	
BuOH		77.3 ± 1.2	100.0	100.0	89.5 ± 0.8	86.1 ± 1.3	
		EtOH	88.6 ± 9.0	93.5 ± 1.1	100.0	79.1 ± 4.5	69.9 ± 2.6
<i>S. reginae</i>	EtOH	37.1 ± 1.1	44.2 ± 8.9	41.8 ± 6.3	7.6 ± 2.1	4.4 ± 4.2	
		37.7 ± 4.1	42.0 ± 1.2	48.5 ± 6.8	27.6 ± 4.8	26.2 ± 3.1	
	Hex	61.1 ± 9.2	68.3 ± 3.5	82.5 ± 7.5	54.8 ± 3.2	33.6 ± 2.6	
		69.0 ± 5.8	71.4 ± 1.4	77.7 ± 8.9	83.9 ± 2.3	59.8 ± 3.7	
	DCM	28.9 ± 6.4	40.9 ± 2.2	41.4 ± 1.1	55.3 ± 6.2	40.6 ± 2.6	
		26.3 ± 5.5	29.2 ± 3.4	30.3 ± 4.3	54.5 ± 2.7	16.7 ± 5.4	
	EtOAc	28.8 ± 2.6	30.0 ± 0.1	28.0 ± 1.4	89.5 ± 4.2	42.5 ± 2.7	
		25.7 ± 4.1	28.1 ± 0.7	29.6 ± 0.7	57.7 ± 2.7	26.0 ± 2.4	
	BuOH	100.0	100.0	100.0	66.9 ± 1.9	25.4 ± 1.9	
		OST-car (1.0 µM)	–	–	–	95 ± 5.0	32 ± 3.0

OST-car, OSTcarboxylate.

In cell viability assay, DMSO was used as a control at 1.0; 0.75 or 0.5% v/v to normalized extracts results.

In anti-influenza screening, DMSO was used as a control at 0.1% v/v, and the cell viability remained at 100%.

$3 \mu\text{g. mL}^{-1}$  for SG and  $37 \pm 5 \mu\text{g. mL}^{-1}$  for SS (Table 2). From cell viability assays, it was possible to calculate the CC<sub>50</sub> value. The cell viability for SG and SS BuOH extracts at  $1000 \mu\text{g. mL}^{-1}$  was  $50.7 \pm 1.3\%$  and  $77.3 \pm 1.2\%$ , respectively. Therefore the CC<sub>50</sub> values were  $1000 \mu\text{g. mL}^{-1}$  for SG and  $>1000 \mu\text{g. mL}^{-1}$  for SS. The selective index (SI), a relative effectiveness of the investigational product in inhibiting viral replication compared to inducing cell death, calculated for SG and SS was 40 and  $>27$ , respectively (Table 2). These SI values are higher than others published in the literature for butanol, methanol, ethanol, acetone and ethyl



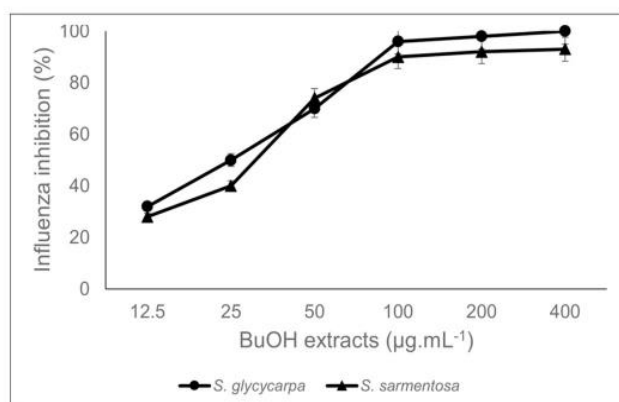


Fig. 1. Influenza inhibition curves of the butanol extracts from *S. glycyrcarpa* and *S. sarmentosa* against influenza A(H1N1)pdm09 virus replication. The curves were established starting from the MDCK cells infected with A(H1N1)pdm09 virus at 400 TCID<sub>50</sub>/well and after 1 hpi, the viral suspension was removed and the monolayers were treated with different extracts concentrations (12.5–400 µg.mL<sup>-1</sup>). These experiments were performed three times and the means were expressed in the graph.

Table 2

The CC<sub>50</sub>, EC<sub>50</sub> and SI values from *S. glycyrcarpa* and *S. sarmentosa* BuOH extracts.

	CC <sub>50</sub>	EC <sub>50</sub>	Selective Index
	µg.mL <sup>-1</sup>		CC <sub>50</sub> /EC <sub>50</sub>
<i>S. glycyrcarpa</i>	1000	25 ± 3	40
<i>S. sarmentosa</i>	1000	37 ± 5	27
OST-car (µM)	2132 µM	0.012 µM	178

CC<sub>50</sub>, the concentration required to reduce normal, non-infected cell viability by 50%. Values represent the mean of duplicate samples from three independent experiments.

EC<sub>50</sub>, the concentration required to reduce inhibition of viral infection-induced cytopathogenicity by 50%. Values represent the mean of duplicate samples from three independent experiments.

SI, selective index is determined by the ratio between CC<sub>50</sub> and EC<sub>50</sub>.

OST-car, OST carboxylate.

acetate extracts from South African, Middle East and Chinese medicinal plants (Mehrbod et al., 2018; Moradi et al., 2019). In these assays, OST-car was used as a positive control for influenza inhibition. The EC<sub>50</sub> value for this compound is not being compared to that observed for the crude extracts, because the crude extracts are formed by a pool of compounds. There is no standard crude extract available for influenza virus inhibition to compare with SG and SS extracts, for this reason the main molecule clinically administered for flu treatment was used as a positive control. Furthermore, the OST-car EC<sub>50</sub> value indicated that the assays were performed with seasonal pandemic influenza strain (sensitive to neuraminidase inhibitor).

According to literature, SI values over 3 and EC<sub>50</sub> values less than 100 µg.mL<sup>-1</sup>, indicate the efficacy of natural products antiviral activity (Mehrbod et al., 2018). These results make SG and SS BuOH extracts a promising starting material for bioguided fractionation and therefore they were chosen for further dereplication by ESI (±) LC-QTOF-MS<sup>2</sup> to obtain more detailed chemical profile (Fig. S36; Table S3).

Compounds n° 1, 2, 4, 5, 1' and 4' (Table 3) showed, in their MS<sup>2</sup> spectra, losses of NH<sub>3</sub> or CH<sub>3</sub>NH<sub>2</sub>, H<sub>2</sub>O, CO, CH<sub>3</sub>OH, and fragment ions at *m/z* 107 and *m/z* 192, characteristics for benzylisoquinoline alkaloids (Fig. S37) (Lima et al., 2020). According to the literature data and characteristic fragments in the MS<sup>2</sup> spectra, the compounds 1 and 1' with *m/z* 272.1288 [M+H]<sup>+</sup> and *m/z* 272.1296 [M+H]<sup>+</sup> (Figs. S38–S39), 2 at *m/z* 300.1627 [M+H]<sup>+</sup> (Fig. S40), 4 at *m/z* 330.1742 [M+H]<sup>+</sup> (Fig. S41), 5 at *m/z* 286.1470 [M+H]<sup>+</sup> and 4' at *m/z* 286.1474 [M+H]<sup>+</sup> (Figs. S42–43) were annotated as norcoclaurine,

*N*-methylcoclaurine, reticuline and coclaurine respectively.

The losses of NH<sub>3</sub> or CH<sub>3</sub>NH<sub>2</sub>, CH<sub>3</sub>OH followed by CO when an OH and an OCH<sub>3</sub> group are vicinal in the aromatic ring, radical losses (CH<sub>3</sub><sup>•</sup> or CH<sub>3</sub>O<sup>•</sup>) and CH<sub>2</sub>O followed by CO in the presence of methylenedioxy group are characteristics in fragmentation of aporphine alkaloids (Stévigny et al., 2004). Therefore, the MS<sup>2</sup> spectra of compounds 3' *m/z* 328.1583 [M+H]<sup>+</sup> (Fig. S44), 3 *m/z* 298.1445 [M+H]<sup>+</sup> (Fig. S45), 9 *m/z* 266.1190 [M+H]<sup>+</sup> (Fig. S46), 2' *m/z* 314.1418 [M+H]<sup>+</sup> (Fig. S47), 5' *m/z* 326.1424 [M+H]<sup>+</sup> (Fig. S48), 6' *m/z* 268.1332 [M+H]<sup>+</sup> (Fig. S49) and 8' *m/z* 342.1360 [M+H]<sup>+</sup> (Fig. S50), displayed characteristic fragment ions for boldine, apoglaziovine, annonaine, lauroitsine, bulbocapnine, caaverine and cassythine (Table 3).

The neutral sugar loss 132 Da (pentosides-C<sub>5</sub>H<sub>6</sub>O<sub>4</sub>), 146 Da (deoxyhexosides-C<sub>6</sub>H<sub>10</sub>O<sub>4</sub>), 162 Da (hexosides-C<sub>6</sub>H<sub>10</sub>O<sub>5</sub>) and *m/z* of quercetin and kaempferol aglycones in MS<sup>2</sup> spectra of compounds 6, 7, 8, 10, 7' and 9' (Table 3) indicated the *O*-glycoside flavonoids. The fragment ions in MS<sup>2</sup> spectra of compounds 6 *m/z* 597.1528 [M+H]<sup>+</sup> (Fig. S51), 7 *m/z* 611.1661 [M+H]<sup>+</sup> and 7' *m/z* 611.1629 [M+H]<sup>+</sup> (Figs. S52–S53), 8 *m/z* 595.1709 [M+H]<sup>+</sup> (Fig. S54), 10 *m/z* 609.1490 [M+H]<sup>+</sup> and 9' *m/z* 609.1522 [M+H]<sup>+</sup> (Fig. S55), were attributed to quercetin 3-*O*-[β-D-xylosyl-(1 → 2)-β-D-glucoside], quercetin 3-*O*-rhamnoside-7-*O*-glucoside or quercetin 3-*O*-glucoside-7-*O*-rhamnoside, kaempferol 3-*O*-glucoside-7-*O*-rhamnoside and quercetin-3-*O*-rutinoside (rutin). Compound 11' *m/z* 593.1525 [M+H]<sup>+</sup> (Fig. S56) showed, in MS<sup>2</sup> spectra, fragments characteristic of *C*-glycosid flavonoids and can correspond to vicenin-2 (Table 3). Compound 10' *m/z* 577.1355 [M+H]<sup>+</sup> (Fig. S57) presented similar fragments to a procyanidin dimer type B (Table 3).

Characteristics losses and A-type fragments ([<sup>1</sup>A-CH<sub>3</sub>]<sup>-</sup>) for dihydrochalcones were observed in the MS<sup>2</sup> spectra of compounds 12 *m/z* 271.1002 [M+H]<sup>+</sup> (Fig. S58) and 11 *m/z* 301.1062 [M+H]<sup>+</sup> (Fig. S59) in *S. glycyrcarpa*, suggesting the presence of 2',6'-dihydroxy-4'-methoxydihydrochalcone and 2',6'-dihydroxy-4,4'-dimethoxydihydrochalcone (Table 3).

Coclaurine, *N*-methylcoclaurine, norcoclaurine, norneolitsine, xylopine, cassythine, caaverine, apoglaziovine, 2',6'-dihydroxy-4'-methoxydihydrochalcone, quercetin 3-*O*-[β-D-xylosyl-(1 → 2)-β-D-glucoside], quercetin 3-*O*-rhamnoside-7-*O*-glucoside or quercetin 3-*O*-glucoside-7-*O*-rhamnoside and kaempferol 3-*O*-glucoside-7-*O*-rhamnoside are being described for the first time in *Siparuna* species.

According to literature, procyanidin B2 (Yang et al., 2014), flavonoids (Grienke et al., 2012), alkaloids with the indole, isoquinoline and quinolizidine skeleton (Moradi et al., 2017) were able to inhibit influenza virus. Therefore, these compounds may be targets in bioguided studies in search of new drugs against influenza virus.

#### 4. Conclusions

The inhibitory effects of Amazonian *Siparuna* species against influenza A(H1N1)pdm09 virus replication is being reported here for the first time, corroborating their folk medicinal use and showing their potential as anti-influenza agents. The metabolic fingerprinting analysis was useful for a quick chemical composition investigation of the 25 *Siparuna* extracts. Fragmentation studies made possible the identification of different metabolites showing the wide variety of chemical compounds in these extracts. These promising results stimulate the continuation of this study with the aim of isolation the compound(s) responsible for this bioactivity, thus contributing to a better knowledge of those species and to the research of natural products with potential anti-influenza activity.

#### Author contributions

Gilda G. Leitão and Suzana G. Leitão conceived the study. Carla M. Leal performed the laboratory work, analyzed the data and wrote the article draft. Rosineide C. Simas developed the ESI (±) LC-QTOF-MS<sup>2</sup> methods. Milene Miranda, Marilda M. Siqueira, Gabrielle do Vale and

**Table 3**ESI ( $\pm$ ) LC-QTOF-MS<sup>2</sup> data of proposed compounds in BuOH extracts from *S. glycyarpa* and *S. sarmentosa* (MS/MS spectra in Figs. S38–S59).

<i>Siparuna</i> Specie	Compound N°	R <sub>f</sub> (min)	[M+H] <sup>+</sup> (m/z)	[M-H] <sup>-</sup> (m/z)	Calculated Mass	Molecular formula	Error (ppm)	RDB	MS/MS (MS <sup>2</sup> )	Proposed compound ( Table S3)
<i>S. glycyarpa</i>	1	7.4	272.1288	–	272.1281	C <sub>16</sub> H <sub>17</sub> NO <sub>3</sub>	2.49	8.5	255.1020, 237.0923, 209.0990, 161.0632, 107.0509	Norcochlorine
<i>S. glycyarpa</i>	2	8.1	300.1627	–	300.1594	C <sub>16</sub> H <sub>21</sub> NO <sub>3</sub>	10.92	8.5	269.1190, 237.0914, 209.0969, 107.0505	N-methylcochlorine
<i>S. glycyarpa</i>	3	8.4	298.1445	–	298.1438	C <sub>16</sub> H <sub>19</sub> NO <sub>3</sub>	2.44	9.5	269.1198, 255.0932, 237.0966, 223.0820, 211.0805	Apoglaziovine
	4		330.1742	–	330.1699	C <sub>19</sub> H <sub>23</sub> NO <sub>4</sub>	12.76	8.5	299.1313, 267.1023, 192.1042, 177.0791, 137.0624, 115.0567	Reticuline
<i>S. glycyarpa</i>	5	9.3	286.1470	–	286.1438	C <sub>17</sub> H <sub>19</sub> NO <sub>3</sub>	11.28	8.5	269.1203, 237.0923, 209.0950, 194.0729, 115.0564, 107.0517	Cochlorine
<i>S. glycyarpa</i>	6	9.5	597.1528	–	597.1450	C <sub>26</sub> H <sub>28</sub> O <sub>16</sub>	13.06	12.5	303.0529	Quercetin 3-O-[[ $\beta$ -D-xylopyranosyl-(1 → 2)- $\beta$ -D-glucoside]
<i>S. glycyarpa</i>	7	9.7	611.1661	–	611.1607	C <sub>27</sub> H <sub>30</sub> O <sub>16</sub>	8.83	12.5	465.1088, 303.0520	Quercetin 3-O-rhamnoside-7- O-glucoside Quercetin 3-O-glucoside-7-O- rhamnoside
<i>S. glycyarpa</i>	8	10.3	595.1709	–	595.1657	C <sub>27</sub> H <sub>30</sub> O <sub>15</sub>	8.65	12.5	449.1128, 287.0580	Kaempferol 3-O-glucoside-7- O-rhamnoside
<i>S. glycyarpa</i>	9	11.2	266.1190	–	266.1175	C <sub>17</sub> H <sub>15</sub> NO <sub>2</sub>	5.42	10.5	249.0913, 219.0787, 202.0773, 191.0851, 189.0696	Annonaine
<i>S. glycyarpa</i>	10	9.8	–	609.1490	609.1450	C <sub>27</sub> H <sub>30</sub> O <sub>16</sub>	6.56	13.5	301.0379, 271.0285, 255.0833, 243.0328	Quercetin-3-O-rutinoside (Rutin)
<i>S. glycyarpa</i>	11	15.2	–	301.1062	301.1070	C <sub>17</sub> H <sub>16</sub> O <sub>5</sub>	-2.65	9.5	283.0977, 268.0788, 253.0520, 165.0219, 152.0135, 124.0183	2',6'-dihydroxy-4,4'- dimethoxydihydrochalcone
<i>S. glycyarpa</i>	12	15.4	–	271.1002	271.0964	C <sub>16</sub> H <sub>16</sub> O <sub>4</sub>	14.01	9.5	253.0871, 238.0647, 210.0693, 173.0609, 152.0139, 124.0184	2',6'-dihydroxy-4'-methoxy- dihydrochalcone
<i>S. sarmentosa</i>	1'	8.1	272.1296	–	272.1281	C <sub>16</sub> H <sub>17</sub> NO <sub>3</sub>	5.51	8.5	255.1028, 237.0918, 209.0995, 161.0629, 107.0507	Norcochlorine
<i>S. sarmentosa</i>	2'	8.8	314.1418	–	314.1386	C <sub>16</sub> H <sub>19</sub> NO <sub>4</sub>	9.91	9.5	297.1156, 265.0885, 237.0925, 222.0678, 207.0793, 194.0735	Lauroitsine
<i>S. sarmentosa</i>	3'	9.0	328.1583	–	328.1543	C <sub>19</sub> H <sub>21</sub> NO <sub>4</sub>	12.08	9.5	297.1163, 265.0892, 222.0689, 205.0655	Boldine
<i>S. sarmentosa</i>	4'	9.7	286.1474	–	286.1438	C <sub>17</sub> H <sub>19</sub> NO <sub>3</sub>	12.68	8.5	269.1210, 237.0933, 209.0963, 194.0742, 175.0764, 107.0514	Cochlorine
<i>S. sarmentosa</i>	5'	10.0	326.1424	–	326.1387	C <sub>19</sub> H <sub>19</sub> NO <sub>4</sub>	11.39	10.5	295.1002, 280.0760, 263.0734, 235.0765, 205.0661, 177.0693	Bulbocapnine
<i>S. sarmentosa</i>	6'	10.1	268.1332	–	268.1328	C <sub>17</sub> H <sub>17</sub> NO <sub>2</sub>	1.49	9.5	251.1078, 219.0806, 191.0867	Caaverine
	7'		611.1629	–	611.1607	C <sub>27</sub> H <sub>30</sub> O <sub>16</sub>	3.59	12.5	465.1070, 303.0520	Quercetin 3-O-rhamnoside-7- O-glucoside Quercetin 3-O-glucoside-7-O- rhamnoside
<i>S. sarmentosa</i>	8'	10.3	342.1360	–	342.1336	C <sub>19</sub> H <sub>19</sub> NO <sub>5</sub>	7.01	10.5	295.0974, 263.0711, 235.0761, 205.0646, 177.0693	Cassythine
<i>S. sarmentosa</i>	9'	10.4	–	609.1522	609.1450	C <sub>27</sub> H <sub>30</sub> O <sub>16</sub>	11.81	13.5	301.0389, 271.0295, 255.0833, 243.0336	Quercetin-3-O-rutinoside (Rutin)
<i>S. sarmentosa</i>	10'	11.8	–	577.1355	577.1340	C <sub>30</sub> H <sub>26</sub> O <sub>12</sub>	2.59	18.5	451.1034, 425.0582, 407.0753, 289.0784, 245.0463, 161.0268, 125.0233, 96.9588	Procyanidin dimer (B1, B2, B3, B4, B5, B6, B7 or B8)
<i>S. sarmentosa</i>	11'	18	–	593.1525	593.1500	C <sub>27</sub> H <sub>30</sub> O <sub>15</sub>	4.21	13.5	503.1205, 473.1010, 413.0850, 383.0750, 353.0822, 300.0254, 285.0722, 259.0294, 151.0408, 125.0242, 96.9578	Vicenin-2

*S.glycyarpa*: 1-12.*S.sarmentosa*: 1'-11'.



Carlos V. G. de Almeida performed influenza virus experiments. Brendo A. Gomes and Mariana F. Campos gave support in DI-ESI(±) IT-MS analyses. Gilda G. Leitão, Suzana G. Leitão, Rosineide C. Simas, Marilda M. Siqueira and Milene Miranda reviewed and contributed to the writing of this manuscript.

#### Declaration of competing interest

The authors declare that there are no conflicts of interest.

#### Acknowledgements

We are grateful to FAPERJ, CNPQ and CAPES for financial support. CNPQ for the PhD scholarships. LaCEM (Laboratório de Cromatografia e Espectrometria de Massas – UFG) for lending the UFLC-MicroTOF-Q III-MS apparatus. Simony C. Mendonça for support with MZmine software.

#### Appendix A. Supplementary data

Supplementary data to this article can be found online at <https://doi.org/10.1016/j.jep.2021.113788>.

#### References

- Ben-Shabat, S., Yarmolinsky, L., Porat, D., Dahan, A., 2020. Antiviral effect of phytochemicals from medicinal plants: applications and drug delivery strategies. *Drug Deliv Transl Res* 1–14.
- Cornejo-Báez, A.A., Peña-Rodríguez, L.M., Alvarez-Zapata, R., Vazquez-Hernández, M., Sánchez-Medina, A., 2019. Chemometrics: a complementary tool to guide the isolation of pharmacologically active natural products. *Drug Discov. Today* 1–11.
- Costa, F.N., Garrard, I., Silva, A.J.R., Leitão, G.G., 2013. Changes in the mobile phase composition on a stepwise counter-current chromatography elution for the isolation of flavonoids from *Siparuna glycyarpa*. *J. Separ. Sci.* 36, 2253–2259.
- Demarque, D.P., Crotti, A.E.M., Vessecchi, R., Lopes, J.L.C., Lopes, N.P., 2016. Fragmentation reactions using electrospray ionization mass spectrometry: an important tool for the structural elucidation and characterization of synthetic and natural products. *Nat. Prod. Rep.* 33 (3), 432–455.
- Denaro, M., Smeriglio, A., Barreca, D., De Francesco, C., Occhiuto, C., Milano, G., Trombetta, D., 2019. Antiviral activity of plants and their isolated bioactive compounds: an update. *Phytother. Res.* 1–27.
- Dixit, R., Khandaker, G., Ilgoutz, S., Rashid, H., Booy, R., 2013. Emergence of Oseltamivir resistance: control and management of influenza before, during and after the pandemic. *Infect. Disord. - Drug Targets* 13, 34–45.
- Ernst, M., Silva, D.B., Silva, R.R., Vencio, R.Z.N., Lopes, N.P., 2014. Mass spectrometry in plant metabolomics strategies: from analytical platforms to data acquisition and processing. *Nat. Prod. Rep.* 31, 784–806.
- Facundo, V.A., Azevedo, M.S., Rodrigues, R.V., Nascimento, L.F., Militão, J.S.L.T., Silva, G.V.J., Braz-Filho, R., 2012. Chemical constituents from three medicinal plants: *Piper renitens*, *Siparuna guianensis* and *Alternanthera brasiliana*. *Rev Bras Farmacogn* 22 (5), 1134–1139.
- Grienke, U., Schmidtke, M., Grafenstein, S.V., Kirchmair, J., Liedl, K.R., Rollinger, J.M., 2012. Influenza neuraminidase: a druggable target for natural products. *Nat. Prod. Rep.* 29, 11–36.
- Leitão, G.G., Simas, N.K., Soares, S.S.V., Brito, A.P.P., Claros, B.M.G., Brito, T.B.M., Monache, F.D., 1999. Chemistry and pharmacology of monimiaceae: a special focus on *Siparuna* and *mollinedia*. *J. Ethnopharmacol.* 65, 87–102.
- Leitão, G.G., Soares, S.S.V., Brito, T.B.M., Monache, F.D., 2000. Kaempferol glycosides from *Siparuna apiosyce*. *Phytochemistry* 55, 679–682.
- Lima, B.R., Da Silva, F.M.A., Soares, E.R., Almeida, R.A., Da Silva-Filho, F.A., Barison, A., Costa, E.V., Koolen, H.H.F., Souza, A.D.L., Pinheiro, M.L.B., 2020. Integrative approach based on leaf spray mass spectrometry, HPLC-DAD-MS/MS, and NMR for comprehensive characterization of isoquinoline-derived alkaloids in leaves of *Onychopetalum amazonicum* R. E. Fr. *J. Braz Chem Soc* 31 (1), 79–89.
- Lopes e Souza, T.M., Fintelman-Rodrigues, N., Resende, P.C., Mesquita, M., Gregianini, T.S., Bozza, F.A., Pecego, A.C., Fernandes, S.B., Cury, A.L.F., Riediger, I. N., Siqueira, M.M., 2015. Oseltamivir-resistant influenza A(H1N1)pdm2009 strains found in Brazil are endowed with permissive mutations, which compensate the loss of fitness imposed by antiviral resistance. *Mem I Oswaldo Cruz* 110, 101–105.
- Mehrbod, P., Abdalla, M.A., Njoya, E.M., Ahmed, A.S., Fotouhi, F., Farahmand, B., Gado, D.A., Tabatabaian, M., Fasanmi, O.G., Eloff, J.N., McGaw, L.J., Fasina, F.O., 2018. South African medicinal plant extracts active against influenza A virus. *BMC Compl. Alternative Med.* 18 (112), 1–10.
- Moradi, M.T., Karimi, A., Lorigooini, Z., 2017. Alkaloids as the natural anti-influenza virus agents: a systematic review. *Toxin Rev.* 1–8.
- Moradi, M.T., Karimi, A., Shahrani, M., Hashemi, L., Goosheh, M.S.C., 2019. Anti-influenza virus activity and phenolic content of pomegranate (*Punica granatum* L.) peel extract and fractions. *Avicenna J. Med. Biotechnol. (AJMB)* 11 (4), 285–291.
- Negri, G., Santi, D., Tabach, R., 2013. Flavonol glycosides found in hydroethanolic extracts from *Tilia cordata*, a species utilized as anxiolytics. *Rev. Bras. Plantas Med.* 15 (2), 217–224.
- Neto, F.C., Andréo, M.A., Raftery, D., Lopes, J.L.C., Lopes, N.P., Castro-Gamboa, I., Maia, B.H.L.N.S., Costa, E.V., Vessecchi, R., 2019. Characterization of aporphine alkaloids by electrospray ionization tandem mass spectrometry and density functional theory calculations. *Rapid Commun. Mass Spectrom.* 1, 11.
- Newman, D.J., Cragg, G., 2020. Natural products as sources of new drugs over the nearly four decades from 01/1981 to 09/2019. *J. Nat. Prod.* 1–10.
- Portet, B., Fabre, N., Rozenberg, R., Habib-Jiwan, J.L., Moulis, C., Quetin-Leclercq, J., 2008. Analysis of minor flavonoids in *Piper hostmannianum* var. *berbicense* using liquid chromatography coupled with atmospheric pressure chemical ionization mass spectrometry. *J. Chromatogr. A* 1210, 45–54.
- Reed, J., Mounch, M., 1938. An endpoint assay to evaluate the 50% tissue cytopathic effect. *J. Gen. Virol.* 5, 25–29.
- Renner, S.S., Hausner, G., 2005. *Siparunaceae in: Flora Neotropica. Monograph 95*, The New York Botanical Garden.
- Setzer, W.N., 2016. Essential oils as complementary and alternative medicines for the treatment of influenza. *Am J Essent Oil Nat Prod* 4, 16–22.
- Stévigny, C., Jiwan, J.L.H., Rozenberg, R., Hoffmann, E., Quetin-Leclercq, J., 2004. Key fragmentation patterns of aporphine alkaloids by electrospray ionization with multistage mass spectrometry. *Rapid Commun. Mass Spectrom.* 18, 523–528.
- Theisen, L.L., Erdelmeier, C.A.J., Spoden, G.A., Boukhallouk, F., Sausy, A., Florin, L., Muller, C.P., 2014. Tannins from *Hamamelis virginiana* bark extract: characterization and improvement of the antiviral efficacy against influenza A virus and human papillomavirus. *PLoS One* 9 (1), e88062. <https://doi.org/10.1371/journal.pone.0088062>.
- Torres-Vega, J., Gómez-Alonso, S., Pérez-Navarro, J., Pastene-Navarrete, E., 2020. Green extraction of alkaloids and polyphenols from *Peumus boldus* leaves with natural deep eutectic solvents and profiling by HPLC-PDA-IT-MS/MS and HPLC-QTOF-MS/MS. *Plants* 9, 1–17.
- Wang, M., Liu, Y., Fu, S., Zhang, Q., Wang, Q., Gao, X., 2017. Applying target data screening followed by characteristic fragment filtering for the comprehensive screening and identification of alkaloids in *Corydalis yanhusuo* W.T. Wang by UPLC-Q-TOF/MS. *RSC Adv.* 7, 53545–53551.
- World Health Organization (WHO), 2018. Influenza (seasonal). Available at: <http://www.who.int/mediacentre/factsheets/fs211/en/>.
- World Health Organization (WHO), 2011. Manual for the laboratory diagnosis and virological surveillance of influenza. World Health Organization. Available at: [http://www.who.int/influenza/gisrs\\_laboratory/manual\\_diagnosis\\_surveillance\\_influenza/en/](http://www.who.int/influenza/gisrs_laboratory/manual_diagnosis_surveillance_influenza/en/).
- Yang, Z.F., Bai, L.P., Huang, W.B., Li, X.Z., Zhao, S.S., Zhong, N.S., Jiang, Z.H., 2014. Comparison of in vitro antiviral activity of tea polyphenols against influenza A and B viruses and structure-activity relationship analysis. *Fitoterapia* 93, 47.



## Supplementary material

**Table S1.** Mzmine parameters for ESI ( $\pm$ ) LC-QTOF-MS<sup>2</sup>

Parameters	UFLC-MicroTOF-QIII-MS (ESI ( $\pm$ ) LC-QTOF-MS <sup>2</sup> data)
Mass detector:	
-Noise level	*1.0E2
FTMS shoulder peaks filter:	
-Mass resolution	*30000
Chromatogram builder:	
-Min time span (min)	*0.3 min
-Min height	*5.0E2
- $m/z$ tolerance	*0.01 $m/z$ or 10 ppm
Chromatogram decovolution (Algorithm):	
-Chromatographic threshold	*5%
-RT range (min)	*0.2 min
-Minimum relative height	*15%
-Minimum absolute height	*5.0E2
-Min ratio of peak top/edge	*5
-Peak duration range (min)	*0.3-45 min
Isotopic peaks grouper:	
- $m/z$ tolerance	*0.01 $m/z$ or 10 ppm
-Retention time tolerance	*0.2 min
Join aligner:	
- $m/z$ tolerance	*0.01 $m/z$ or 10 ppm
-Weight for $m/z$	*15
-Retention time tolerance	*0.2 min

-Weight for RT	*10
-Isotope $m/z$ tolerance	*0.01 $m/z$ or 10 ppm
-Minimum absolute intensity	*5.0E2
- Minimum score	*65%
Peak finder:	
-Intensity tolerance	*1.0%
- $m/z$ tolerance	*0.01 $m/z$ or 10 ppm
-Retention time tolerance	*0.2 min
Identification (Adduct search):	
- $m/z$ tolerance	*0.01 $m/z$ or 10 ppm
-Max relative adduct peak height	*50%
Identification (Complex search):	
-Ionization method	*[M+H] <sup>+</sup> and [M-H] <sup>-</sup>
-Retention time tolerance	*0.2 min
- $m/z$ tolerance	*0.01 $m/z$ or 10 ppm
-Max complex peak height	*50%
Identification (Custom database search):	
- $m/z$ tolerance	*0.01 $m/z$ or 10 ppm
-Retention time tolerance	*0.2 min

**Table S2.** ESI ( $\pm$ ) LC-QTOF-MS<sup>2</sup> analysis of the EtOH extracts from *S. cristata*, *S. decipiens*, *S. reginae*, *S. sarmentosa* and *S. glycyarpa* (MS/MS spectra in Figures S3-S25).

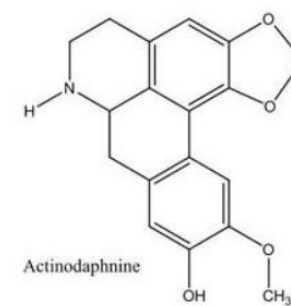
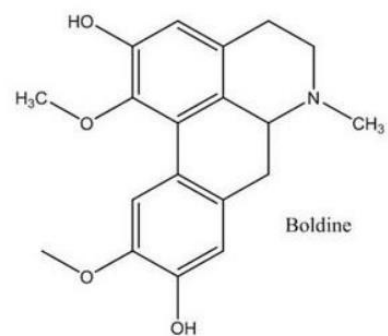
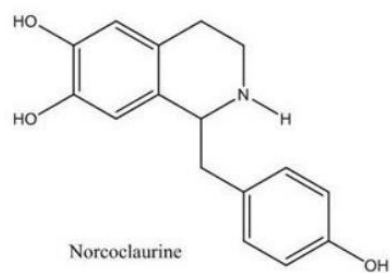
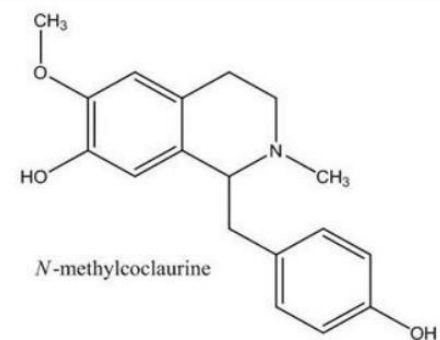
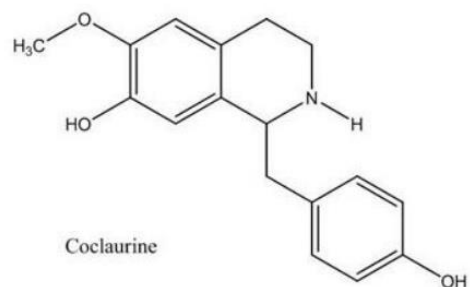
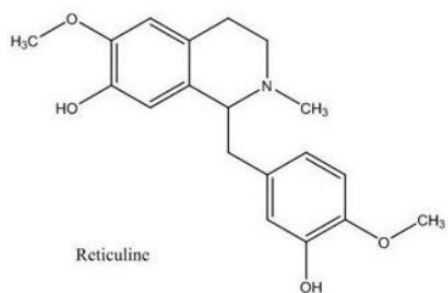
<i>Siparuna</i> Species	$R_t$ (min)	[M+H] <sup>+</sup> ( $m/z$ )	MS/MS (MS <sup>2</sup> )	[M-H] <sup>-</sup> ( $m/z$ )	MS/MS (MS <sup>2</sup> )	Proposed compound (Table S3)
<i>S. cristata</i>	10.5	342.1709	311.1284; 296.1058; 280.1107; 265.0866; 237.0919; 205.0651; 178.0845	-	-	<i>N</i> -methyl-laurotetanine
<i>S. cristata</i>	11.0	330.1773	299.1335; 265.0888; 192.1064; 177.0818; 137.0647; 115.0588	-	-	Reticuline
<i>S. cristata</i>	11.2	328.1617	297.1164; 265.0900; 251.0750; 237.0936; 222.0701; 205.0687	-	-	Boldine
<i>S. cristata</i>	12.8	340.1563	309.1134; 294.0902; 278.0949; 263.0698; 251.0715; 235.0750; 223.0752; 205.0630	-	-	Nantenine or Dicentrine
<i>S. cristata</i>	17.0	-	-	313.0814	283.0330; 255.0371; 117.0385; 93.0366	Kaempferol 3,7-dimethyl ether
<i>S. decipiens</i>	10.1	328.1570	297.1119; 265.0851; 251.0695; 237.0903; 222.0661; 205.0624	-	-	Boldine

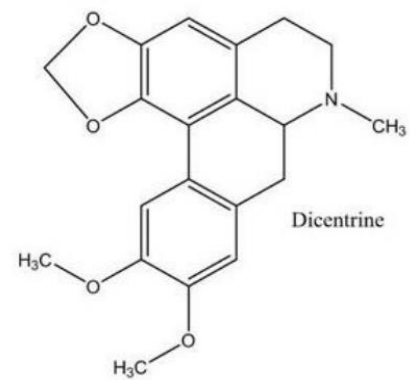
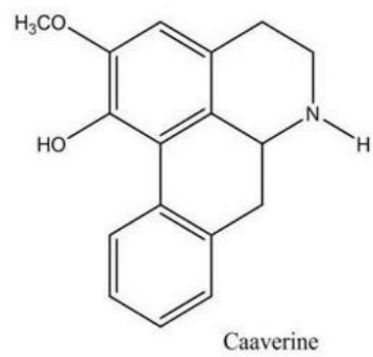
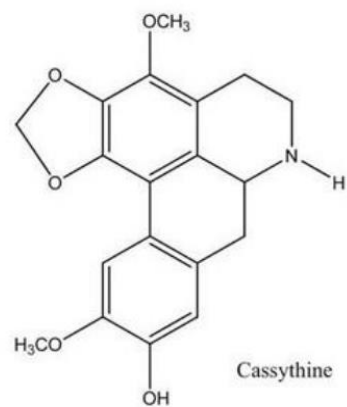
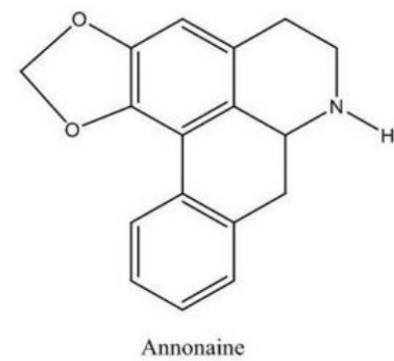
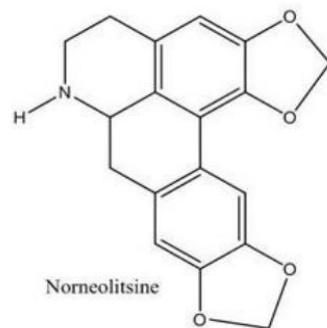
<i>S. decipiens</i>	10.5	286.1459	269.1184; 254.0934; 237.0900; 209.0949; 194.0719	-	-	Coclaurine
<i>S. decipiens</i>	10.8	330.1737	299.1304; 267.1017; 192.1029; 177.0776; 137.0613; 115.0556; 94.0414	-	-	Reticuline
<i>S. decipiens</i>	12.0	312.1255	295.0982; 265.0869; 251.0725; 237.0890; 222.0671; 205.0637; 194.0712; 177.0680	-	-	Actinodaphnine
<i>S. reginae</i>	10.7	286.1493	269.1228; 254.0988; 237.0942; 209.0994; 194.0753; 175.0769; 115.0587; 107.0540	-	-	Coclaurine
<i>S. reginae</i>	10.8	314.1399	297.1173; 282.0929; 265.0910; 237.0951; 222.0704; 205.0676; 194.0755; 177.0726	-	-	Laurokitsine
<i>S. reginae</i>	10.8	330.1768	299.1339; 267.1053; 192.1064; 177.0816; 115.0584	-	-	Reticuline
<i>S. reginae</i>	12.9	310.1140	293.0876; 263.0758; 235.0793; 205.0686; 177.0727	-	-	Norneolitsine

<i>S. sarmentosa</i>	10.2	328.1583	297.1140; 265.0857; 237.0910; 222.0667; 205.0644	-	-	Boldine
<i>S. sarmentosa</i>	10.5	286.1477	269.1204; 254.0971; 237.0925; 209.0964; 194.0730; 175.0762; 115.0558; 107.0513; 91.0555	-	-	Coclaurine
<i>S. sarmentosa</i>	11.6	314.1453	297.1154, 282.0921, 265.0886, 237.0914, 222.0680, 205.0653, 194.0731, 177.0686	-	-	Laurolicsine
<i>S. sarmentosa</i>	13.6	296.1294	279.1032, 264.0759, 249.0887, 233.0600, 221.0909, 205.0644, 178.0763	-	-	Xylopine
<i>S. sarmentosa</i>	14.3	-	-	609.1584	300.0338; 271.0308; 255.0363	Quercetin-3- <i>O</i> -rutinoside (Rutin)
<i>S. sarmentosa</i>	21.4	871.5923	593.2892; 533.2655	-	-	Pheophytin a
<i>S. glycyarpa</i>	10.5	330.1736	299.1302; 267.1028; 192.1030; 177.0778; 137.0610; 115.0550	-	-	Reticuline
<i>S. glycyarpa</i>	11.4	286.1462	269.1183; 254.0955; 237.0906; 209.0959;	-	-	Coclaurine

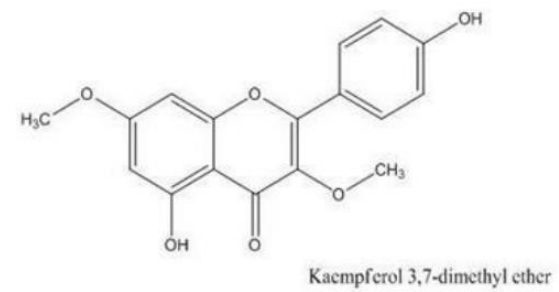
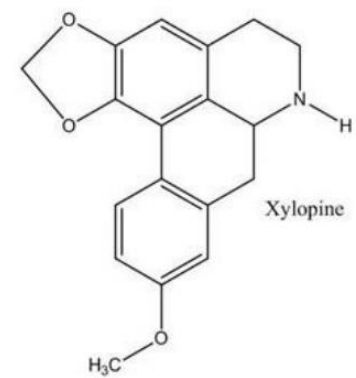
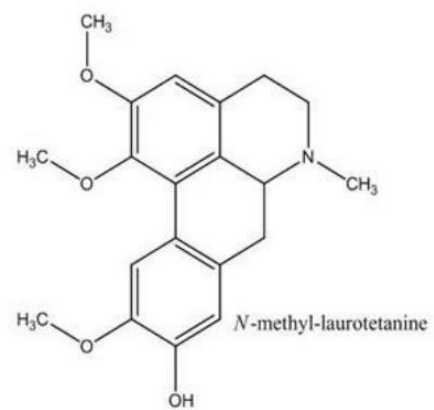
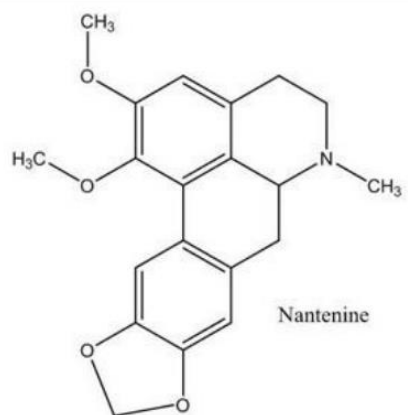
				194.0687; 175.0753; 115.0549; 107.0499		
<i>S. glycyarpa</i>	17	-	-	271.1072	238.0691; 210.0738; 165.0248; 152.0177; 139.0421; 124.0219; 96.0236	2',6'-dihydroxy-4'-methoxy- dihydrochalcone
<i>S. glycyarpa</i>	17.3	-	-	301.1185	268.0797; 253.0580; 225.0608; 188.0533; 165.0249; 152.0178; 139.0429; 124.0220; 95.0162	2',6'-dihydroxy-4,4'- dimethoxydihydrochalcone

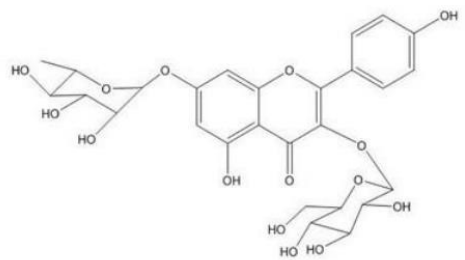
**Table S3.** Proposed compounds in EtOH extracts from *S. cristata*, *S. decipiens*, *S. glycyarpa*, *S. reginae*, *S. sarmentosa* and in BuOH extracts from *S. glycyarpa* and *S. sarmentosa*.



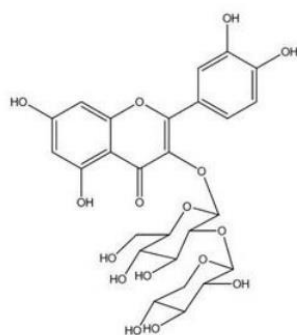




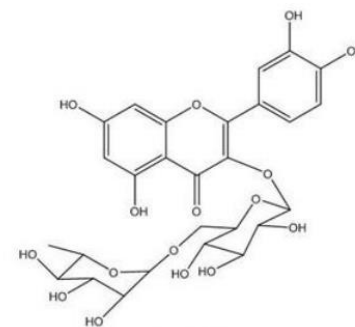
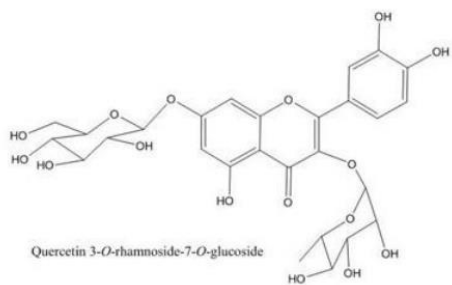




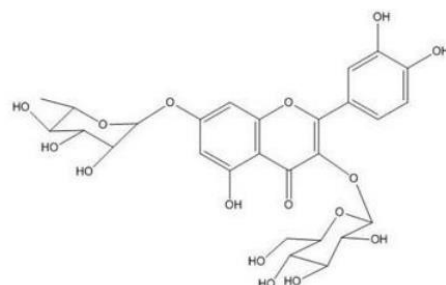
Kaempferol 3-O-glucoside-7-O-rhamnoside



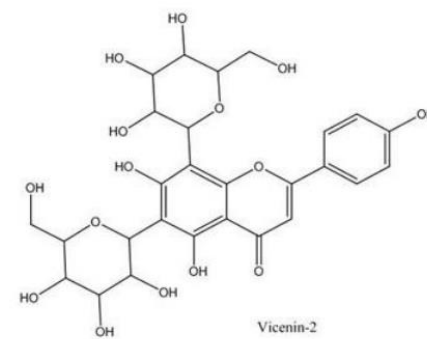
Quercetin 3-O-[β-D-xylosyl-(1→2)-β-D-glucoside]

Quercetin-3-O-rutinoside  
(Rutin)

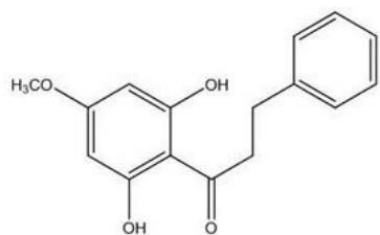
Quercetin 3-O-rhamnoside-7-O-glucoside



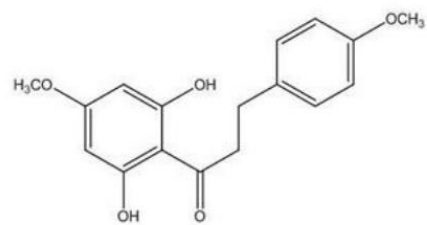
Quercetin 3-O-glucoside-7-O-rhamnoside



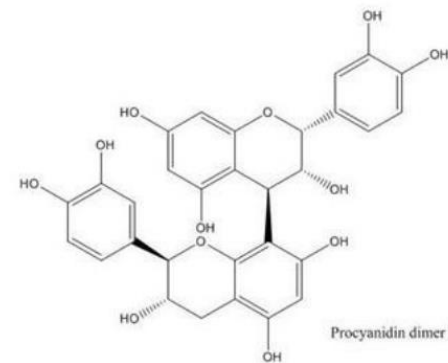
Vicenin-2



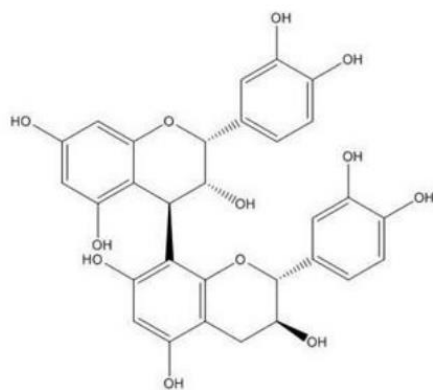
2',6'-dihydroxy-4'-methoxy-dihydrochalcone



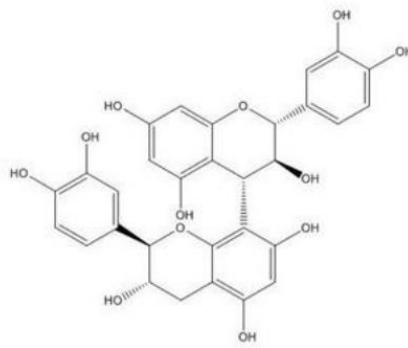
2',6'-dihydroxy-4,4'-dimethoxydihydrochalcone



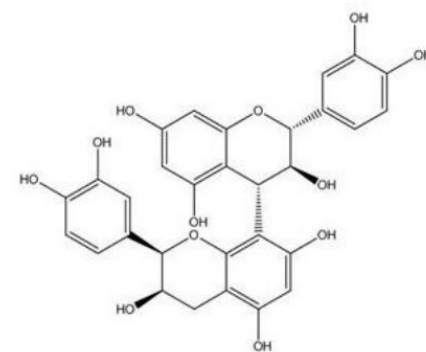
Procyanidin dimer B1



Procyanidin dimer (B2)



Procyanidin dimer (B3)



Procyanidin dimer (B4)



**Table S4.** Infectivity assay of the BuOH extracts from *S. glycyarpa* and *S. sarmentosa* by Reed and Muench method (TCID<sub>50</sub>.mL<sup>-1</sup>).

	TCID <sub>50</sub> .mL <sup>-1</sup>	Inhibition of control (%)
<i>S. glycyarpa</i>	1.0x10 <sup>6</sup>	87.0
<i>S. sarmentosa</i>	2.0x10 <sup>6</sup>	72.6
Non-treated control	7.6x10 <sup>6</sup>	NA

NA not applicable

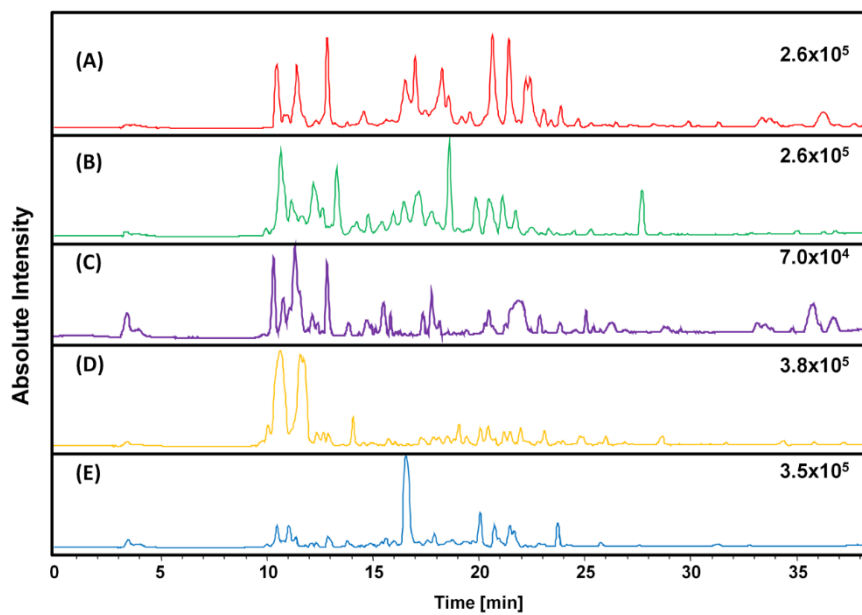


**Figure S1.** Base Peak Chromatograms by ESI (+) LC-QTOF-MS<sup>2</sup> of EtOH extracts. (A) *S. cristata*, (B) *S. decipiens*, (C) *S. reginae*, (D) *S. sarmentosa*, (E) *S. glycyarpa*.

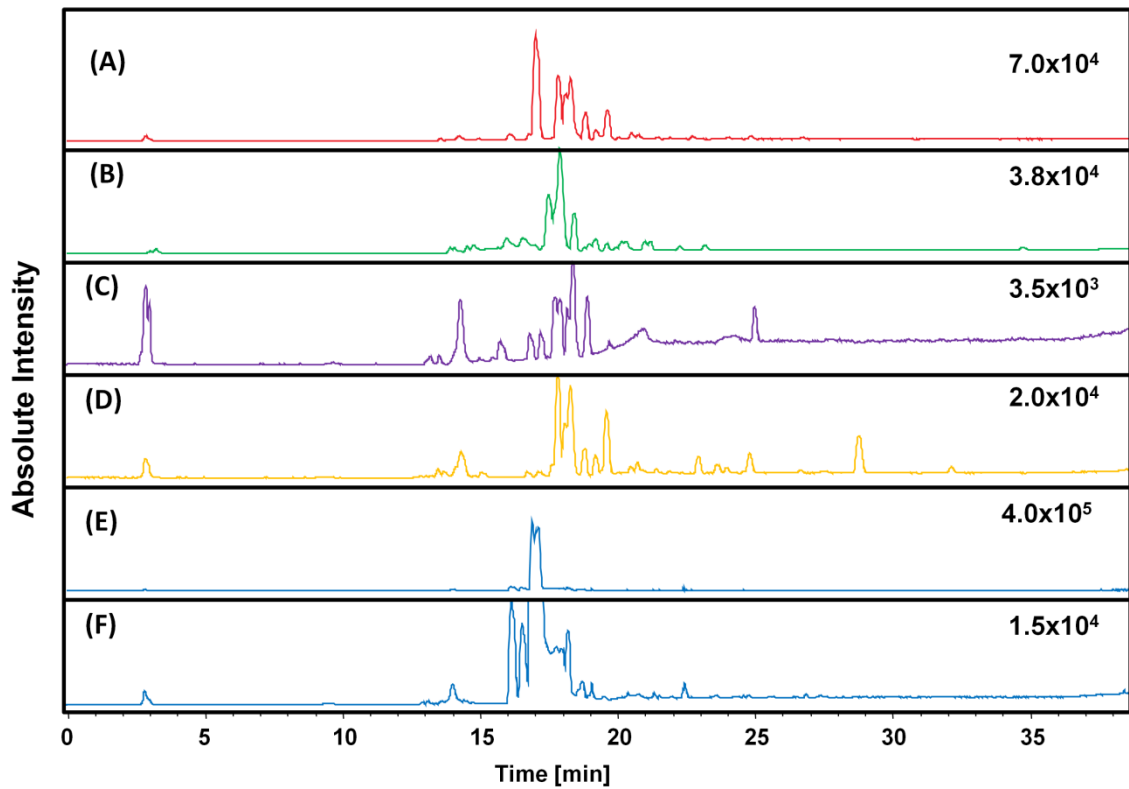


**Figure S2.** Base Peak Chromatograms by ESI (-) LC-QTOF-MS<sup>2</sup> of EtOH extracts. **(A)** *S. cristata*, **(B)** *S. decipiens*, **(C)** *S. reginae*, **(D)** *S. sarmentosa*, **(E)** *S. glyycarpa*, **(F)** expansion of the minority peak region in chromatogram **E**.

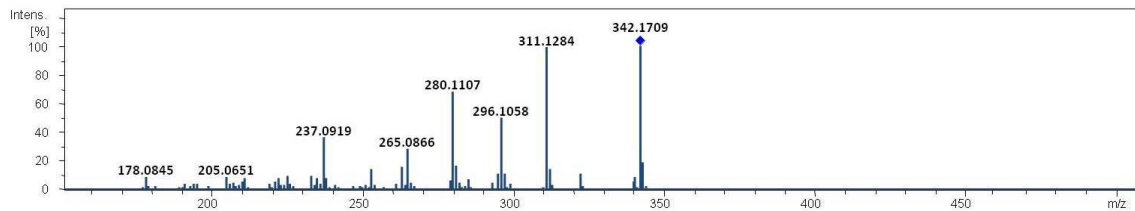


**Figure S3.** *Siparuna cristata* EtOH extract: MS<sup>2</sup> spectrum of compound  $m/z$  342.1709 [M+H]<sup>+</sup>.

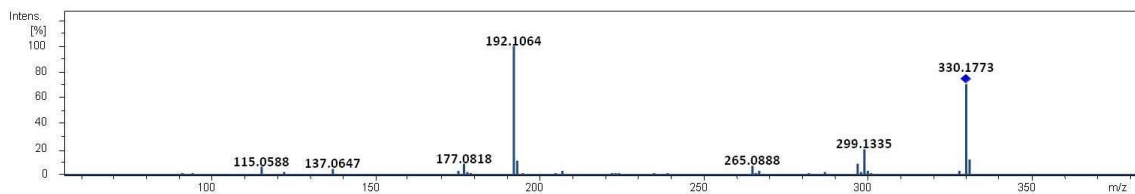


**Figure S4.** *Siparuna cristata* EtOH extract: MS<sup>2</sup> spectrum of compound  $m/z$  330.1773 [M+H]<sup>+</sup>.

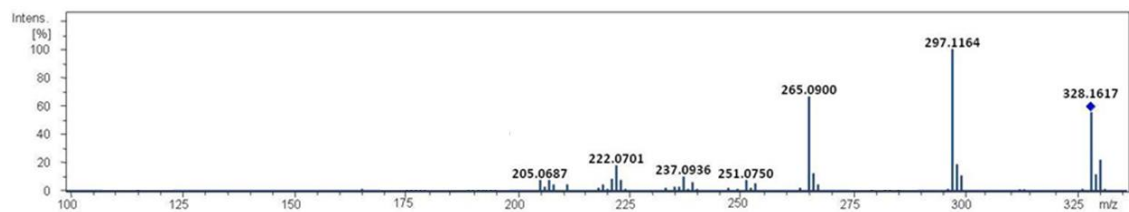


**Figure S5.** *Siparuna cristata* EtOH extract: MS<sup>2</sup> spectrum of compound  $m/z$  328.1617 [M+H]<sup>+</sup>.

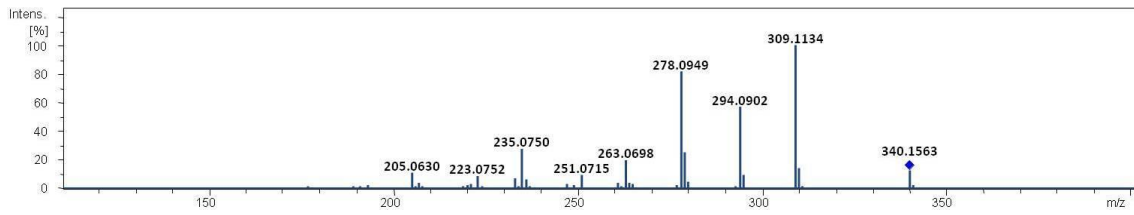


**Figure S6.** *Siparuna cristata* EtOH extract: MS<sup>2</sup> spectrum of compound  $m/z$  340.1563 [M+H]<sup>+</sup>.

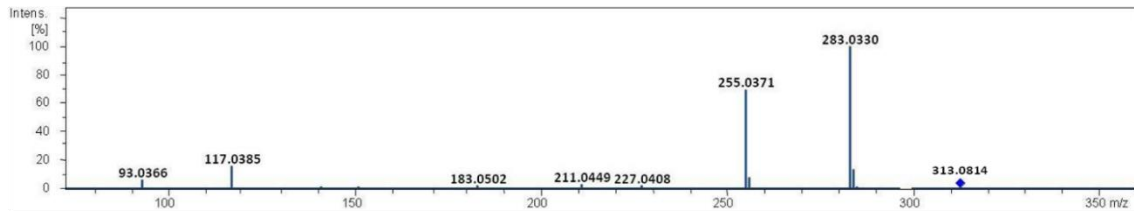


**Figure S7.** *Siparuna cristata* EtOH extract: MS<sup>2</sup> spectrum of compound  $m/z$  313.0814 [M-H]<sup>-</sup>.

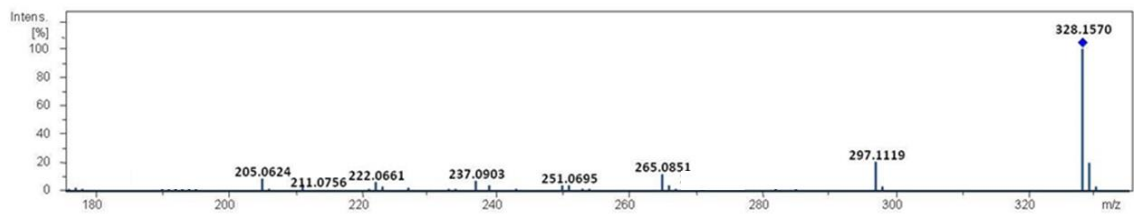


**Figure S8.** *Siparuna decipiens* EtOH extract: MS<sup>2</sup> spectrum of compound  $m/z$  328.1570 [M+H]<sup>+</sup>.

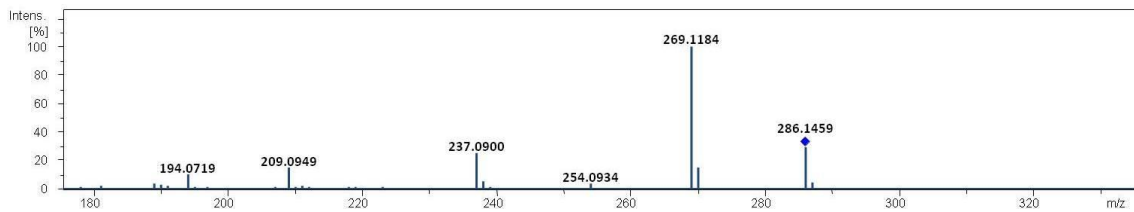


**Figure S9.** *Siparuna decipiens* EtOH extract: MS<sup>2</sup> spectrum of compound  $m/z$  286.1459 [M+H]<sup>+</sup>.

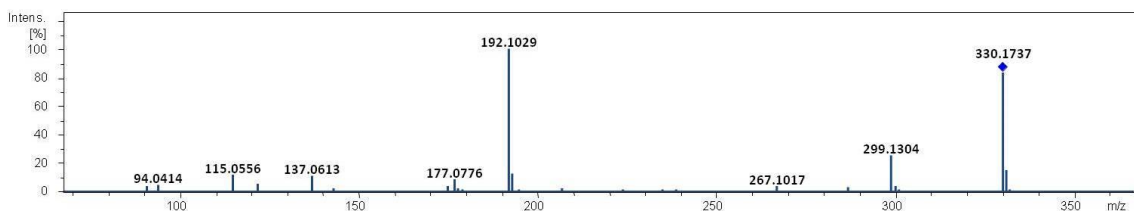


**Figure S10.** *Siparuna decipiens* EtOH extract: MS<sup>2</sup> spectrum of compound  $m/z$  330.1737 [M+H]<sup>+</sup>.

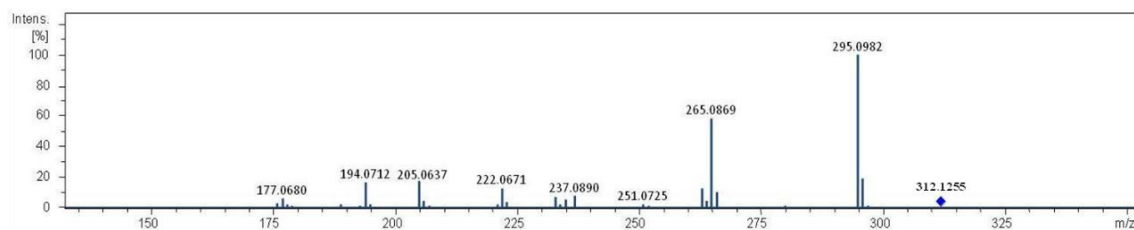


**Figure S11.** *Siparuna decipiens* EtOH extract: MS<sup>2</sup> spectrum of compound  $m/z$  312.1255 [M+H]<sup>+</sup>.

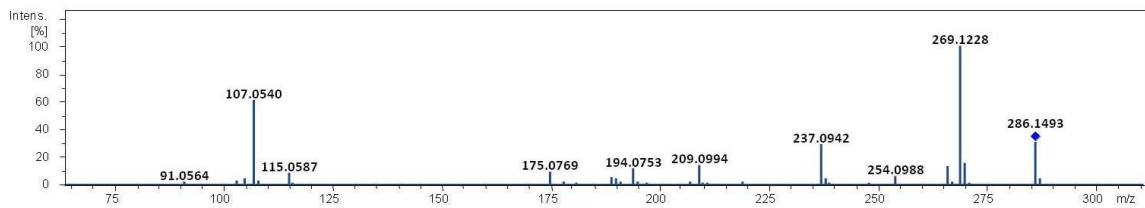


**Figure S12.** *Siparuna reginae* EtOH extract: MS<sup>2</sup> spectrum of compound  $m/z$  286.1493 [M+H]<sup>+</sup>.

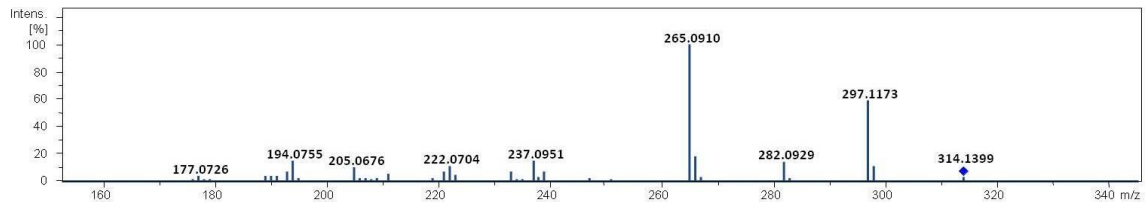


**Figure S13.** *Siparuna reginae* EtOH extract: MS<sup>2</sup> spectrum of compound  $m/z$  314.1399 [M+H]<sup>+</sup>.

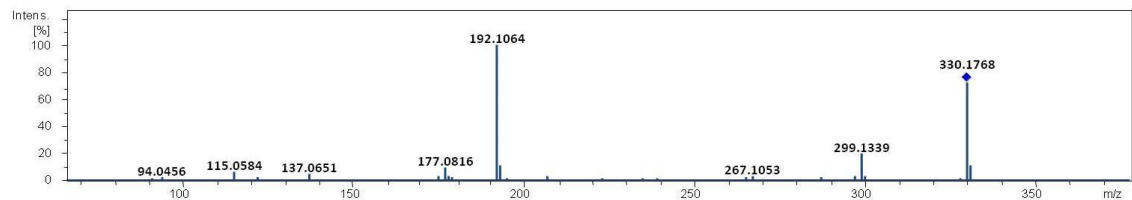


**Figure S14.** *Siparuna reginae* EtOH extract: MS<sup>2</sup> spectrum of compound  $m/z$  330.1768 [M+H]<sup>+</sup>.

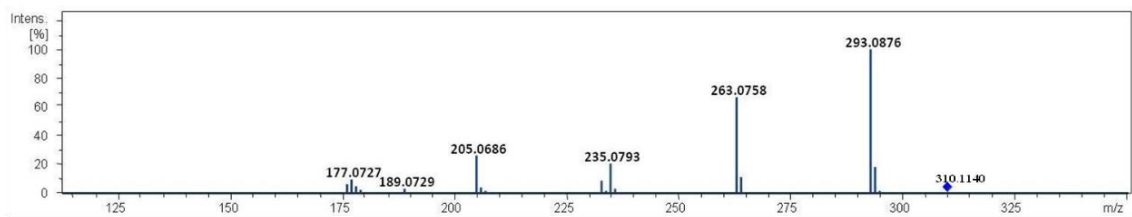


**Figure S15.** *Siparuna reginae* EtOH extract: MS<sup>2</sup> spectrum of compound  $m/z$  310.1140 [M+H]<sup>+</sup>.

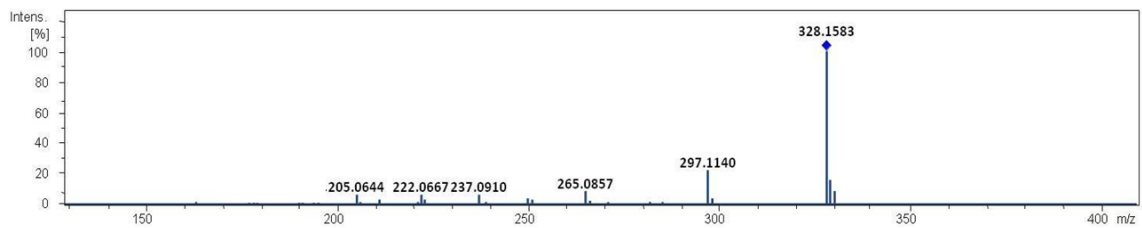


**Figure S16.** *Siparuna sarmentosa* EtOH extract: MS<sup>2</sup> spectrum of compound  $m/z$  328.1583 [M+H]<sup>+</sup>.

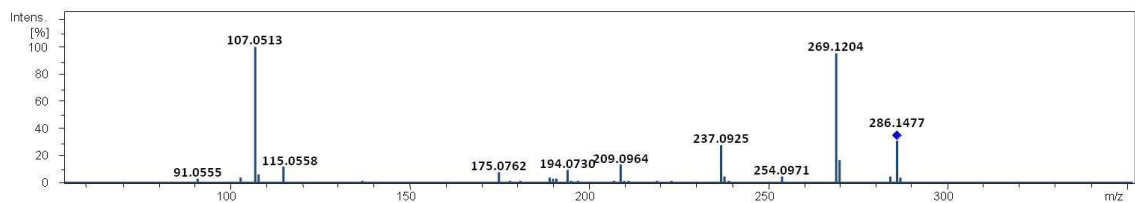


**Figure S17.** *Siparuna sarmentosa* EtOH extract: MS<sup>2</sup> spectrum of compound  $m/z$  286.1477 [M+H]<sup>+</sup>.



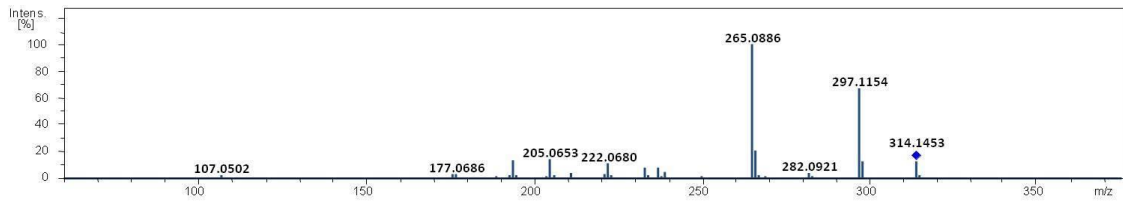


**Figure S18.** *Siparuna sarmentosa* EtOH extract: MS<sup>2</sup> spectrum of compound  $m/z$  314.1453 [M+H]<sup>+</sup>.

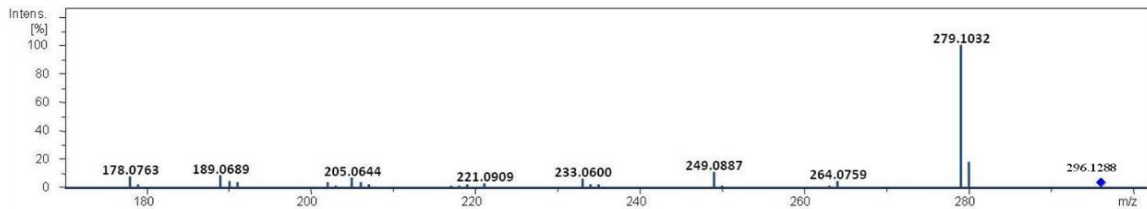


**Figure S19.** *Siparuna sarmentosa* EtOH extract: MS<sup>2</sup> spectrum of compound  $m/z$  296.1288 [M+H]<sup>+</sup>.

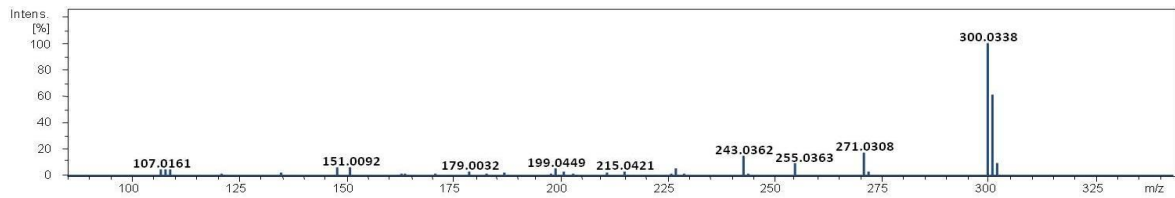


**Figure S20.** *Siparuna sarmentosa* EtOH extract: MS<sup>2</sup> spectrum of compound  $m/z$  609.1584 [M-H]<sup>-</sup>.

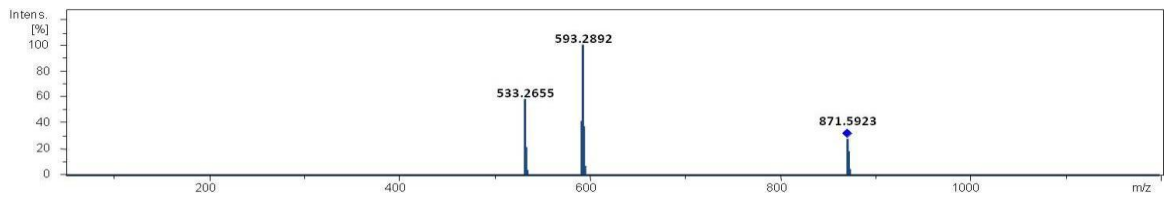


**Figure S21.** *Siparuna sarmentosa* EtOH extract: MS<sup>2</sup> spectrum of compound  $m/z$  871.5923 [M+H]<sup>+</sup>.

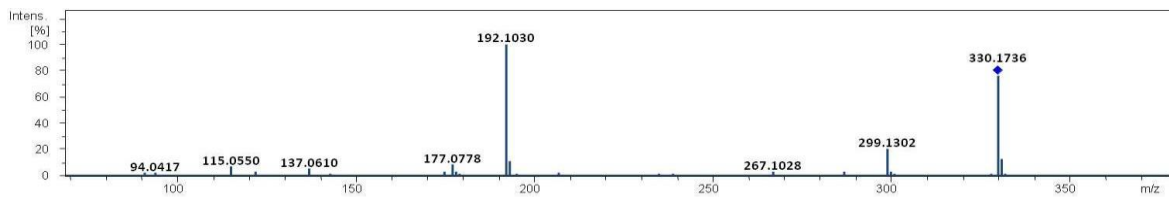


**Figure S22.** *Siparuna glycyarpa* EtOH extract: MS<sup>2</sup> spectrum of compound  $m/z$  330.1736 [M+H]<sup>+</sup>.

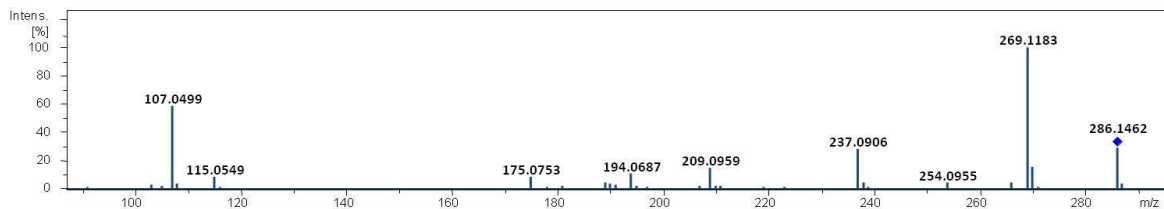


**Figure S23.** *Siparuna glycyarpa* EtOH extract: MS<sup>2</sup> spectrum of compound  $m/z$  286.1462 [M+H]<sup>+</sup>.

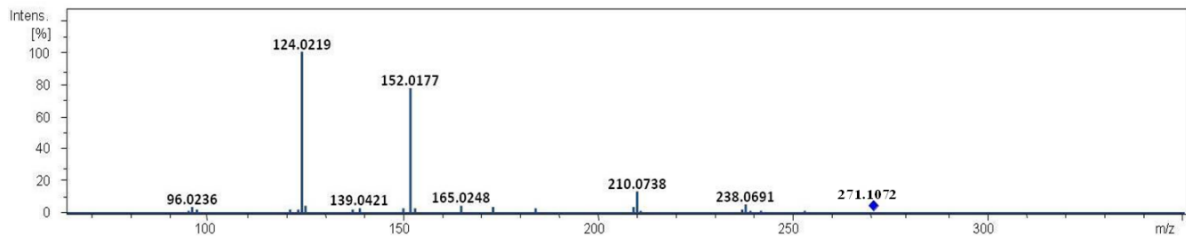


**Figure S24.** *Siparuna glycyarpa* EtOH extract: MS<sup>2</sup> spectrum of compound  $m/z$  271.1072 [M-H]<sup>-</sup>.

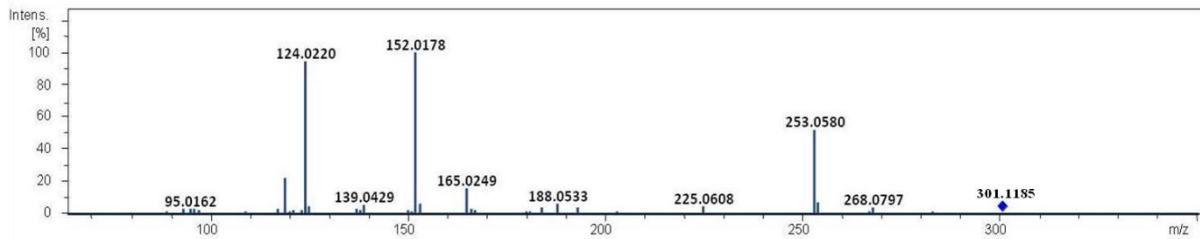


**Figure S25.** *Siparuna glycyarpa* EtOH extract: MS<sup>2</sup> spectrum of compound  $m/z$  301.1185 [M-H]<sup>-</sup>.

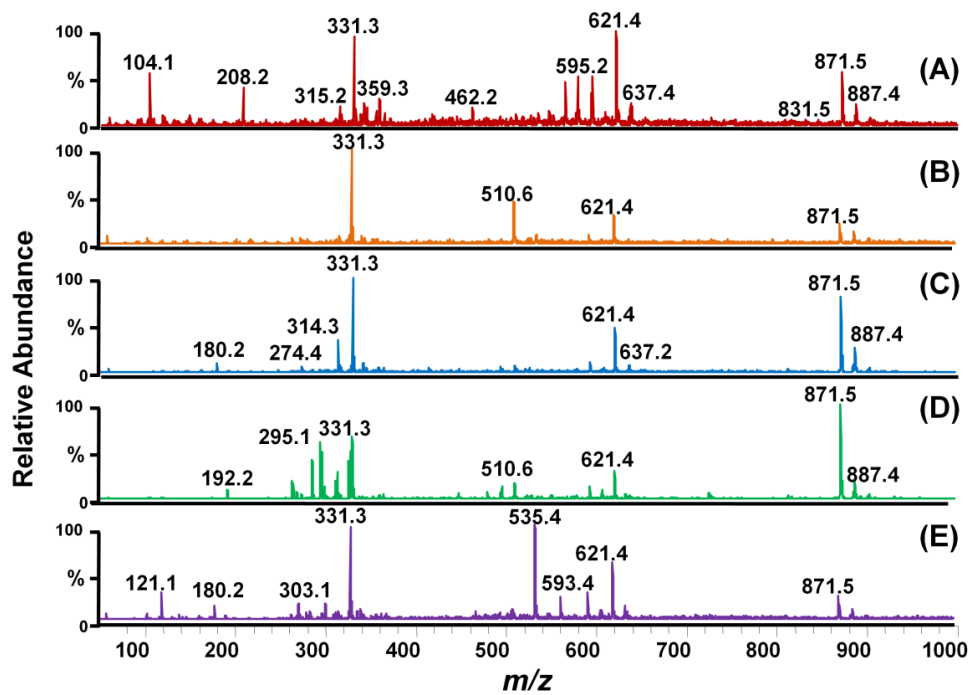


**Figure S26.** Fingerprinting by DI-ESI(+) IT-MS of EtOH extracts. **A)** *S. cristata*, **B)** *S. decipiens*, **C)** *S. reginae*, **D)** *S. sarmentosa* and **E)** *S. glycyarpa*.

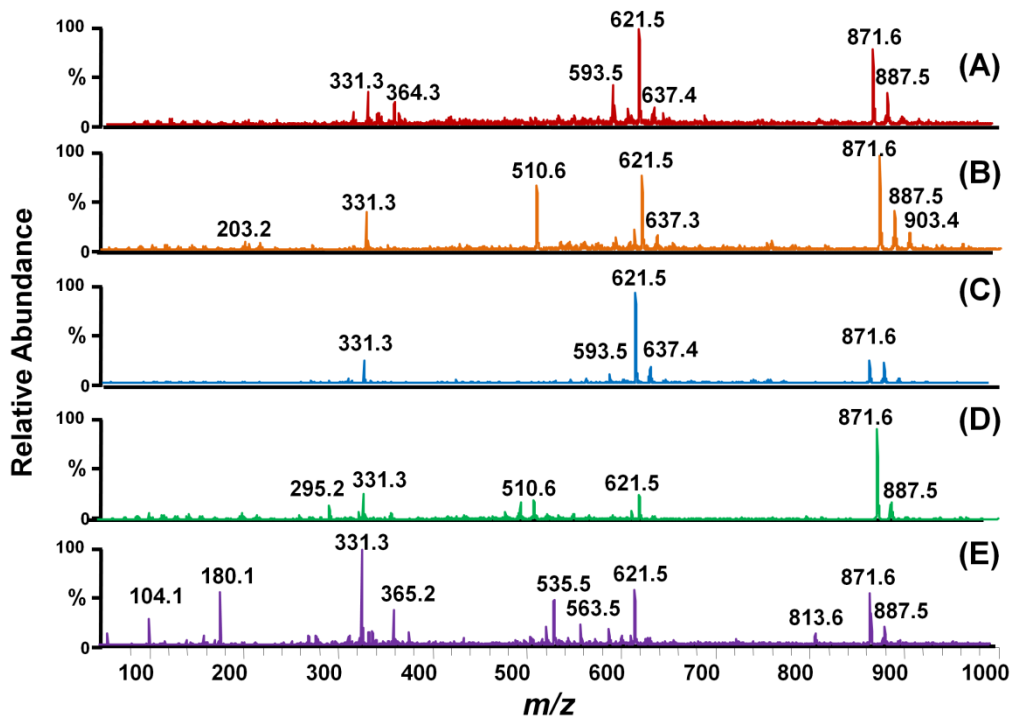


**Figure S27.** Fingerprinting by DI-ESI(+) IT-MS of Hex extracts. **A)** *S. cristata*, **B)** *S. decipiens*, **C)** *S. reginae*, **D)** *S. sarmentosa* and **E)** *S. glycyarpa*.

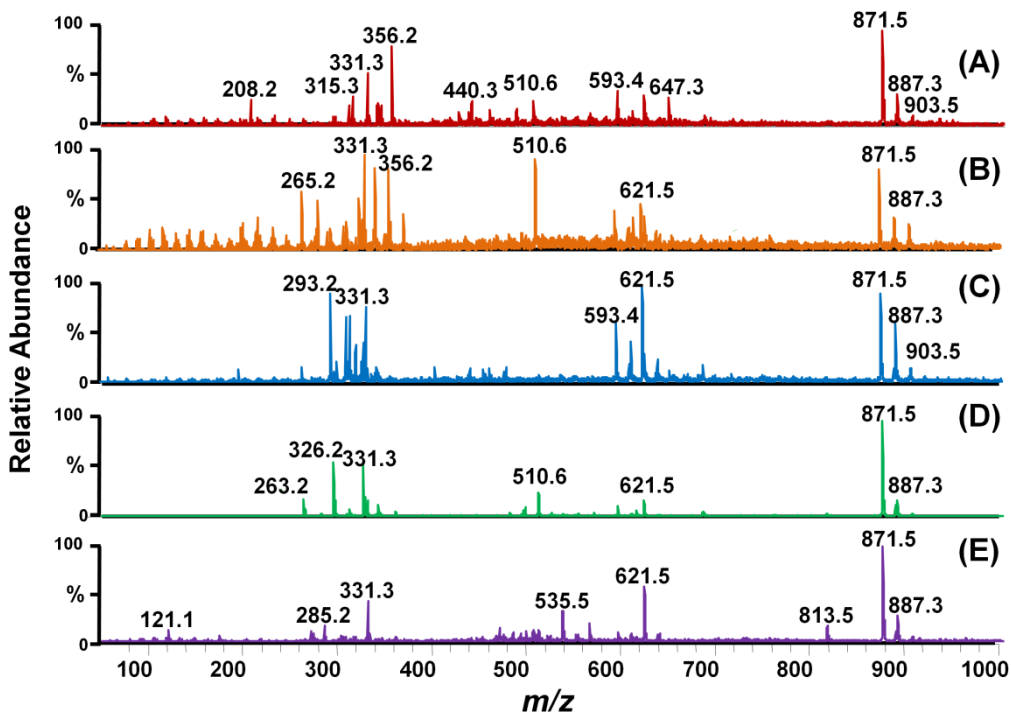


**Figure S28.** Fingerprinting by DI-ESI(+) IT-MS of DCM extracts. **A)** *S. cristata*, **B)** *S. decipiens*, **C)** *S. reginae*, **D)** *S. sarmentosa* and **E)** *S. glycyarpa*.

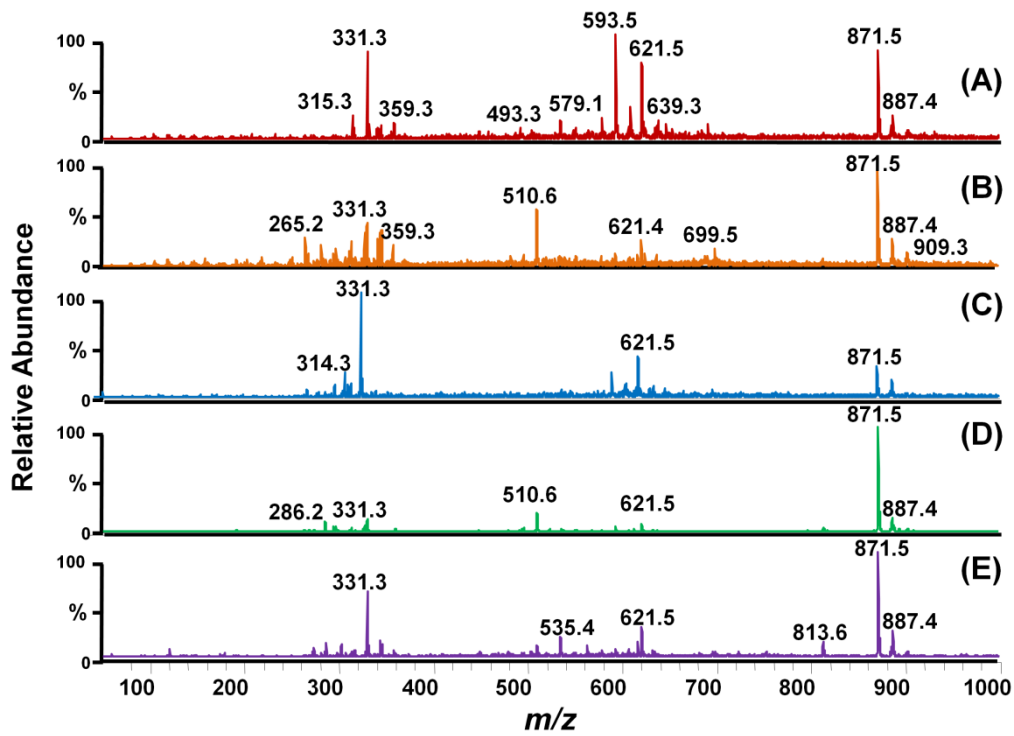


**Figure S29.** Fingerprinting by DI-ESI(+) IT-MS of EtOAc extracts. **A)** *S. cristata*, **B)** *S. decipiens*, **C)** *S. reginae*, **D)** *S. sarmentosa* and **E)** *S. glycyarpa*.

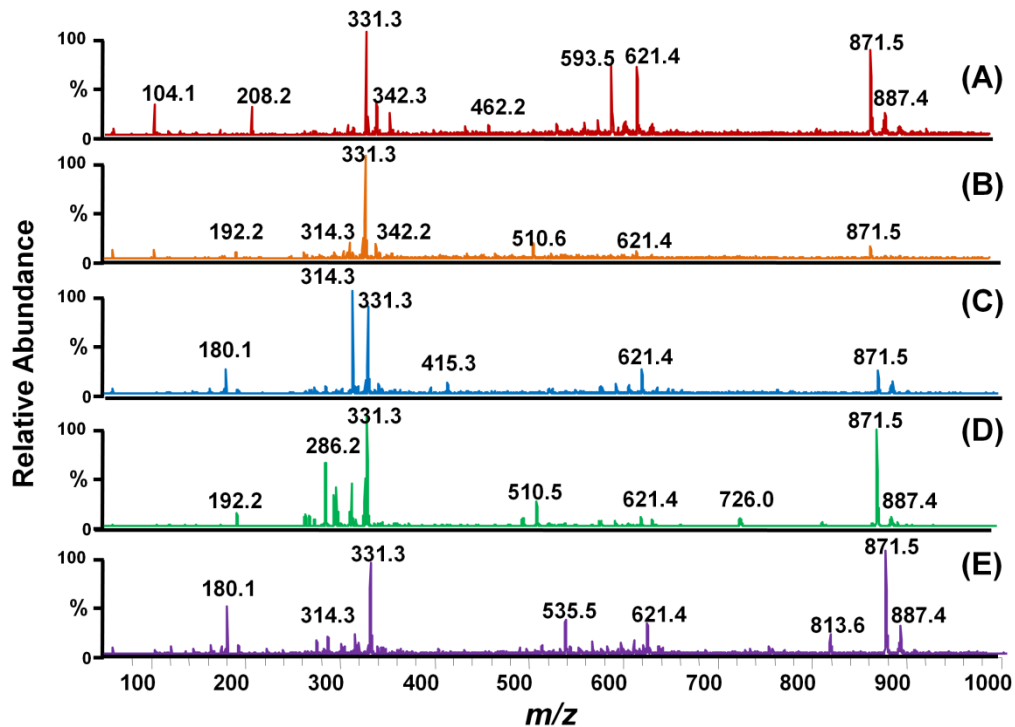


**Figure S30.** Fingerprinting by DI-ESI(+) IT-MS of BuOH extracts. **A)** *S. cristata*, **B)** *S. decipiens*, **C)** *S. reginae*, **D)** *S. sarmentosa* and **E)** *S. glycyarpa*.

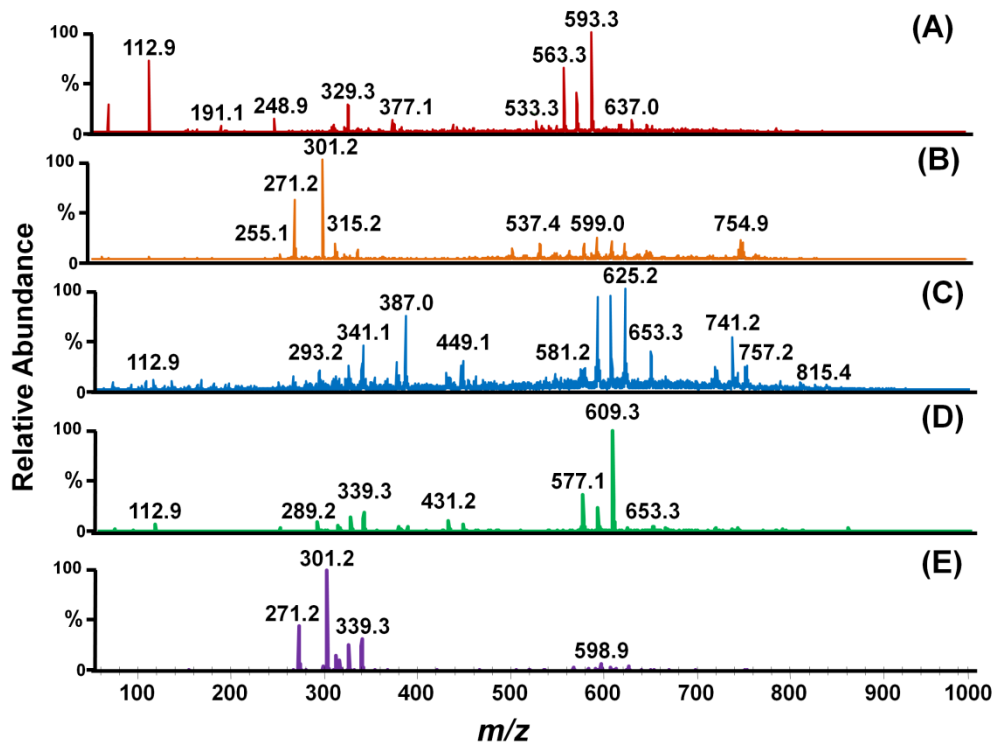


**Figure S31.** Fingerprinting by DI-ESI(-) IT-MS of EtOH extracts. **A)** *S. cristata*, **B)** *S. decipiens*, **C)** *S. reginae*, **D)** *S. sarmentosa* and **E)** *S. glycyarpa*.

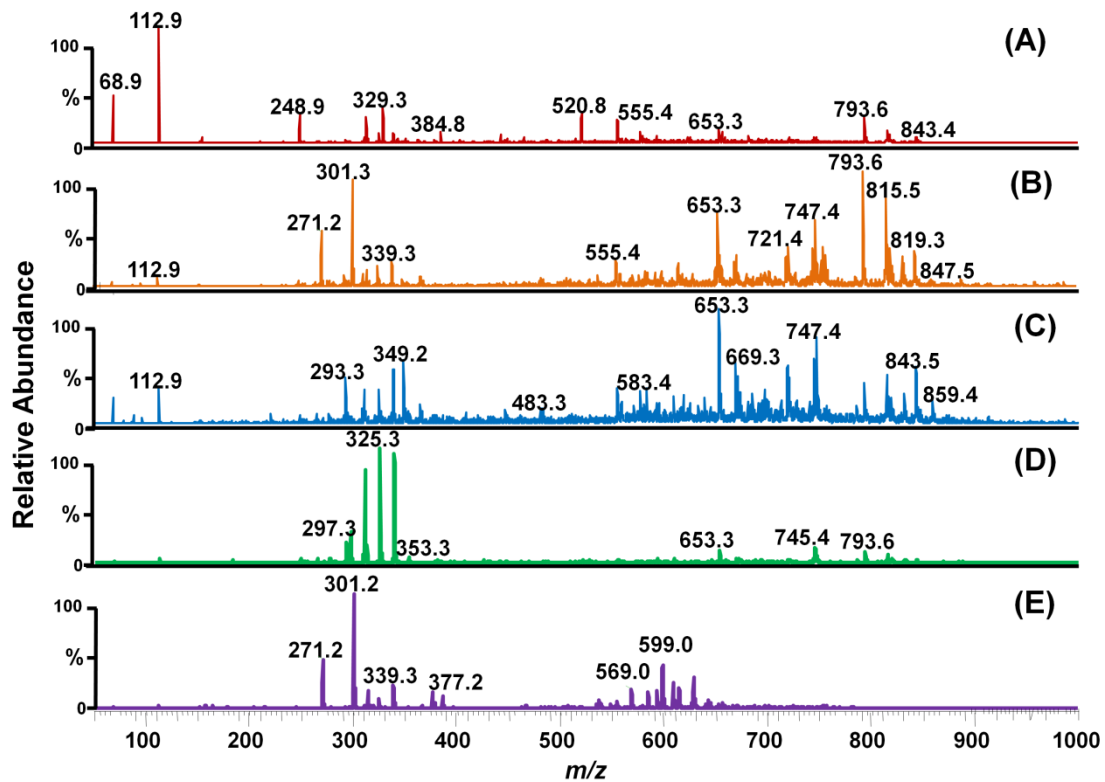


**Figure S32.** Fingerprinting by DI-ESI(-) IT-MS of Hex extracts. **A)** *S. cristata*, **B)** *S. decipiens*, **C)** *S. reginae*, **D)** *S. sarmentosa* and **E)** *S. glycyarpa*.

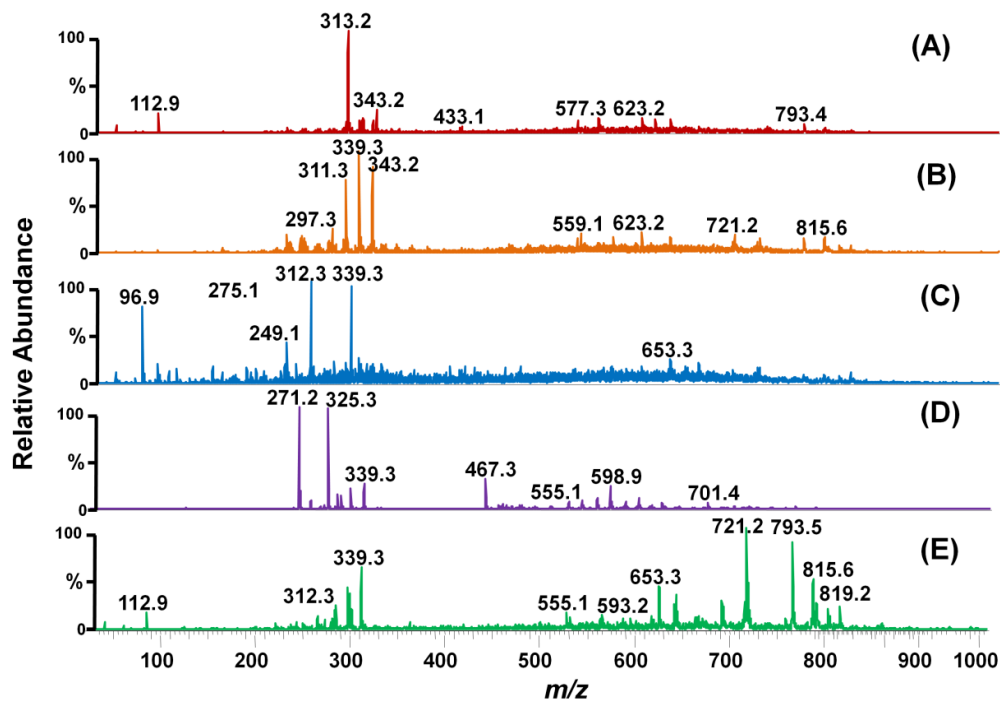


**Figure S33.** Fingerprinting by DI-ESI(-) IT-MS of DCM extracts. **A)** *S. cristata*, **B)** *S. decipiens*, **C)** *S. reginae*, **D)** *S. sarmentosa* and **E)** *S. glycyarpa*.

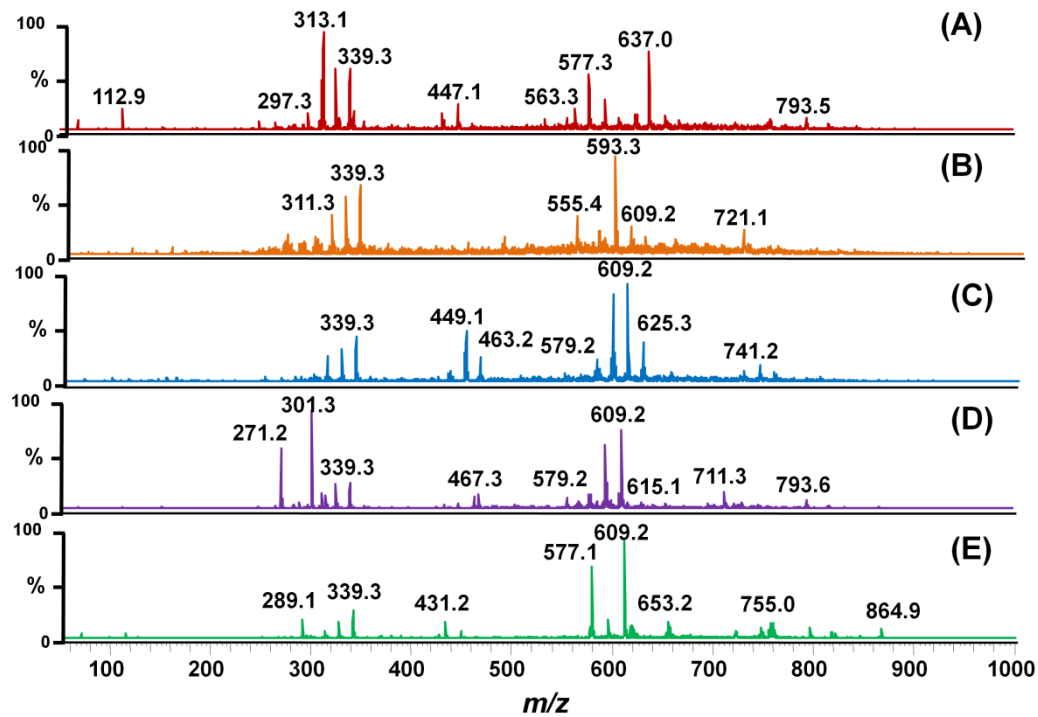


**Figure S34.** Fingerprinting by DI-ESI(-) IT-MS of EtOAc extracts. **A)** *S. cristata*, **B)** *S. decipiens*, **C)** *S. reginae*, **D)** *S. sarmentosa* and **E)** *S. glycyarpa*.

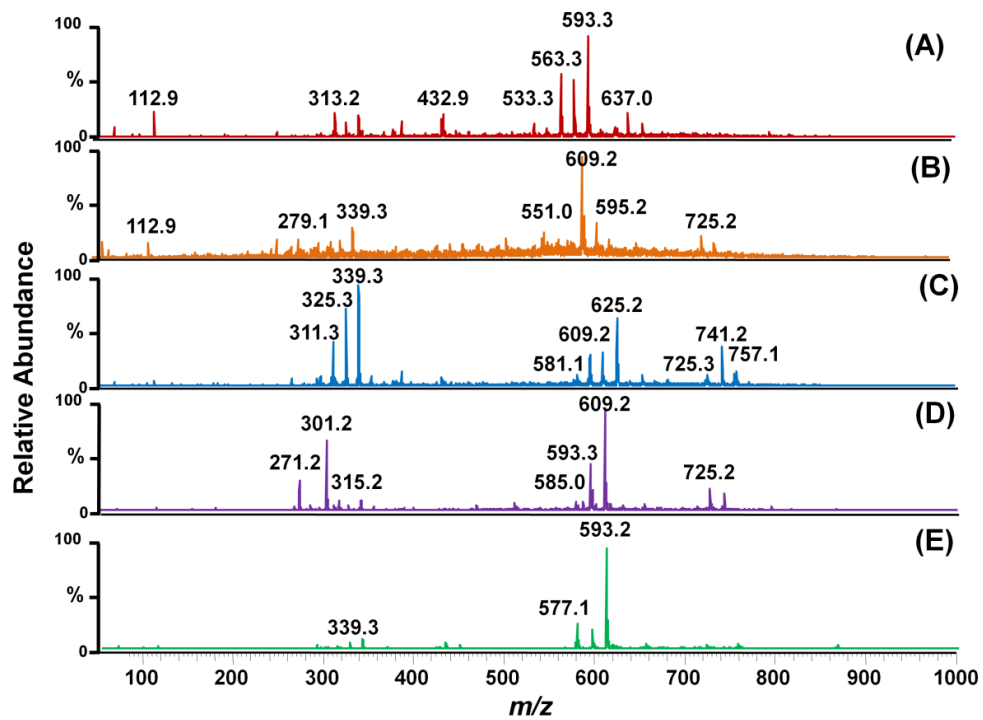


**Figure S35.** Fingerprinting by DI-ESI(-) IT-MS of BuOH extracts. **A)** *S. cristata*, **B)** *S. decipiens*, **C)** *S. reginae*, **D)** *S. sarmentosa* and **E)** *S. glycyarpa*.

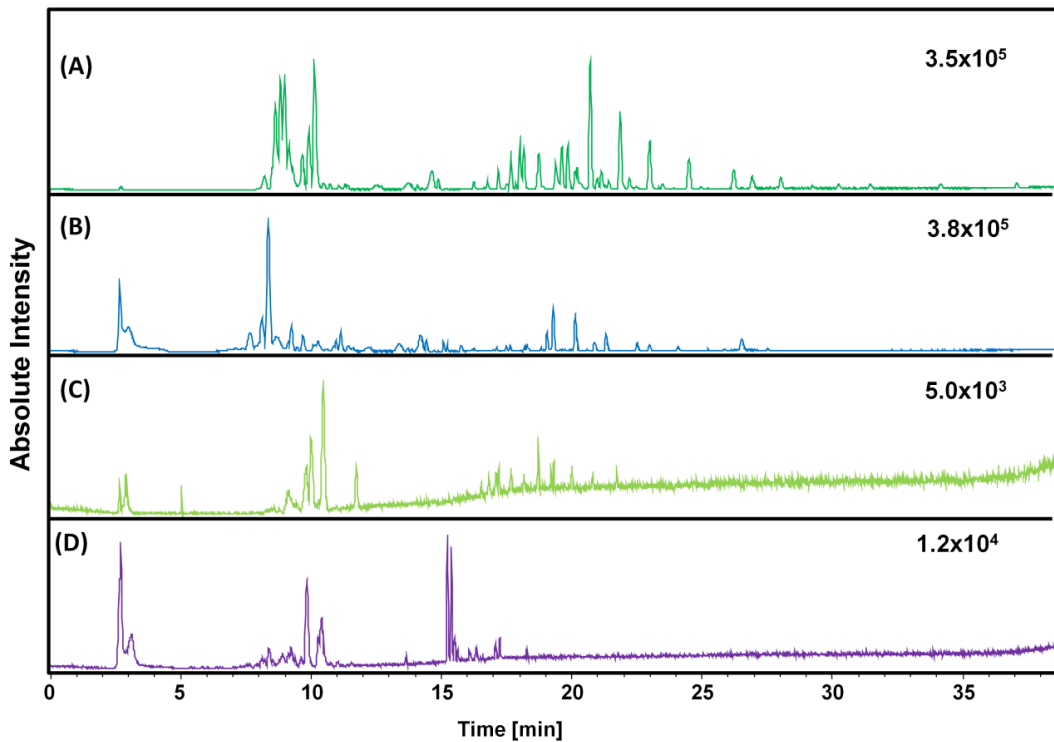


**Figure S36.** Base Peak Chromatograms by LC-ESI ( $\pm$ ) QTOF-MS/MS of the BuOH extracts. **A)** *S. sarmentosa*, ESI (+), **B)** *S. glycyarpa*, ESI (+), **C)** *S. sarmentosa*, ESI (-) and **D)** *S. glycyarpa*, ESI (-).

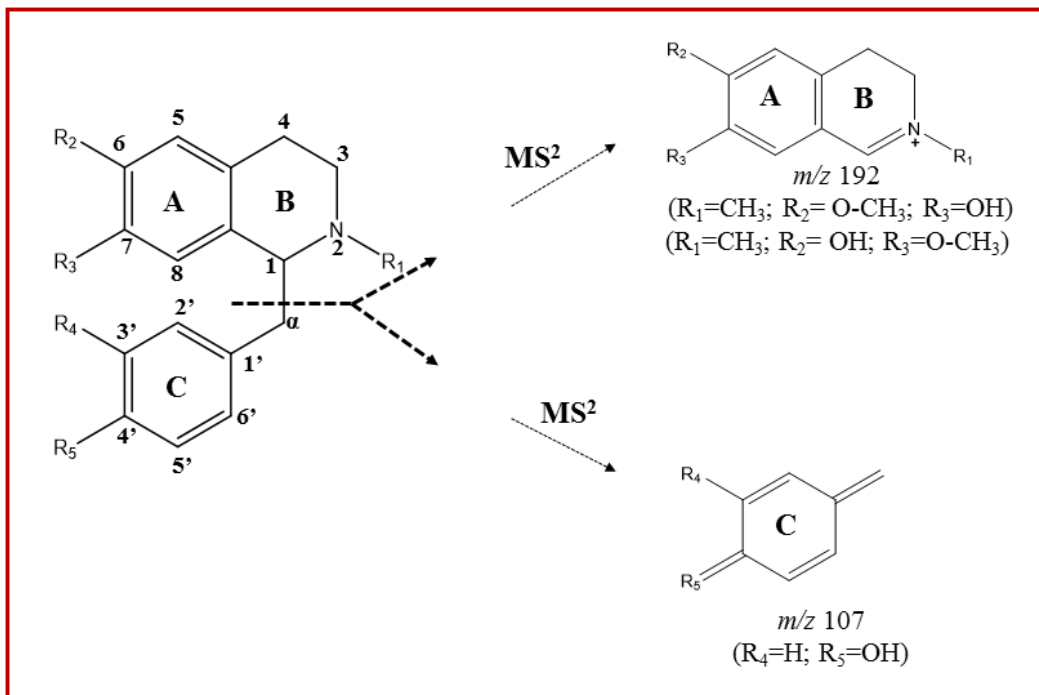


**Figure S37.** Benzylisoquinoline alkaloid skeleton and fragment ions at  $m/z$  107 and  $m/z$  192 after cleavage between C-1 and C- $\alpha$ .

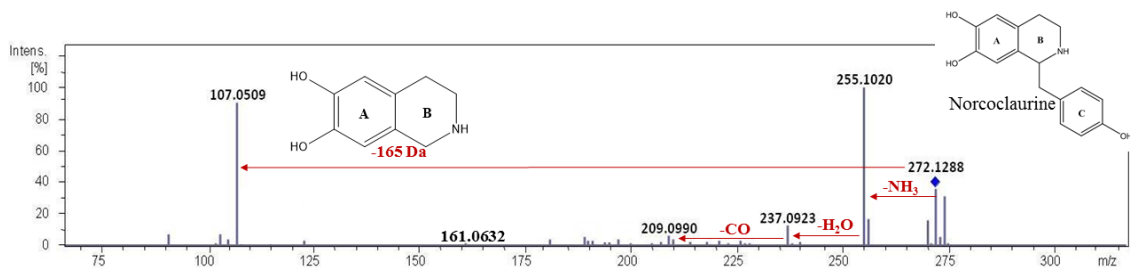


**Figure S38.** *Siparuna glycyarpa* butanol extract:  $MS^2$  spectrum of compound 1  $m/z$  272.1288  $[M+H]^+$  in 7.4 min.

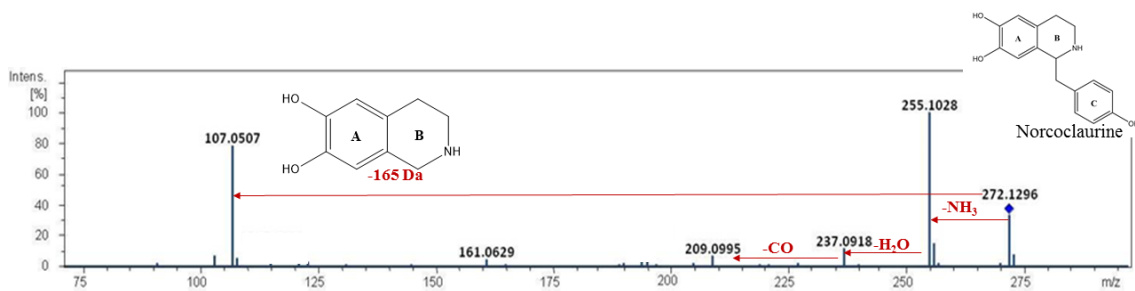


**Figure S39.** *Siparuna sarmentosa* butanol extract:  $MS^2$  spectrum of compound 1'  $m/z$  272.1296  $[M+H]^+$  in 8.1 min.



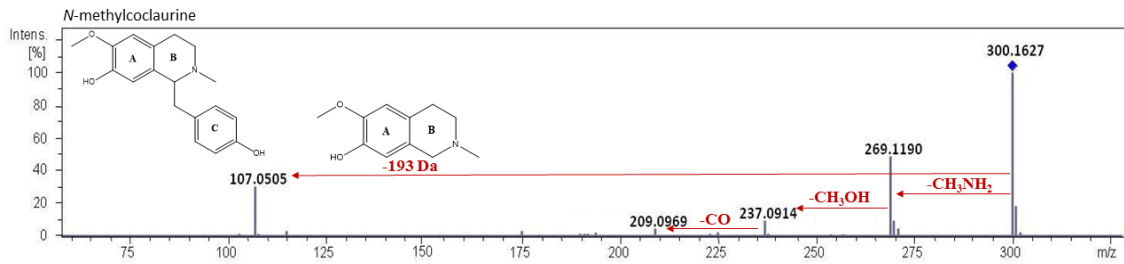


**Figure S40.** *Siparuna glycyrcarpa* butanol extract: MS<sup>2</sup> spectrum of compound 2  $m/z$  300.1627 [M+H]<sup>+</sup> in 8.1 min.

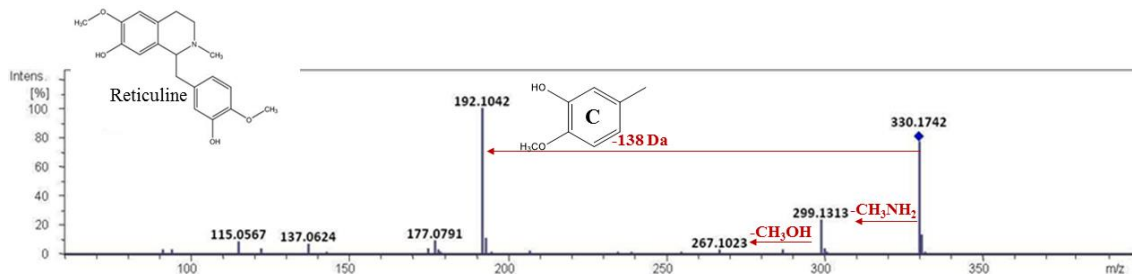


**Figure S41.** *Siparuna glycyrcarpa* butanol extract: MS<sup>2</sup> spectrum of compound 4  $m/z$  330.1742 [M+H]<sup>+</sup> in 8.4 min.

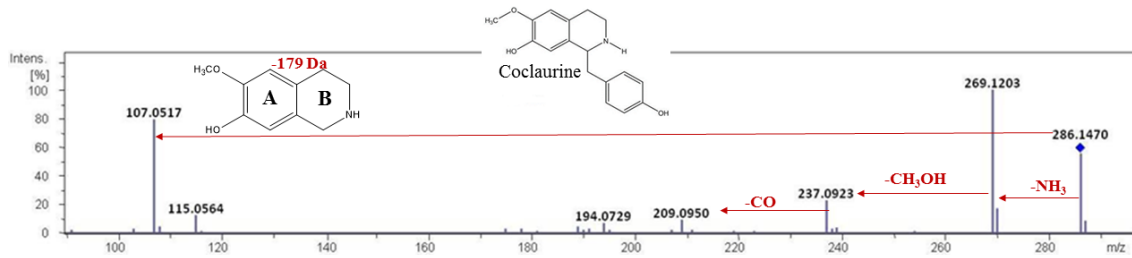


**Figure S42.** *Siparuna glycyrcarpa* butanol extract: MS<sup>2</sup> spectrum of compound 5  $m/z$  286.1470 [M+H]<sup>+</sup> in 9.3 min.

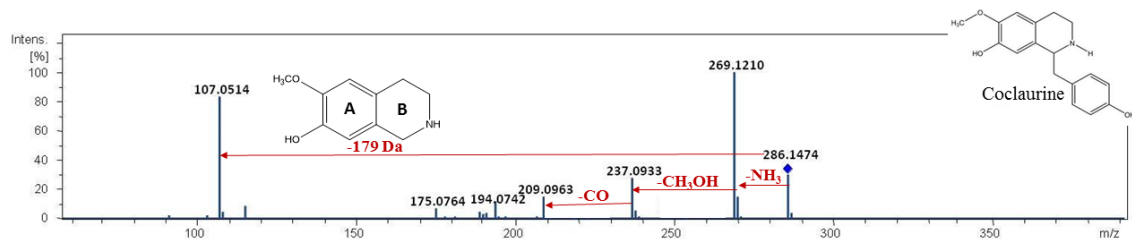


**Figure S43.** *Siparuna sarmentosa* butanol extract: MS<sup>2</sup> spectrum of compound 4'  $m/z$  286.1474 [M+H]<sup>+</sup> in 8.6 min.

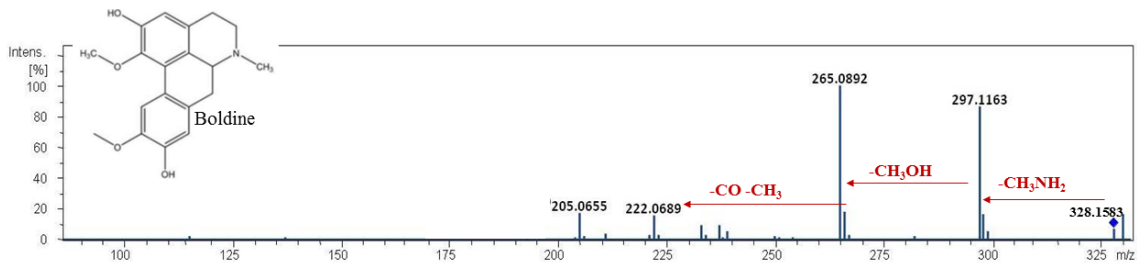


**Figure S44.** *Siparuna sarmentosa* butanol extract: MS<sup>2</sup> spectrum of compound 3'  $m/z$  328.1583 [M+H]<sup>+</sup> in 9.0 min.

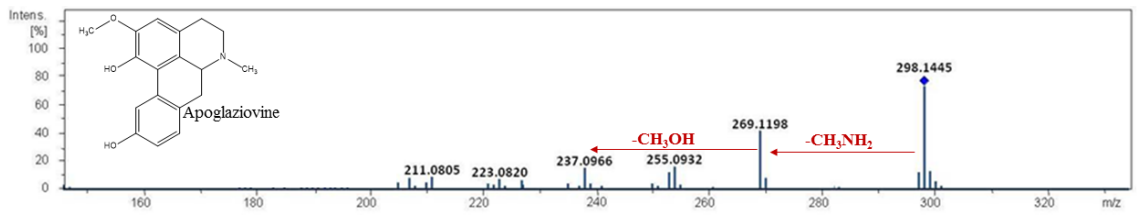


**Figure S45.** *Siparuna glycyrcarpa* butanol extract: MS<sup>2</sup> spectrum of compound 3  $m/z$  298.1445 [M+H]<sup>+</sup> in 8.4 min.

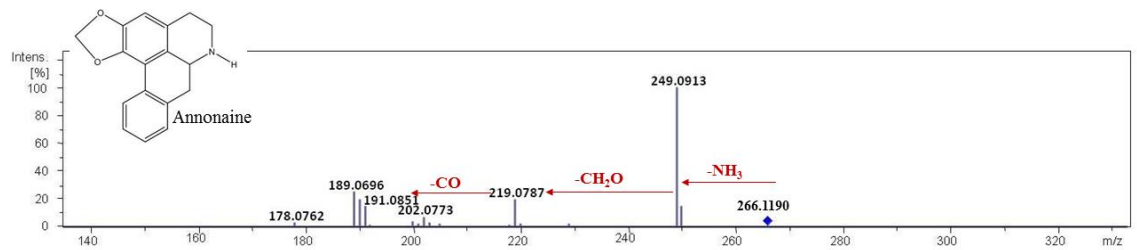


**Figure S46.** *Siparuna glycyrcarpa* butanol extract: MS<sup>2</sup> spectrum of compound 9  $m/z$  266.1190 [M+H]<sup>+</sup> in 11.2 min.

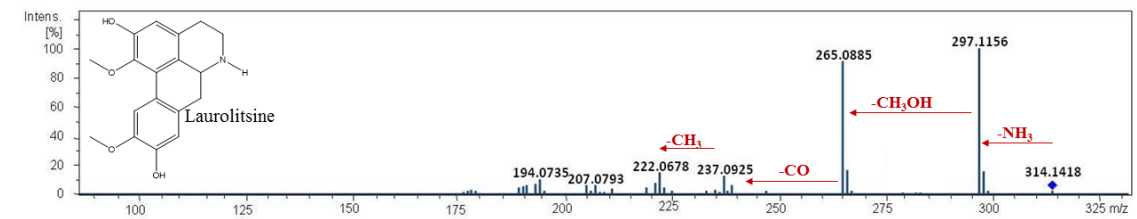


**Figure S47.** *Siparuna sarmentosa* butanol extract: MS<sup>2</sup> spectrum of compound 2'  $m/z$  314.1418 [M+H]<sup>+</sup> in 8.8 min.

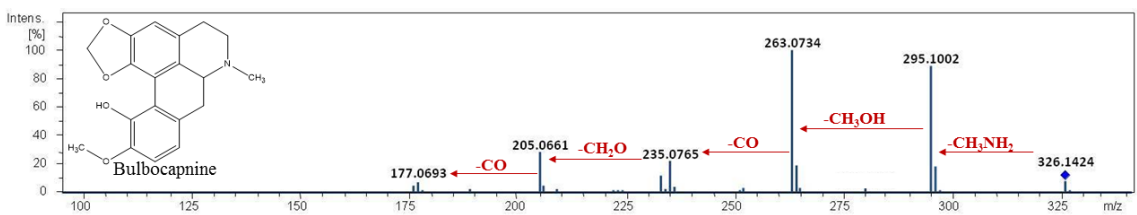


**Figure S48.** *Siparuna sarmentosa* butanol extract: MS<sup>2</sup> spectrum of compound 5'  $m/z$  326.1424 [M+H]<sup>+</sup> in 10.0 min.

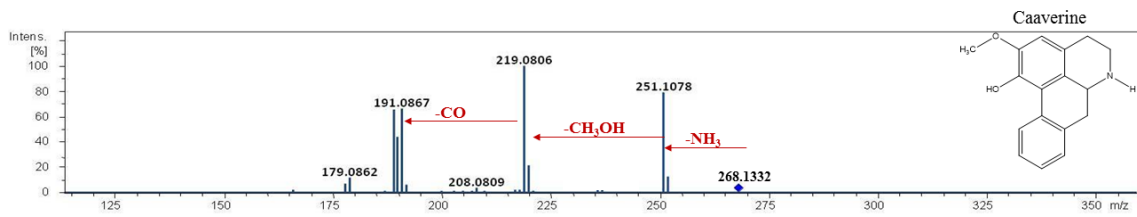


**Figure S49.** *Siparuna sarmentosa* butanol extract: MS<sup>2</sup> spectrum of compound 6'  $m/z$  268.1332 [M+H]<sup>+</sup> in 10.1 min.

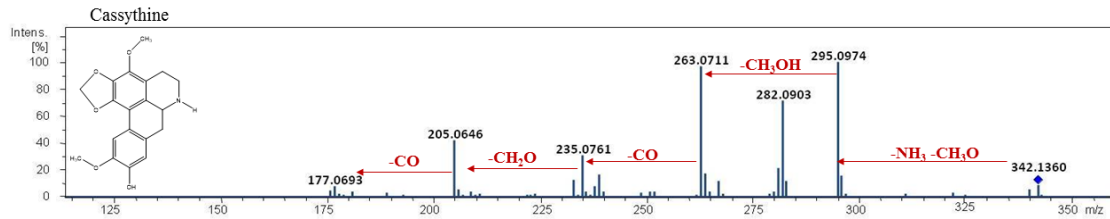


**Figure S50.** *Siparuna sarmentosa* butanol extract: MS<sup>2</sup> spectrum of compound 8'  $m/z$  342.1360 [M+H]<sup>+</sup> in 10.3 min.

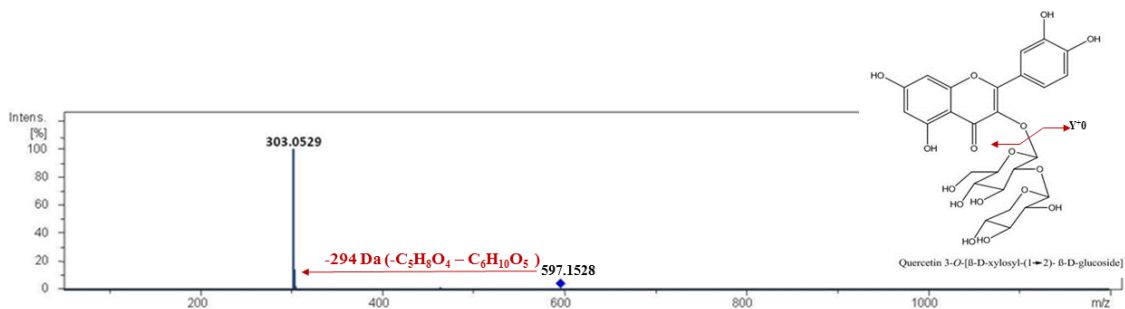


**Figure S51.** *Siparuna glycyrcarpa* butanol extract: MS<sup>2</sup> spectrum of compound 6  $m/z$  597.1528 [M+H]<sup>+</sup> in 9.5 min.

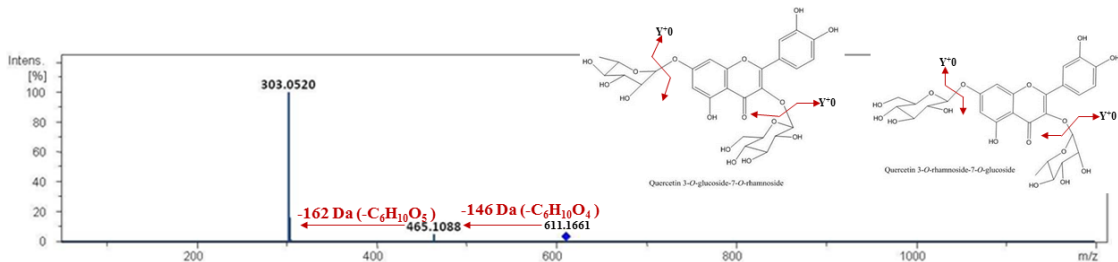


**Figure S52.** *Siparuna glycyrcarpa* butanol extract: MS<sup>2</sup> spectrum of compound 7  $m/z$  611.1661 [M+H]<sup>+</sup> in 9.7 min.

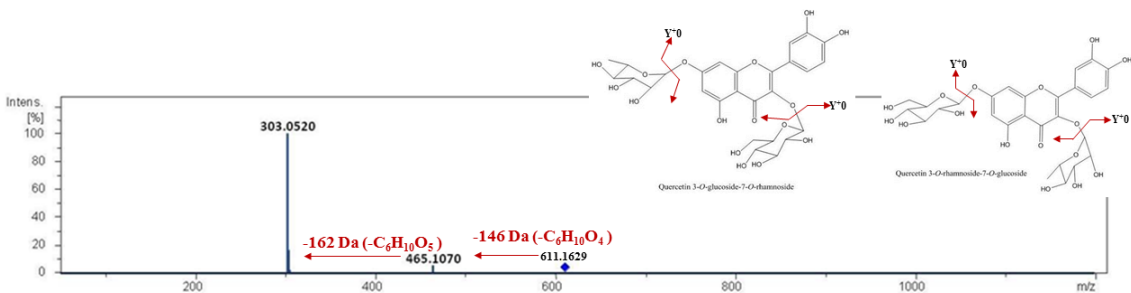


**Figure S53.** *Siparuna sarmentosa* butanol extract: MS<sup>2</sup> spectrum of compound 7'  $m/z$  611.1629 [M+H]<sup>+</sup> in 10.1 min.

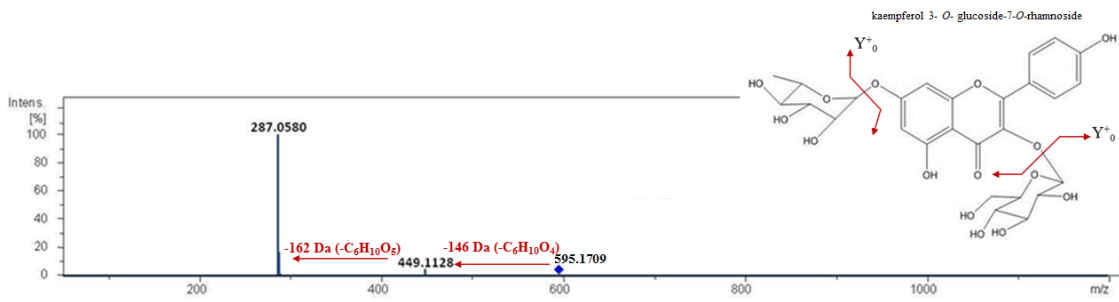


**Figure S54.** *Siparuna glycyrcarpa* butanol extract: MS<sup>2</sup> spectrum of compound 8 *m/z* 595.1709 [M+H]<sup>+</sup> in 10.3 min.

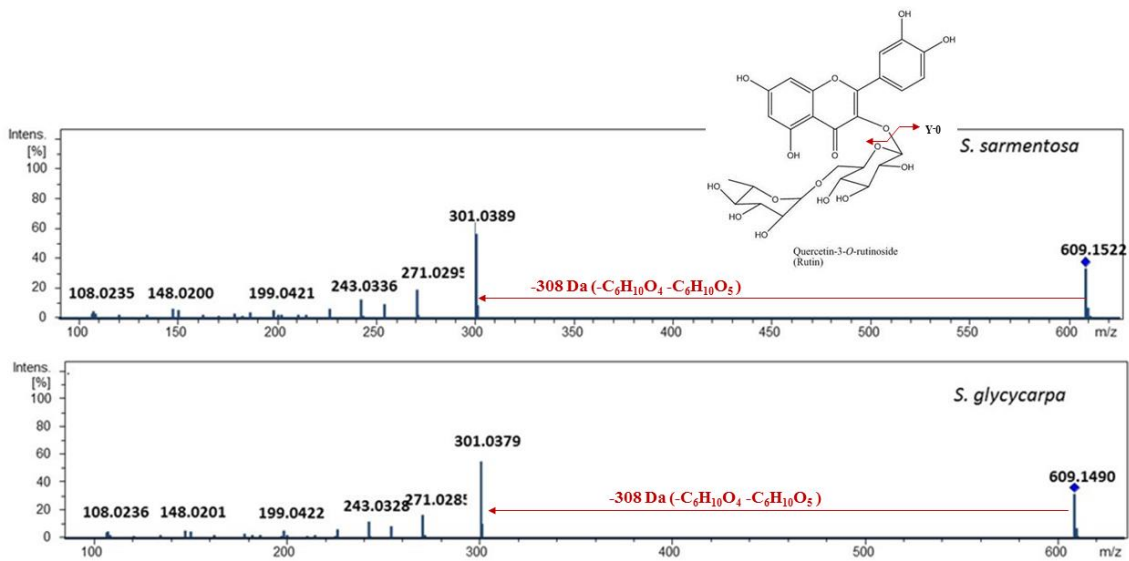


**Figure S55.** *Siparuna sarmentosa* and *Siparuna glycyrcarpa* butanol extracts: MS<sup>2</sup> spectra of compound 9' *m/z* 609.1522 [M-H]<sup>-</sup> in 10.4 min and compound 10 *m/z* 609.1490 [M-H]<sup>-</sup> in 9.8 min.

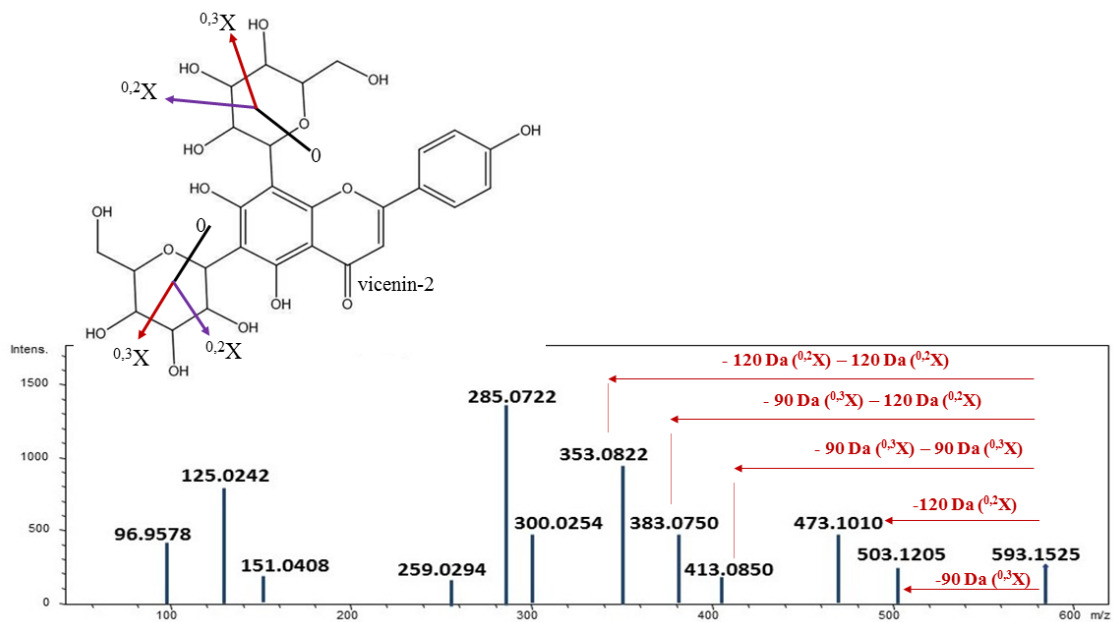


**Figure S56.** *Siparuna sarmentosa* butanol extract: MS<sup>2</sup> spectrum of compound 11' *m/z* 593.1525 [M-H]<sup>-</sup> in 18.0 min.

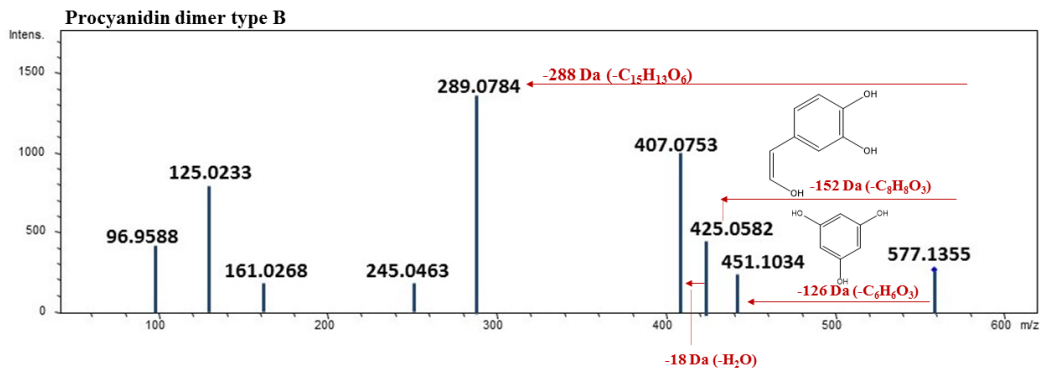


**Figure S57.** *Siparuna sarmentosa* butanol extract: MS<sup>2</sup> spectrum of compound 10'  $m/z$  577.1355 [M-H]<sup>-</sup> in 11.8 min.

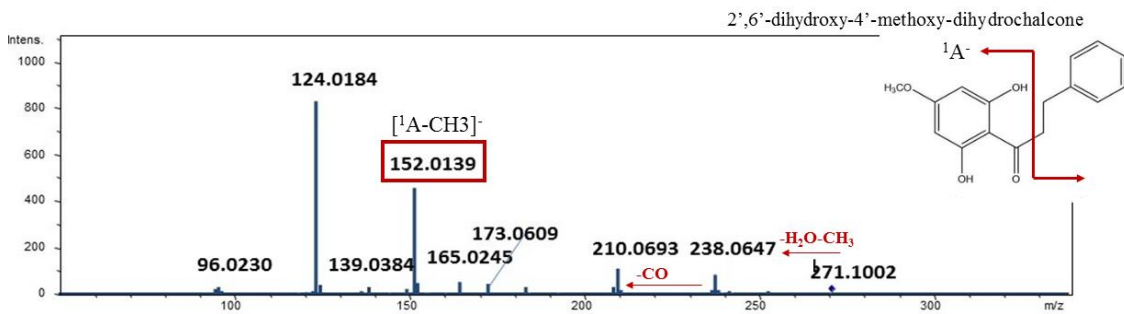


**Figure S58.** *Siparuna glycyrcarpa* butanol extract: MS<sup>2</sup> spectrum of compound 12  $m/z$  271.1002 [M-H]<sup>-</sup> in 15.4 min.

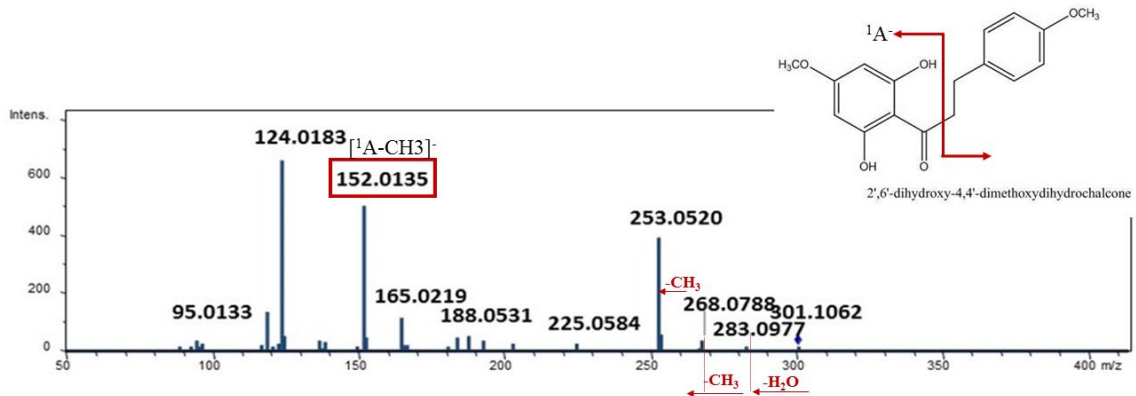


**Figure S59.** *Siparuna glycyrcarpa* butanol extract: MS<sup>2</sup> spectrum of compound 11  $m/z$  301.1062 [M-H]<sup>-</sup> in 15.2 min.

**4.2 Capítulo II.** Bioassay-Guided Fractionation of *Siparuna glycyarpa* n-Butanol Extract with Inhibitory Activity against Influenza A(H1N1)pdm09 Virus by Centrifugal Partition Chromatography (CPC)







Trabalho publicado em *Molecules*, in the special issue “Analytical and Preparative Hyphenation of Countercurrent Chromatography (CCC/CPC) to Structure Elucidation Methods in the Field of Natural Product Recovery and Identification”

(doi: 10.3390/molecules27020399)



Article

# Bioassay-Guided Fractionation of *Siparuna glycyarpa* *n*-Butanol Extract with Inhibitory Activity against Influenza A(H1N1)pdm09 Virus by Centrifugal Partition Chromatography (CPC)

Carla Monteiro Leal <sup>1,2</sup>, Suzana Guimarães Leitão <sup>3</sup> , Leonardo Luiz Oliveira de Mello <sup>2</sup>, Isabel de Castro Rangel <sup>2</sup>, Carlos Vinicius Azevedo da Silva <sup>4</sup> , Milene Dias Miranda <sup>5</sup> , Amanda Resende Tucci <sup>5</sup>, Camilla Blanco de Assis <sup>6,7</sup>, Carolina de Queiroz Sacramento <sup>6,7</sup>, Natalia Fintelman-Rodrigues <sup>6,7</sup> , Hector Henrique Ferreira Koolen <sup>4</sup>, Boniek Gontijo Vaz <sup>8</sup>, Rosineide Costa Simas <sup>8</sup> , and Gilda Guimarães Leitão <sup>2,\*</sup> 



**Citation:** Leal, C.M.; Leitão, S.G.; de Mello, L.L.O.; Rangel, I.d.C.; da Silva, C.V.A.; Miranda, M.D.; Tucci, A.R.; de Assis, C.B.; Sacramento, C.d.Q.; Fintelman-Rodrigues, N.; et al. Bioassay-Guided Fractionation of *Siparuna glycyarpa* *n*-Butanol Extract with Inhibitory Activity against Influenza A(H1N1)pdm09 Virus by Centrifugal Partition Chromatography (CPC). *Molecules* **2022**, *27*, 399. <https://doi.org/10.3390/molecules27020399>

Academic Editor: Gerold Jerz

Received: 17 December 2021

Accepted: 5 January 2022

Published: 8 January 2022

**Publisher's Note:** MDPI stays neutral with regard to jurisdictional claims in published maps and institutional affiliations.



**Copyright:** © 2022 by the authors. Licensee MDPI, Basel, Switzerland. This article is an open access article distributed under the terms and conditions of the Creative Commons Attribution (CC BY) license (<https://creativecommons.org/licenses/by/4.0/>).

- Programa de Pós-Graduação em Biotecnologia Vegetal e Bioprocessos (PBV), Centro de Ciências da Saúde, Universidade Federal do Rio de Janeiro, Rio de Janeiro 21941-902, Brazil; carlam.leal@yahoo.com.br
- Instituto de Pesquisas de Produtos Naturais, Centro de Ciências da Saúde, Universidade Federal do Rio de Janeiro, Rio de Janeiro 21941-902, Brazil; leonardo\_tuiz\_@outlook.com (L.L.O.d.M.); isabeldecastror@gmail.com (I.d.C.R.)
- Faculdade de Farmácia, Centro de Ciências da Saúde, Universidade Federal do Rio de Janeiro, Rio de Janeiro 21941-902, Brazil; sgleitao@pharma.ufrj.br
- Grupo de Pesquisas em Metabolômica e Espectrometria de Massas, Escola Superior de Ciências da Saúde, Universidade do Estado do Amazonas, Manaus 69065-000, Brazil; cv25066@gmail.com (C.V.A.d.S.); hkoolen@uea.edu (H.H.F.K.)
- Laboratório de Vírus Respiratórios e do Sarampo, Instituto Oswaldo Cruz, Fundação Oswaldo Cruz, Rio de Janeiro 21041-210, Brazil; milenediasmiranda@gmail.com (M.D.M.); biologa.t@gmail.com (A.R.T.)
- Laboratório de Imunofarmacologia, Instituto Oswaldo Cruz, Fundação Oswaldo Cruz, Rio de Janeiro 21041-210, Brazil; camillablanco.a@gmail.com (C.B.d.A.); carol.qsacramento@gmail.com (C.d.Q.S.); nataliafintelman@gmail.com (N.F.R.)
- Centro de Desenvolvimento Tecnológico em Saúde, Instituto Nacional de Ciência e Tecnologia de Gestão da Inovação em Doenças Negligenciadas, Fundação Oswaldo Cruz, Rio de Janeiro 21041-210, Brazil
- Laboratório de Cromatografia e Espectrometria de Massas (LaCEM), Instituto de Química, Universidade Federal de Goiás, Goiânia 74690-900, Brazil; boniek@gmail.com (B.G.V.); simas.rc@gmail.com (R.C.S.)
- \* Correspondence: ggleitao@ippn.ufrj.br

**Abstract:** *Siparuna glycyarpa* occurs in the Amazon region, and some species of this genus are used in Brazilian folk medicine. A recent study showed the inhibitory effect of this species against influenza A(H1N1)pdm09 virus, and in order to acquire active fractions, a polar solvent system *n*-butanol-methanol-water (9:1:10, *v/v*) was selected and used for bioassay-guided fractionation of *n*-butanol extract by centrifugal partition chromatography (CPC). The upper phase was used as stationary phase and the lower phase as mobile (descending mode). Among the collected fractions, the ones coded SGA, SGC, SGD, and SGO showed the highest antiviral inhibition levels (above 74%) at 100 µg·mL<sup>-1</sup> after 24 h of infection. The bioactive fractions chemical profiles were investigated by LC-HRMS/MS data in positive and negative ionization modes exploring the Global Natural Products Social Molecular Networking (GNPS) platform to build a molecular network. Benzylisoquinoline alkaloids were annotated in the fractions coded SGA, SGC, and SGD collected during elution step. Aporphine alkaloids, *O*-glycosylated flavonoids, and dihydrochalcones in SGO were acquired with the change of mobile phase from lower aqueous to upper organic. Benzylisoquinolinic and aporphine alkaloids as well as glycosylated flavonoids were annotated in the most bioactive fractions suggesting this group of compounds as responsible for antiviral activity.

**Keywords:** centrifugal partition chromatography; influenza virus; mass spectrometry; off-line LC-MS/MS; Siparunaceae; solvent system

## 1. Introduction

Influenza viruses are one of the most relevant etiological agents of acute respiratory infections. Influenza A viruses are highly mutagenic and can infect both animals and humans, causing seasonal epidemics and pandemics, for instance the influenza A(H1N1) 2009 pandemic, which led to significant morbidity, mortality rates, and burden to public health [1,2]. In July 2020, during the worldwide pandemic of COVID-19, an outbreak of another influenza A subtype, A(H3N2), occurred in the Kingdom of Cambodia. Among the Pagoda residents, 82.5% tested positive for this virus [3]. Therefore, the search for anti-influenza compounds that may prevent and treat serious infections and reduce transmissibility is pivotal.

Plants and their derived natural products could be a source for new antiviral drugs [4,5]. Some species of the genus *Siparuna* are used in Brazilian folk medicine [6,7], and recently, our group showed that the extracts from Amazonian *Siparuna* species presented inhibitory effect against influenza A(H1N1)pdm09 virus replication [8]. The *n*-butanol extracts from *Siparuna glycyarpa* (SG) and *Siparuna sarmentosa* (SS) demonstrated high antiviral activity, inhibiting, respectively,  $96.0 \pm 1.3\%$  and  $89.5 \pm 0.8\%$  of influenza virus replication 24 h post-infection. The selective index (SI) values for SG and SS were 40 and  $>27$ , higher than those for other *n*-butanol extracts published in the literature [8,9]. Alkaloids, *O*- and *C*-flavonoid glycosides, dihydrochalcones, and a procyanidin dimer were annotated in these extracts, and according to the literature, they have been demonstrated as potential inhibitors of influenza virus [8,10,11].

Plant extracts are generally complex mixtures composed of many different compounds within the several classes of secondary metabolites. According to ethnopharmacological knowledge, the bio-guided fractionation approach has been employed for the screening and fractionation of extracts in natural products research for the obtention of bioactive fractions and identification of active compounds [12,13]. Many chromatographic techniques can be employed in this approach. However, depending on the applied technique, some bioactive compounds may be lost due to irreversible adsorption on the chromatographic column, common in solid stationary phase techniques [14–17].

Thus, a liquid–liquid extraction method such as countercurrent chromatography (CCC) is an excellent alternative, as it is a liquid–liquid partition chromatography technique in which the stationary liquid phase is retained in a column without the use of solid supports. CCC is extremely useful in the purification of compounds from complex matrices such as plant extracts. In modern CCC, the equipment operates in a centrifugal way. The rotational movement of the column can be of two types, generating hydrostatic equilibrium between the two liquid phases or the hydrodynamic equilibrium. Centrifugal partition chromatography (CPC) uses a hydrostatic column with a constant-gravity force field produced by a single-axis rotating column [18,19]. The sample properties, solvent system choice, instrument, and instrumental method influence the efficiency within the separation procedure by CPC [20]. Among the advantages of the hydrostatic techniques such as high-flow rates working possibility, one stands out, which is the excellent retention of all solvent systems, especially of those composed of high-polarity and viscous solvents, including the aqueous two-phase solvent systems (ATPS), which are not retained in hydrodynamic columns [18,20].

CPC has been applied in different natural products studies for the isolation and purification of compounds, and for obtaining simplified fractions from crude extracts [19,21–23]. The off-line coupling of CPC with liquid chromatography–mass spectrometry is an efficient tool for giving access to the chemical profile of fractions [24]. By employing tandem mass spectrometry, it is possible to annotate the known and unknown compounds through spectra fragmentation data [14,24].

In this study, the *n*-butanol extract from *S. glycyarpa*, previously shown to be active against influenza A(H1N1)pdm09 replication, was fractionated by CPC using *n*-butanol-methanol-water (BuMWat), a polar solvent system that failed stationary phase retention on hydrodynamic equipment. The acquired fractions were evaluated for their inhibitory effects



against influenza A(H1N1) virus replication, and the bioactive fractions were analyzed by LC-HRMS/MS and molecular networking for the compound's annotation.

## 2. Results and Discussion

### 2.1. Centrifugal Partition Chromatography of the *n*-Butanol Extract from *S. glycyarpa*

The choice of an adequate solvent system is essential for the success of fractionation in CCC. When dealing with polar extracts, the composition of a suitable solvent system generally involves a ternary mixture of polar organic solvents such as ethyl acetate, *n*-butanol, a short-chain alcohol, and water [24,25]. The *n*-butanol–methanol–water (BuMWat) solvent system is a hydrophilic-organic solvent system that can be applied for the purification of some peptides, glycans, phenolic acids, glycosylated polyphenols, and hydrophilic alkaloids [20,23,26,27]. The presence of high-viscosity solvents such as *n*-butanol, results in lower retention (or even no retention at all) of the stationary phase in equipment with a hydrodynamic column as in high-speed countercurrent chromatography (HSCCC), affecting chromatographic peak resolution [23]. Thus, better stationary phase control is one of the advantages of CPC over HSCCC, which allow using hydrophilic systems [20].

Previous chemical profiling of the extract under study by ion-trap liquid chromatography–high resolution mass spectrometry revealed its complex composition, containing different compounds of high polarity [8]. Thus, a solvent system such as *n*-butanol–methanol–water (BuMWat) would be suitable for covering the large range of high polarity of the compounds present in this extract and was proposed for its bioguided fractionation. To do this, different volume ratios of *n*-butanol–methanol–water were tested: (1) 10:0:10, *v/v*, (2) 9:1:10, *v/v*, and (3) 8:2:10, *v/v* (Supplementary Figure S1). Solvent system 2 was selected, as it provided good solubility of the extract and homogenous distribution of compounds between the two liquid phases. Due to compounds of interest being mainly found in the upper organic phase, this phase was chosen as stationary and the lower aqueous phase as mobile (descending mode).

Three 500 mg fractionations of the *n*-butanol extract from *S. glycyarpa* were performed in the elution–extrusion mode, allowing the recovery of retained compounds in the stationary phase [28]. During the first experiment 47 fractions of 12 mL were collected with a flow rate of 6 mL·min<sup>−1</sup> and a rotor spinning at 1000 rpm (Supplementary Figure S2). In these conditions a loss of stationary phase (102 mL) was observed in the first collected tubes (1–17) and, consequently, a low retention of stationary phase (59.2%). Flow rate and rotation speed are essential for the fluid dynamics in CPC and can influence the quality of separation [24,29]. Therefore, a second fractionation was carried out with the same conditions, adjusting the rotation to 1300 rpm to improve stationary phase retention. Indeed, there was an increase in the stationary phase retention to 70% and an improvement in the chromatographic separation (Supplementary Figure S3). Through the CPC–UV chromatogram of collected fractions it was possible to monitor (UV detection) the presence of compounds with absorption bands at about 220 nm and 280 nm in the elution step (fractions 7 to 12), which may account for alkaloids [30]. Fractions 33 to 40, collected during the extrusion step, showed the presence of absorption maxima that ranged from 300–380 nm and 240–285 nm, characteristic, respectively, of bands I and II of flavonoids [31] (Supplementary Figure S4).

Aiming at improving the chromatographic separation, the local minimum function was applied in the last fractionation. This tool of the Glider CPC software moves the probe to the next tube during a collection phase when an inflection of the signal appears on the chromatogram, allowing us to separate fractions in different tubes regardless of their volume and, although an accurate prediction of sample volume and tube quantity, as in a conventional CPC separation does not seem to be observed, it can help to separate poorly resolved chromatographic peaks.

For this, the rotor spinning was adjusted to 1300 rpm with a flow rate of 6 mL·min<sup>−1</sup>. The stationary phase retention was maintained at 70%, and 167 fractions were obtained with the local minimum function. Although a larger number of fractions were collected, TLC analysis showed an improvement in the separation profile (Supplementary Figure S5). The obtained fractions with different chemical compounds distribution were pooled into

18 final fractions, according to their chemical and chromatographic similarities by TLC profile (Supplementary Table S1). The anti-influenza activity of the simplified fractions was evaluated to target the active fractions and the chemical compounds annotation through LC-HRMS/MS analysis.

### 2.2. In Vitro Anti-Influenza Activity of Fractions Acquired by CPC

The 18 final fractions from the third fractionation of the *n*-butanol extract from *S. glycyarpa* were first screened for their cytotoxicity at  $100 \mu\text{g}\cdot\text{mL}^{-1}$ , evaluated in Madin-Darby Canine Kidney (MDCK) cells by the MTT (3-[4,5-dimethylthiazol-2-yl]-2,5 diphenyl tetrazolium bromide) assay. Most of the fractions, as well as the crude *n*-butanol extract (SGBu) and OST-car (control), were not cytotoxic and maintained cell viability above 80%, except for SGJ, SGL, SGM, SGN, SGP, SGQ, and SGR, which reduced cell viability to values below 50% (Supplementary Table S2).

In the sequence, viral replication inhibition assays were performed with the least cytotoxic fractions (cell viability > 80%) to verify their antiviral activity against influenza virus. MDCK cells were infected with influenza A(H1N1) virus and then treated for 24 and 48 hours post-infection (hpi) with concentrations of 25 and  $100 \mu\text{g}\cdot\text{mL}^{-1}$  of the fractions, which, based on our previous results of *S. glycyarpa* *n*-butanol extract (SGBu)  $\text{EC}_{50}$  [8], were expected to inhibit virus replication by 50 and 90%, respectively. The results showed that the treatment with  $100 \mu\text{g}\cdot\text{mL}^{-1}$  of the fractions, for 24 h, was more potent than that with  $25 \mu\text{g}\cdot\text{mL}^{-1}$  (Figure 1 and Supplementary Table S3). The fractions SGA, SGC, SGD, and SGO presented the highest inhibition levels (above 74%) at a concentration of  $100 \mu\text{g}\cdot\text{mL}^{-1}$ . Although less pronounced, viral replication inhibition was maintained until 48 h of treatment with  $100 \mu\text{g}\cdot\text{mL}^{-1}$  (Figure 1 and Supplementary Table S3). The clinically approved anti-influenza drug oseltamivir (OST) and the previously described SGBu were used as positive controls and inhibited influenza replication by 100 and 95% at  $100 \mu\text{g}\cdot\text{mL}^{-1}$ , respectively, after 24 hpi, remaining with high percentages of inhibition even after 48 hpi (Figure 1 and Supplementary Table S3).

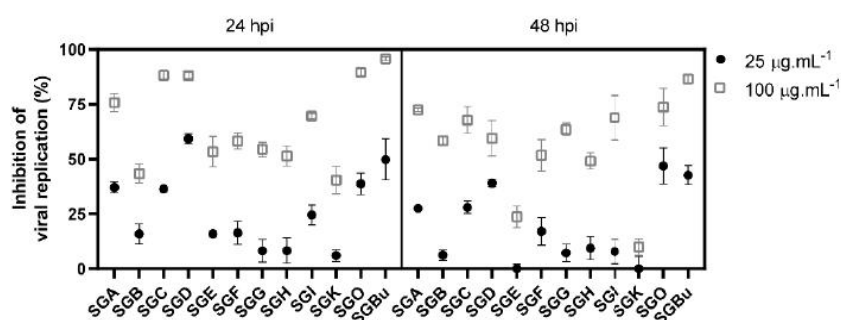


**Figure 1.** Inhibition of influenza virus replication by CPC pooled fractions with cell viability above 80%.

### 2.3. LC-HRMS/MS and Molecular Networking Analyses of CPC Fractions

Untargeted LC-HRMS/MS analyses in positive and negative ionization modes were performed in the CPC fractions to characterize their metabolites. The resulting spectral data of fractions with cell viability above 80% and antiviral activity against influenza virus (Figure 1) were analyzed using the GNPS platform to generate molecular networks. For this, molecular network creation was based on mass spectrometry data analysis of the SGBu extract (G1), the most active fractions (enumerated as decreasing activity results) SGO (G2), SGD (G3), SGC (G4), and SGA (G5) (Supplementary Figure S6), and the least active fractions (LAF), which were SGB, SGE, SGF, SGG, SGH, SGI and SGK, all placed into the same group (G6). After data processing, a total of 30 networks were obtained, comprising 592 nodes for positive mode and 8 networks with 23 nodes for negative mode (Figure 2). Several hits were obtained, all of them checked manually by MS/MS data interpretation



to validate the identifications. Most of the annotated compounds in the CPC fractions belong to the isoquinoline alkaloid class, in addition to other compounds, such as flavonoid glycosides and dihydrochalcones.

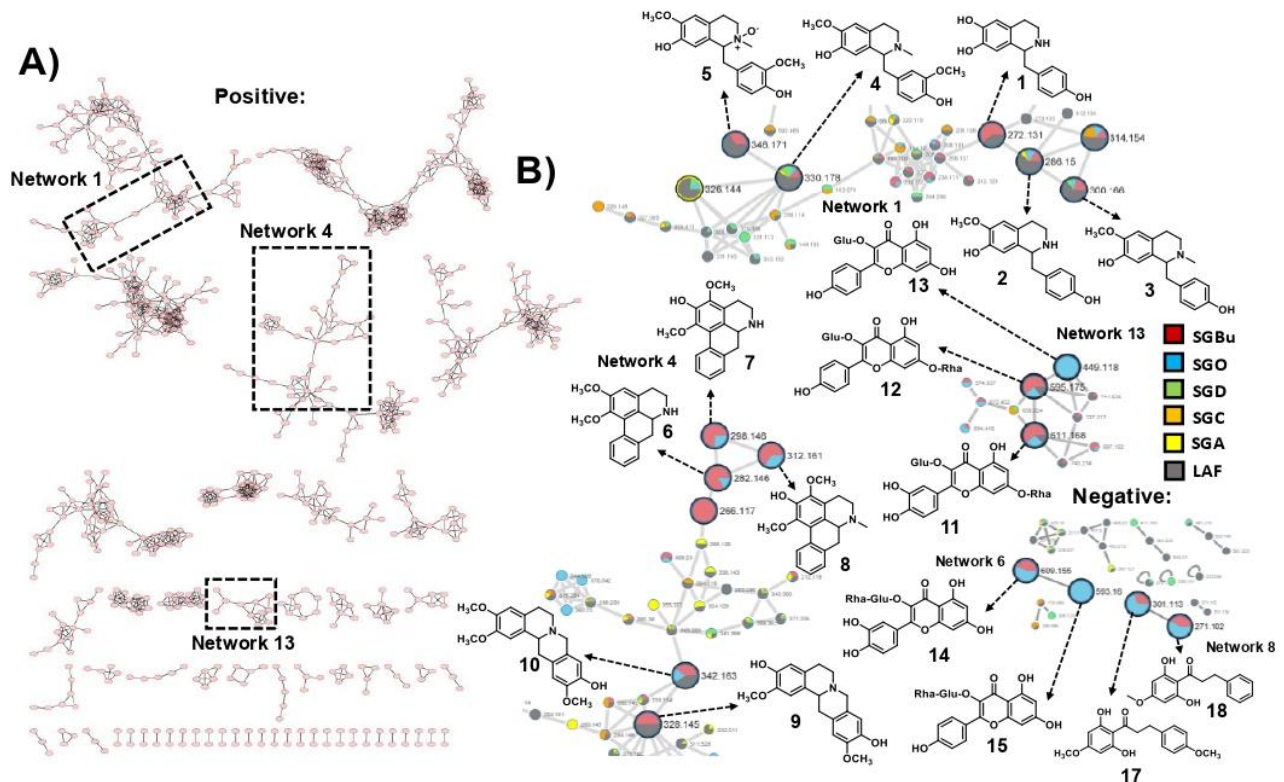


**Figure 2.** (A) Molecular networking through LC-HRMS/MS data in positive ionization mode of SGBu and bioactive CPC fractions. (B) Focusing on the networks with the annotated compounds in bioactive fractions through LC-HRMS/MS data in positive and negative ionization modes. Crude *n*-butanol extract (SGBu) ■; the most active fractions (SGO) ■, (SGD) ■, (SGC) ■ and (SGA) ■; the least active fractions (LAF) ■, which were SGB, SGE, SGF, SGG, SGH, SGI and SGK.

Among the most active fractions, all displayed alkaloids within their composition. SGA, SGC, and SGD, collected during elution step within the first 43 min of process, are composed of coclaurine **2** and reticuline **4**, in addition to *N*-methylcoclaurine **3** for SGD. The molecular network 1 displays the nodes of **2** ( $m/z$  286.1444), **3** ( $m/z$  300.1593), and **4** ( $m/z$  330.1720), whereas other nodes with  $m/z$  272.1283 and  $m/z$  346.1655, which can correspond to demethyl-coclaurine **1** and reticuline *N*-oxide **5**, were annotated in LAF only (Table 1); (Figure 2). These attributions were proposed based on diagnostic fragment ions and neutral losses characteristic for benzyloisoquinoline alkaloids as previously described [32].

Moreover, other nodes in network 4 ( $m/z$  328.1564, **9** and  $m/z$  342.1704, **10**) are consistent with the structures of alkaloids. However, their fragmentation indicates that they are tetrahydroprotoberberine derivatives, especially due to the appearance of the diagnostic fragment ion of  $m/z$  178, formed via a retro-Diels-Alder ring opening, typical in MS/MS spectra of this type of alkaloid skeleton [32]. Therefore, these compounds were annotated as stepholidine **9** and isocorypalmine **10**. All these compounds were eluted and detected in LAF. In addition, compound **10** also appeared at SGO active fraction (Table 1); (Figure 2).

**Table 1.** LC-HRMS/MS data of annotated compounds in CPC bioactive fractions (MS/MS spectra in Supplementary Figures S7–S23).

CPC Fractions	[M + H] <sup>+</sup> ( <i>m/z</i> )	[M – H] <sup>–</sup> ( <i>m/z</i> )	Molecular Formula	Error (ppm)	MS/MS (MS <sup>2</sup> )	Proposed Compound
<b>Network 1 (Positive Ionization Mode Data)</b>						
LAF	272.1283	-	C <sub>16</sub> H <sub>17</sub> NO <sub>3</sub>	–1.10	255.10, 237.08, 223.07, 209.09, 194.06	Demethyl-coclaurine <b>1</b>
All fractions	286.1444	-	C <sub>17</sub> H <sub>19</sub> NO <sub>3</sub>	0.35	269.12, 237.09, 209.09, 194.07, 178.08, 115.05, 107.05	Coclaurine <b>2</b>
SGO, SGD, LAF	300.1593	-	C <sub>18</sub> H <sub>21</sub> NO <sub>3</sub>	–1.99	269.11, 257.11, 237.09, 225.08, 209.09, 194.07, 181.06, 107.04	N-methylcocclaurine <b>3</b>
All fractions	330.1720	-	C <sub>19</sub> H <sub>23</sub> NO <sub>4</sub>	4.54	299.13, 265.08, 207.0793, 192.10, 178.08, 163.06, 137.06	Reticuline <b>4</b>
LAF	346.1655	-	C <sub>19</sub> H <sub>23</sub> NO <sub>5</sub>	0.28	329.16, 312.12, 299.13, 286.11, 267.09, 238.08, 185.08, 137.06, 115.05, 91.05	Reticuline N-oxide <b>5</b>
<b>Network 4 (Positive Ionization Mode Data)</b>						
SGO	282.1475	-	C <sub>18</sub> H <sub>19</sub> NO <sub>2</sub>	–6.73	265.12, 250.10, 234.10, 219.07, 207.08, 189.07, 179.08	Nornuciferine <b>6</b>
SGO	298.1438	-	C <sub>18</sub> H <sub>19</sub> NO <sub>3</sub>	–1.67	281.11, 266.09, 250.09, 233.06, 221.09, 205.06, 189.06, 178.07	Isopiline <b>7</b>
SGO	312.1595	-	C <sub>19</sub> H <sub>21</sub> NO <sub>3</sub>	–1.28	295.13, 280.10, 264.11, 249.08, 234.06, 219.07	O-Methylisopiline <b>8</b>
LAF	328.1564	-	C <sub>19</sub> H <sub>21</sub> NO <sub>4</sub>	4.87	313.13, 192.10, 178.08	Stepholidine <b>9</b>
SGO, LAF	342.1704	-	C <sub>20</sub> H <sub>23</sub> NO <sub>4</sub>	–0.29	324.19, 312.12, 297.11, 194.08, 178.08, 163.06	Isocorypalmine <b>10</b>
<b>Network 13 (Positive Ionization Mode Data)</b>						
SGO, LAF	611.1639	-	C <sub>27</sub> H <sub>30</sub> O <sub>16</sub>	4.41	465.10, 303.05	Quercetin-3-O- rhamnoside-7-O-glucoside <b>11</b> Quercetin-3-O-glucoside- 7-O-rhamnoside <b>11</b>
SGO, LAF	595.1705	-	C <sub>27</sub> H <sub>30</sub> O <sub>15</sub>	7.05	449.11, 287.05	Kaempferol-3-O- glucoside-7-O-rhamnoside <b>12</b>
SGO	449.1096	-	C <sub>21</sub> H <sub>20</sub> O <sub>11</sub>	2.67	287.05, 249.14, 227.17, 100.11	Kaempferol 3-O-glucoside <b>13</b>

Table 1. Cont.

CPC Fractions	[M + H] <sup>+</sup> ( <i>m/z</i> )	[M – H] <sup>–</sup> ( <i>m/z</i> )	Molecular Formula	Error (ppm)	MS/MS (MS <sup>2</sup> )	Proposed Compound
Networks 6 and 8 (Negative Ionization Mode Data)						
SGO	-	609.1524	C <sub>27</sub> H <sub>30</sub> O <sub>16</sub>	11.0	300.03, 271.02, 243.03, 199.04, 151.00, 148.01, 108.02	Quercetin-3- <i>O</i> -rutinoside (Rutin) <b>14</b>
SGO	-	593.1579	C <sub>27</sub> H <sub>30</sub> O <sub>15</sub>	–12.0	285.04, 255.03, 227.04, 211.0433, 183.05, 107.01	Kaempferol-3- <i>O</i> - rutinoside <b>15</b>
SGO	-	301.1104	C <sub>17</sub> H <sub>18</sub> O <sub>5</sub>	9.30	253.05, 225.05, 188.05, 165.02, 152.01, 124.01	2',6'-Dihydroxy-4,4'- dimethoxydihydrochalcone <b>16</b>
SGO	-	271.1012	C <sub>16</sub> H <sub>16</sub> O <sub>4</sub>	15.5	238.06, 210.07, 184.00, 165.02, 152.01, 124.01	2',6'-Dihydroxy-4'- methoxy-dihydrochalcone <b>17</b>

On the other hand, in fractions collected in the extrusion step with the change from mobile phase to upper organic phase, aporphine alkaloids, *O*-glycosylated flavonoids, and dihydrochalcones eluted in SGO fraction appeared in networks 4, 6, 8, and 13 (Table 1); (Figure 2). Three aporphine derivatives grouped at network 4 were annotated based on their fragmentation pattern. As expected for aporphines, the initial losses of 17 u were observed, and intense corresponding fragments were formed. Moreover, some fragmentation features suggested adjacent methoxy and hydroxy-groups in compound 7 (CH<sub>3</sub>OH followed by CO losses, –32 u and –28 u) and adjacent methoxy groups in compounds 6 and 8 (CH<sub>3</sub> and CH<sub>3</sub>O group radical losses, –15 u and –31 u, respectively) [32,33]. Thus, nornuciferine 6, isopiline 7, and *O*-methylisopiline 8 were annotated.

Additionally, the ions at *m/z* 611.1639 **11**, *m/z* 595.1705 **12**, and *m/z* 449.1096 **13** in the positive mode, and *m/z* 609.1524 **14** and *m/z* 593.1579 **15** in the negative mode, showed neutral sugar losses of 146 u (deoxyhexosides) and 162 u (hexosides) on their MS/MS spectra. Compounds **11** and **14**, displayed fragments consistent with the aglycone quercetin, while compounds **12**, **13**, and **15** displayed those of kaempferol as their aglycone. Thus **11**, **12**, **13**, **14**, and **15** were annotated as quercetin 3-*O*-rhamnoside-7-*O*-glucoside or quercetin 3-*O*-glucoside-7-*O*-rhamnoside, kaempferol 3-*O*-glucoside-7-*O*-rhamnoside, kaempferol 3-*O*-glucoside, quercetin-3-*O*-rutinoside (rutin), and kaempferol 3-*O*-rutinoside, respectively [34–36]. In addition, the MS/MS spectra for the compounds of *m/z* 301.1104 **16** and *m/z* 271.1012 **17** observed at the negative mode displayed diagnostic ions of A-type fragment [<sup>1</sup>A-CH<sub>3</sub>]<sup>–</sup>, common for dihydrochalcones [37]. Therefore, these compounds **16** and **17** were assigned as 2',6'-dihydroxy-4,4'-dimethoxydihydrochalcone and 2',6'-dihydroxy-4'-methoxy-dihydrochalcone, respectively.

The SGJ, SGL, SGM, SGN, SGP, SGQ, and SGR fractions, with cell viability values below 50%, also had their chemical profile investigated by LC-HRMS/MS. The ion of *m/z* 328.1564 [M + H]<sup>+</sup> corresponding to stepholidine **9** (Supplementary Figure S15) was common for SGJ, SGL, SGM, SGN, SGP, and SGQ. Furthermore, the MS/MS spectrum of compound of *m/z* 314.1792 [M]<sup>+</sup> in the SGP, SGQ and SGR showed characteristic fragment ions for magnocurarine (Supplementary Figure S24) [38]. In addition to alkaloids in SGJ, SGL, and SGQ, flavonoids were observed with galloyl units and *O*-triglycosylated flavonoid. The ion of *m/z* 727.2089 [M + H]<sup>+</sup> in SGJ and SGL showed, in MS/MS spectrum, fragments of *m/z* 449 and *m/z* 287, which likely result from a loss of pentose, deoxyhexose, and hexose units, corresponding to kaempferol-3-*O*-hexose-*O*-deoxyhexose-*O*-pentoside (Supplementary Figure S25) [39]. In SGQ, the ions of *m/z* 585.2190 [M – H]<sup>–</sup> and *m/z* 615.2335 [M – H]<sup>–</sup> produced the product ions of *m/z* 301 [M – H-152-132]<sup>–</sup> (Supplementary



Figure S26) and  $m/z$  301  $[M - H-152-162]^-$  (Supplementary Figure S27), indicating a galloyl-pentoside and galloyl-hexoside moiety losses, respectively. Through this fragmentation pattern, these compounds were annotated as quercetin-3-*O*-(2''-*O*-galloyl)-pentoside and quercetin-3-*O*-(6'-*O*-galloyl)- $\beta$ -galactopyranoside [40,41].

### 3. Materials and Methods

#### 3.1. Solvents and Chemical Reagents

Analytical grade solvents from Tedia<sup>®</sup> Brazil (Tedia, Rio de Janeiro, Brazil) were used for the preparation of extracts. CPC fractionation was performed with ultrapure water (18.2 M $\Omega$ -cm) prepared with a PURELAB<sup>®</sup> Classic system (ELGA, Woodridge, IL, USA), and analytical grade solvents from Tedia<sup>®</sup> Brazil (Rio de Janeiro, Brazil). LC-HRMS/MS analyses were carried out using analytical grade solvents from Tedia<sup>®</sup> Brazil (Rio de Janeiro, Brazil), ammonium formate (CAS number: 540-69-2) purchased from Sigma-Aldrich<sup>®</sup>, formic acid from Vetec Química Fina<sup>®</sup>, LTDA (Rio de Janeiro, Brazil), and ultrapure water (18.2 M $\Omega$ -cm).

#### 3.2. Plant Material and Extracts Preparation

Leaves of *Siparuna glycyarpa* (Ducke) S.S. Renner & Hausner were collected at Reserva Adolpho Ducke, Manaus, Brazil, in August 2015 and deposited at Instituto Nacional de Pesquisas da Amazônia (INPA) herbarium (Manaus, Brazil) under the registration INPA 269732. This research was authorized by the Directing Council of Genetic Heritage (Conselho de Gestão do Patrimônio Genético, CGEN) under the authorization A3C04CB. The leaves were dried and ground (101.97 g) and were extracted by percolation with ethanol 96° GL. Part of the crude ethanol extract (14.1 g, 13.8%  $w/w$ ) was fractionated by liquid-liquid extraction between water-methanol 7:3 ( $v/v$ ) and organic solvents affording *n*-hexane (2.80 g), dichloromethane (2.20 g), ethyl acetate (2.33 g), and *n*-butanol (2.18 g) extracts.

#### 3.3. Thin Layer Chromatography (TLC)

The preliminary analyses of the *n*-butanol extract, solvent system selection tests, and CPC fractions were performed on silica gel TLC plates (AL 60 F254 20 cm  $\times$  20 cm MERCK<sup>®</sup>, Darmstadt, Germany). The TLC plates were eluted with the organic phase of *n*-butanol-acetic acid-water (BAW) (8:2:10,  $v/v$ ), and the results were visualized under ultraviolet light (UV) (Spectroline CL-80 model) at 254 nm and 365 nm.

#### 3.4. Centrifugal Partition Chromatography (CPC)

##### 3.4.1. Apparatus

The fractionation step was performed on a CPC Lab System (Gilson, Middleton, WI, USA) that combines a PLC purification system (model 2050) with a CPC 250. The column has a total volume of 250 mL and can be used with a pressure up to 100 bar, flow rate up to 15 mL $\cdot$ min<sup>-1</sup>, and a maximum rotation speed of 3000 rpm. The PLC features a fraction collector and a built-in detector that measures the absorbance and sends the chromatogram to the onboard control software, Gilson Glider Prep (GGP) software. The dissolved sample was injected through the sample loop of 10 mL.

##### 3.4.2. Solvent System Selection

The solvent system composed of *n*-butanol-methanol-water was selected, and different volume ratios (10:0:10,  $v/v$ ), (9:1:10,  $v/v$ ), and (8:2:10,  $v/v$ ) were screened. The *n*-butanol extract (2 mg) was dissolved in test tubes containing 2 mL of each phase of the solvent systems and were shaken to allow compounds to partition between the two phases (Supplementary Figure S1).

##### 3.4.3. Solvent System and Sample Preparation

The selected solvent system *n*-butanol-methanol-water (9:1:10,  $v/v$ ) was thoroughly equilibrated and the two separated phases were degassed by ultra-sonication for 10 min.

The sample solution was prepared dissolving 500 mg of the *n*-butanol extract in 10 mL of the solvent system (1:1, *v/v*).

#### 3.4.4. CPC Fractionation Procedure

The fractionations were performed with the lower aqueous phase as mobile phase and upper organic phase as stationary phase (descending mode). The CPC column was first entirely filled with the upper organic stationary phase and then the lower aqueous mobile phase was pumped through the column at 6 mL·min<sup>-1</sup> flow rate in the descending mode until hydrostatic equilibrium, when the sample was injected into the CPC column. Three fractionations of the *n*-butanol extract were performed with different rotation speeds: 1000 and 1300 rpm and the UV monitoring at different wavelength (254 nm, 365 nm and 200–400 nm-full scan). In the first and second fractionations 47 tubes of 12 mL were collected (22 tubes with classic elution step and 25 tubes with extrusion step). For the last fractionation, the local minimum function was applied for the fraction collection step. A total of 167 fractions were collected: 94 fractions in the elution step, corresponding to 250 mL mobile phase (1.0 column-volume) and 73 fractions in the extrusion step, corresponding to 302.2 mL (1.2 column-volume) of pumped upper phase.

#### 3.5. CPC Fractions Preparation for Antiviral and Cytotoxicity Assays

Dried fractions and *S. glycyarpa* *n*-butanol extract were dissolved in dimethyl sulfoxide (DMSO) to a final concentration of 100 mg·mL<sup>-1</sup> (stock solution) for the *in vitro* tests. Cell culture medium was used to dilute fractions, and *n*-butanol extract and oseltamivir carboxylate (OST-car) were used to obtain the assays concentrations. For all assays, DMSO did not exceed 1% (*v/v*).

#### 3.6. Cells and Viruses

Madin-Darby Canine Kidney (MDCK) cells were cultured in Dulbecco's Modified Eagle Medium (DMEM; Life Technologies, Grand Island, NY, USA) supplemented with 10% fetal bovine serum (FBS; HyClone, Logan, UT, USA), 100 U/mL penicillin, and 100 mg/mL streptomycin (Sigma-Aldrich, Burlington, MA, USA) and maintained at 37 °C in a 5% CO<sub>2</sub> atmosphere.

Cell infection assays were performed with influenza A (IAV) strain (A/Michigan/45/2015), an influenza A(H1N1)pdm09 virus, propagated in MDCK cells. IAV was grown and titrated according to the World Health Organization (WHO) manual for the laboratory diagnosis and virological surveillance of influenza [42]. Viral stocks were aliquoted and stored at -70 °C for further studies.

The cell and virus were kindly provided by the Centers for Disease Control and Prevention (CDC, Atlanta, GA, USA) and Influenza Reagent Resources (IRR).

#### 3.7. Cell Viability (Cytotoxicity Assay)

Monolayers of 2 × 10<sup>4</sup> MDCK cells in 96-well plates were treated with 100 µg/mL of *n*-butanol extract from *S. glycyarpa* and fractions for 3 days. OST-car at 0.05 µM was used as control. The culture medium was removed and 5 mg/mL of (3-[4,5-dimethylthiazol-2-yl]-2,5 diphenyl tetrazolium bromide) (MTT) in phosphate-buffered saline (PBS) 1x was added. Cells were incubated for 2 h at 37 °C. A 10% *w/v* sodium dodecyl sulfate (SDS) solution was added followed by another 2 h-incubation period. The plate was read in a spectrophotometer at 570 nm.

#### 3.8. Influenza Replication Inhibition Assay

Monolayers of MDCK cells in 96-well plates (2 × 10<sup>4</sup> cells/well) were infected with influenza A/H1N1 virus at a multiplicity of infection (MOI) of 0.01 for 1 h at 37 °C. The inoculum was removed, and cells were treated with 25 or 100 µg/mL of *n*-butanol extract from *S. glycyarpa* and fractions for 24 h at 37 °C. OST-car at 0.0125 or 0.05 was used as control. These concentrations are equivalent to EC<sub>50</sub> and 4 times the EC<sub>50</sub> values for *S.*



*glycyarpa* *n*-butanol extract and OST-car [8]. After the incubation, the culture supernatant was collected, and viruses were quantified by viral neuraminidase activity.

### 3.9. Neuraminidase Activity

The activity of viral neuraminidase (NA) was measured in the viruses present in the supernatants harvested from the influenza replication inhibition assays using the NA-Star kit (Applied Biosystems, Foster City, CA, USA), according to the manufacturer's instructions. Briefly, culture supernatants were incubated for 30 min with a chemiluminescent neuraminidase substrate at room temperature, and then an accelerator solution was added triggering light emission from the cleaved substrate. The chemiluminescent signal was read in the luminometer.

### 3.10. Statistical Analysis

All the antiviral and cytotoxicity tests were performed at least three times, and the results are displayed as the mean  $\pm$  standard error, calculated using Excel 2010 for Windows software (Microsoft).

### 3.11. LC-HRMS/MS Analysis

Analysis of the CPC fractions were performed on an ultra-fast liquid chromatography (UFLC) apparatus (Shimadzu), coupled to a MicrOTOF-QIII-MS (Bruker Daltonics, Inc., Billerica, MA, USA) mass spectrometer with ESI ionization source. The samples (0.5 mg) were dissolved in 2 mL of methanol, and 3  $\mu$ L was injected on a column Acquity UPLC<sup>®</sup> BEH C18 (2.1 mm  $\times$  150 mm internal diameter (i.d.); 1.7  $\mu$ m particle size; Waters, Dublin, Ireland) heated at 40  $^{\circ}$ C. The mobile phase consisted of water–5 mM ammonium formate–0.1% formic acid (A) and methanol (B). The gradient conditions were set as B = 50% at 0 min, B = 99% at 10 min, B = 100% at 30 min and remains at 100% until 32 min, B = 50% at 35 min and remains at 50% until 45 min at a flow rate of 0.2 mL $\cdot$ min<sup>-1</sup>. The source temperature was set at 200  $^{\circ}$ C, 8 L $\cdot$ min<sup>-1</sup> dry gas (nitrogen) flow rate and 4 bar nebulizer gas pressure (nitrogen). Data were acquired in positive and negative ionization modes in the mass range of *m/z* 50–1200, and collision-induced dissociation (CID) cell energy was set to 20 eV. The chromatograms and mass spectra were processed in Bruker Daltonics ESI Compass Data Analysis software version 5.0 SR1 (Bruker Daltonics, Inc., Billerica, MA, USA).

### 3.12. Global Natural Products Social Molecular Networking (GNPS)

Product ion spectra arising from the LC-HRMS/MS analysis of the *S. glycyarpa* *n*-butanol extract and its bioactive fractions were analyzed and organized in molecular networks by using the GNPS platform (<http://gnps.ucsd.edu>, accessed on 21 October 2021) [43]. The MS/MS data were converted to the mzXML format with MS-Convert [44] and then uploaded on the GNPS Web platform. Parameters for molecular network generation were set as follows: the precursor ion mass tolerance of 0.05 Da, product ion tolerance of 0.5 Da, and fragment ions below 10 counts were removed from the MS/MS spectra. Molecular networks were generated using four minimum matched peaks and a cosine score of 0.65. Data were visualized using Cytoscape 3.7.0 software. Annotation of chemical compounds was performed by manual interpretation of MS/MS spectra in comparison with the databases inside GNPS. The MS/MS molecular network is accessible at the GNPS Web site with the following links: <https://gnps.ucsd.edu/ProteoSAFe/status.jsp?task=daf5b5b0355e4862b3f163d3d62052cc>, accessed on 21 October 2021, and <https://gnps.ucsd.edu/ProteoSAFe/status.jsp?task=9dc29a10767344f5902b709fdb440722>, accessed on 21 October 2021.

## 4. Conclusions

The search for new anti-influenza agents is essential for public health. In this study, the application of CPC enabled the bioassay-guided fractionation of *S. glycyarpa* *n*-butanol extract by using a solvent system that failed stationary phase retention on HSCCC, therefore



acquiring bioactive fractions. With the use of a local minimum function tool, it was possible to improve resolution during chromatographic separation. Different compounds were annotated through dereplication tools, while changing the mobile phase nature made it possible to obtain a distinct chemical profile of bioactive fractions composition. Furthermore, different compounds such as flavonoids with galloyl units and *O*-triglycosylated flavonoid were annotated in fractions with cell viability values below 50%. Benzyloisoquinolinic and aporphine alkaloids were annotated in the most bioactive fractions, whereas tetrahydroprotoberberines were at the least active ones. Moreover, glycosylated flavonoids derived from quercetin and kaempferol and dihydrochalcones were also annotated in one of the most active fractions, suggesting this group of compounds, along with the described alkaloids, were responsible for antiviral activity. Compound isolation is the aim of future research in order to assay their individual antiviral potential.

**Supplementary Materials:** The following are available online, Figure S1: TLC results for solvent system selection with the test tube partitioning test. Tested solvent systems: *n*-butanol–methanol–water (1) 10:0:10, (2) 9:1:10, (3) 8:2:10 (*v/v*). (UP) upper phase and (LP) lower phase. The TLC plate was eluted with the organic phase of *n*-butanol–acetic acid–water (8:2:10, *v/v*) solvent system followed by visualized under UV light (254 nm (A) and 365 nm (B)). Figure S2: (A) CPC-UV chromatogram of the *n*-butanol extract fractionation at 1000 rpm rotation (— 254 nm; — 365 nm; — 200–400 nm). (B) TLC analysis of CPC fractions pooled according to chemical and chromatographic similarities. Figure S3: (A) CPC-UV chromatogram of the *n*-butanol extract fractionation at 1300 rpm rotation (— 254 nm; — 365 nm; — 200–400 nm). (B) CPC fractions by TLC analysis. Figure S4: Ultraviolet spectra of selected fractions acquired by CPC fractionation at 1300 rpm rotation. Figure S5: (A) CPC-UV chromatogram of the *n*-butanol extract fractionation at 1300 rpm rotation and local minimum function (— 254 nm; — 365 nm; — 200–400 nm). (B) CPC fractions by TLC analysis. Figure S6: (A) SGO, (B) SGD, (C) SGA, (D) SGC LC-HRMS/MS analysis in positive ionization mode. (E) SGO LC-HRMS/MS analysis in negative ionization mode. Figure S7: (A) MS spectrum with  $m/z$  272.1283 [M + H]<sup>+</sup> and (B) MS<sup>2</sup> spectrum of demethyl-coclaurine 1. Figure S8: (A) MS spectrum with  $m/z$  286.1444 [M + H]<sup>+</sup> and (B) MS<sup>2</sup> spectrum of coclaurine 2. Figure S9: (A) MS spectrum with  $m/z$  300.1593 [M + H]<sup>+</sup> and (B) MS<sup>2</sup> spectrum of *N*-methylcoclaurine 3. Figure S10: (A) MS spectrum with  $m/z$  330.1720 [M + H]<sup>+</sup> and (B) MS<sup>2</sup> spectrum of reticuline 4. Figure S11: (A) MS spectrum with  $m/z$  346.1655 [M + H]<sup>+</sup> and (B) MS<sup>2</sup> spectrum of reticuline *N*-oxide 5. Figure S12: (A) MS spectrum with  $m/z$  282.1475 [M + H]<sup>+</sup> and (B) MS<sup>2</sup> spectrum of nornuciferine 6. Figure S13: (A) MS spectrum with  $m/z$  298.1438 [M + H]<sup>+</sup> and (B) MS<sup>2</sup> spectrum of isopiline 7. Figure S14: (A) MS spectrum with  $m/z$  312.1595 [M + H]<sup>+</sup> and (B) MS<sup>2</sup> spectrum of *O*-methylisopiline 8. Figure S15: (A) MS spectrum with  $m/z$  328.1564 [M + H]<sup>+</sup> and (B) MS<sup>2</sup> spectrum of stepholidine 9. Figure S16: (A) MS spectrum with  $m/z$  342.1704 [M + H]<sup>+</sup> and (B) MS<sup>2</sup> spectrum of isocorypalmine 10. Figure S17: (A) MS spectrum with  $m/z$  611.1639 [M + H]<sup>+</sup> and (B) MS<sup>2</sup> spectrum of quercetin-3-*O*-rhamnoside-7-*O*-glucoside or quercetin-3-*O*-glucoside-7-*O*-rhamnoside 11. Figure S18: (A) MS spectrum with  $m/z$  595.1705 [M + H]<sup>+</sup> and (B) MS<sup>2</sup> spectrum of kaempferol-3-*O*-glucoside-7-*O*-rhamnoside 12. Figure S19: (A) MS spectrum with  $m/z$  449.1096 [M + H]<sup>+</sup> and (B) MS<sup>2</sup> spectrum of kaempferol 3-*O*-glucoside 13. Figure S20: (A) MS spectrum with  $m/z$  609.1524 [M – H]<sup>–</sup> and (B) MS<sup>2</sup> spectrum of quercetin-3-*O*-rutinoside (Rutin) 14. Figure S21: (A) MS spectrum with  $m/z$  593.1579 [M – H]<sup>–</sup> and (B) MS<sup>2</sup> spectrum of kaempferol-3-*O*-rutinoside 15. Figure S22: (A) MS spectrum with  $m/z$  301.1104 [M – H]<sup>–</sup> and (B) MS<sup>2</sup> spectrum of 2',6'-dihydroxy-4,4'-dimethoxydihydrochalcone 16. Figure S23: (A) MS spectrum with  $m/z$  271.1012 [M – H]<sup>–</sup> and (B) MS<sup>2</sup> spectrum of 2',6'-dihydroxy-4'-methoxydihydrochalcone 17. Figure S24. MS<sup>2</sup> spectrum of magnocurarine  $m/z$  314.1792 [M]<sup>+</sup>. Figure S25. MS<sup>2</sup> spectrum of kaempferol-3-*O*-hexose-*O*-deoxyhexose-*O*-pentoside  $m/z$  727.2089 [M + H]<sup>+</sup>. Figure S26. MS<sup>2</sup> spectrum of quercetin-3-*O*-(2'-*O*-galloyl)-pentoside  $m/z$  585.2190 [M – H]<sup>–</sup>. Figure S27. MS<sup>2</sup> spectrum of quercetin-3-*O*-(6'-*O*-galloyl)-β-galactopyranoside  $m/z$  615.2335 [M – H]<sup>–</sup>. Table S1: Pooled fractions from the *n*-butanol extract fractionation at 1300 rpm rotation and local minimum function (Supplementary Figure S5). Table S2: Cell viability of pooled fractions from the *n*-butanol extract fractionation by CPC. Table S3: Anti-influenza activity of CPC pooled fractions with cell viability above 80%.

**Author Contributions:** Data curation, C.M.L., C.V.A.d.S., H.H.F.K., M.D.M., C.d.Q.S. and N.F.-R.; Funding acquisition, G.G.L., S.G.L., M.D.M. and B.G.V.; Investigation, C.M.L., M.D.M., A.R.T. and C.B.d.A.; Methodology, L.L.O.d.M., I.d.C.R., C.M.L., C.V.A.d.S., A.R.T., C.B.d.A., H.H.F.K., R.C.S. and B.G.V.; Supervision, R.C.S., M.D.M., C.d.Q.S. and N.F.-R.; Visualization, L.L.O.d.M. and I.d.C.R.; Writing—original draft preparation, C.M.L.; Writing—review and editing, M.D.M., C.d.Q.S., N.F.-R., H.H.F.K., G.G.L. and S.G.L. All authors have read and agreed to the published version of the manuscript.

**Funding:** This research was funded by FAPERJ, CNPQ and CAPES.

**Institutional Review Board Statement:** Not applicable.

**Informed Consent Statement:** Not applicable.

**Data Availability Statement:** Not applicable.

**Acknowledgments:** We are grateful to FAPERJ, CNPq, and CAPES for the funding and CNPq for the scholarship. Nova Analítica and Gilson for lending the Gilson CPC apparatus. Mario de la Torre, ALH Field Application Specialist Gilson, for support with CPC apparatus and Gilson Glider Prep (GGP) software.

**Conflicts of Interest:** The authors declare no conflict of interest.

**Sample Availability:** Samples are not available.

## References

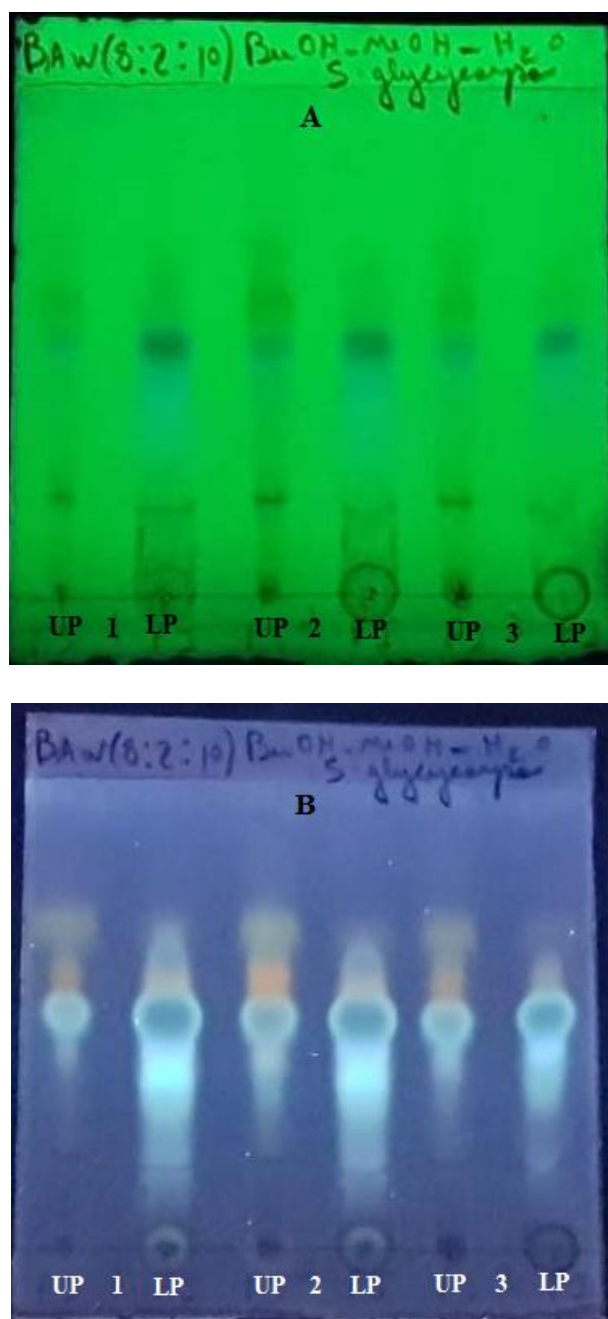
- Silva, T.; Salomon, P.S.; Hamerski, L.; Walter, J.; Menezes, R.B.; Siqueira, J.E.; Santos, A.; Santos, J.A.M.; Ferme, N.; Guimarães, T.; et al. Inhibitory effect of microalgae and cyanobacteria extracts on influenza virus replication and neuraminidase activity. *PeerJ* **2018**, *6*, e5716. [CrossRef]
- World Health Organization (WHO). Influenza (Seasonal). Available online: <http://www.who.int/mediacentre/factsheets/fs211/en/> (accessed on 14 June 2021).
- Sovann, L.Y.; Sar, B.; Kab, V.; Yann, S.; Kinzer, M.; Raftery, P.; Albalak, R.; Patel, S.; Hay, P.L.; Seng, H.; et al. An influenza A (H3N2) virus outbreak in the Kingdom of Cambodia during the COVID-19 pandemic of 2020. *Int. J. Infect. Dis.* **2021**, *103*, 352–357. [CrossRef]
- Newman, D.J.; Cragg, G. Natural products as sources of new drugs over the nearly four decades from 01/1981 to 09/2019. *J. Nat. Prod.* **2020**, *83*, 770–803. [CrossRef] [PubMed]
- Wani, A.R.; Yadav, K.; Khursheed, A.; Rather, M.A. An update and comprehensive review of the antiviral potential of essential oils and their chemical constituents with special focus on their mechanism of action against various influenza and coronaviruses. *Microb. Pathog.* **2021**, *152*, 1–14. [CrossRef] [PubMed]
- Leitão, G.G.; Soares, S.S.V.; Brito, T.B.M.; Monache, F.D. Kaempferol glycosides from *Siparuna apiosyce*. *Phytochemistry* **2000**, *55*, 679–682. [CrossRef]
- Renner, S.S.; Hausner, G. Siparunaceae. In *Flora Neotropica*; Monograph 95; The New York Botanical Garden: New York, NY, USA, 2005.
- Leal, C.M.; Simas, R.C.; Miranda, M.; Campos, M.F.; Gomes, B.A.; Siqueira, M.M.; Do Valle, G.; De Almeida, C.V.G.; Leitão, S.G.; Leitão, G.G. Amazonian *Siparuna* extracts as potential anti-influenza agents: Metabolic fingerprinting. *J. Ethnopharmacol.* **2021**, *270*, 1–7. [CrossRef] [PubMed]
- Moradi, M.T.; Karimi, A.; Shahrani, M.; Hashemi, L.; Goosheh, M.S.C. Anti-influenza virus activity and phenolic content of pomegranate (*Punica granatum* L.) peel extract and fractions. *Avicenna J. Med. Biotechnol.* **2019**, *11*, 285–291.
- Grienke, U.; Schmidtke, M.; Grafenstein, S.V.; Kirchmair, J.; Liedl, K.R.; Rollinger, J.M. Influenza neuraminidase: A druggable target for natural products. *Nat. Prod. Rep.* **2012**, *29*, 11–36. [CrossRef]
- Yang, Z.F.; Bai, L.P.; Huang, W.B.; Li, X.Z.; Zhao, S.S.; Zhong, N.S.; Jiang, Z.H. Comparison of in vitro antiviral activity of tea polyphenols against influenza A and B viruses and structure-activity relationship analysis. *Fitoterapia* **2014**, *93*, 47–53. [CrossRef]
- Giri, G.F.; Viarengo, G.; Furlán, R.L.E.; Suárez, A.G.; Eleonora, G.V.; Spanevello, R.A. Soybean hulls, an alternative source of bioactive compounds: Combining pyrolysis with bioguided fractionation. *Ind. Crop. Prod.* **2017**, *105*, 113–123. [CrossRef]
- Rufatto, L.C.; Luchtenberg, P.; Garcia, C.; Thomassigny, C.; Bouttier, S.; Henriques, J.A.P.; Roesch-Ely, M.; Dumas, F.; Moura, S. Brazilian red propolis: Chemical composition and antibacterial activity determined using bioguided fractionation. *Microbiol. Res.* **2018**, *214*, 74–82. [CrossRef]
- Nothias, L.F.; Nothias-Esposito, M.; Da Silva, R.; Wang, M.; Protsyuk, I.; Zhang, Z.; Sarvepalli, A.; Leyssen, P.; Touboul, D.; Costa, J.; et al. Bioactivity-based molecular networking for the discovery of drug leads in natural product bioassay-guided fractionation. *J. Nat. Prod.* **2018**, *81*, 758–767. [CrossRef]



15. Ma, R.; Zhou, R.; Tong, R.; Shi, S.; Chen, X. At-line hyphenation of high-speed countercurrent chromatography with sephadex LH-20 column chromatography for bioassay-guided separation of antioxidants from vine tea (*Ampelopsis grossedentata*). *J. Chromatogr. B* **2017**, *1040*, 112–117. [[CrossRef](#)]
16. Xu, F.; Huang, Y.; Ding, S.; Cai, X.; Liu, C.; Ji, Z.; Tang, J.; Yang, Y.; Tian, J. Counter-current fractionation-assisted bioassay-guided separation of active composition from the edible medicinal insect *Blaps rynchopetera* Fairmaire. *J. Chromatogr. A* **2019**, *1603*, 433–437. [[CrossRef](#)]
17. Xue, H.; Tan, J.; Zhu, X.; Li, Q.; Tang, J.; Cai, X. Counter-current fractionation assisted and bioassay-guided separation of active compounds from cranberry and their interaction with  $\alpha$ -glucosidase. *LWT* **2021**, *145*, 1–10. [[CrossRef](#)]
18. Costa, F.d.N.; Hubert, J.; Borie, N.; Kotland, A.; Hewitson, P.; Ignatova, S.; Renault, J.H. *Schinus terebinthifolius* countercurrent chromatography (part III): Method transfer from small CCC column to preparative CPC ones as a part of method development. *J. Chromatogr. A* **2017**, *1487*, 77–82. [[CrossRef](#)] [[PubMed](#)]
19. Messaili, S.; Colas, C.; Fougere, L.; Destandau, E. Combination of molecular network and centrifugal partition chromatography fractionation for targeting and identifying *Artemisia annua* L. antioxidant compounds. *J. Chromatogr. A* **2020**, *1615*, 1–21. [[CrossRef](#)]
20. Bojczuk, M.; Zyzelewicz, D.; Hodurek, P. Centrifugal partition chromatography- a review of recent applications and some classic references. *J. Sep. Sci.* **2017**, *40*, 1429–1630. [[CrossRef](#)] [[PubMed](#)]
21. Lima, A.S.; De Oliveira, B.S.; Shabudin, S.V.; Almeida, M.; Freire, M.G.; Bica, K. Purification of anthocyanins from grape pomace by centrifugal partition chromatography. *J. Mol. Liq.* **2021**, *326*, 1–9. [[CrossRef](#)]
22. Chami, M.C.; Bouju, E.; Lequemener, C.; De Vaumas, R.; Hadji-Minaglou, F.; Fernandez, X.; Michel, T. Purification of two valepotriates from *Centranthus ruber* by centrifugal partition chromatography: From analytical to preparative scale. *J. Chromatogr. A* **2018**, *1580*, 126–133. [[CrossRef](#)] [[PubMed](#)]
23. Zhang, Y.; He, Y.; Liu, C.; Li, S. Screening and isolation of potential neuraminidase inhibitors from leaves of *Ligustrum lucidum* Ait. Based on ultrafiltration, LC/MS, and online extraction-separation methods. *J. Chromatogr. B* **2018**, *1083*, 102–109. [[CrossRef](#)]
24. Mandova, T.; Audo, G.; Michel, S.; Grougnet, R. Off-line coupling of new generation centrifugal partition chromatography device with preparative high pressure liquid chromatography-mass spectrometry triggering fraction collection applied to the recovery of secoiridoid glycosides from *Centaurium erythraea* Rafn. (Gentianaceae). *J. Chromatogr. A* **2017**, *1513*, 149–156.
25. Kim, J.H.; Jung, E.J.; Lee, Y.J.; Gao, E.M.; Syed, A.S.; Kim, C.Y. Bioassay-guided separation of *Centipeda minima* using comprehensive linear gradient centrifugal partition chromatography. *Molecules* **2020**, *25*, 3077. [[CrossRef](#)]
26. Zhang, Y.; Liu, C.; Zhang, Z.; Qi, Y.; Wu, G.; Li, S. Solvent gradient elution for comprehensive separation of constituents with wide range of polarity in *Apocynum venetum* leaves by high-speed counter-current chromatography. *J. Sep. Sci.* **2010**, *33*, 2743–2748. [[CrossRef](#)]
27. Ren, D.B.; Yi, L.Z.; Qin, Y.H.; Yun, Y.H.; Deng, B.C.; Lu, H.M.; Chen, X.Q.; Liang, Y.Z. Systematic and practical solvent system selection strategy based on the nonrandom two-liquid segment activity coefficient model for real-life counter-current chromatography separation. *J. Chromatogr. A* **2015**, *1393*, 47–56. [[CrossRef](#)]
28. Michel, T.; Destandau, E.; Pecher, V.; Renimel, I.; Pasquier, L.; André, P.; Elfakir, C. Two-step centrifugal partition chromatography (CPC) fractionation of *Butea monosperma* (Lam.) biomarkers. *Sep. Purif. Technol.* **2011**, *80*, 32–37. [[CrossRef](#)]
29. Fromme, A.; Fischer, C.; Keine, K.; Schembecker, G. Characterization and correlation of mobile phase dispersion of aqueous-organic solvent systems in centrifugal partition chromatography. *J. Chromatogr. A* **2020**, *1620*, 460990. [[CrossRef](#)] [[PubMed](#)]
30. Sangster, A.W.; Stuart, K.L. Ultraviolet spectra of alkaloids. *Chem. Rev.* **1965**, *65*, 69–130. [[CrossRef](#)]
31. Villiers, A.; Venter, P.; Pasch, H. Recent advances and trends in the liquid-chromatography-mass-spectrometry analysis of flavonoids. *J. Chromatogr. A* **2016**, *1430*, 16–78. [[CrossRef](#)]
32. Lima, B.R.; Da Silva, F.M.A.; Soares, E.R.; De Almeida, R.A.; Da Silva-Filho, F.A.; Barison, A.; Costa, E.V.; Koolen, H.H.F.; De Souza, A.D.L.; Pinheiro, M.L.B. Integrative approach based on leaf spray mass spectrometry, HPLC-DAD-MS/MS, and NMR for comprehensive characterization of isoquinoline-derived alkaloids in leaves of *Onychopetalum amazonicum* R. E. Fr. *J. Braz. Chem. Soc.* **2020**, *31*, 79–89.
33. Stévigny, C.; Jiwan, J.L.H.; Rozenberg, R.; Hoffmann, E.; Quetin-Leclercq, J. Key fragmentation patterns of aporphine alkaloids by electrospray ionization with multistage mass spectrometry. *Rapid Commun. Mass Spectrom.* **2004**, *18*, 523–528. [[CrossRef](#)]
34. Sobral, F.; Calhelha, R.C.; Barros, L.; Dueñas, M.; Tomás, A.; Santos-Buelga, C.; Vilas-Boas, M.; Ferreira, I.C.F.R. Flavonoid composition and antitumor activity of bee bread collected in northeast Portugal. *Molecules* **2017**, *22*, 248. [[CrossRef](#)] [[PubMed](#)]
35. Ju, W.T.; Kwon, O.C.; Kim, H.B.; Sung, G.B.; Kim, H.W.; Kim, Y.S. Qualitative and quantitative analysis of flavonoids from 12 species of Korean mulberry leaves. *J. Food Sci. Technol.* **2018**, *55*, 1789–1796. [[CrossRef](#)] [[PubMed](#)]
36. Francescato, L.N.; Debenedetti, S.L.; Schwanz, T.G.; Bassani, V.L.; Henriques, A.T. Identification of phenolic compounds in *Equisetum giganteum* by LC-ESI-MS/MS and a new approach to total flavonoid quantification. *Talanta* **2013**, *105*, 192–203. [[CrossRef](#)] [[PubMed](#)]
37. Portet, B.; Fabre, N.; Rozenberg, R.; Habib-Jiwan, J.L.; Moulis, C.; Quetin-Leclercq, J. Analysis of minor flavonoids in *Piper hostmannianum* var. *berbicense* using liquid chromatography coupled with atmospheric pressure chemical ionization mass spectrometry. *J. Chromatogr. A* **2008**, *1210*, 45–54.
38. Nikolic, D.; Godecke, T.; Chen, S.N.; White, J.; Lankin, D.C.; Pauli, G.F.; Breemen, R.B.V. Mass spectrometric dereplication of nitrogen-containing constituents of black cohosh (*Cimicifuga racemosa* L.). *Fitoterapia* **2012**, *83*, 441–460. [[CrossRef](#)]

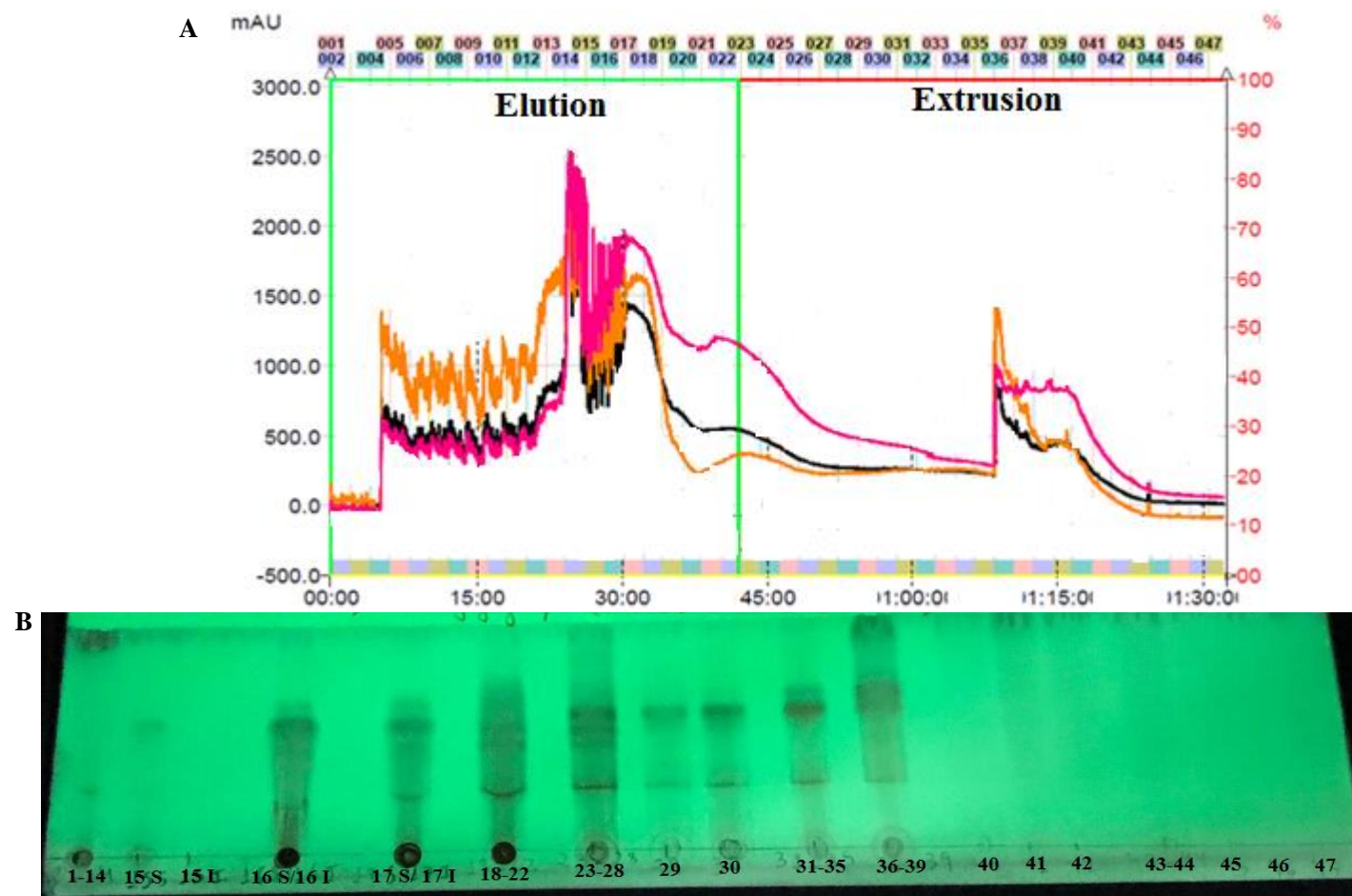
39. Martucci, M.E.P.; De Vos, R.C.H.; Carollo, C.A.; Gobbo-Neto, L. Metabolomics as a potential chemotaxonomical tool: Application in the genus *Vernonia* Schreb. *PLoS ONE* **2014**, *9*, e93149. [CrossRef]
40. Sobeh, M.; ElHawary, E.; Peixoto, H.; Labib, R.M.; Handoussa, H.; Swilam, N.; El-Khatib, A.H.; Sharapov, F.; Mohamed, T.; Krstin, S.; et al. Identification of phenolic secondary metabolites from *Schotia brachypetala* Sond. (Fabaceae) and demonstration of their antioxidant activities in *Caenorhabditis elegans*. *PeerJ* **2016**, *4*, e2404. [CrossRef]
41. Saldanha, L.L.; Vilegas, W.; Dokkedal, A.L. Characterization of flavonoids and phenolic acids in *Myrcia bella* Cambess. using FIA-ESI-IT-MS<sup>n</sup> and HPLC-PAD-ESI-IT-MS combined with NMR. *Molecules* **2013**, *18*, 8402–8416. [CrossRef]
42. World Health Organization (WHO). Manual for the Laboratory Diagnosis and Virological Surveillance of Influenza. 2011. Available online: [http://www.who.int/influenza/gisrs\\_laboratory/manual\\_diagnosis\\_surveillance\\_influenza/en/](http://www.who.int/influenza/gisrs_laboratory/manual_diagnosis_surveillance_influenza/en/) (accessed on 20 October 2021).
43. Aron, A.T.; Gentry, E.C.; McPhail, K.L.; Nothias, L.F.; Nothias-Esposito, M.; Bouslimani, A.; Petras, D.; Gauglitz, J.M.; Sikora, N.; Vargas, F.; et al. Reproducible molecular networking of untargeted mass spectrometry data using GNPS. *Nat. Protoc.* **2020**, *15*, 1954–1991. [CrossRef]
44. Holman, J.D.; Tabb, D.L.; Mallick, P. Employing ProteoWizard to convert raw mass spectrometry data. *Curr. Protoc. Bioinform.* **2014**, *46*, 13–24. [CrossRef] [PubMed]

## Supplementary material

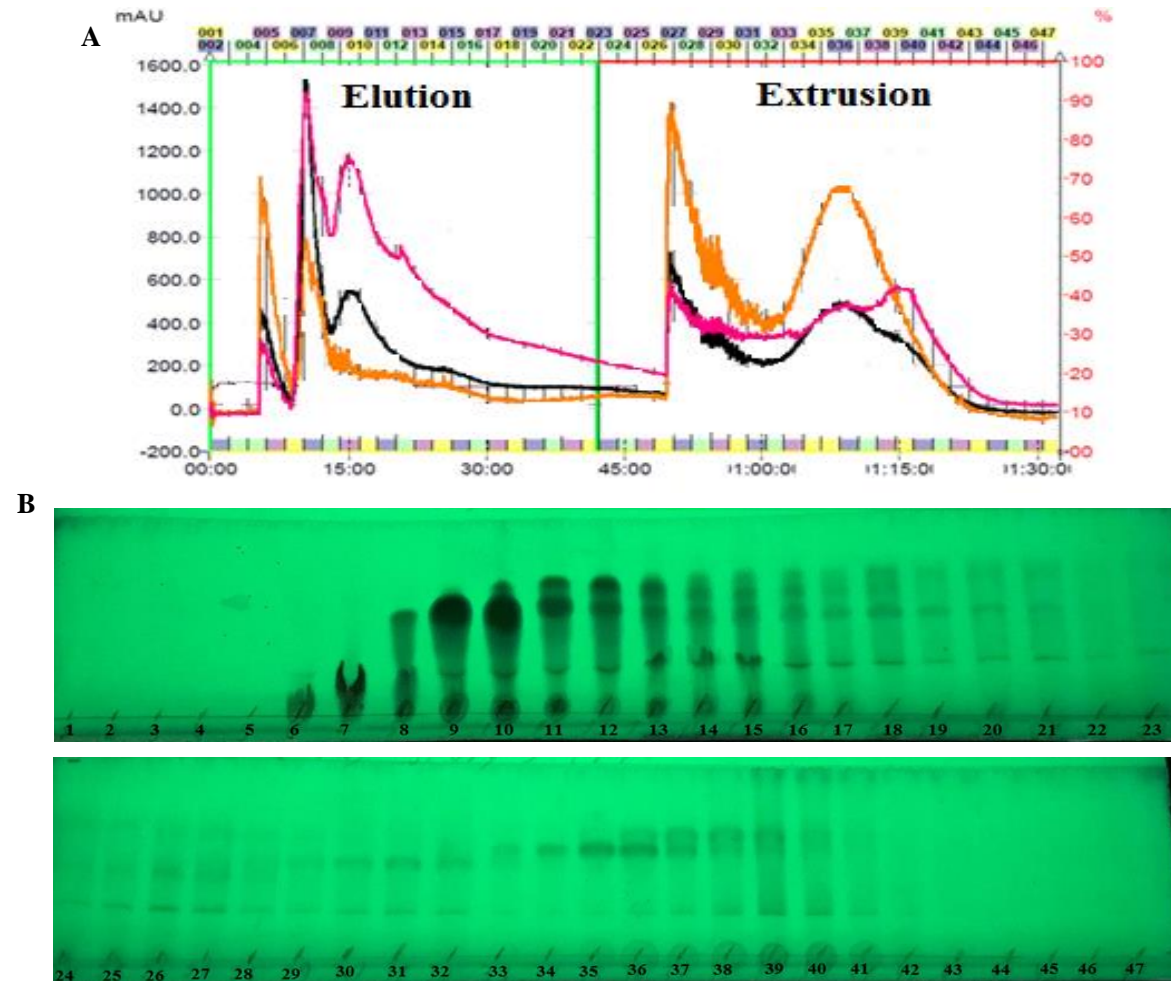


**Supplementary Figure S1.** TLC results for solvent system selection with the test tube partitioning test. Tested solvent systems: butanol-methanol-water (1) 10:0:10, (2) 9:1:10, (3) 8:2:10 (v/v). (UP) upper phase and (LP) lower phase. The TLC plate was eluted with the organic phase of butanol-acetic acid-water (8:2:10, v/v) solvent system followed by visualized under UV light (254 nm (A) and 365 nm (B)).

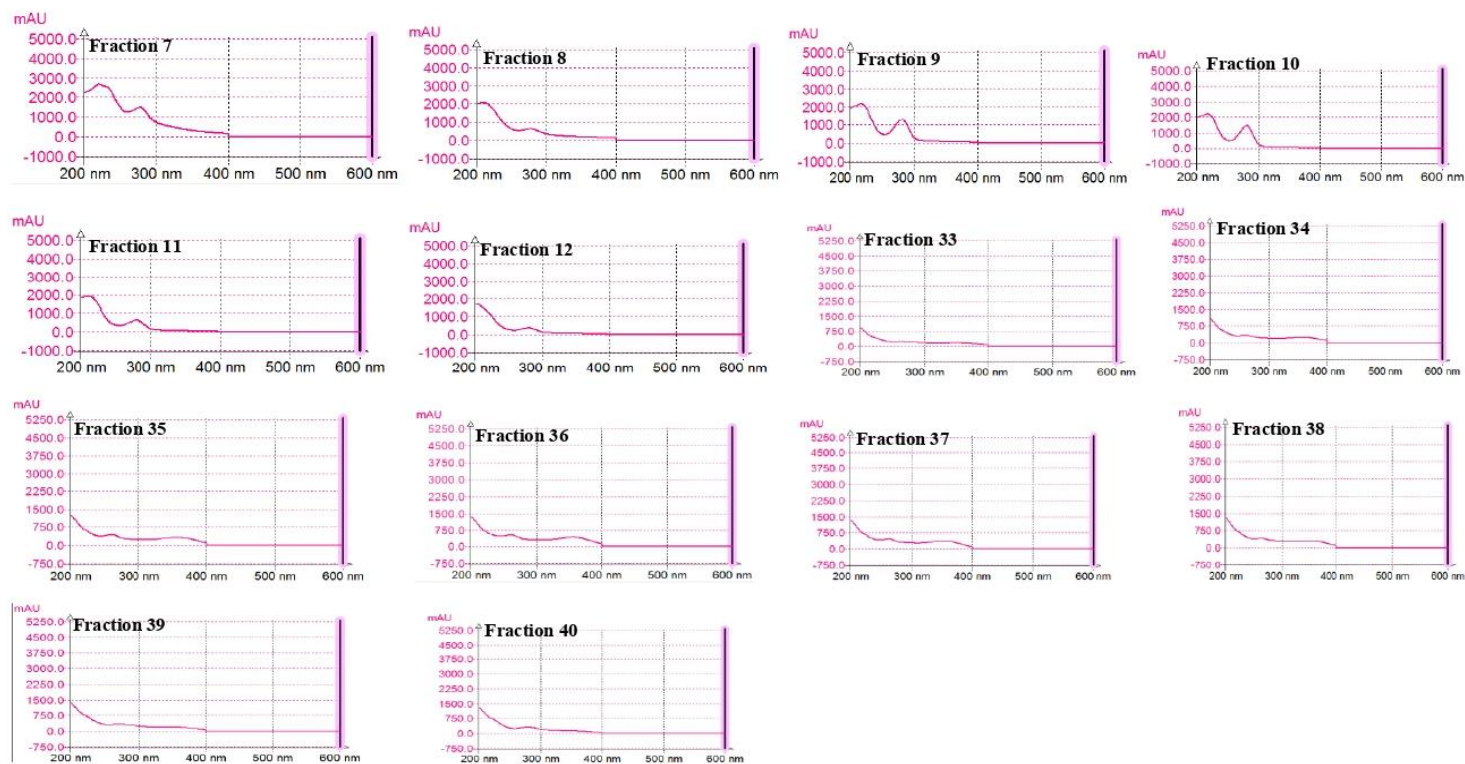




**Supplementary Figure S2.** (A) CPC-UV chromatogram of the *n*-butanol extract fractionation at 1000 rpm rotation (— 254 nm; — 365 nm; — 200-400 nm). (B) TLC analysis of CPC fractions pooled according to chemical and chromatographic similarities.

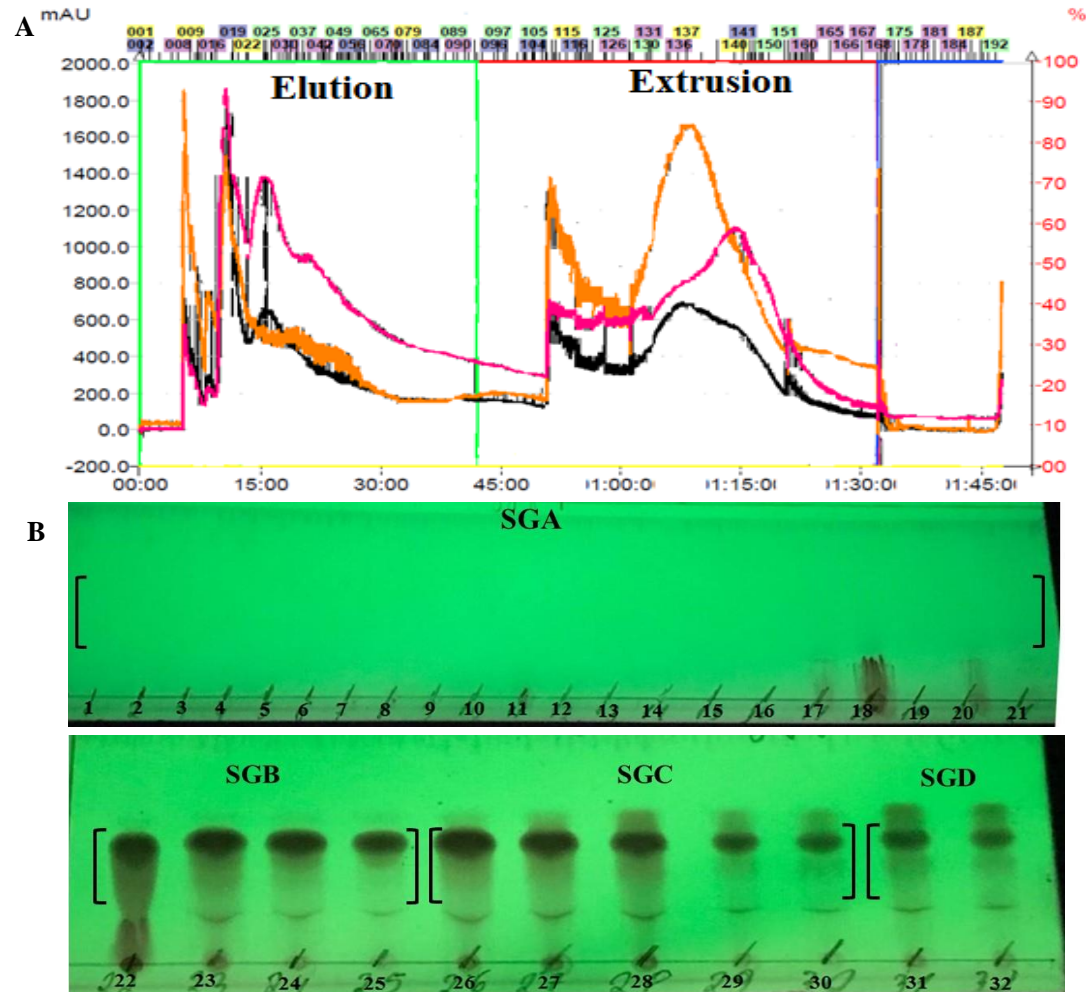


**Supplementary Figure S3.** (A) CPC-UV chromatogram of the *n*-butanol extract fractionation at 1300 rpm rotation (— 254 nm; — 365 nm; — 200-400 nm). (B) CPC fractions by TLC analysis.

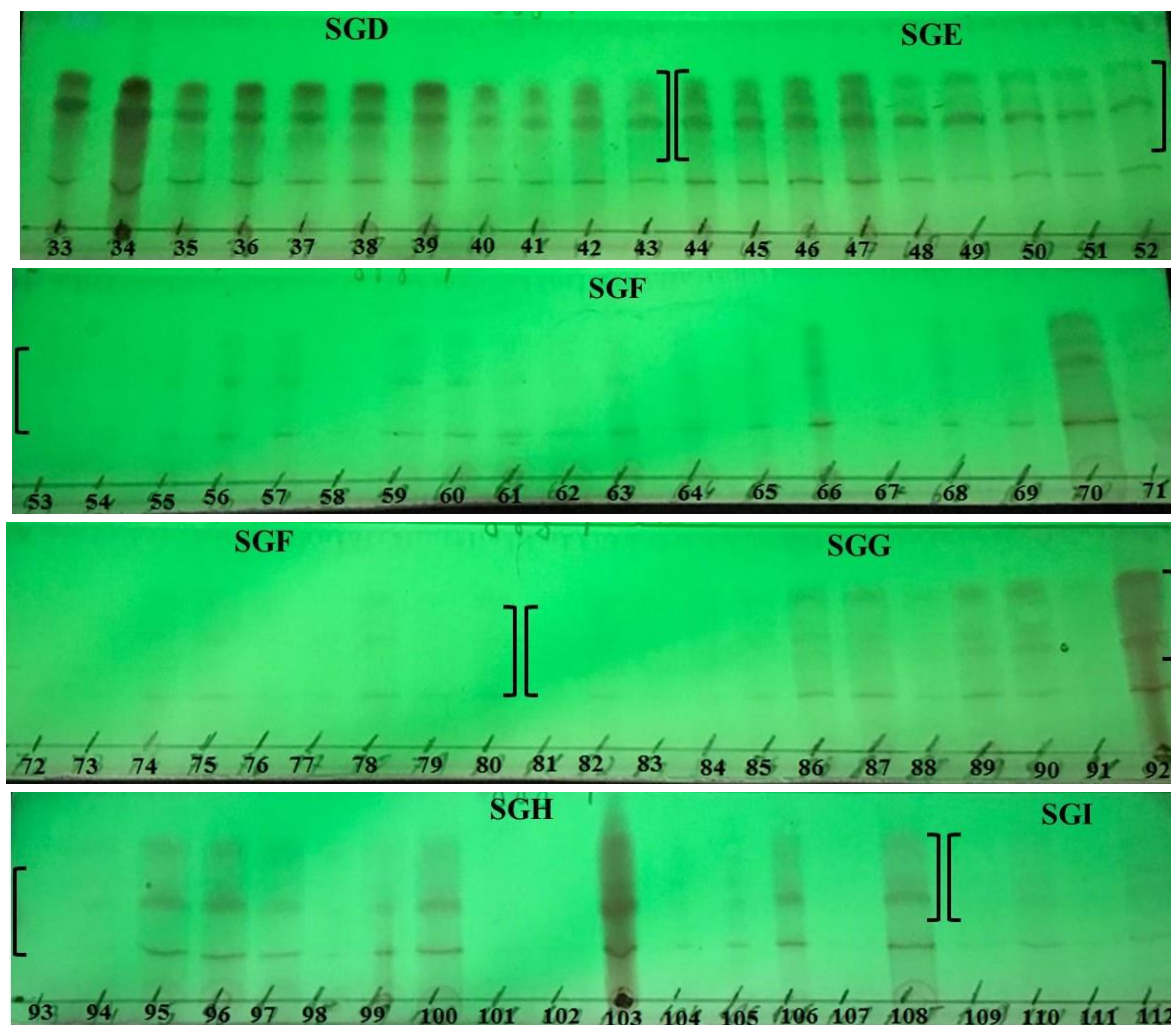


Supplementary Figure S4. Ultraviolet spectra of selected fractions acquired by CPC fractionation at 1300 rpm rotation.

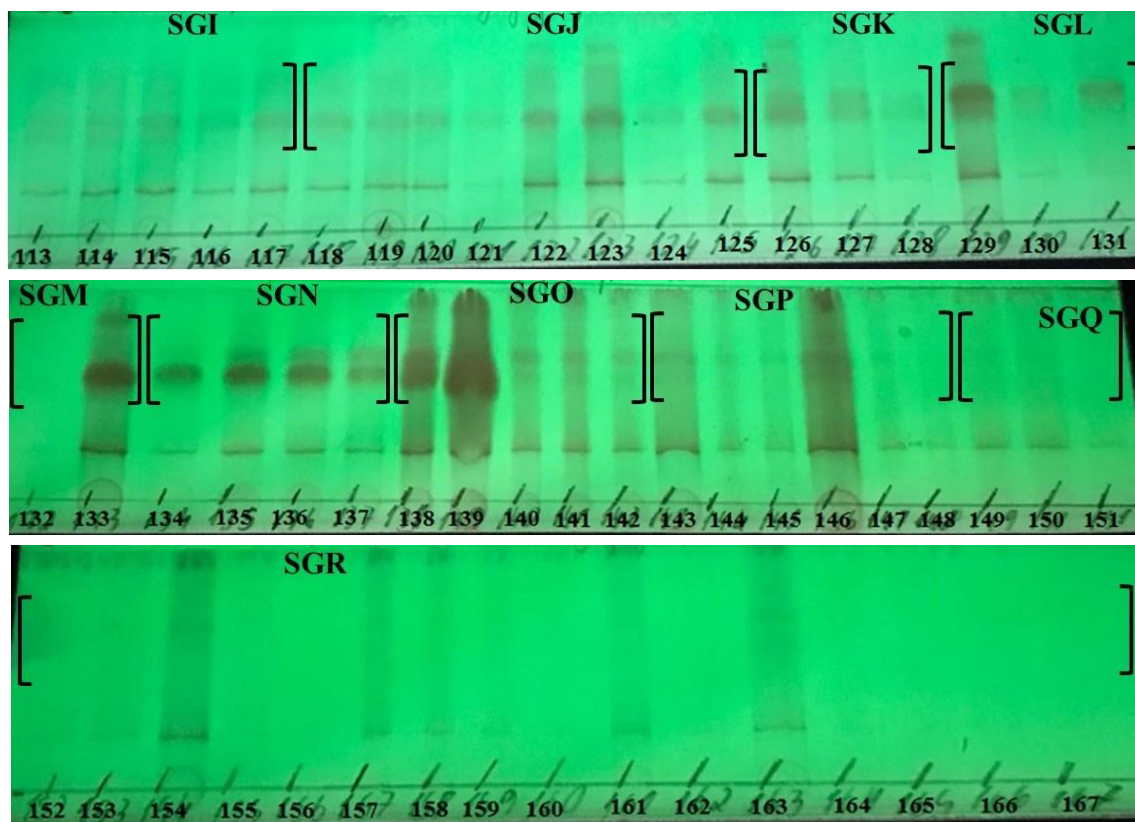




**Supplementary Figure S5.** (A) CPC-UV chromatogram of the *n*-butanol extract fractionation at 1300 rpm rotation and local minimum function (— 254 nm; — 365 nm; — 200-400 nm). (B) CPC fractions by TLC analysis.



Supplementary Figure S5 continuation sequence. (B) CPC fractions by TLC analysis.



Supplementary Figure S5 continuation sequence. (B) CPC fractions by TLC analysis.

**Supplementary Table S1.** Pooled fractions from the *n*-butanol extract fractionation by CPC at 1300 rpm rotation and local minimum function (**Supplementary Figure S5**).

Pooled fractions	Sample code	Weight (mg)
1-21	SGA	80.6 mg
22-25	SGB	55.2 mg
26-30	SGC	23.4 mg
31-43	SGD	18 mg
44-52	SGE	6.3 mg
53-80	SGF	15 mg
81-92	SGG	16.8 mg
93-108	SGH	28.3 mg
109-117	SGI	13.5 mg
118-125	SGJ	22.9 mg
126-128	SGK	10.8 mg
129-131	SGL	15 mg
132-133	SGM	8.8 mg
134-137	SGN	14.1 mg
138-142	SGO	22.5 mg
143-148	SGP	21.8 mg
149-151	SGQ	10 mg
152-167	SGR	40.7 mg

**Supplementary Table S2.** Cell viability of pooled fractions from the *n*-butanol extract fractionation by CPC.

Fractions	Cell viability (%)* at 100 µg.mL <sup>-1</sup>
SGA	81±5
SGB	88±1
SGC	100
SGD	100
SGE	100
SGF	83±5
SGG	86±6
SGH	91±2
SGI	80±5
SGJ	< 50
SGK	80±1
SGL	< 50
SGM	< 50
SGN	< 50
SGO	79±2
SGP	< 50

SGQ	< 50
SGR	< 50
SGBu	100
OST-car	87±3

SGBu, *n*-butanol extract from *Siparuna glycyarpa*.

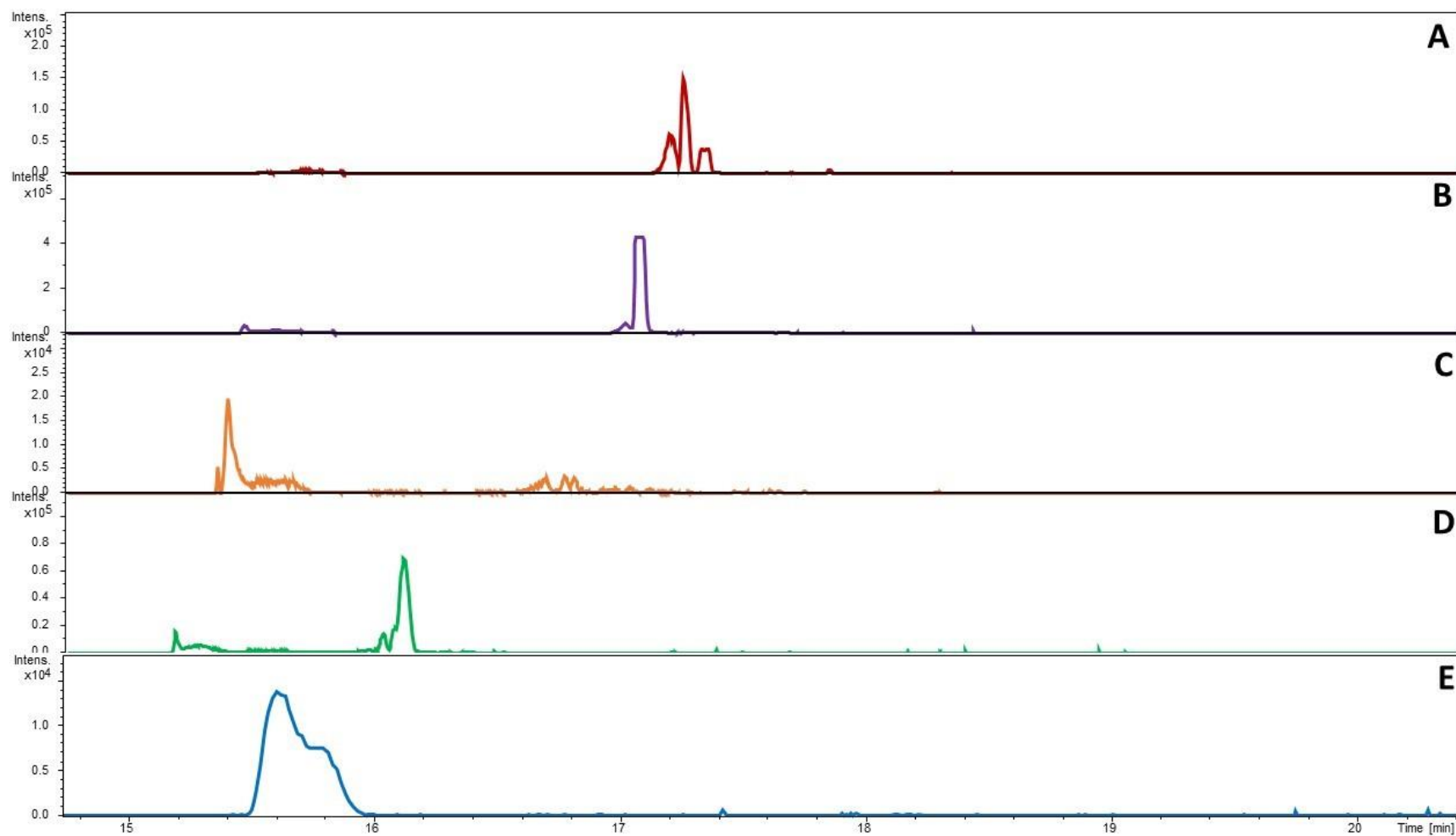
OST-car, OST-carboxylate.

\*DMSO was used as a cell control at 0.1 % v/v and the cell viability remained at least 95 % of cells exposed just to culture medium.

**Supplementary Table S3.** Anti-influenza activity of CPC pooled fractions with cell viability above 80%.

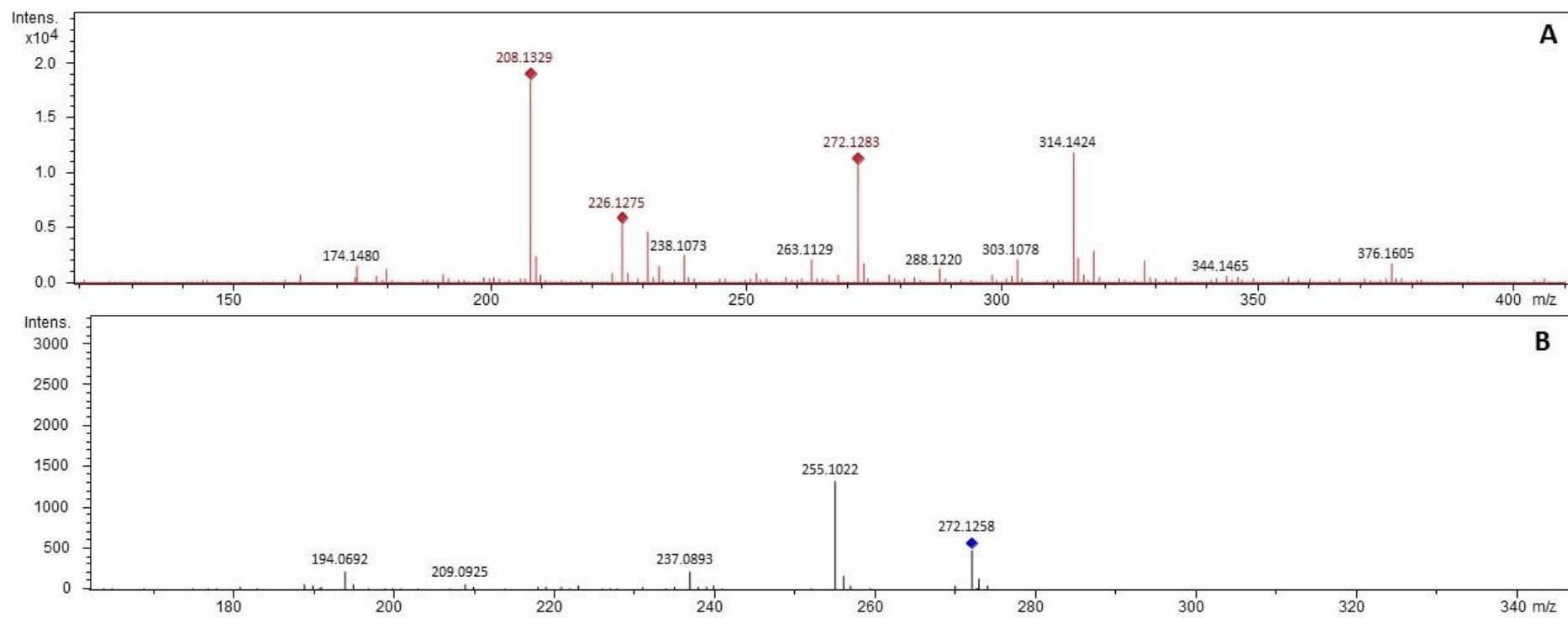
Fractions	Anti-influenza Screening (% of inhibition of viral replication)			
	24 hpi		48 hpi	
	25 $\mu\text{g.mL}^{-1}$	100 $\mu\text{g.mL}^{-1}$	25 $\mu\text{g.mL}^{-1}$	100 $\mu\text{g.mL}^{-1}$
SGA	37.0 $\pm$ 2.5	75.8 $\pm$ 3.9	27.6 $\pm$ 0.5	72.4 $\pm$ 0.6
SGB	15.8 $\pm$ 4.5	43.4 $\pm$ 4.4	6.2 $\pm$ 2.4	58.4 $\pm$ 1.7
SGC	36.4 $\pm$ 1.2	88.2 $\pm$ 2.3	27.9 $\pm$ 2.8	67.9 $\pm$ 6.1
SGD	59.2 $\pm$ 2.2	88.1 $\pm$ 1.4	39.1 $\pm$ 1.5	59.6 $\pm$ 7.9
SGE	15.9 $\pm$ 1.4	53.3 $\pm$ 6.9	NA	23.7 $\pm$ 4.9
SGF	16.3 $\pm$ 5.3	58.2 $\pm$ 3.7	17.1 $\pm$ 6.3	51.8 $\pm$ 7.1
SGG	8.2 $\pm$ 5.0	54.5 $\pm$ 3.3	7.2 $\pm$ 3.9	63.6 $\pm$ 2.8
SGH	8.3 $\pm$ 5.7	51.4 $\pm$ 4.6	9.4 $\pm$ 5.3	49.1 $\pm$ 3.8
SGI	24.5 $\pm$ 4.6	69.6 $\pm$ 1.2	7.8 $\pm$ 5.5	68.9 $\pm$ 10.1
SGK	6.1 $\pm$ 2.7	40.4 $\pm$ 6.3	NA	9.9 $\pm$ 3.7
SGO	38.8 $\pm$ 4.9	89.6 $\pm$ 1.5	46.8 $\pm$ 8.2	73.8 $\pm$ 8.5
SGBu	49.9 $\pm$ 3.3	95.7 $\pm$ 0.8	42.7 $\pm$ 4.3	86.5 $\pm$ 1.8
OST-car	94.4 $\pm$ 0.9	100	87.2 $\pm$ 4.3	98.9 $\pm$ 1.8

SGBu, *n*-butanol extract from *Siparuna glycyarpa*. OST-car, OST-carboxylate. NA, not applicable. Influenza not titrated, because cell monolayer was damaged due to viral growth.

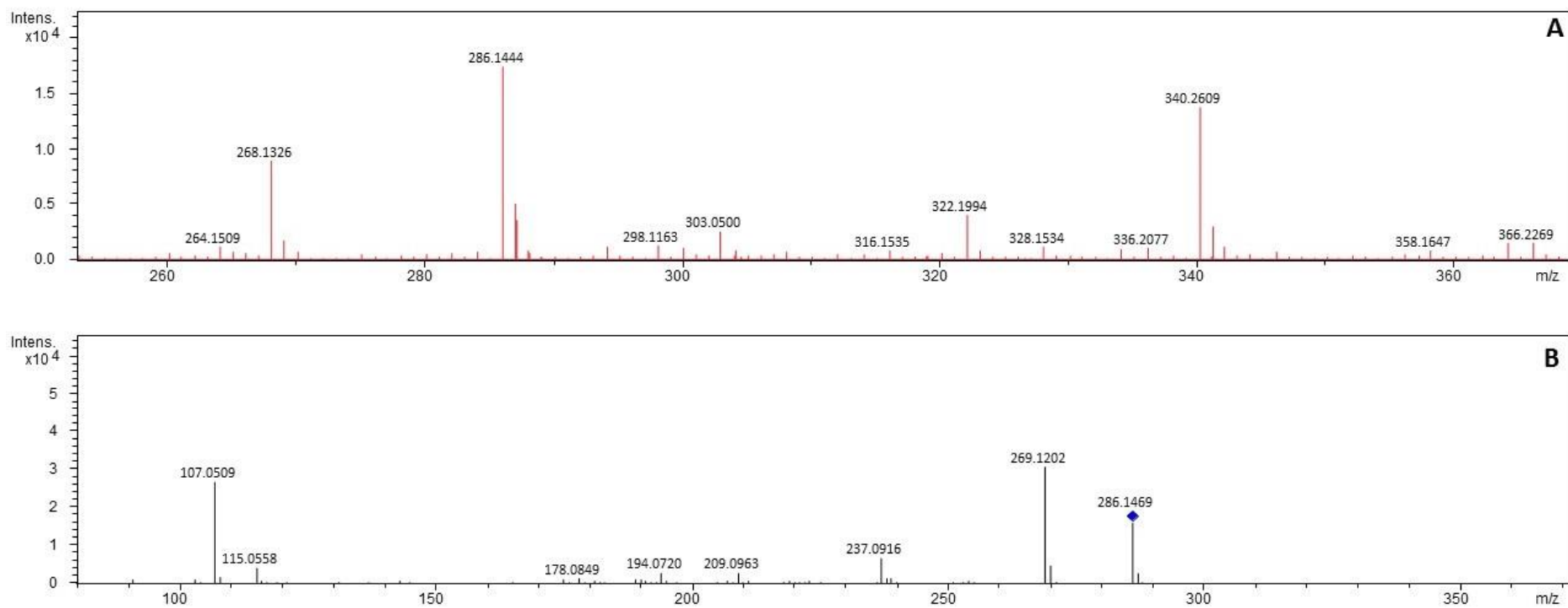


**Supplementary Figure S6.** (A) SGO, (B) SGD, (C) SGA and (D) SGC LC-HRMS/MS analysis in positive ionization mode. (E) SGO LC-HRMS/MS analysis in negative ionization mode.

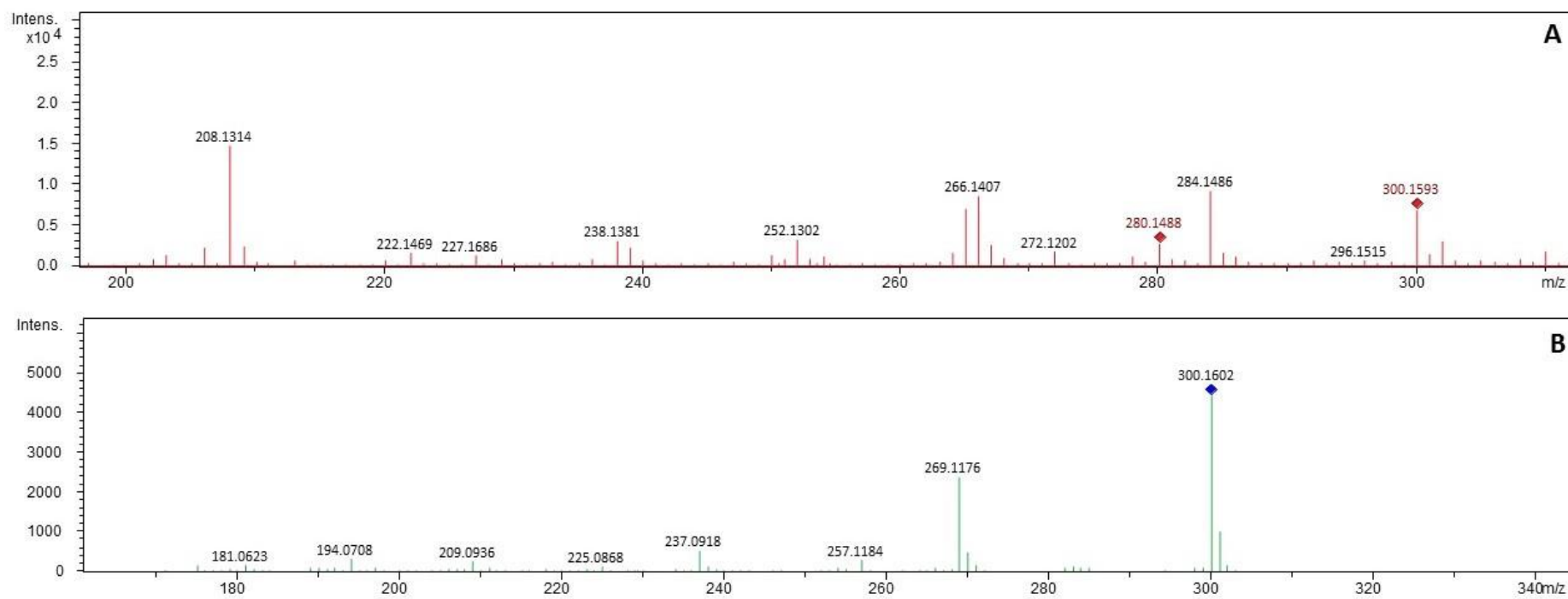




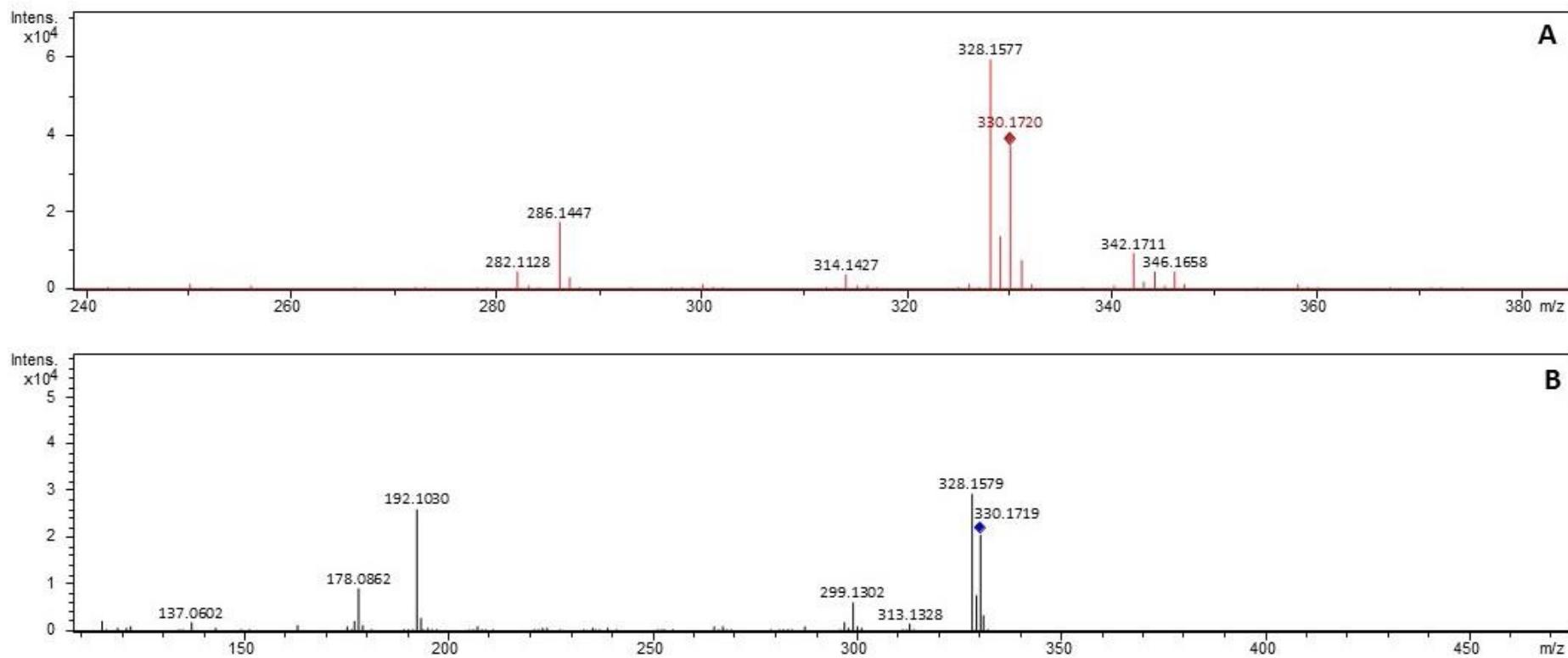
**Supplementary Figure S7.** (A) MS spectrum with  $m/z$  272.1283  $[M+H]^+$  and (B) MS<sup>2</sup> spectrum of demethyl-coclaurine **1**.



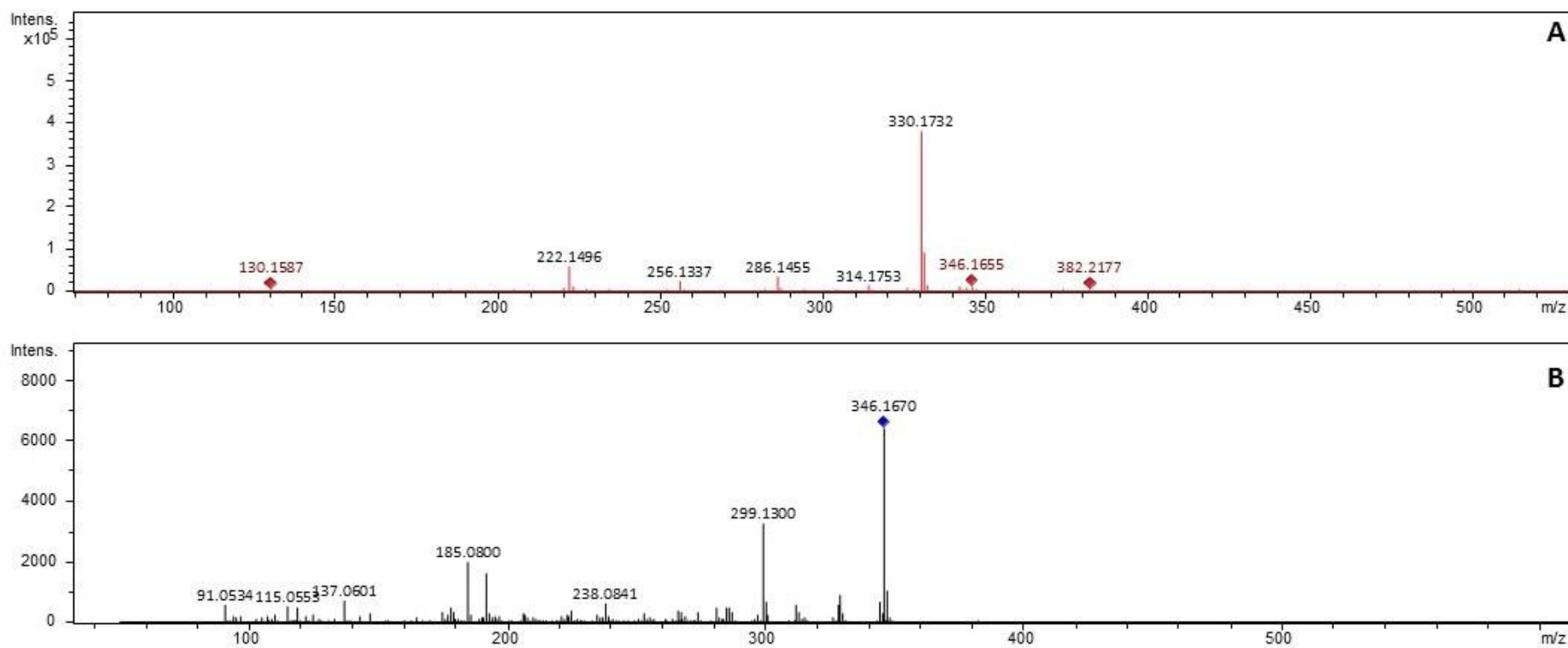
**Supplementary Figure S8.** (A) MS spectrum with  $m/z$  286.1444  $[M+H]^+$  and (B)  $MS^2$  spectrum of coclaurine 2.



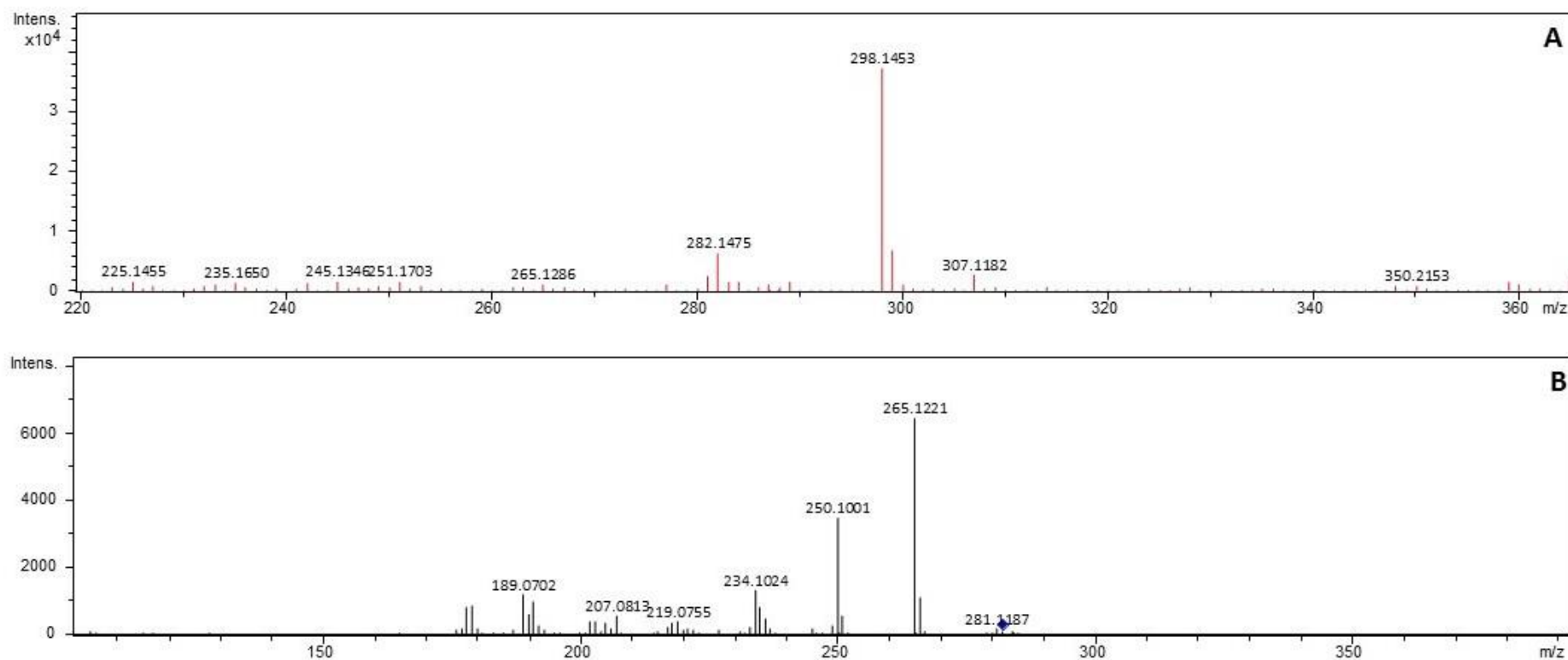
**Supplementary Figure S9.** (A) MS spectrum with  $m/z$  300.1593  $[M+H]^+$  and (B) MS<sup>2</sup> spectrum of *N*-methylcoclaurine **3**.



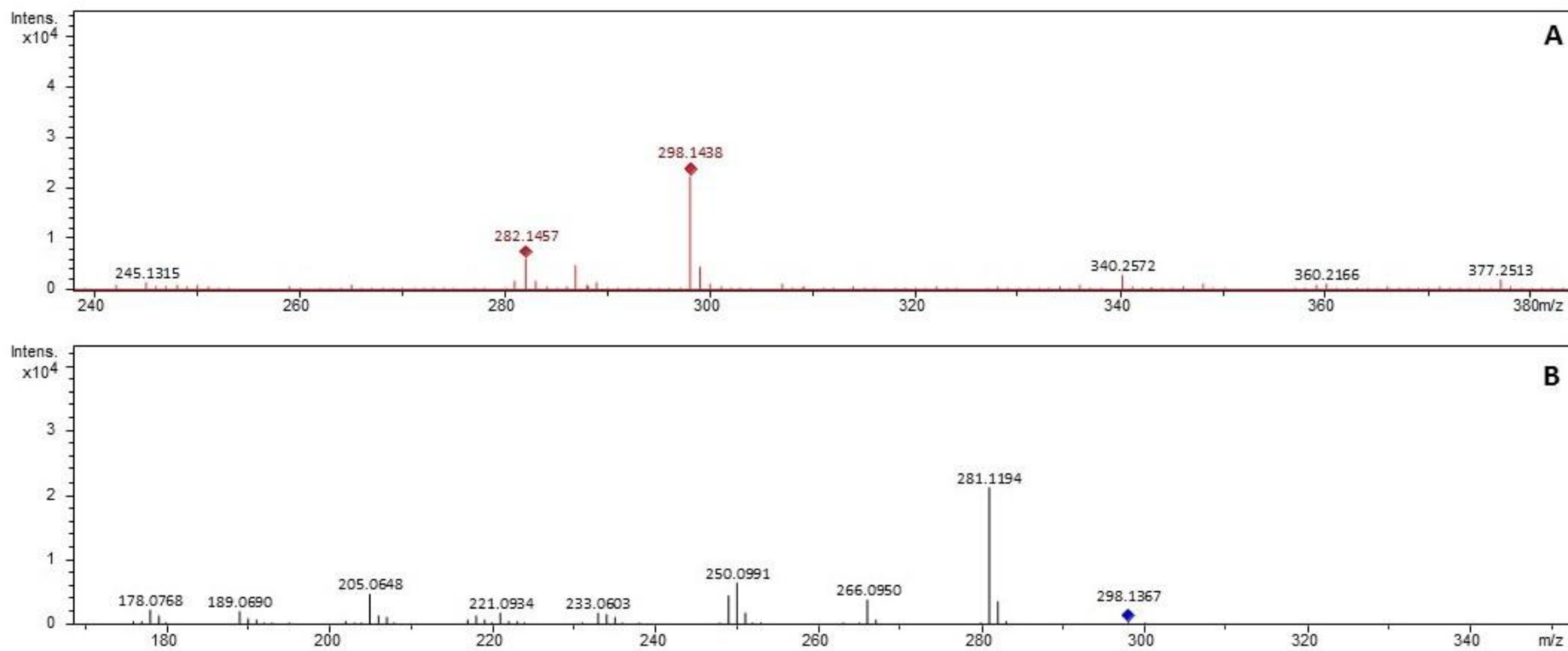
**Supplementary Figure S10.** (A) MS spectrum with  $m/z$  330.1720  $[M+H]^+$  and (B)  $MS^2$  spectrum of reticuline 4.



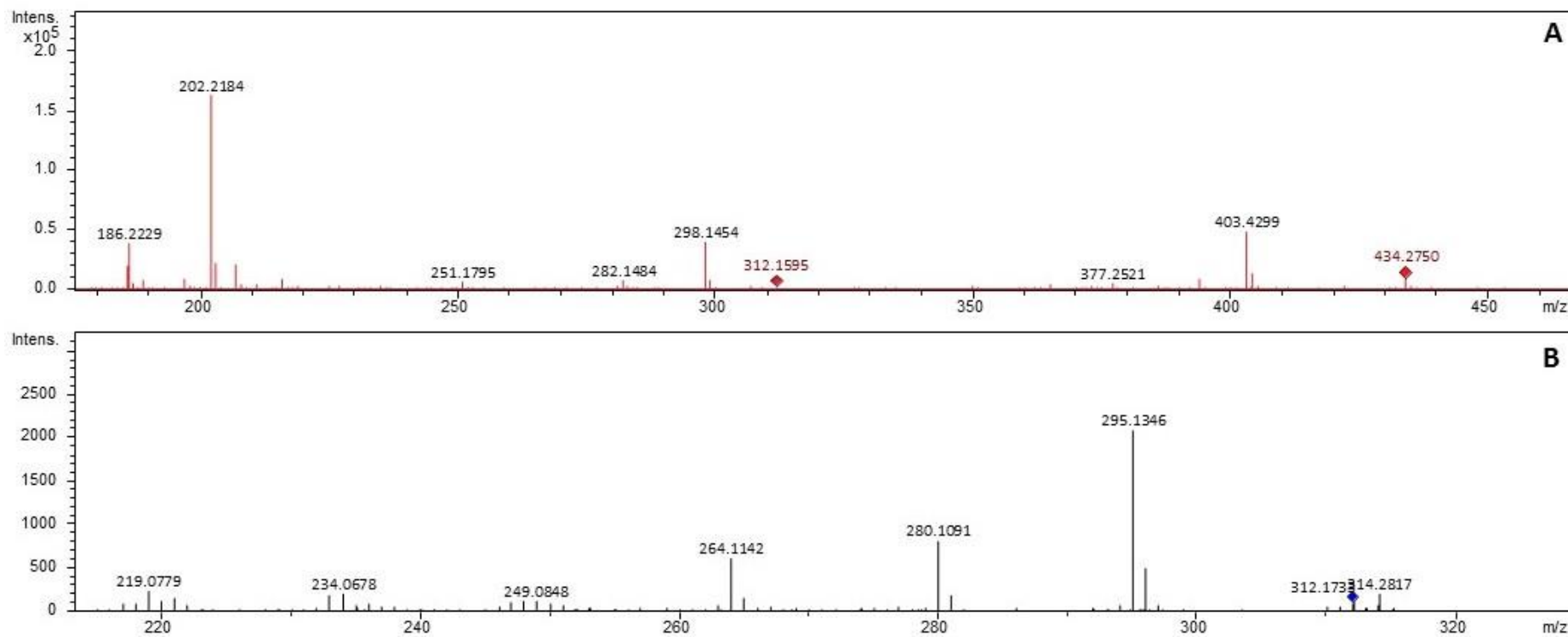
**Supplementary Figure S11.** (A) MS spectrum with  $m/z$  346.1655  $[M+H]^+$  and (B) MS<sup>2</sup> spectrum of reticuline *N*-oxide **5**.



**Supplementary Figure S12.** (A) MS spectrum with  $m/z$  282.1475  $[M+H]^+$  and (B)  $MS^2$  spectrum of normuciferine 6.

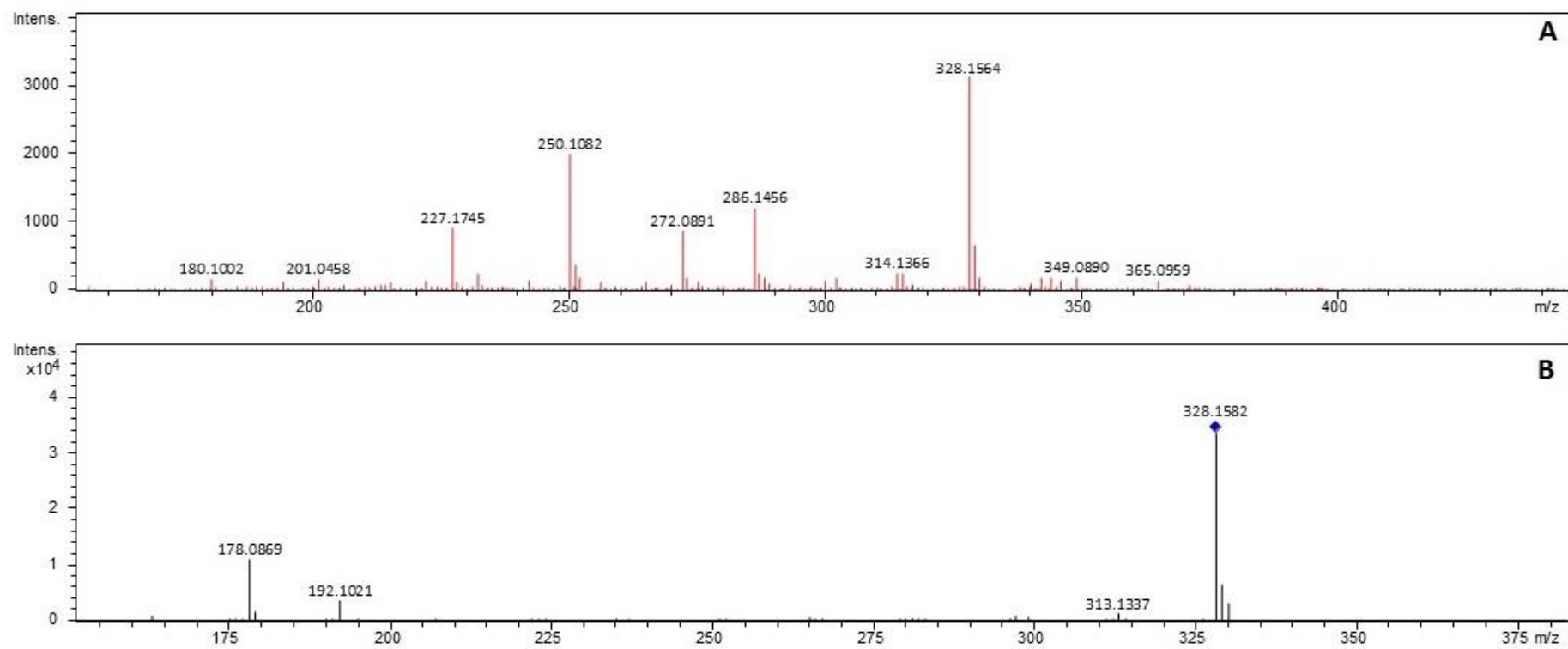


**Supplementary Figure S13.** (A) MS spectrum with  $m/z$  298.1438  $[M+H]^+$  and (B) MS<sup>2</sup> spectrum of isopiline 7.

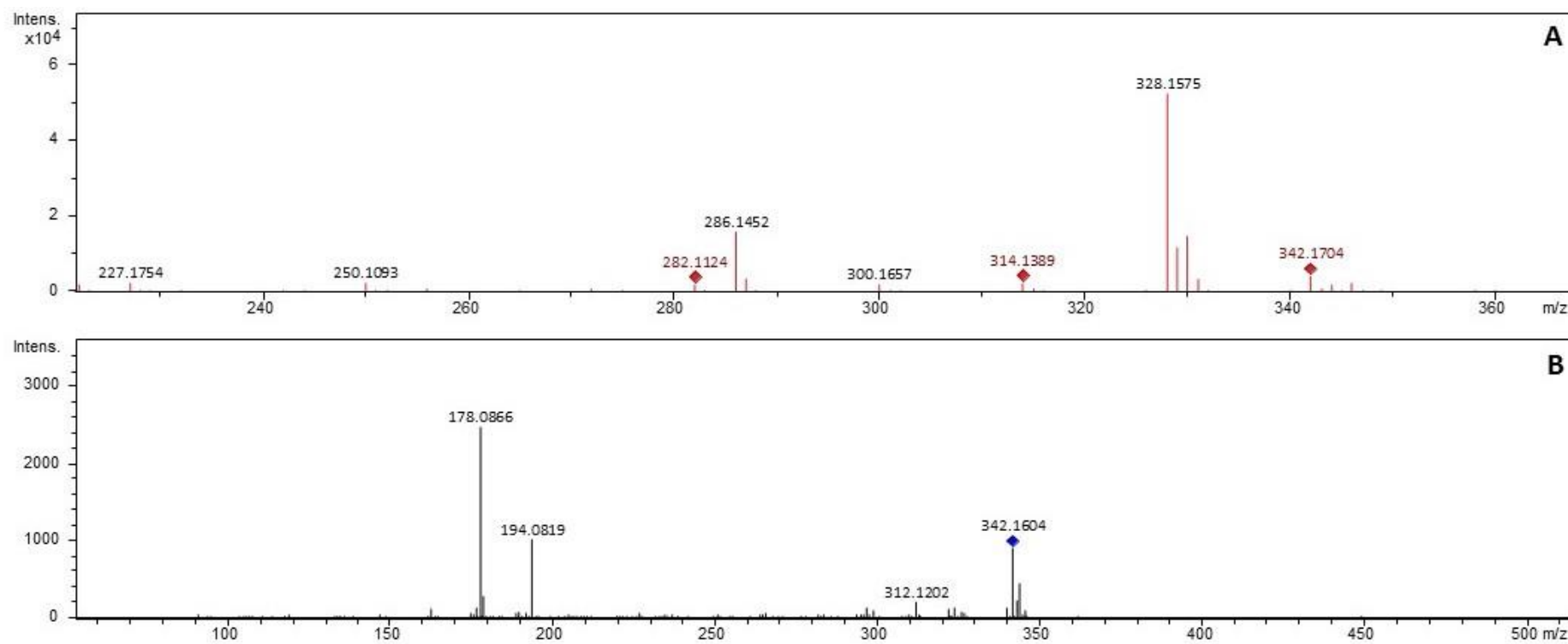


**Supplementary Figure S14.** (A) MS spectrum with  $m/z$  312.1595  $[M+H]^+$  and (B) MS<sup>2</sup> spectrum of *O*-methylisopiline **8**.

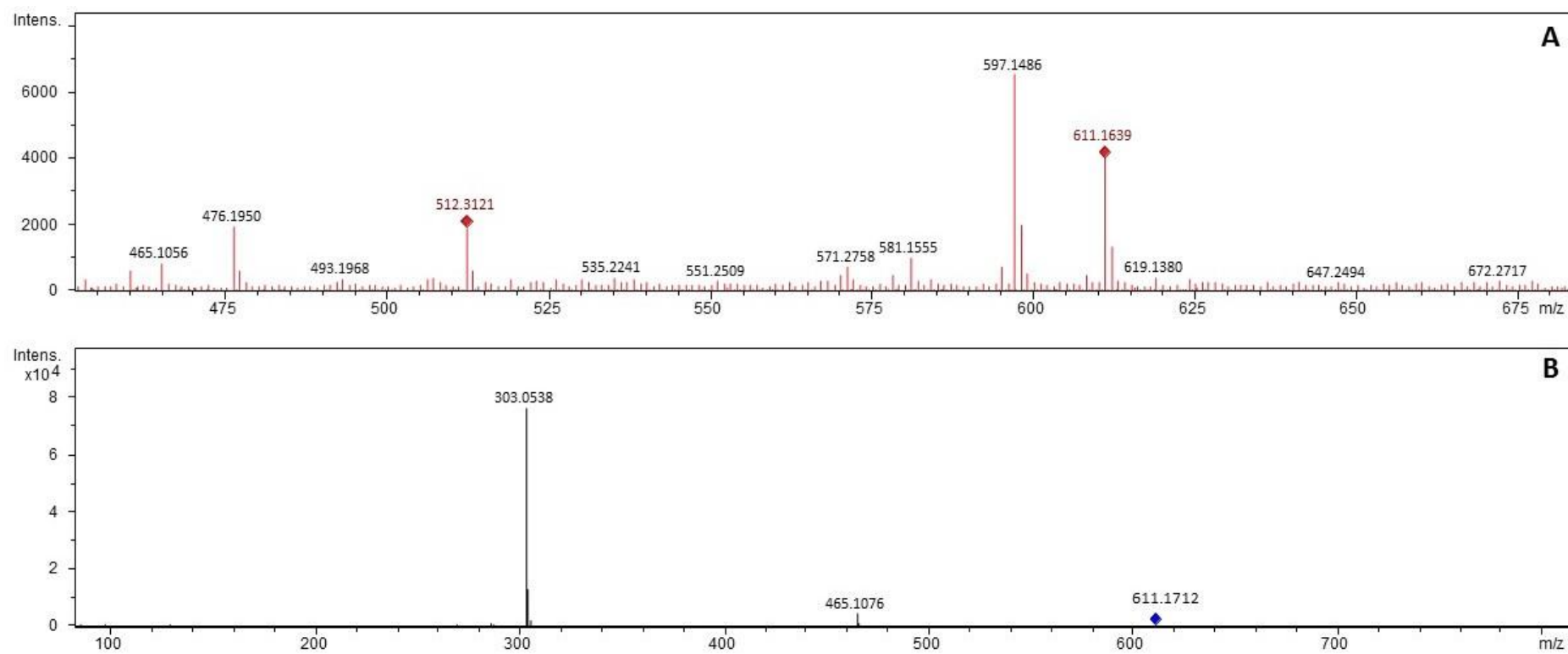




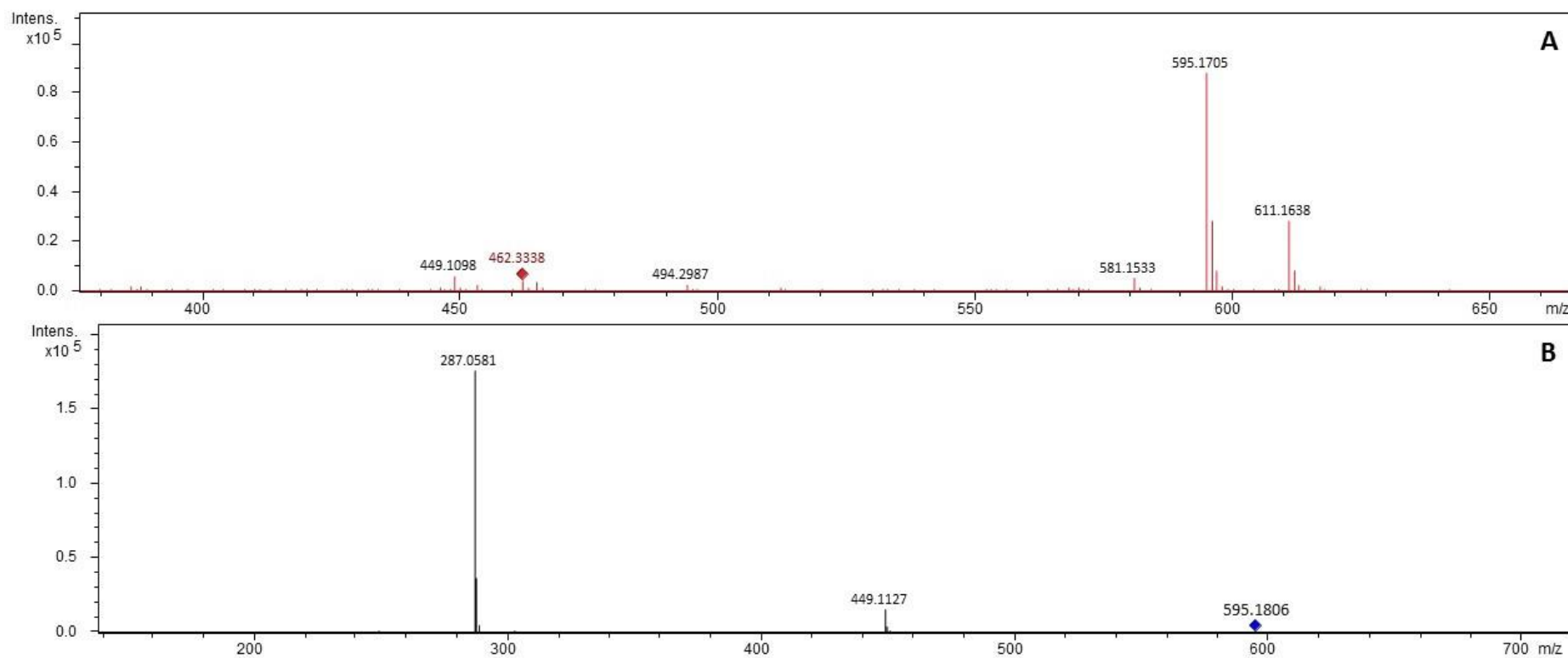
**Supplementary Figure S15.** (A) MS spectrum with  $m/z$  328.1564  $[M+H]^+$  and (B) MS<sup>2</sup> spectrum of stepholidine 9.



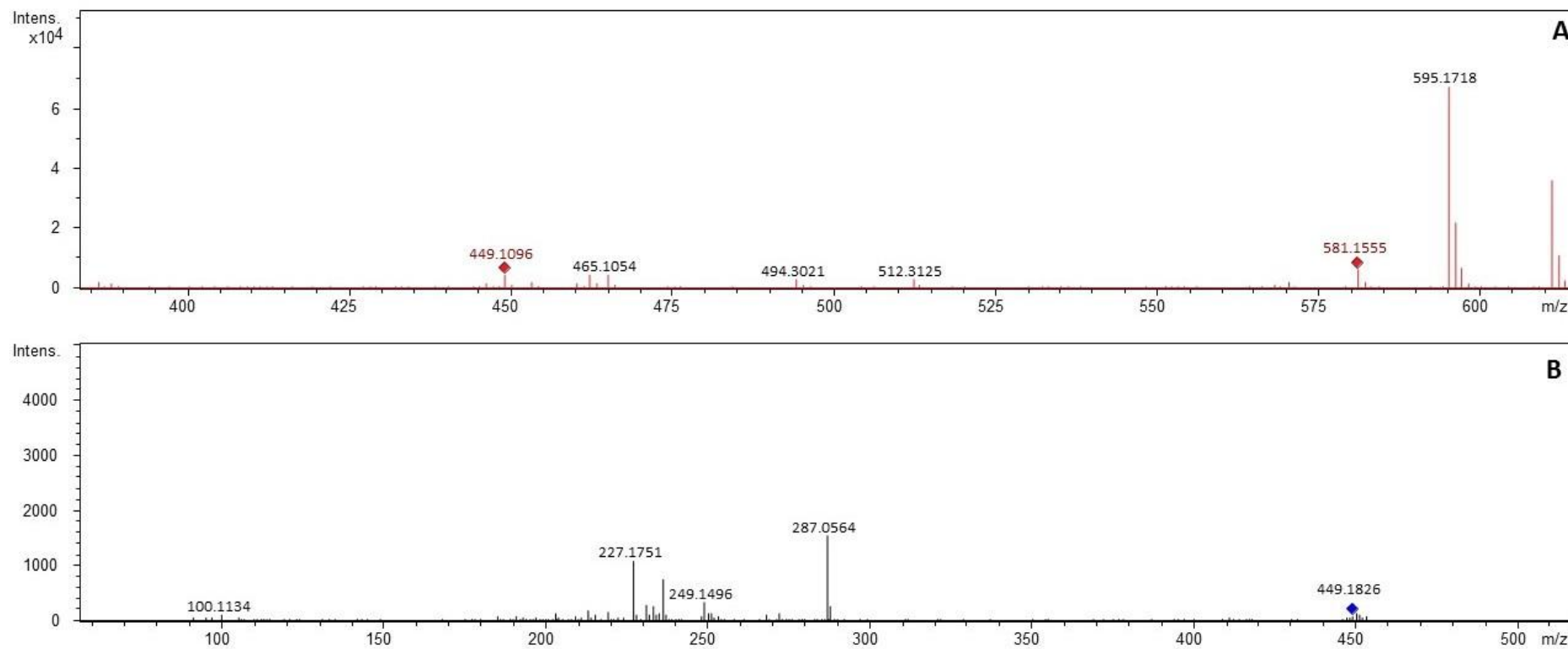
**Supplementary Figure S16.** (A) MS spectrum with  $m/z$  342.1704  $[M+H]^+$  and (B) MS<sup>2</sup> spectrum of isocorypalmine **10**.



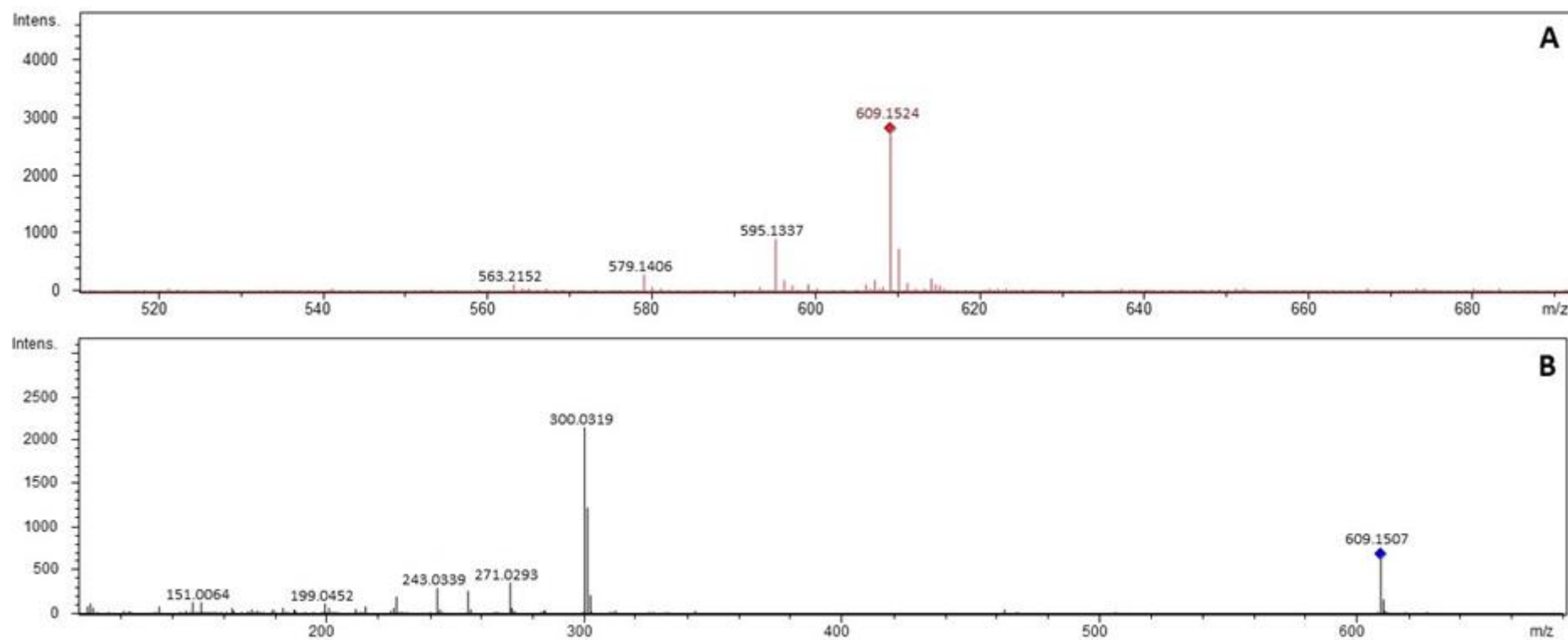
**Supplementary Figure S17.** (A) MS spectrum with  $m/z$  611.1639  $[M+H]^+$  and (B) MS<sup>2</sup> spectrum of quercetin-3-*O*-rhamnoside-7-*O*-glucoside or quercetin-3-*O*-glucoside-7-*O*-rhamnoside **11**.



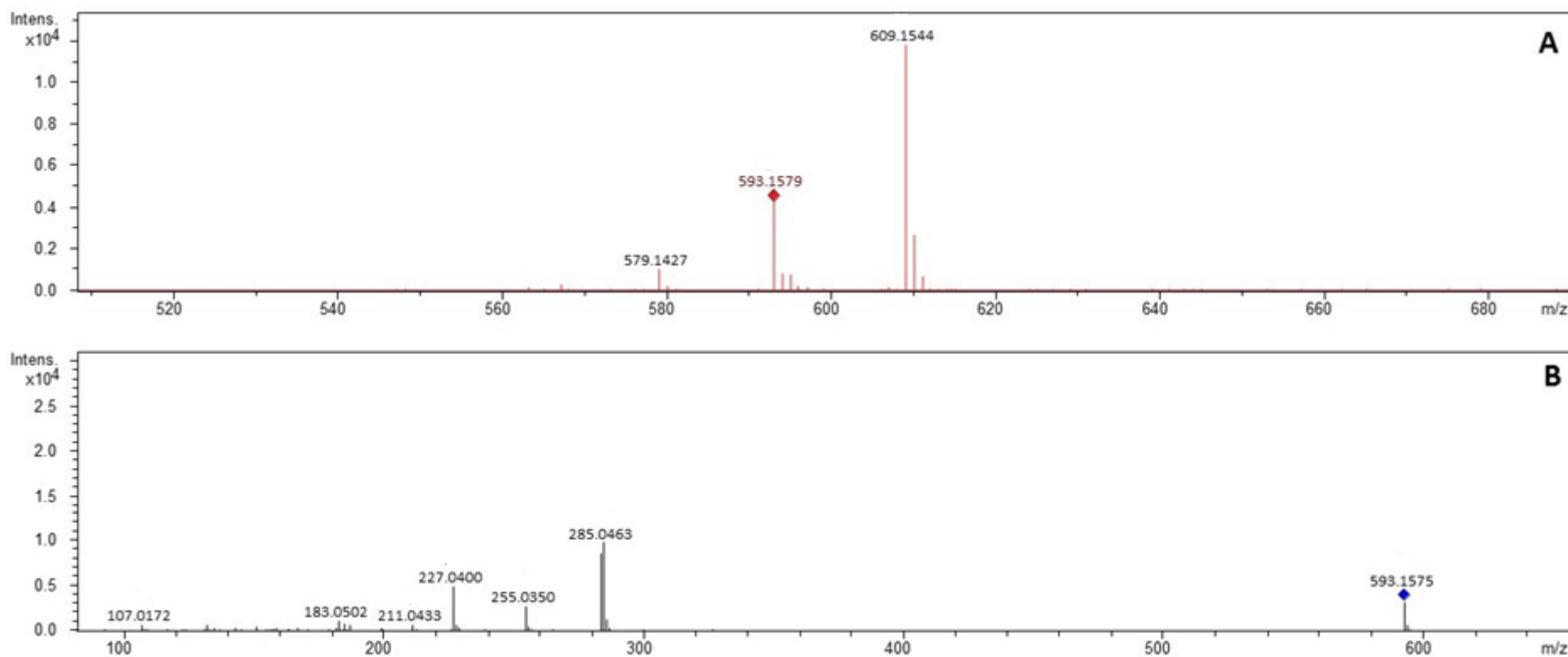
**Supplementary Figure S18.** (A) MS spectrum with  $m/z$  595.1705  $[M+H]^+$  and (B) MS<sup>2</sup> spectrum of kaempferol-3-*O*-glucoside-7-*O*-rhamnoside **12**.



**Supplementary Figure S19.** (A) MS spectrum with  $m/z$  449.1096  $[M+H]^+$  and (B) MS<sup>2</sup> spectrum of kaempferol 3-*O*-glucoside **13**.

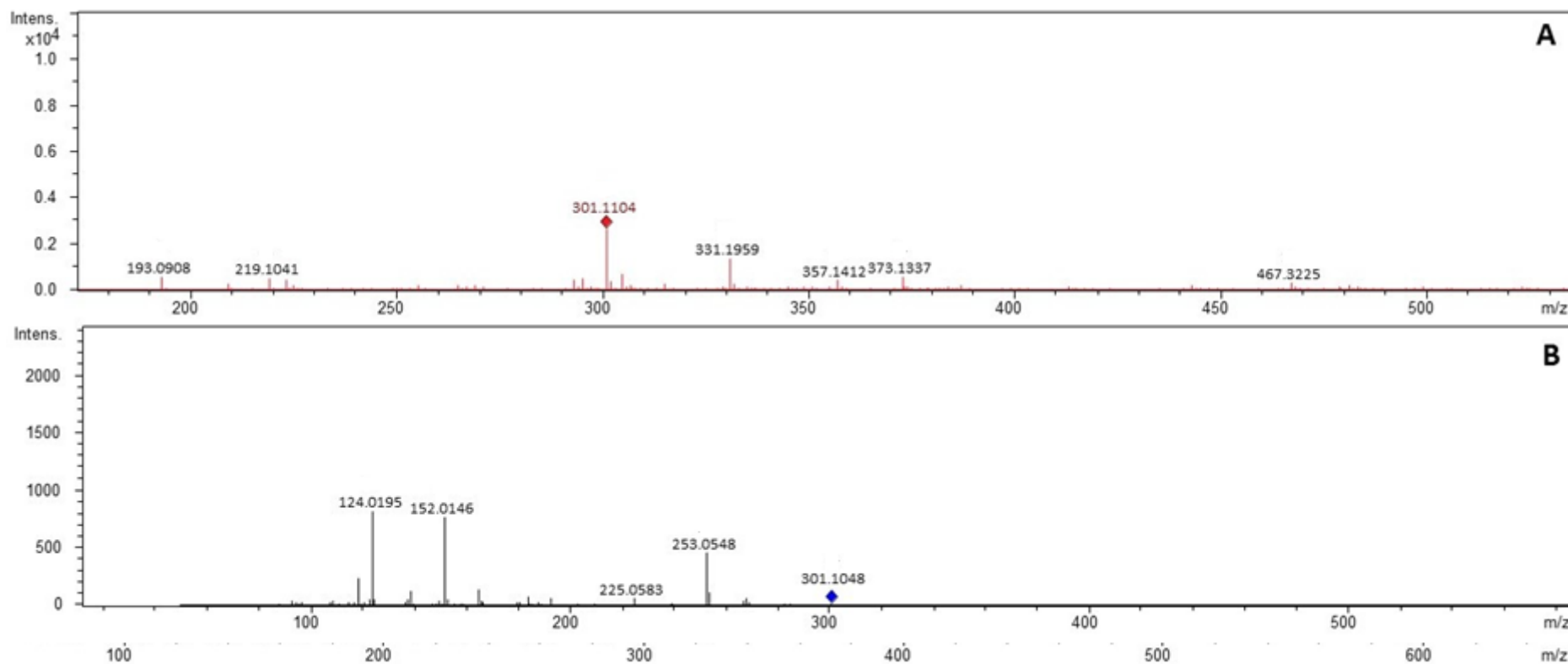


**Supplementary Figure S20.** (A) MS spectrum with  $m/z$  609.1524  $[M-H]^-$  and (B) MS<sup>2</sup> spectrum of quercetin-3-*O*-rutinoside (Rutin) **14**.

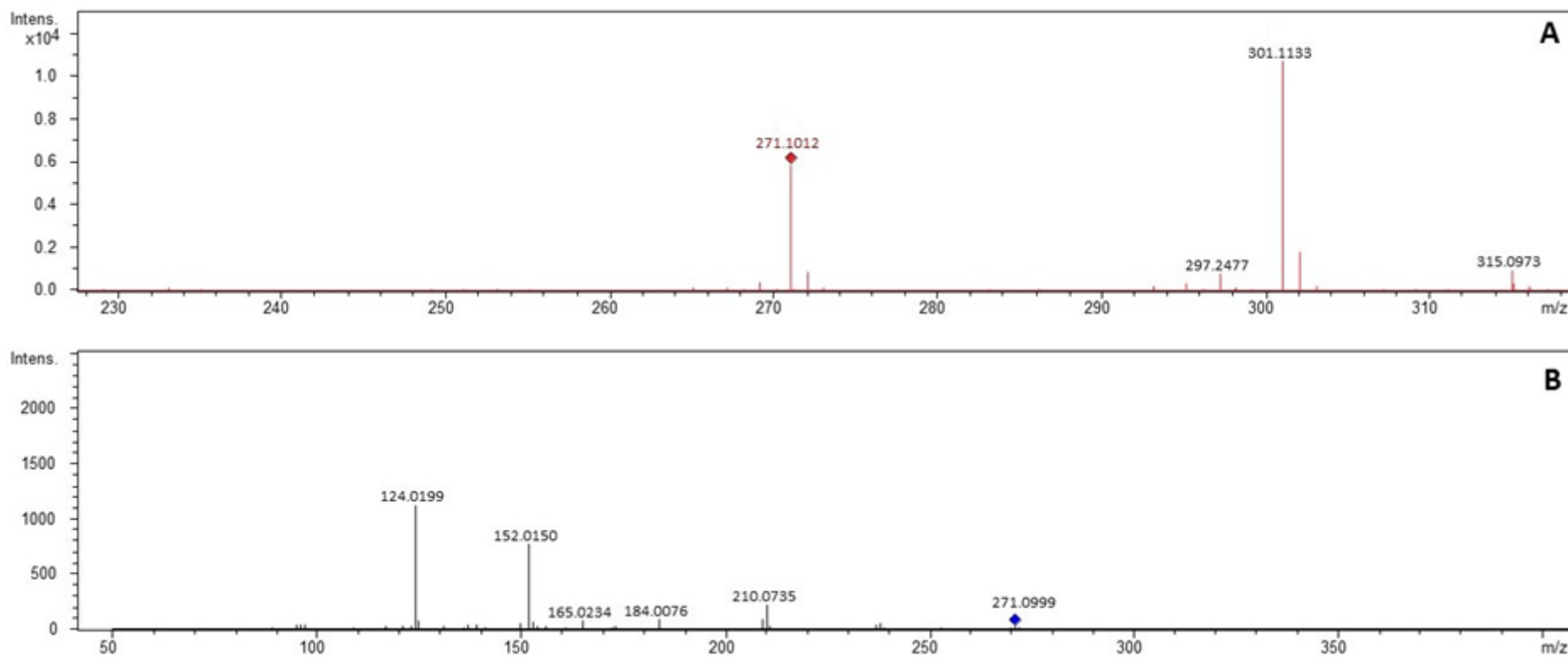


**Supplementary Figure S21.** (A) MS spectrum with  $m/z$  593.1579  $[M-H]^-$  and (B)  $MS^2$  spectrum of kaempferol-3-*O*-rutinoside **15**.

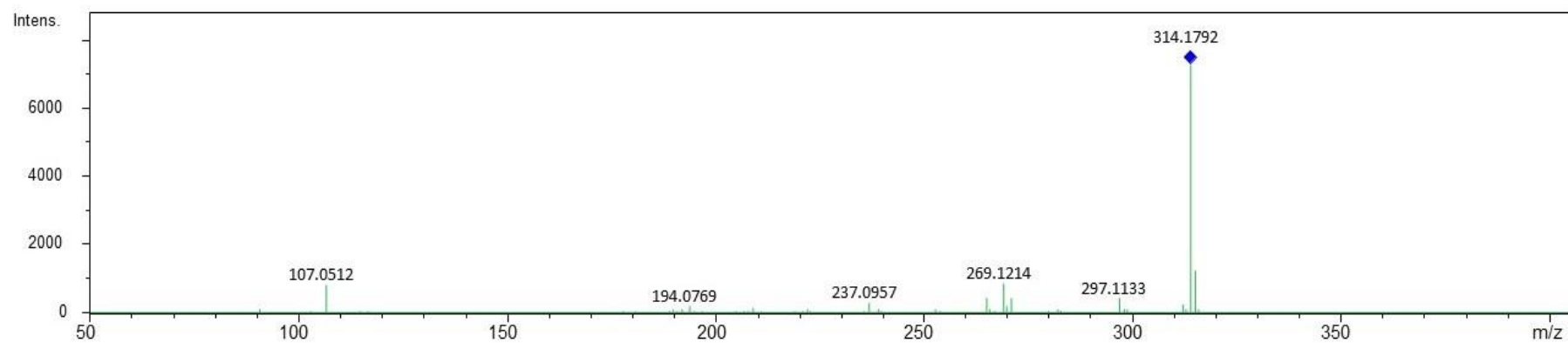




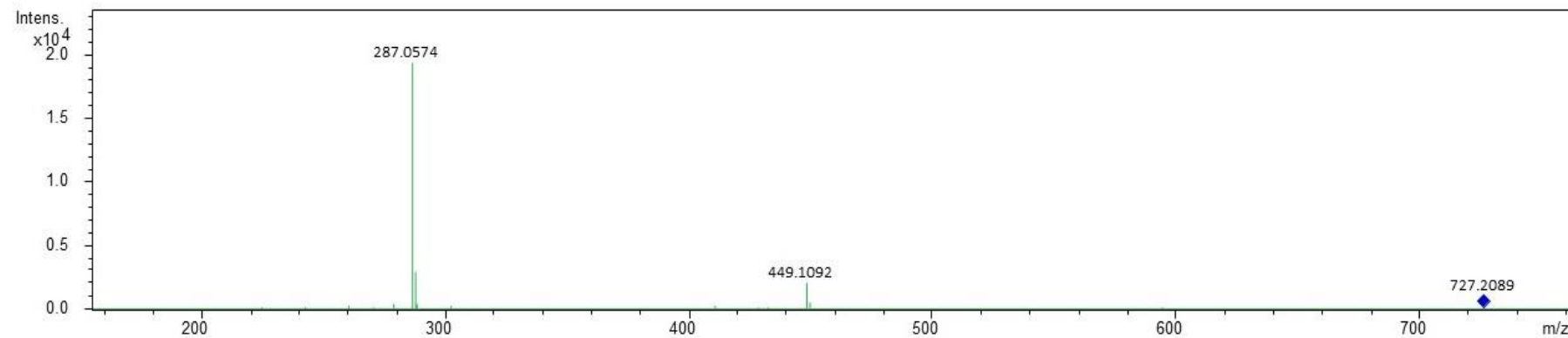
**Supplementary Figure S22.** (A) MS spectrum with  $m/z$  301.1104  $[M-H]^-$  and (B)  $MS^2$  spectrum of 2',6'-dihydroxy-4,4'-dimethoxydihydrochalcone **16**.



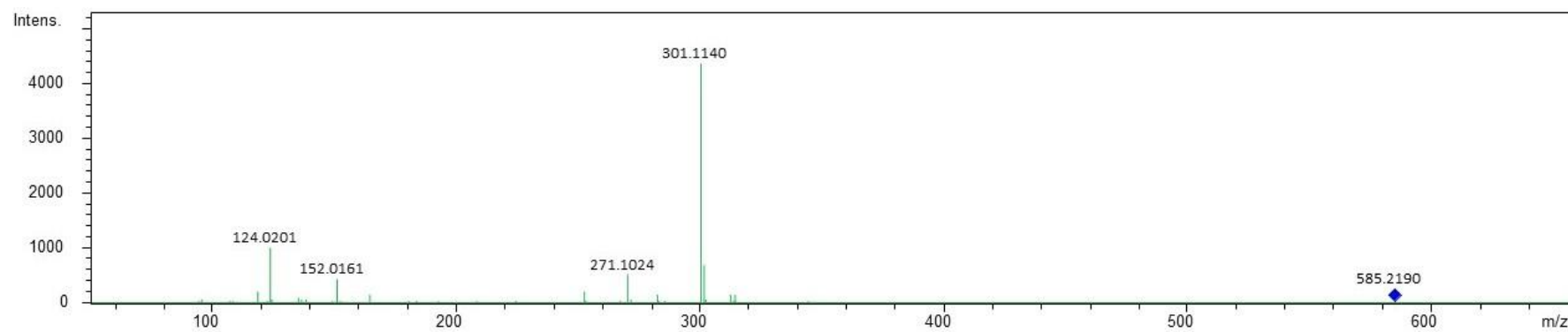
**Supplementary Figure S23.** (A) MS spectrum with  $m/z$  271.1012 [M-H]<sup>-</sup> and (B) MS<sup>2</sup> spectrum of 2',6'-dihydroxy-4'-methoxy-dihydrochalcone **17**.



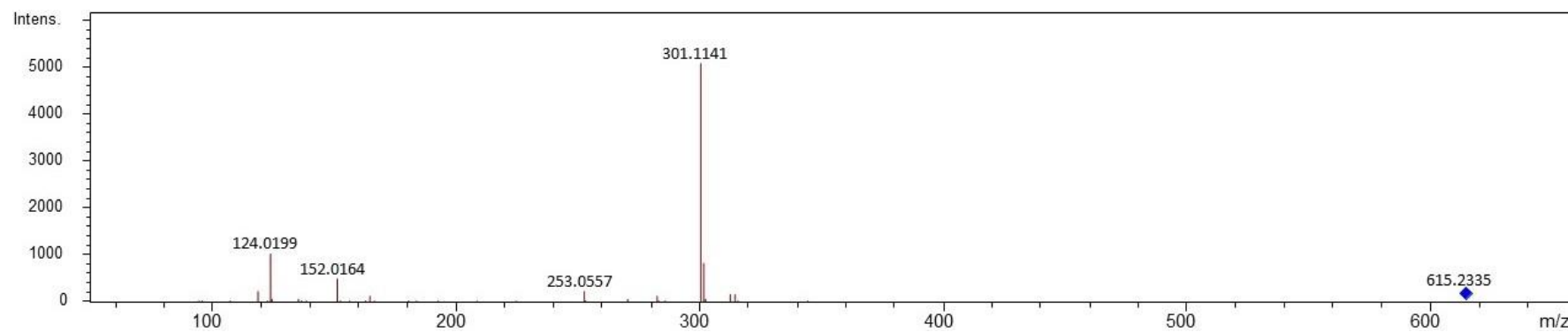
**Supplementary Figure S24.** MS<sup>2</sup> spectrum of magnocurarine *m/z* 314.1792 [M]<sup>+</sup>.



**Supplementary Figure S25.** MS<sup>2</sup> spectrum of kaempferol-3-*O*-hexose-*O*-deoxyhexose-*O*-pentoside *m/z* 727.2089 [M+H]<sup>+</sup>.



**Supplementary Figure S26.** MS<sup>2</sup> spectrum of quercetin-3-O-(2''-O-galloyl)-pentoside  $m/z$  585.2190 [M-H].



**Supplementary Figure S27.** MS<sup>2</sup> spectrum of quercetin-3-O-(6''-O-galloyl)- $\beta$ -galactopyranoside  $m/z$  615.2335 [M-H].

### **4.3 Capítulo III. Flavonoids from *Siparuna cristata* as Potential Inhibitors of SARS-CoV-2 Replication**

Trabalho publicado em *Brazilian Journal of Pharmacognosy in the special issue to celebrate the 35<sup>th</sup> anniversary of the Brazilian Journal of Pharmacognosy*

(doi: 10.1007/s43450-021-00162-5)



## Flavonoids from *Siparuna cristata* as Potential Inhibitors of SARS-CoV-2 Replication

Carla Monteiro Leal<sup>1,2</sup> · Suzana Guimarães Leitão<sup>3</sup> · Romain Sausset<sup>2,4</sup> · Simony C. Mendonça<sup>2</sup> · Pedro H. A. Nascimento<sup>2</sup> · Caio Felipe de Araujo R. Cheohen<sup>5</sup> · Maria Eduarda A. Esteves<sup>6</sup> · Manuela Leal da Silva<sup>5,6</sup> · Tayssa Santos Gondim<sup>7</sup> · Maria Eduarda S. Monteiro<sup>7</sup> · Amanda Resende Tucci<sup>7</sup> · Natália Fintelman-Rodrigues<sup>8,9</sup> · Marilda M. Siqueira<sup>7</sup> · Milene Dias Miranda<sup>7</sup> · Fernanda N. Costa<sup>2</sup> · Rosineide C. Simas<sup>10</sup> · Gilda Guimarães Leitão<sup>2</sup>

Received: 11 February 2021 / Accepted: 3 June 2021  
 © Sociedade Brasileira de Farmacognosia 2021

### Abstract

The novel coronavirus SARS-CoV-2 has been affecting the world, causing severe pneumonia and acute respiratory syndrome, leading people to death. Therefore, the search for anti-SARS-CoV-2 compounds is pivotal for public health. Natural products may present sources of bioactive compounds; among them, flavonoids are known in literature for their antiviral activity. *Siparuna* species are used in Brazilian folk medicine for the treatment of colds and flu. This work describes the isolation of 3,3',4'-tri-*O*-methyl-quercetin, 3,7,3',4'-tetra-*O*-methyl-quercetin (retusin), and 3,7-di-*O*-methyl-kaempferol (kumatakenin) from the dichloromethane extract of leaves of *Siparuna cristata* (Poepp. & Endl.) A.DC., Siparunaceae, using high-speed countercurrent chromatography in addition to the investigation of their inhibitory effect against SARS-CoV-2 viral replication. Retusin and kumatakenin inhibited SARS-CoV-2 replication in Vero E6 and Calu-3 cells, with a selective index greater than lopinavir/ritonavir and chloroquine, used as control. Flavonoids and their derivatives may stand for target compounds to be tested in future clinical trials to enrich the drug arsenal against coronavirus infections.

**Keywords** Countercurrent chromatography · Siparunaceae · Mass spectrometry · *O*-Methyl flavonoids · Coronavirus

This article is part of a Special Issue to celebrate the 35th anniversary of the *Brazilian Journal of Pharmacognosy*

✉ Suzana Guimarães Leitão  
 sgleitao@pharma.ufrj.br

✉ Gilda Guimarães Leitão  
 ggleitao@ippn.ufrj.br

<sup>1</sup> Programa de Pós-graduação em Biotecnologia Vegetal e Bioprocessos, Universidade Federal do Rio de Janeiro, Rio de Janeiro, RJ 21941-902, Brazil

<sup>2</sup> Instituto de Pesquisas de Produtos Naturais, Centro de Ciências da Saúde, Bl. H, Ilha do Fundão, Universidade Federal do Rio de Janeiro, Rio de Janeiro, RJ 21941-902, Brazil

<sup>3</sup> Faculdade de Farmácia, Centro de Ciências da Saúde, Bl. A 2º andar, Ilha do Fundão, Universidade Federal do Rio de Janeiro, Rio de Janeiro, RJ 21941-902, Brazil

<sup>4</sup> Muséum National D'Histoire Naturelle, 75005 Paris, France

<sup>5</sup> Programa de Pós-graduação Multicêntrico em Ciências Fisiológicas, Centro de Ciências da Saúde, Instituto de

Biodiversidade e Sustentabilidade NUPEM, Universidade Federal do Rio de Janeiro, Macaé, RJ 27965-045, Brazil

<sup>6</sup> Programa de Pós-graduação em Biologia Computacional e Sistemas, Instituto Oswaldo Cruz, Manguinhos, Rio de Janeiro, RJ 21041-361, Brazil

<sup>7</sup> Laboratório de Vírus Respiratórios e do Sarampo, Instituto Oswaldo Cruz, Fundação Oswaldo Cruz, Rio de Janeiro 21041-210, Brazil

<sup>8</sup> Laboratório de Imunofarmacologia, Instituto Oswaldo Cruz, Fundação Oswaldo Cruz, Rio de Janeiro 21041-210, Brazil

<sup>9</sup> Instituto Nacional de Ciência e Tecnologia de Gestão da Inovação em Doenças Negligenciadas, Centro de Desenvolvimento Tecnológico em Saúde, Fundação Oswaldo Cruz, Rio de Janeiro, RJ 21041-210, Brazil

<sup>10</sup> Laboratório de Cromatografia e Espectrometria de Massas, Instituto de Química, Universidade Federal de Goiás, Goiânia, GO 74690-900, Brazil



## Introduction

Coronaviruses (CoVs), Coronaviridae family, are subdivided into the *Alphacoronavirus*, *Betacoronavirus*, *Gammacoronavirus*, and *Deltacoronavirus* genera, which are etiologic agents causing several acute and chronic respiratory, enteric, and central nervous system diseases (Chinsembu, 2020; Mani et al. 2020). The betacoronaviruses SARS-CoV and MERS-CoV are the etiologic agents of the severe acute respiratory syndrome (SARS) and Middle East respiratory syndrome (MERS) that occurred from 2002 and 2012. In 2019, the new coronavirus SARS-CoV-2 (*Betacoronavirus*) appeared in Wuhan, China, causing the worldwide pandemic of COVID-19 and public health concerns (Mani et al. 2020). Due to the highly complex pathophysiology of SARS-CoV-2 infection (Elizalde-González 2020), involving not only the activation of the immune and hematologic systems but also the involvement and impairment of different organs and potential for systemic complications, the term multiple organ dysfunction syndrome, MODS-CoV-2 was proposed (Maisch, 2020; Robba et al. 2020). As of May 2021, there are over 160 million positive cases reported in 220 affected countries and regions, with death numbers surpassing the figure of 3 million (WHO 2021). In Brazil, the deaths from the disease have so far surpassed the number of 500,000 (JHU CSSE COVID-19 Data 2021). Due to this worldwide scenario, the search for vaccines, medicines, monoclonal antibodies, interferon therapies, peptides, and natural medicines has been developed for fighting the new coronavirus. The non-structural proteins 3-chymotrypsin-like protease (3CLpro), papain-like protease (PLpro), and RNA-dependent RNA polymerase (RdRp) and the structural protein spike (S) protein, present in the SARS-CoV-2 genome, have been research targets for drug interventions against this new virus (Mani et al. 2020). Proteases are important therapeutic targets due their crucial activity in the replicative cycle of the virus. Both main protease (Mpro) and PLpro act by cleaving the pp1a and pp1ab polyproteins that are translated from the viral genome shortly after SARS-CoV-2 enters the host cell. Together, they give rise to sixteen functional non-structural proteins. PLpro does proteolytic cleavage from nsp1 to nsp3, while nsp4 to nsp16 are excised by Mpro (Abdul et al., 2021). Earlier studies showed SARS-CoV 3CLpro and SARS-CoV PLpro have been considered potential targets for the design and development of antiviral drugs. Several in silico simulations suggested the possibility that flavonoids can affect key factors responsible for the virus viability replication. In the course of 2020 and 2021, works have been published dealing with the screening of natural flavonoids as a promising class of SARS-CoV-2 inhibitors (Komolafe et al. 2021), blocking

its entry or replication (El-Mordy et al. 2020; Jo et al. 2020; Cherrak et al. 2020; Russo et al. 2020; Mouffouk et al. 2021; Pandey et al. 2021).

In silico screening studies with different plant species from traditional Chinese medicines (TCMs) showed that flavonoids such as baicalin, epigallocatechin gallate, herbacetin, isobavaschalcone, kaempferol derivatives, luteolin, myricetin, quercetin 3- $\beta$ -D-glucoside, rhoifolin, and scutellarein have been described as potential inhibitors of SARS-CoV-2 PLpro and 3CLpro (Chinsembu, 2020; Mani et al. 2020). Flavonoids commonly present in propolis samples have also been highlighted as promising agents that could attenuate SARS-CoV-2 infection and its consequences (Berretta et al. 2020). A recent work described three flavonoids that were found to efficiently block the enzymatic activity of SARS-CoV 3CLpro, among them is pectolinarin, a dimethylated flavone glycoside (Jo et al. 2020). Furthermore, flavonoids have demonstrated an efficient modulation potential against the SARS-CoV-2-induced inflammatory storm and counteracting lung inflammation (Liskova et al. 2021; Santana et al., 2021).

According to “Diagnosis and Treatment Program for Corona Virus Disease 2019 (COVID-19)” in China, treatment with traditional medicine is recommended, which has achieved good clinical effects (Ren et al. 2020). In the same way, a recent work (Cock and Vuuren 2020) revealed the potential of South African medicinal plants used to treat viral respiratory diseases in screening studies against the SARS-CoV-2 virus. Brazil has a long tradition of medicinal plant use, and in many regions of the country where medical care units are scarce or inexistent, traditional medicinal therapies are the only option which is being used to overcome COVID-19. Plants of the genus *Siparuna* are commonly used in Brazilian folk medicine in the treatment of colds, fever, headache, and rheumatism, as well as in rituals (Leitão et al. 1999). A syrup prepared with *Siparuna apiosyce*, a species from the first Brazilian Pharmacopeia, has long been commercialized in Brazil for the treatment of colds and flu with the name of “limão-bravo.” During the investigation on the chemistry of *Siparuna* species for the management of colds and fever, we came across a methylated flavonoid-rich extract with anti-influenza activity (Leal et al. 2021) from the Amazonian species *Siparuna cristata* (Poepp. & Endl.) A.DC., Siparunaceae. In this paper, metabolic profiling by HPLC, isolation by high-speed countercurrent chromatography (HSCCC), structure elucidation, and molecular docking studies of the methylated flavonoids 1–3 from *S. cristata* were performed to investigate their in vitro inhibitory effect against SARS-CoV-2 and to evaluate their in silico inhibitory effect against 3CLpro and PLpro SARS-CoV-2 proteases.



## Materials and Methods

### Plant Material

Leaves of *Siparuna cristata* (Poepp. & Endl.) A.DC., Siparunaceae, were collected at Reserva Ducke, Manaus, in August 2015. A voucher specimen is deposited at Instituto Nacional de Pesquisas da Amazônia (INPA) herbarium (Manaus, AM) under the registration INPA 269,731. This work was authorized by the Directing Council of Genetic Heritage (Conselho de Gestão do Patrimônio Genético, CGEN) by the authorization A3C04CB. The leaves were dried in a ventilated oven (Marconi, model IMA037) and ground in a Wiley-type mill (Marconi, model MA340, serial 9,304,176). The powdered material of leaves (1325.72 g) was exhaustively extracted by percolation with ethanol 96° GL, filtrated, and evaporated under reduced pressure. Then, the ethanol extract (151 g, 11.4% yield dry weight) was sequentially partitioned in a separatory funnel between water–methanol 7:3 (v/v) and hexane (23.72 g), dichloromethane (20.11 g), ethyl acetate (25.46 g), and butanol (35.43 g) in this order. The solvents were removed by rotary evaporation.

### Fractionation by Countercurrent Chromatography

Part of the CH<sub>2</sub>Cl<sub>2</sub> (DCM) extract (600 mg) from leaves of *S. cristata* was submitted to HSCCC fractionation using a Quattro HTPrep apparatus equipped with two bobbins containing two polytetrafluoroethylene multilayer coils each (26 ml, 1.0 mm i.d., + 224 ml, 3.2 mm i.d., and 95 ml, 2.0 mm i.d., + 98 ml, 2.0 mm i.d.). The 98-ml coil was used, and the solvent system chosen was hexane–ethyl acetate–methanol–water 1:1:1:1 (v/v). The upper organic layer served as a stationary phase (reversed-phase elution mode), and the aqueous phase was the mobile phase at a flow rate of 2 ml/min. The sample was dissolved in 5 ml of the solvent system (1:1, v/v), and the solution was introduced in the coil through a manual sample injection valve using a 5-ml sample loop. Thirty fractions of 4 ml were collected during elution with a rotation of 860 rpm followed by extrusion of another 30 fractions of 4 ml. Fractions were analyzed by TLC and grouped into 13 subfractions: Fr-1 (54.4 mg), Fr-2 (40.6 mg), Fr-3 (47.6 mg), Fr-4 (43.5 mg), Fr-5 (40.2 mg), Fr-6 (64.2 mg), Fr-7 (45.5 mg), 3,3',4'-tri-*O*-methyl-quercetin, **1**, Fr-8 (53.1 mg), Fr-9 (45.2 mg), Fr-10 (49.3 mg, 3,7-di-*O*-methyl-kaempferol or kumatakenin, **3**), Fr-11 (16 mg), Fr-12 (53.2 mg), and Fr-13 (47.2 mg). Fraction Fr-11 (16 mg) was further fractionated by HSCCC under the same conditions as above, to afford Fr-11A (7 mg, tetra-*O*-methyl-quercetin or retusin,

**2**) and Fr-11B (9 mg, 3,7-di-*O*-methyl-kaempferol or kumatakenin, **3**) (Fig. S1).

3,3',4'-Tri-*O*-methyl-quercetin (**1**): UV–Vis  $\lambda$ /nm ( $\lambda_{\max}$ , 253, 355); <sup>1</sup>H and <sup>13</sup>C NMR data (Figs. S20 and S27), see Table S1. Positive DI-APCI-MS/MS  $m/z$  345.2 [M+H]<sup>+</sup> (calcd for C<sub>18</sub>H<sub>17</sub>O<sub>7</sub><sup>+</sup>, 345.1), which was identified by comparison with previously described data (Awad et al. 2018).

3,7,3',4'-Tetra-*O*-methyl-quercetin (retusin) (**2**): UV–Vis  $\lambda$ /nm ( $\lambda_{\max}$ , 250, 350); <sup>1</sup>H and <sup>13</sup>C NMR data (Figs. S41 and S44). Positive DI-APCI-MS/MS  $m/z$  359.3 [M+H]<sup>+</sup> (calcd for C<sub>19</sub>H<sub>19</sub>O<sub>7</sub><sup>+</sup>, 359.1), which was identified by comparison with previously described data (Silva et al. 2009).

3,7-Di-*O*-methyl-kaempferol (kumatakenin) (**3**): UV–Vis  $\lambda$ /nm ( $\lambda_{\max}$ , 265, 345); <sup>1</sup>H and <sup>13</sup>C NMR data (Figs. S30 and S37), see Table S2. Positive DI-APCI-MS/MS  $m/z$  315.2 [M+H]<sup>+</sup> (calcd for C<sub>17</sub>H<sub>15</sub>O<sub>6</sub><sup>+</sup>, 315.1), which was identified by comparison with previously described data (Silva et al. 2009).

### Analysis by HPLC–DAD

HPLC–DAD (280 nm) analyses were performed using an Agilent 1260 Infinity Series with a Poroshell 120 EC-C18 column (2.1 × 100 mm i.d.; 2.7  $\mu$ m particle size; Agilent) at 30 °C. Gradient conditions were as follows: solvent A = water–0.01% formic acid, solvent B = acetonitrile, B = 60% in  $t = 40$  min, and B = 100% in  $t = 45$  min.

### Analysis by APCI-MS/MS

The MS analyses were performed using LCQ Fleet (Thermo Fisher Scientific, Waltham, MA, USA) through direct infusion of the diluted samples in MeOH:H<sub>2</sub>O (9:1) containing 0.1% formic acid as a modifier for positive ionization mode in a flow rate of 0.1 ml/min. The mass spectrometer, equipped with APCI font and ion trap analyzer, was operated in positive mode. High-purity nitrogen (N<sub>2</sub>) was used as sheath gas (10 arbitrary units) and auxiliary gas (5 arbitrary units). High-purity helium (He) was used as collision gas. Mass spectrometry parameters used were a source voltage of 6.0 kV, a capillary voltage of 10 V, a tube lens voltage of –13 V, a capillary temperature of 400 °C, and an APCI vaporizer temperature of 450 °C. Full-scan data acquisition (mass range:  $m/z$  50–1000). The normalized collision energy of the collision-induced dissociation (CID) cell was set at 35 eV. The spectra were processed using the Xcalibur software, version 2.2 SP1.

### Identification of Isolated Compounds

<sup>1</sup>H, <sup>13</sup>C, APT, HMBC, and HSQC NMR data were acquired in deuterated dimethyl sulfoxide (DMSO-*d*<sub>6</sub>) and chloroform-*d* (CDCl<sub>3</sub>) at 25 °C (Varian VNMRS 500 MHz



spectrometer). UV-1240 ultraviolet spectrometer (Shimadzu, Japan) uses MeOH and anhydrous sodium acetate (NaOAc) P.A. as displacement reagent.

### Inhibition of SARS-CoV-2 Replication

Vero E6 (African green monkey kidney) and Calu-3 (human lung adenocarcinoma) cells were infected with SARS-CoV-2 isolate (GISAID EPI\_ISL\_#414,045) in multiplicity of infection (MOI) 0.01 and 0.1, respectively. After 1 h, the supernatants were harvested, and the cells were incubated with 1–3 at log and semi-log concentrations (from 10 to 0.01  $\mu\text{M}$ ) or DCM extract from leaves of *Siparuna cristata* (from 250 to 31.25  $\mu\text{g}/\text{ml}$ ). Lopinavir/ritonavir (LPV/RTV) in combination and chloroquine (CLQ) were used as control. LPV/RTV was prepared in the proportion of 3:1 as the pharmaceutical pills were composed of 300 mg LPV and 100 mg RTV (Fintelman-Rodrigues et al. 2020). The concentrations of LPV/RTV showed in the present study were based on LPV concentration. After 24 h of infection in Vero E6 cells or 48 h of infection in Calu-3 cells, the supernatants were titrated by plaque-forming units (PFU/ml).

For PFU assay, monolayers of Vero E6 ( $10^5$  cell/well) in 24-well plates were infected with 300  $\mu\text{l}$  of supernatant dilutions ( $10^{-3}$ ,  $10^{-4}$ , or  $10^{-5}$ ). After 1 h at 37 °C in 5%  $\text{CO}_2$ , the medium was replaced by 500  $\mu\text{l}$  of carboxymethylcellulose solution (DMEM-HG 10 $\times$ , 1.8% carboxymethylcellulose and 2% fetal bovine serum). After 72 h of infection, the cytopathic effect (CPE) was analyzed on an optical microscope and 500  $\mu\text{l}$  of 10% formalin was added to fix the cells. After 3 h, this solution was harvested, and plaques were colored by 0.4% bromophenol blue and PFU was counted. All procedures related to virus culture were handled at biosafety level 3 (BSL3) multiuser facility, according to WHO guidelines (WHO 2020).

For cytotoxicity analysis, monolayers of  $10^4$  Vero E6 cells and  $10^5$  Calu-3 cells in 96-well plates were treated for 72 h with semi-log dilutions (from 6000 to 50  $\mu\text{M}$ ) of all compounds tested or DCM extract (200  $\mu\text{g}/\text{ml}$ ). Then, 5 mg/ml of 3-(4,5-dimethylthiazol-2-yl)-2,5-diphenyltetrazolium bromide (MTT, Sigma) in 1 $\times$  PBS was added to the cells, according to the manufacturer's instructions. After 4 h at 37 °C, 10% SDS was added. After incubating for 2 h at 37 °C, the plates were read in a spectrophotometer at 570 nm. The 50% cytotoxic concentration ( $\text{CC}_{50}$ ) was calculated by a non-linear regression analysis of the dose–response curves. All the compounds were resuspended in 100% dimethyl sulfoxide (DMSO) for the in vitro tests. In the assays, the DMSO final concentrations were equal or lower than 1% (v/v) diluted in Dulbecco's modified Eagle's medium (DMEM, Gibco), not affecting the growth of the cells.

## In Silico Analyses

### Preparation of Receptors and Ligands

The selected crystal structures for 3CLpro (PDBid 6XQT) and for PLpro (PDBid 7JRN) were obtained from the Protein Data Bank. Through the Pymol and UCSF Chimera software programs, all ligands and identical chains present in the molecules were removed (De Lano 2002; Pettersen et al. 2004). The ligand files were processed by the PDB2PQR server (<http://server.poissonboltzmann.org/pdb2pqr>) (Dolinsky et al. 2007) with AMBER force field in order to assess the pKa prediction of the ionizable protein residuals at pH 7.4. For 3CLpro, the selection of the probable 3D-structure protonation state was performed through the *pdb2gm* module from the computational package GROMACS with the AMBER99SB-ILDN protein field force, nucleic AMBER94 (Abraham et al. 2015). The conversion of the structure and the bind to the *pdbqt* format was performed with AutoDock tools (Morris et al. 2009), while the PLpro PDB2PQR output was converted by using UCSF Chimera.

### Molecular Docking

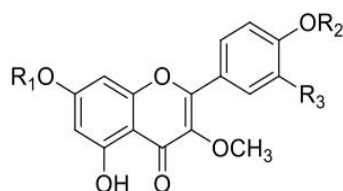
Through the Zone function, which is available at the Chimera software (Pettersen et al. 2004), the far residuals were selected until 5 Å from the selected bind is achieved. With this selected perimeter, it was developed with the grid center  $x = -11$ , center  $y = 1$ , and center  $z = 45$ , and size  $x = 32$ , size  $y = 35$ , and size  $z = 33$  for 3CLpro, and center  $x = 13$ , center  $y = -9$ , and center  $z = 30$ , and size  $x = 30$ , size  $y = 30$ , and size  $z = 30$  for PLpro. The protein redocking was performed with the AutoDock Vina software (Trott et al. 2009). Six different dockings were performed for both receptors using the following substances: lopinavir, ritonavir, chloroquine, 3,3',4'-tri-*O*-methyl-quercetin (1), 3,7,3',4'-tetra-*O*-methyl-quercetin (2), and 3,7-di-*O*-methyl-kaempferol (3). The results were reranked based on the distances in Å from hydrogen bonds between the His41, Cys145, and Glu166 residues for 3CLpro, and from the one created with residue Tyr268, described as the main bonding interaction for PLpro.

## Results and Discussion

### Isolation and Characterization of Flavonoids

To isolate the flavonoids (1–3) from *S. cristata*, the DCM extract was fractionated by HSCCC. DCM extracts normally contain compounds of medium polarity, and therefore, the solvent system hexane–ethyl acetate–methanol–water (HEMWat) was used because of the versatility

and range of polarity of this solvent system family (Costa and Leitão 2010; Costa et al. 2013). In general, the selection of HEMWat ratios should start with 1:1:1:1 (v/v) and then be adjusted with the proper polarity for  $K$  near 1 for the target compounds (Costa and Leitão 2010). In the present case, these ratios were appropriate for the fractionation of the DCM extract of leaves of *S. cristata*. HPLC–DAD analysis of the resulting 13 fractions (Figs. S2 to S7) revealed the presence of the flavonoids in fractions Fr-7 to Fr-12 (Tables S1–S3), which annotation results and data obtained with HPLC–DAD and DI-APCI (+)-MS/MS analyses are summarized in Table S3. A detailed description of fraction annotations can be found in the Supplementary Material.



- 1  $R_1=H$ ;  $R_2=CH_3$ ;  $R_3=OCH_3$   
 2  $R_1=R_2=CH_3$ ;  $R_3=OCH_3$   
 3  $R_1=CH_3$ ;  $R_2=R_3=H$

### Cell Toxicity and Inhibition of SARS-CoV-2 Replication

Flavonoids 1–3 and DCM extract were evaluated against SARS-CoV-2 replication and cell viability (Table 1). The combination of LPV/RTV and CLQ was used as a positive control to inhibit viral protease and replication. Retusin (2), kumatakenin (3), and the DCM extract were able to inhibit

SARS-CoV-2 replication, while the flavonoid 3,3',4'-tri-*O*-methyl-quercetin (1) did not exert any inhibition, in both Vero E6 and Calu-3 cells. In Vero E6 and Calu-3 cells, retusin (2) was active at the lowest concentrations tested and displayed a lower  $EC_{50}$  than the tested controls (LPV/RTV and CLQ), with a selective index (SI) which is 1257 and 7 times greater than LPV/RTV and CLQ, respectively, in Vero E6 cells. In Calu-3, retusin (2) showed an inhibitory effect 417 times greater than LPV/RTV. CLQ did not have an inhibitory effect, as shown in previous studies (Hoffmann et al. 2020). The three analyzed flavonoids have high  $CC_{50}$  values and are less toxic than the compounds used as control in both cell lineages analyzed (Table 1).

The inhibitory activity of 3CLpro and PLpro SARS-CoV-2 proteases by flavonoids was recently described through attaching to their active site and inactivating them (Tutunchi et al. 2020). Quercetin reduced the infectivity of human and bovine coronaviruses, showing activities against SARS-CoV and MERS-CoV (Russo et al. 2020; Solnier et al. 2020). Tetramethyl derivatives of quercetin have shown to display antiviral and cytotoxic activities; e.g., retusin (2), isolated from rhizomes of *Kaempferia parviflora* Wall. ex Baker, Zingiberaceae, showed an inhibitory effect on the feline foamy virus (FFV) (Lee et al. 2017). Also, 5,7,3',4'-tetra-*O*-methyl-quercetin, isolated from *Sambucus nigra* L., Adoxaceae, inhibited influenza A (H1N1) infection in vitro (Roschek Jr. et al. 2009). Studies show inhibition of neuraminidase activity for kumatakenin (3) (Ryu et al. 2010). Recently, pectolinarin (5,7-dihydroxy-4',6-dimethoxyflavone-7-rutinoside) demonstrated inhibitory activity by efficiently blocking the enzymatic activity of SARS-CoV-2 3CL-Pro (Jo et al. 2020). Therefore, the study with flavonoids is interesting from the point of view of viral proteases.

**Table 1**  $CC_{50}$ ,  $EC_{50}$ , and SI values for 3,3',4'-tri-*O*-methyl-quercetin, 1; 3,7,3',4'-tetra-*O*-methyl-quercetin (retusin), 2; 3,7-di-*O*-methyl-kaempferol (kumatakenin) 3; LPV/RTV; and CLQ

	Vero E6			Calu-3		
	$CC_{50}$ ( $\mu$ M)	$EC_{50}$ ( $\mu$ M)	SI	$CC_{50}$ ( $\mu$ M)	$EC_{50}$ ( $\mu$ M)	SI
3,3',4'-Tri- <i>O</i> -methyl-quercetin (1)	3000 $\pm$ 150	NA	NA	3500 $\pm$ 130	NA	NA
3,7-Di- <i>O</i> -methyl-kaempferol (kumatakenin) (3)	2000 $\pm$ 230	10 $\pm$ 0.7	200	2080 $\pm$ 135	0.3 $\pm$ 0.02	6933
3,7,3',4'-Tetra- <i>O</i> -methyl-quercetin (retusin) (2)	4575 $\pm$ 300	0.4 $\pm$ 0.05	11,438	5000 $\pm$ 200	0.6 $\pm$ 0.06	8333
LPV/RTV	91 $\pm$ 3	10 $\pm$ 3	9.1	100 $\pm$ 3	5 $\pm$ 0.5	20
CLQ	1664 $\pm$ 75	1 $\pm$ 0.15	1664	500 $\pm$ 50	NA	NA
<i>Siparuna cristata</i> dichloromethane crude extract	> 200 $\mu$ g/ml	< 31.25 $\mu$ g/ml	> 6.4	> 200 $\mu$ g/ml	< 31.25 $\mu$ g/ml	> 6.4

$CC_{50}$ , the concentration required to reduce normal, non-infected cell viability by 50%. The values represent the mean of duplicate samples from three independent experiments.  $EC_{50}$ , the concentration required to reduced inhibition of viral infection-induced cytopathogenicity by 50%. The values represent the mean of duplicate samples from three independent experiments

SI selective index determined by the ratio between  $CC_{50}$  and  $EC_{50}$ . LPV/RTV the combination of lopinavir/ritonavir, CLQ chloroquine, NA not applicable



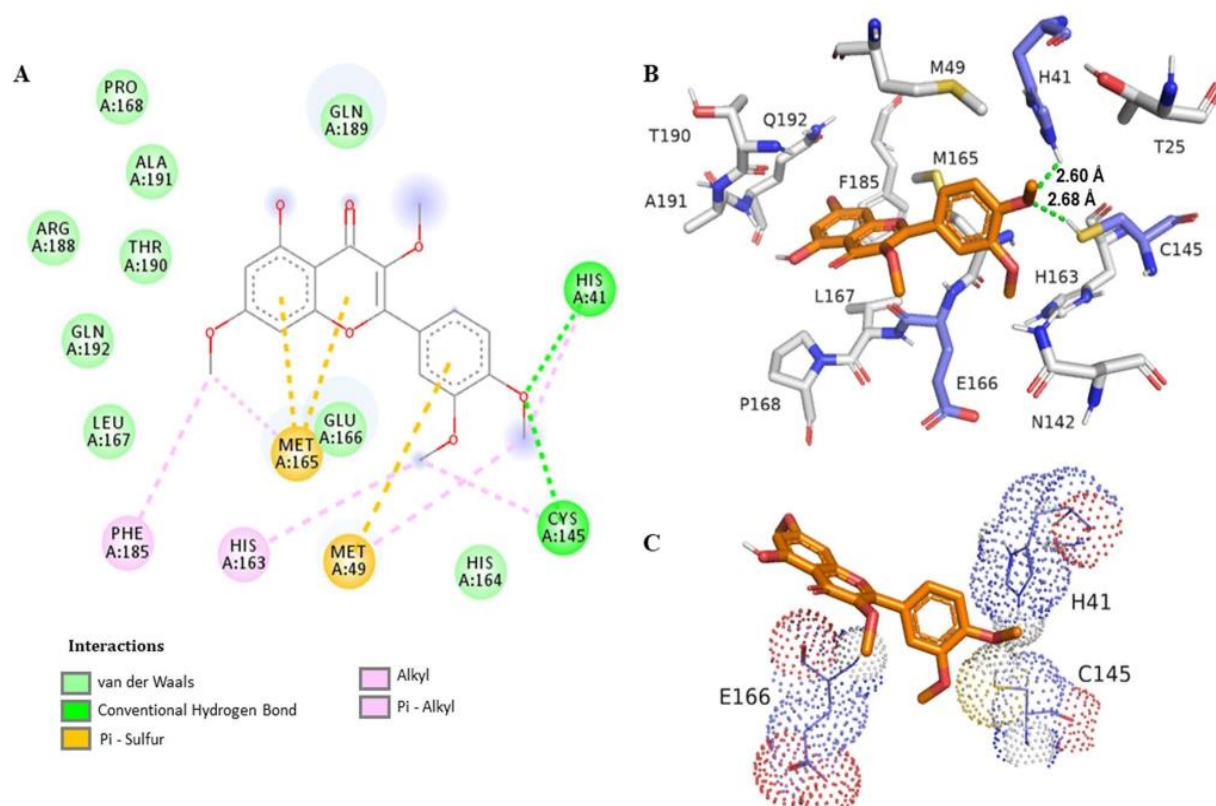


**Fig. 1** Interaction of SARS-CoV-2 3CLpro protease residues with retusin (**2**). **A** Map of the interaction of residues. **B** Protease 3CLpro (PDBid: 6XQT) in gray and residues within a radius of proximity equal to 5 Å of the ligand, represented by sticks. The ligand is in

orange, and the catalytic dyad residues His41 and Cys145 and the residue Glu166 are in lavender. **C** The representation shows the interaction of these residues with the ligand

## Molecular Docking with 3CLpro

Previous studies have shown hydrophobic  $\pi$ - $\pi$  stacking interactions with His41 residue via molecular docking (Xu et al. 2020). Therefore, His41 was the choice to analyze the binding distance from the ligand, due the importance of this residue on the enzyme activity. Also, flavonoids have

demonstrated a wide range of binding affinity to SARS-CoV-2 3CLpro due to their hydrophobic aromatic rings and hydrophilic hydroxyl groups (Jo et al. 2020). The first bind mode generated on the redocking step presented a bind energy of  $-10.4$  kcal/mol, and the root mean square deviation (RMSD) is equal to  $0.97$  Å (Fig. S51) between the pose and the crystal original bind (PDBid 6XQT) calculated

**Table 2** Energy docking values for 3CLpro and PLpro hydrogen-bonding interaction with compounds 1–3

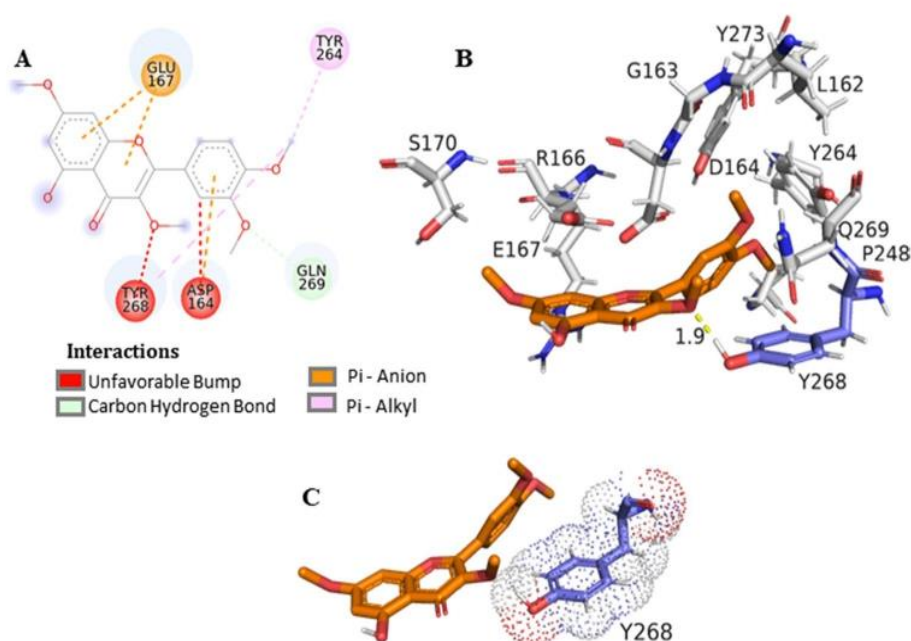
Compound	3CLpro			PLpro				
	Affinity for the best distance mode (kcal/mol)	Mode	Distance His41 (Å)	Distance Cys145 (Å)	Distance Glu166 (Å)	Affinity for the best distance mode (kcal/mol)	Mode	Distance Tyr268 (Å)
<b>1</b>	-6.5	9	-	2.77	-	-7.1	1	2.2
<b>2</b>	-6.3	6	2.60	2.68	-	-5.5	7	1.9
<b>3</b>	-7.2	3	-	3.01	2.19	-5.7	7	2.1
LPV <sup>a</sup>	-5.1	9	2.92	-	-	-5.7	9	1.8
RTV <sup>b</sup>	-8.1	11	2.41	2.68	2.42	-6.9	2	1.6
CLQ <sup>c</sup>	-6.4	1	-	-	2.11	-5.9	8	1.1

<sup>a</sup>Positive control: lopinavir

<sup>b</sup>Positive control: ritonavir

<sup>c</sup>Positive control: chloroquine

**Fig. 2** Interaction of SARS-CoV-2 PLpro residues with retusin (**2**). **A** Map of the interaction of residues. **B** Protease PLpro (PDBid:7JRN) in gray and residues within a radius of proximity equal to 5 Å of the ligand, represented by sticks. The ligand is in orange, and the residue Tyr268 is in lavender. **C** This representation shows the interaction of this residue with the ligand



with the Open Babel software (Table S4) (Murray-Rust et al. 2004). The simulations revealed the best interactions with their respective binding energy value: thus, the value of  $-6.5$  kcal/mol was obtained for **1** (Fig. S53),  $-7.2$  kcal/mol for **3** (Fig. S54), and  $-6.3$  kcal/mol for **2**, and finally, the following values were obtained for the control drugs:  $-6.4$  kcal/mol for CLQ,  $-5.1$  kcal/mol (Fig. S52) for LPV, and  $-8.1$  kcal/mol for RTV. Figure 1 illustrates the most frequent and stable retusin (**2**)–3CLpro protease complex where it was possible to identify a hydrogen-bonding interaction of the  $\text{OCH}_3$  at C-4' with the His41 residue with a distance of  $2.6$  Å. Table 2 summarizes the best binding energies, as well as the distances between the His41, Cys145, and Glu166 residues from the receptor protein 3CLpro (PDBid: 6XQT).

### Molecular Docking with PLpro

The first bind mode generated on the redocking step presented a bind energy of  $-9.6$  kcal/mol and the RMSD of  $0.45356$  Å (Fig. S55) between the pose and the crystal original bind (PDBid: 7JRN) calculated with the Open Babel software (Table S4) (Murray-Rust et al. 2004). Molecular docking simulations afforded the following results based on affinity energy and distances for ligands and the Tyr268 residue (Table 2): RTV  $-6.9$  kcal/mol, distance  $1.6$  Å; LPV  $-5.7$  kcal/mol, distance  $1.8$  Å; CLQ  $-5.9$  kcal/mol, distance  $1.1$  Å (Fig. S56); 3,3',4'-tri-*O*-methyl-quercetin (**1**)  $-7.2$  kcal/mol, distance  $2.2$  Å (Fig. S57); retusin (**2**)  $-5.5$  kcal/mol, distance  $1.9$  Å; and kumatakenin (**3**)  $-5.7$  kcal/mol, distance  $2.1$  Å (Fig. S58). Based on these

results, the interaction between PLpro and the ligand retusin (**2**) may be favorable due the proximity of the  $\text{OCH}_3$  at C-3 from the Tyr268 residue (Fig. 2). Docking simulations have shown the SARS-CoV-2 PLpro BL2 loop having significant flexibility in ligand-free proteins. Residues Asn267, Gln269, and most importantly, Tyr268 account for most of this motion, making Tyr268 the key residue to calculate the distance in Å between the enzyme and inhibitor (Bosken et al. 2020). Flavonoids were previously described as potential inhibitors, by assuming that the hydrophobic flavonoids have shown higher affinity to SARS-CoV PLpro than to other proteases, which might be due to certain structural differences in the protein sequences (Solnier et al. 2020).

### Conclusions

In this work, we describe the anti-SARS-CoV-2 potential of a Brazilian medicinal plant traditionally used to treat respiratory infections such as colds and flu with a long history of commercialization for this purpose. Two isolated flavonoids inhibited SARS-CoV-2 viral replication with higher efficiency and lower cytotoxicity than lopinavir/ritonavir and chloroquine treatment. Among the isolated flavonoids, tetra-*O*-methyl-quercetin is being reported for the first time in the genus as well as the inhibitory potential of free *O*-methyl-flavonoids against SARS-CoV-2. The in silico results demonstrated the potential interaction between flavonoids and key residues of COVID-19 3CLpro as well as PLpro, in a similar way to that of the screened potential inhibitors against COVID-19. Retusin (3,7,3',4'-tetra-*O*-methyl-quercetin) demonstrated the best results in the assays and in



the molecular docking, based on the hydrogen-bonding distance between selected amino acid residues of the catalytic site from 3CLpro and PLpro SARS-CoV-2 proteases and all tested flavonoids. This study highlights the possible application of methylated flavonoids, for example retusin, as an antiviral or adjuvant therapy in the treatment of COVID-19.

**Supplementary Information** The online version contains supplementary material available at <https://doi.org/10.1007/s43450-021-00162-5>.

**Acknowledgements** We are indebted to the Laboratório Multiusuário de Análises por RMN at the Federal University of Rio de Janeiro for the access to NMR facilities, and to the Central Analítica, Departamento de Produtos Naturais e Alimentos for the MS analyses. Thanks are due to Dr. Carmen Beatriz Wagner Giacoia Gripp for the assessments related to BSL3 facility.

**Author Contribution** Collecting and identifying plant material: PHAN; HSCCC experiments: CML, RS, and PHAN; interpretation of the spectrometric data: CML and SCM; supervision of the chromatographic and MS analyses: FNC, RCS, SGL, and GGL; biological assays: TSG, MESM, ART, NFR, MMS, and MDM; molecular docking: CFARC, MEAE, and MLS; drafting the manuscript: all authors; critical revision of the manuscript: GGL, SGL, RCS, MDM, and MLS. All the authors have read the final manuscript and approved its submission.

**Funding** Financial support was provided by the Conselho Nacional de Desenvolvimento Científico e Tecnológico, Fundação de Amparo à Pesquisa do Estado do Rio de Janeiro, and Coordenação de Aperfeiçoamento de Pessoal de Nível Superior.

## Declarations

**Competing Interests** The authors declare no competing interests.

## References

- Abdul S, Banerjee S, Ghosh K, Gayen S, Jha T (2021) Protease targeted COVID-19 drug discovery and its challenges: insight into viral main protease (Mpro) and papain-like protease (PLpro) inhibitors. *Bioorgan Med Chem* 29:115860. <https://doi.org/10.1016/j.bmc.2020.115860>
- Awad HM, Abd-Alla HI, Ibrahim MA, El-Sawy ER, Abdalla MM (2018) Flavones from heavenly blue as modulators of Alzheimer's amyloid-beta peptide (A $\beta$ ) production. *Med Chem Res* 27:768–776. <https://doi.org/10.1007/s00044-017-2100-x>
- Berretta AA, Silveira MAD, Capcha JMC, De Jong D (2020) Propolis and its potential against SARS-CoV-2 infection mechanisms and COVID-19 disease. *Biomed Pharmacother* 131:110622. <https://doi.org/10.1016/j.biopha.2020.110622>
- Bosken YK, Cholko T, Lou YC, Wu KP, Chang CA (2020) Insights into dynamics of inhibitor and ubiquitin-like protein binding in SARS-CoV-2 papain-like protease. *Front Mol Biosci* 7:174. <https://doi.org/10.3389/fmolb.2020.00174>
- Cherrak SA, Merzouk H, Mokhtari-Soulimane N (2020) Potential bioactive glycosylated flavonoids as SARS-CoV-2 main protease inhibitors: a molecular docking and simulation studies. *PLoS ONE* 15:e0240653. <https://doi.org/10.1371/journal.pone.0240653>
- Chinsebu KC (2020) Coronaviruses and nature's pharmacy for the relief of coronavirus disease 2019. *Rev Bras Farmacogn* 30:603–621. <https://doi.org/10.1007/s43450-020-00104-7>
- Cock IE, Vuuren SFV (2020) The traditional use of southern African medicinal plants in the treatment of viral respiratory diseases: a review of the ethnobotany and scientific evaluations. *J Ethnopharmacol* 262:113194. <https://doi.org/10.1016/j.jep.2020.113194>
- Costa FN, Leitão GG (2010) Strategies of solvent system selection for the isolation of flavonoids by countercurrent chromatography. *J Sep Sci* 33:336–347. <https://doi.org/10.1002/jssc.200900632>
- Costa FN, Garrard I, Da Silva AJ, Leitão GG (2013) Changes in the mobile phase composition on a stepwise counter-current chromatography elution for the isolation of flavonoids from *Siparuna glycyarpa*. *J Sep Sci* 36:2253–2259. <https://doi.org/10.1002/jssc.201201054>
- Dolinsky TJ, Czodrowski P, Li H, Nielsen JE, Jensen JH, Klebe G, Baker NA (2007) PDB2PQR: expanding and upgrading automated preparation of biomolecular structures for molecular simulations. *Nucleic Acids Res* 35(Suppl. 2):522–525. <https://doi.org/10.1093/nar/gkm276>
- Elizalde-González JJ (2020) SARS-CoV-2 and COVID-19. A pandemic review. *Med Crit* 3:53–67. <https://doi.org/10.35366/93281>
- El-Mordy FMA, El-Hamouly MM, Ibrahim MT, El-Rheem GA, Aly OM, El-Kader AMA, Youssif KA, Abdelmohsen UR (2020) Inhibition of SARS-CoV-2 main protease by phenolic compounds from *Manilkara hexandra* (Roxb.) Dubard assisted by metabolite profiling and *in silico* virtual screening. *RSC Adv* 10:32148–32155. <https://doi.org/10.1039/d0ra05679k>
- Fintelman-Rodrigues N, Sacramento SQ, Lima CR, Da Silva FS, Ferreira AC, Mattos M, De Freitas CS, Soares VC, Dias SSG, Temer-ozo JR, Miranda MD, Matos AR, Bozza FA, Carels N, Alves CR, Siqueira MM, Bozza PT, Souza TM (2020) Atazanavir, alone or in combination with ritonavir, inhibits SARS-CoV-2 replication and proinflammatory cytokine production. *Antimicrob Agents Chemother* 64:e00825-e920. <https://doi.org/10.1128/AAC.00825-20>
- Hoffmann M, Mosbauer K, Hofmann-Winkler H, Kaul A, Kleine-Weber H, Kruger N, Gassen NC, Muller MA, Drosten C, Pohlmann S (2020) Chloroquine does not inhibit infection of human lung cells with SARS-CoV-2. *Nature* 585:588–590. <https://doi.org/10.1038/s41586-020-2575-3>
- Jo S, Kim S, Kim DY, Kim MS, Shin DH (2020) Flavonoids with inhibitory activity against SARS-CoV-2 3CLpro. *J Enzyme Inhib Med Chem* 35:1539–1544. <https://doi.org/10.1080/14756366.2020.1801672>
- Komolafe K, Komolafe TR, Fatoki TH, Akinmoladun AC, Brai BIC, Olaleye MT, Akindahunsi AA (2021) Coronavirus disease 2019 and herbal therapy: pertinent issues relating to toxicity and standardization of phytopharmaceuticals. *Rev Bras Farmacogn* 31:142–161. <https://doi.org/10.1007/s43450-021-00132-x>
- Leal CM, Simas RC, Miranda M, Campos MF, Gomes BA, Siqueira MM, Do Vale G, De Almeida CVG, Leitão SG, Leitão GG (2021) Amazonian *Siparuna* extracts as potential anti-influenza agents: metabolic fingerprinting. *J Ethnopharmacol* 270:113788. <https://doi.org/10.1016/j.jep.2021.113788>
- Lee GE, Kim J, Shin CG (2017) Antiviral activities of hydroxylated flavones on feline foamy viral proliferation. *Appl Biol Chem* 60:419–425. <https://doi.org/10.1007/s13765-017-0294-8>
- Leitão GG, Simas NK, Soares SS, De Brito AP, Claros BM, Brito TB, DelleMonache F (1999) Chemistry and pharmacology of Monimiaceae: a special focus on *Siparuna* and *Mollinedia*. *J Ethnopharmacol* 65:87–102. [https://doi.org/10.1016/s0378-8741\(98\)00233-5](https://doi.org/10.1016/s0378-8741(98)00233-5)
- Leitão GG, Soares SSV, Brito M, DelleMonache F, De Barros T (2000) Kaempferol glycosides from *Siparuna apiosyce*. *Phytochemistry* 55:679–682. [https://doi.org/10.1016/S0031-9422\(00\)00222-3](https://doi.org/10.1016/S0031-9422(00)00222-3)



- Leitão GG, El-Adji SS, De Melo WAL, Leitão SG, Brown L (2005) Separation of free and glycosylated flavonoids from *Siparuna guianensis* by gradient and isocratic CCC. *J Liq Chromatogr R T* 28:2041–2051. <https://doi.org/10.1081/JLC-200063669>
- Liskova A, Samec M, Koklesova L, Samuel SM, Zhai K, Al-Ishaq RK, Abotaleb M, Nosal V, Kajo K, Ashrafizadeh M, Zarrabi A, Brockmueller A, Shakibaei M, Sabaka P, Mozos I, Ullrich D, Prosecky R, La Rocca G, Caprnda M, Busselberg D, Rodrigo L, Kruzliak P, Kubatka P (2021) Flavonoids against the SARS-CoV-2 induced inflammatory storm. *Biomed Pharmacother* 138:111430. <https://doi.org/10.1016/j.biopha.2021.111430>
- Maisch B (2020) SARS-CoV-2 as potential cause of cardiac inflammation and heart failure. Is it the virus, hyperinflammation, or MODS? *Herz* 22:321–322. <https://doi.org/10.1007/s00059-020-04925-z>
- Mani JS, Johnson JB, Steel JC, Broszczak DA, Neilsen PM, Walsh KB, Naiker M (2020) Natural product-derived phytochemicals as potential agents against coronaviruses: a review. *Virus Res* 284:197989. <https://doi.org/10.1016/j.virusres.2020.197989>
- Morris GM, Ruth H, Lindstrom W, Sanner MF, Belew RK, Goodsell DS, Olson AJ (2009) Software news and updates AutoDock4 and AutoDockTools4: automated docking with selective receptor flexibility. *J Comput Chem* 30:2785–2791. <https://doi.org/10.1002/jcc.21256>
- Mouffouk C, Mouffouk S, Mouffouk S, Hambaba L, Haba H (2021) Flavonols as potential antiviral drugs targeting SARS-CoV-2 proteases (3CLpro and PLpro), spike protein, RNA-dependent RNA polymerase (RdRp) and angiotensin-converting enzyme II receptor (ACE2). *Eur J Pharmacol* 891:173759. <https://doi.org/10.1016/j.ejphar.2020.173759>
- Murray-Rust P, Rzepa HS, Williamson MJ, Willighagen EL (2004) Chemical markup, XML, and the world wide web. 5. Applications of chemical metadata in RSS aggregators. *J Chem Inform Comput Sci* 44:462–469. <https://doi.org/10.1021/ci034244p>
- Pandey P, Khan F, Rana AK, Srivastava Y, Jha SK, Jha NK (2021) A drug repurposing approach towards elucidating the potential of flavonoids as COVID-19 spike protein inhibitors. *Biointerface Res Appl Chem* 11:8482–8501. <https://doi.org/10.33263/BRIAC111.84828501>
- Pettersen EF, Goddard TD, Huang CC, Couch GS, Greenblatt DM, Meng EC, Ferrin TE (2004) UCSF Chimera. A visualization system for exploratory research and analysis. *J Comput Chem* 25:1605–1612. <https://doi.org/10.1002/jcc.20084>
- Ren X, Shao XX, Li XX, Jia XH, Song T, Zhou WY, Wang P, Li Y, Wang XL, Cui QH, Qiu PJ, Zhao YG, Li XB, Zhang FC, Li ZY, Zhong Y, Wang ZG, Fu XJ (2020) Identifying potential treatments of COVID-19 from traditional Chinese medicine (TCM) by using a data-driven approach. *J Ethnopharmacol* 258:112932. <https://doi.org/10.1016/j.jep.2020.112932>
- Robba C, Battaglini D, Pelosi P, Rocco PRM (2020) Multiple organ dysfunction in SARS-CoV-2: MODS-CoV-2. *Expert Rev Respir Med* 9:865–868. <https://doi.org/10.1080/17476348.2020.1778470>
- Roschek B Jr, Fink RC, McMichael MD, Li D, Alberte RS (2009) Elderberry flavonoids bind to and prevent H1N1 infection *in vitro*. *Phytochemistry* 70:1255–1261. <https://doi.org/10.1016/j.phytochem.2009.06.003>
- Russo M, Moccia S, Spagnuolo C, Tedesco I, Russo GL (2020) Roles of flavonoids against coronavirus infection. *Chem-Biol Interact* 328:109211. <https://doi.org/10.1016/j.cbi.2020.109211>
- Ryu YB, Kim JH, Park SJ, Chang JS, Rho MC, Bae KH, Park KH, Lee WS (2010) Inhibition of neuraminidase activity by polyphenol compounds isolated from the roots of *Glycyrrhiza uralensis*. *Bioorg Med Chem Lett* 20:971–974. <https://doi.org/10.1016/j.bmcl.2009.12.106>
- Santana FPR, Thevenard F, Gomes KS, Taguchi L, Câmara NOS, Stilhano RS, Ureshino RP, Prado CM, Lago JHG (2021) New perspectives on natural flavonoids on COVID-19-induced lung injuries. *Phytoter Res*. <https://doi.org/10.1002/ptr.7131>
- Solnier J, Fladerer JP (2020) Flavonoids: a complementary approach to conventional therapy of COVID-19?. *Phytochem Rev*. <https://doi.org/10.1007/s11101-020-09720-6>
- Trott O, Olson AJ (2009) AutoDock Vina: improving the speed and accuracy of docking with a new scoring function, efficient optimization, and multithreading. *J Comput Chem* 31:455–461. <https://doi.org/10.1002/jcc.21334>
- Tutunchi H, Naeini F, Ostadrahimi A, Hosseinzadeh-Attar MJ (2020) Naringenin, a flavanone with antiviral and anti-inflammatory effects: a promising treatment strategy against COVID-19. *Phytoter Res* 34:3137–3147. <https://doi.org/10.1002/ptr.6781>
- Xu Z, Yang L, Zhang X, Zhang Q, Yang Z, Liu Y, Wei S, Liu W (2020) Discovery of potential flavonoid inhibitors against COVID-19 3CL proteinase based on virtual screening strategy. *Front Mol Biosci* 7:556481. <https://doi.org/10.3389/fmolb.2020.556481>



## Supplementary material

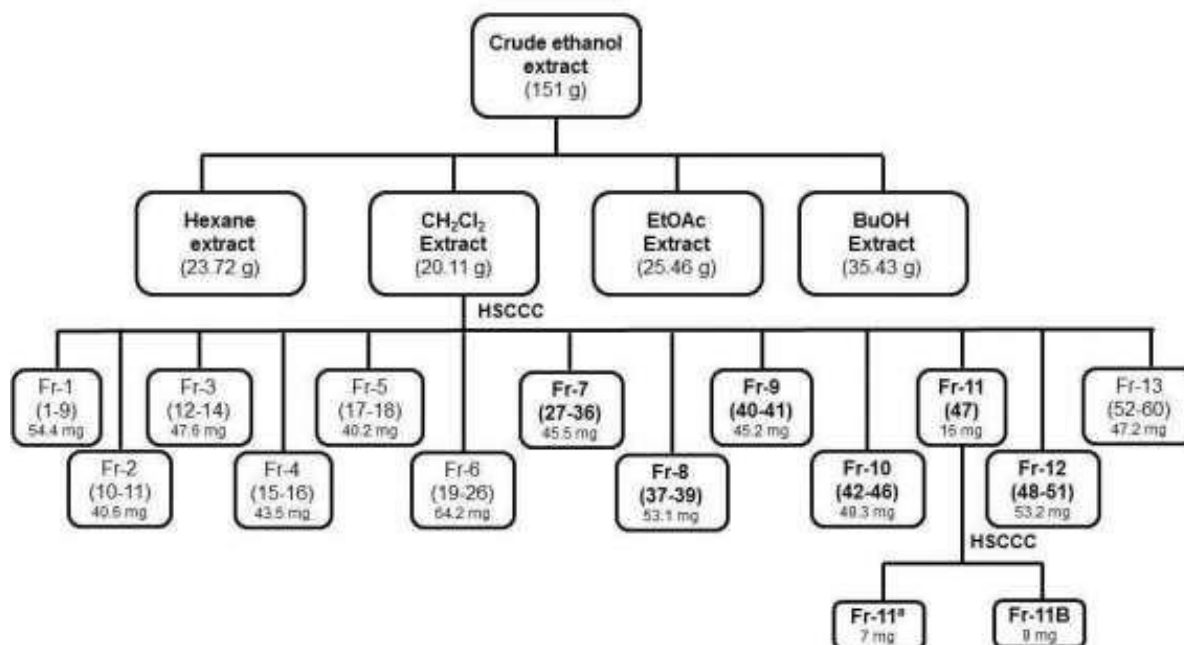


**Fig. S1** Flowchart of the fractionation of the crude ethanol extract of *S. cristata* leaves.

### Detailed description of fractions Fr-7 to Fr-12 annotations

The HPLC-DAD chromatogram of fractions Fr-7 to Fr-12 showed only two different ultraviolet profiles compatible with kaempferol and quercetin derivatives (Fig. S2 to S7), a common feature in *Siparuna* genus. Flavonoids with these two aglycones have been previously isolated from *S. apiosyce* (Leitão et al. 2000), *S. guianensis* (Leitão et al. 2005), *S. glycyarpa* (Costa et al. 2013) and *S. gigantotepala*. Kaempferol and quercetin display two absorption maxima in the ultraviolet- visible for Bands I and II, in the ranges 300-380 nm and 240-285 nm, respectively, which is in accordance with our data, suggesting the presence of three major derivatives of quercetin in peaks at *Rt* 29.4, 32.7 and 36.7min; as well as one kaempferol derivative at *Rt* 32.2 min.

The positive mode APCI ionization source was chosen for the MS analyzes (Table S1 and Fig. S8 to S19) of the fractions. The profile showed three major compounds with intense protonatedmolecular ions  $[M + H]^+$ , in the range of  $m/z$  100 to 1000, so three major masses were detected: i) DI-APCI-MS/MS for compound **1** (obtained from Fr-7, *Rt* 29.4 min, Fig. S8 to S9) displayed fragments

at  $m/z$  330  $[M + H - CH_3]^+$  and 315  $[M + H - 2 \times CH_3]^+$  corresponding to the neutral losses of two methyl groups. The molecular mass obtained was 345  $[M + H]^+$ , compatible with the molecular formula  $C_{18}H_{16}O_7$ , and the compound was identified as tri-*O*-methyl-quercetin (**1**) by comparison with  $^1H$ ,  $^{13}C$  and 2D NMR (Fig. S20 to S27). Compound **1** was therefore identified as 3,3',4'-tri-*O*-methyl-quercetin (Table S1) (Awad et al. 2018). As far as we know, the  $^{13}C$  NMR data for this compound, isolated for the first time from *Ericameria diffusa* is being reported here for the first time (Urbatsch et al. 1976); ii) Fr-10 consisted of compound **3** ( $R_t$  32.2 min), showing  $[M + H]^+$  at  $m/z$  315, with its CID MS spectra contain peaks at  $m/z$  300  $[M + H - CH_3]^+$  and 287  $[aglycone + H]^+$  compatible with di-*O*-methyl-kaempferol structure,  $C_{17}H_{14}O_6$  (Fig. S14 to S15). The structure of 3,7-di-*O*-methyl-kaempferol or kumatakenin (**3**) was confirmed by NMR analyses and is in accordance with those reported in the literature (Fig. S30 to S37, Table S2) (Silva et al. 2009). This compound was also isolated from Fr-11 (Fig. S16 to S17; Fig. S38 to S40) by further purification by HSCCC (fraction 11B; Fig. S45 to S50), which also afforded tetra-*O*-methyl-quercetin or retusin (**2**) ( $R_t$  36.7 min,  $[M + H]^+$  359), in fraction 11A (Fig. S41 to S44); and ii) The analysis of fraction 11A by NMR showed in the  $^1H$  spectrum signals of methoxyl groups with integration for 4 MeO (Fig. S44) and aromatic protons from the AB and ABC systems (Fig. S42 to S43) corresponding to tetra-*O*-methyl-quercetin. The signal at  $\delta_H$  12.65 (Fig. S41) confirmed the presence of the free 5-OH group in a hydrogen bond with C-4 carbonyl, confirming the presence of 3,7,3',4'-tetra-*O*-methyl-quercetin (retusin) (**2**) (Silva et al. 2009) in this fraction.

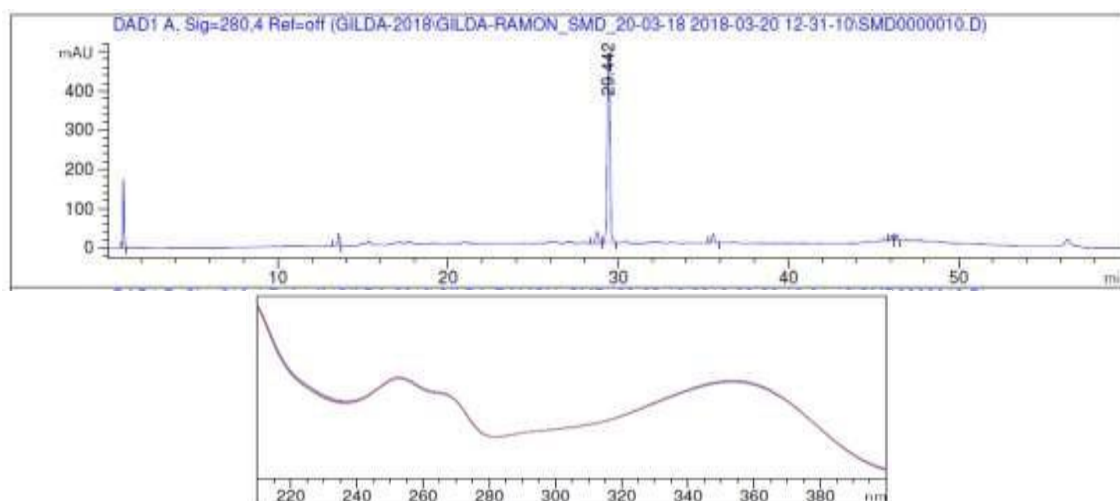


**Fig. S2** HPLC-DAD profile of Fr-7 and UV spectrum of peak at 29.4 min at 280nm (3,3',4'-tri-*O*-methyl-*quercetin*, **1**).

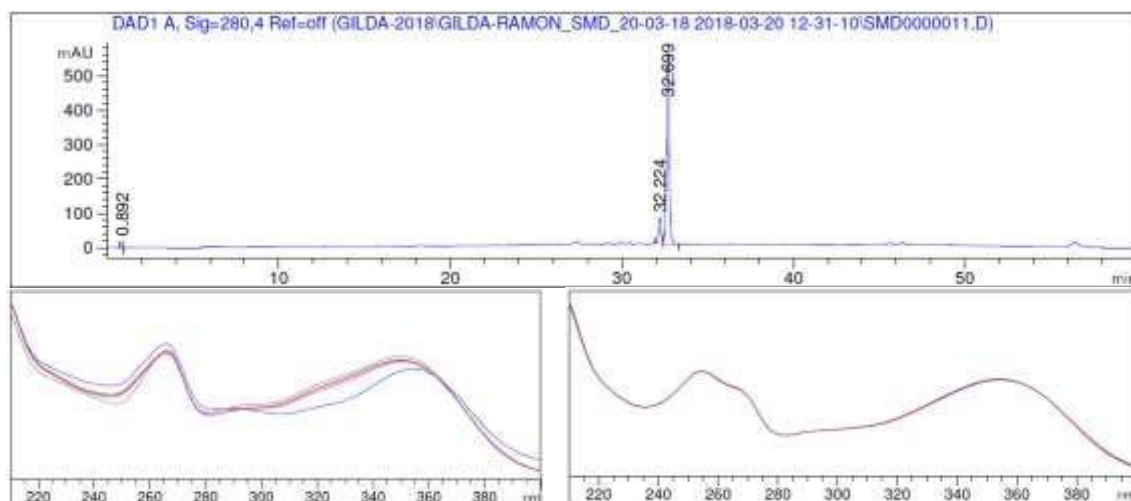


**Fig. S3** HPLC-DAD profile of Fr-8 and UV spectra of peaks at 32.2 and 32.7 min at 280nm (di-*O*-methyl-*kaempferol* and tri-*O*-methyl-*quercetin*).

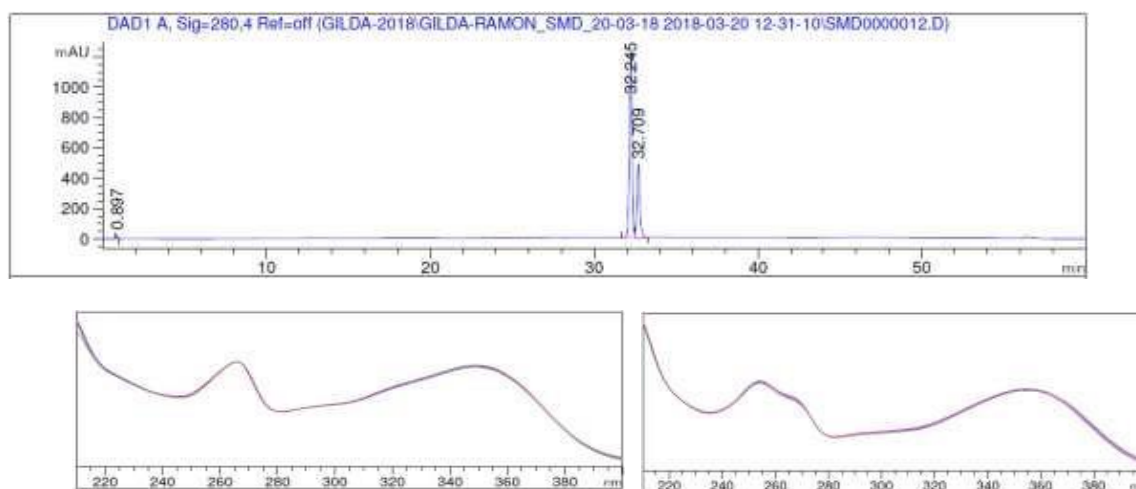


**Fig. S4** HPLC-DAD profile of Fr-9 and UV spectra of peaks at 32.2 and 32.7 min at 280nm (di-*O*-methyl-*kaempferol* and tri-*O*-methyl-*quercetin*).

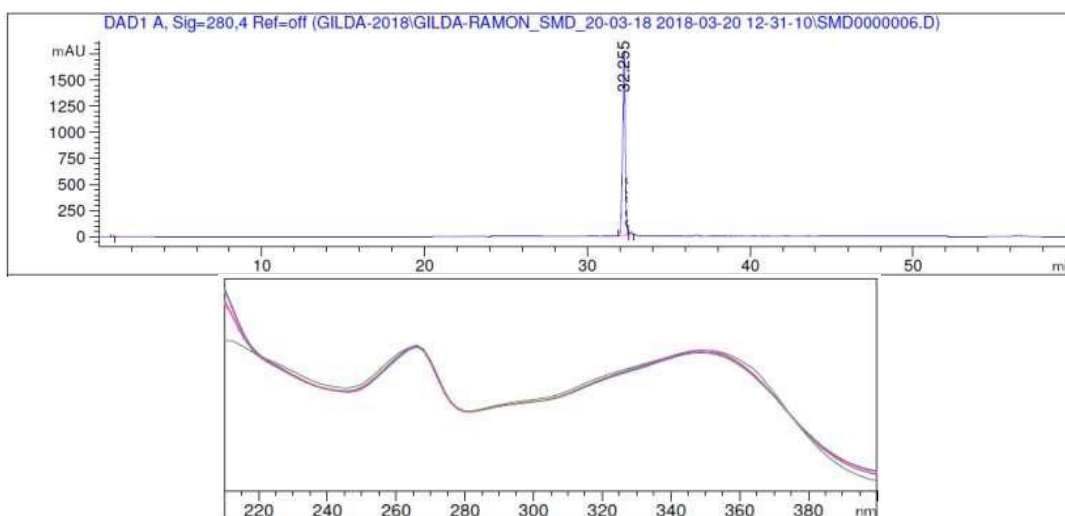


**Fig. S5** HPLC-DAD profile of Fr-10 and UV spectrum of peak at 32.2 min at 280nm (di-*O*-methyl-kaempferol (kumatakenin), **3**).

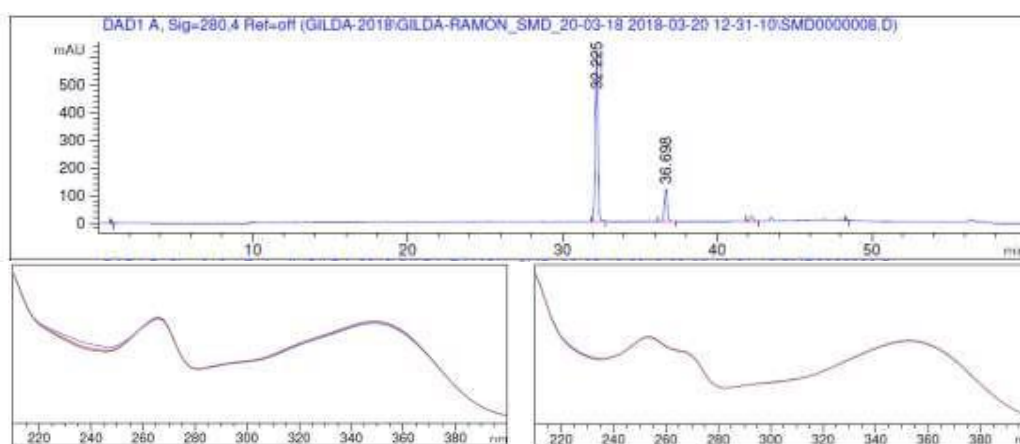


**Fig. S6** HPLC-DAD profile of Fr-11 and UV spectra of peaks at 32.2 and 36.7 min at 280nm (3,7-di-*O*-methyl-kaempferol (kumatakenin), **3** and tetra-*O*-methyl-queracetin (retusin), **2**).

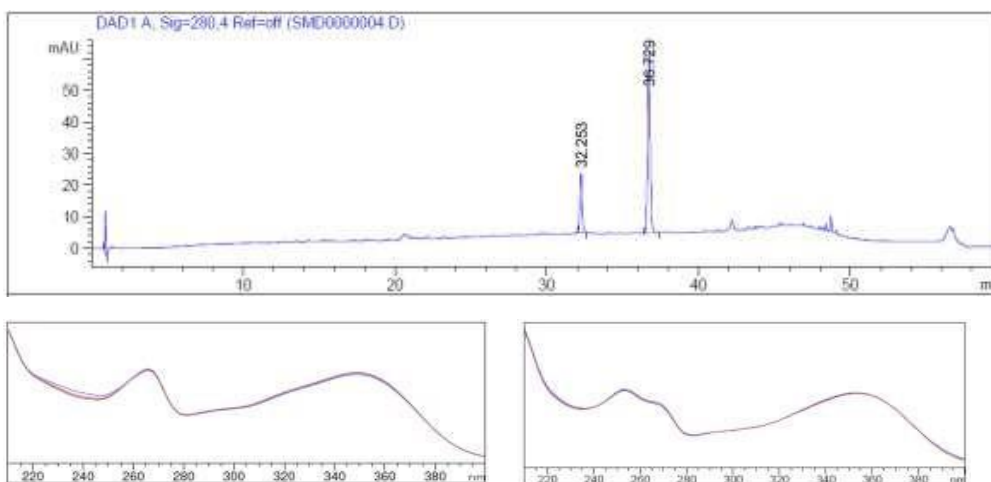


**Fig. S7** HPLC-DAD profile of Fr-12 and UV spectra of peaks at 32.2 and 36.7 min at 280nm (3,7-di-*O*-methyl-kaempferol (kumatakenin), **3** and tetra-*O*-methyl-queracetin (retusin), **2**).

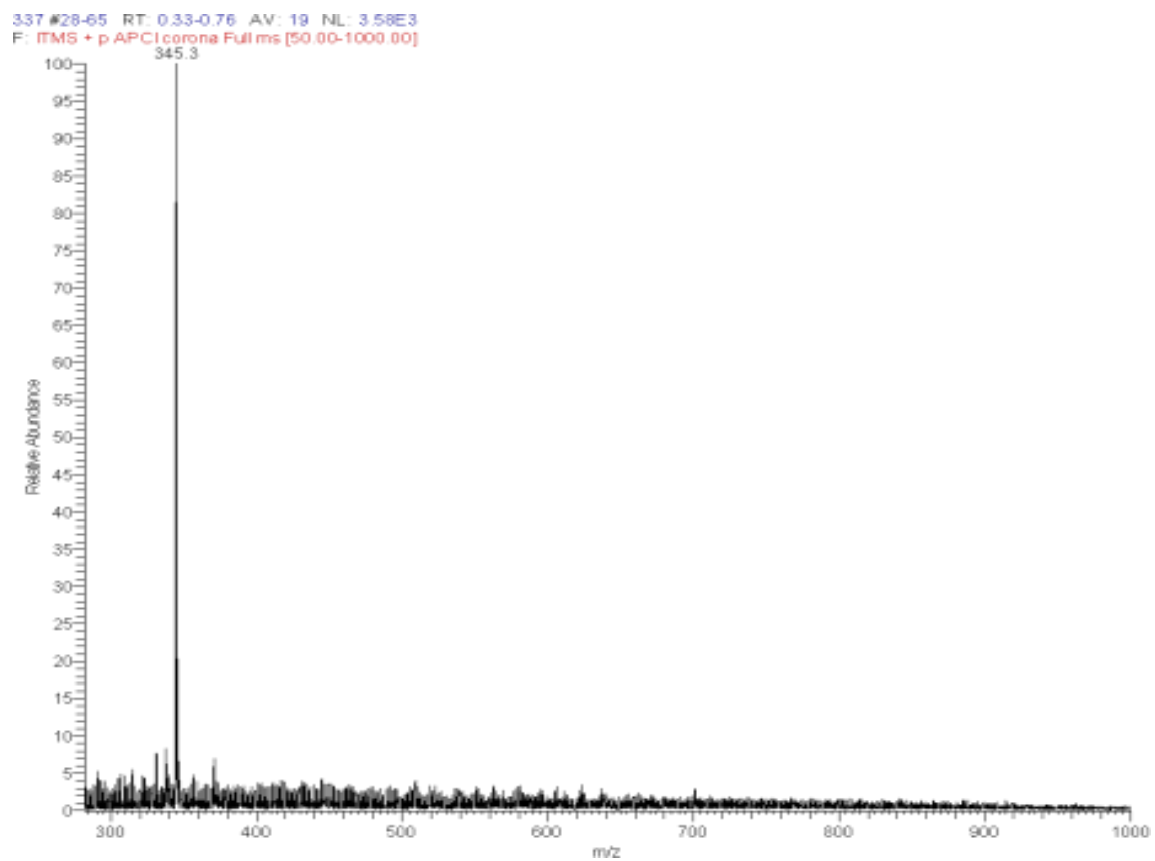


**Fig. S8** MS profile of **Fr-7** ( $R_t = 29.4$  min; (3,3',4'-tri-*O*-methyl-queretin, **1**).

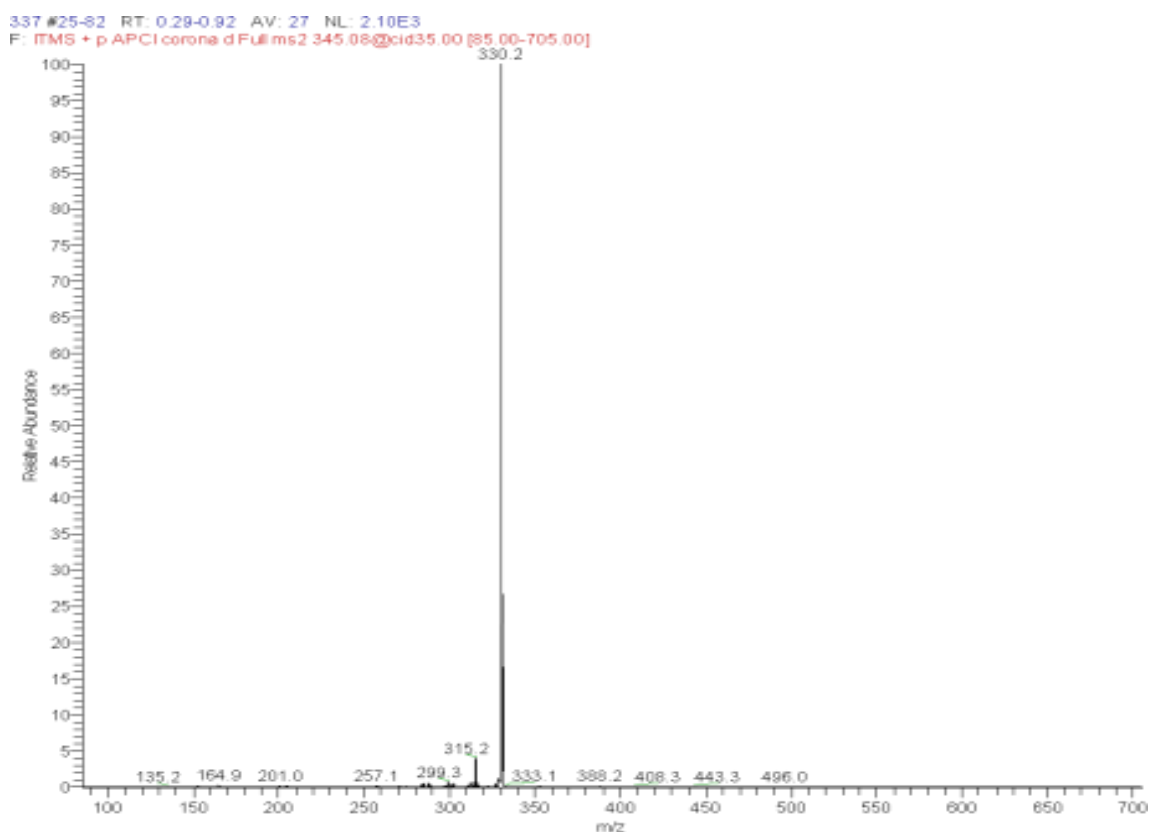


**Fig. S9** Product ion spectrum obtained by CID (35eV) of the precursor ion  $m/z$  345 in **Fr-7** produced by APCI ionization of 3,3',4'-tri-*O*-methyl-quercetin, **1**.

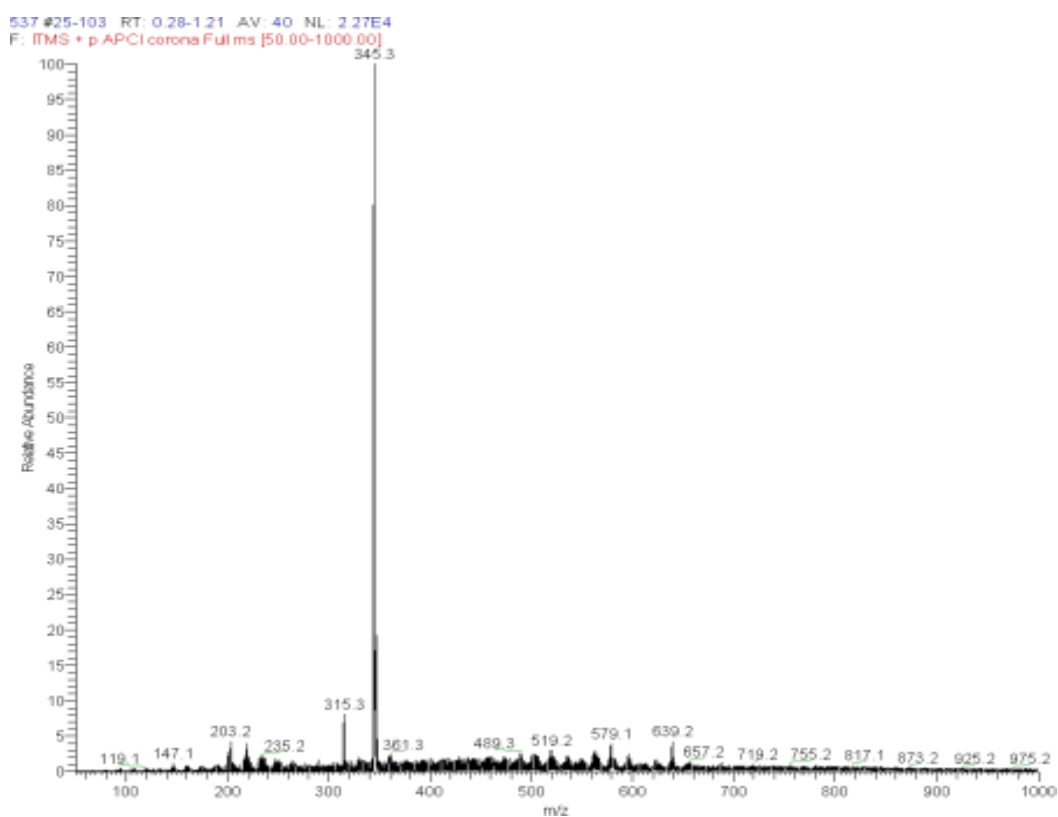


**Fig. S10** MS profile of **Fr-8** ( $R_t=$  32.2 min; di-*O*-methyl-kaempferol and  $R_t=$  32.7 min; tri-*O*-methyl-quercetin).



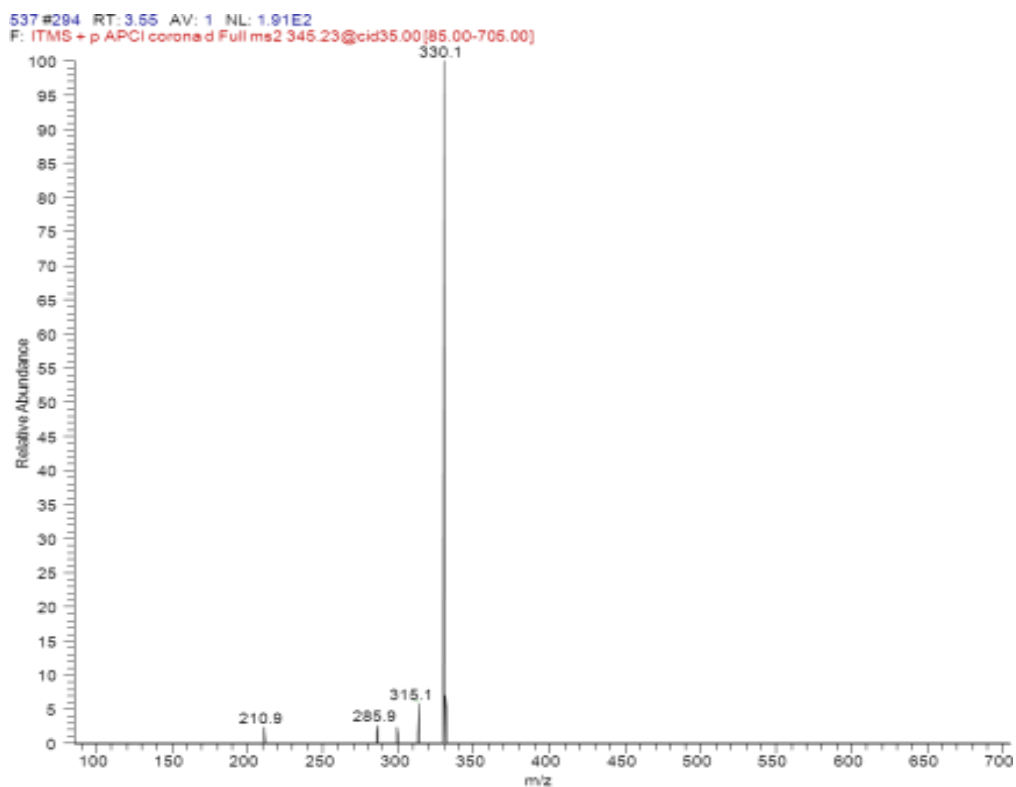


**Fig. S11** Product ion spectrum obtained by CID (35eV) of the precursor ion  $m/z$  345 in **Fr-8** produced by APCI ionization of tri-*O*-methyl-quercetin.

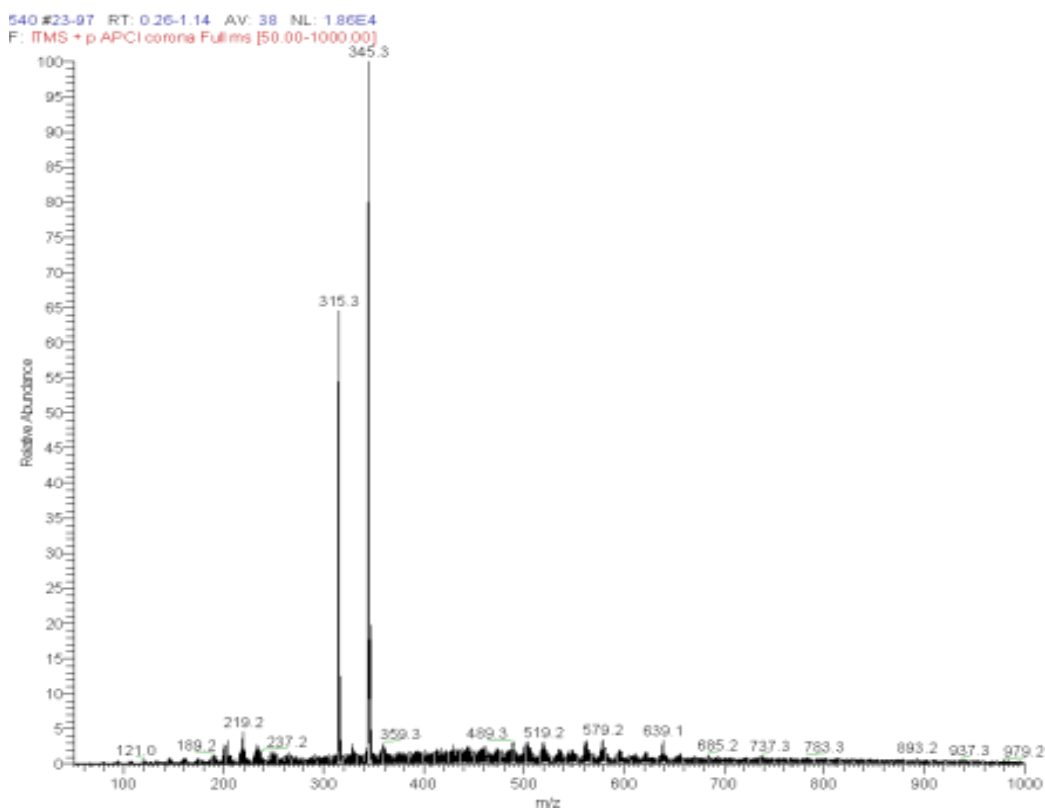


**Fig. S12** MS profile of **Fr-9** ( $R_t = 32.2$  min; di-*O*-methyl-kaempferol and  $R_t = 32.7$  min; tri-*O*-methyl-quercetin).

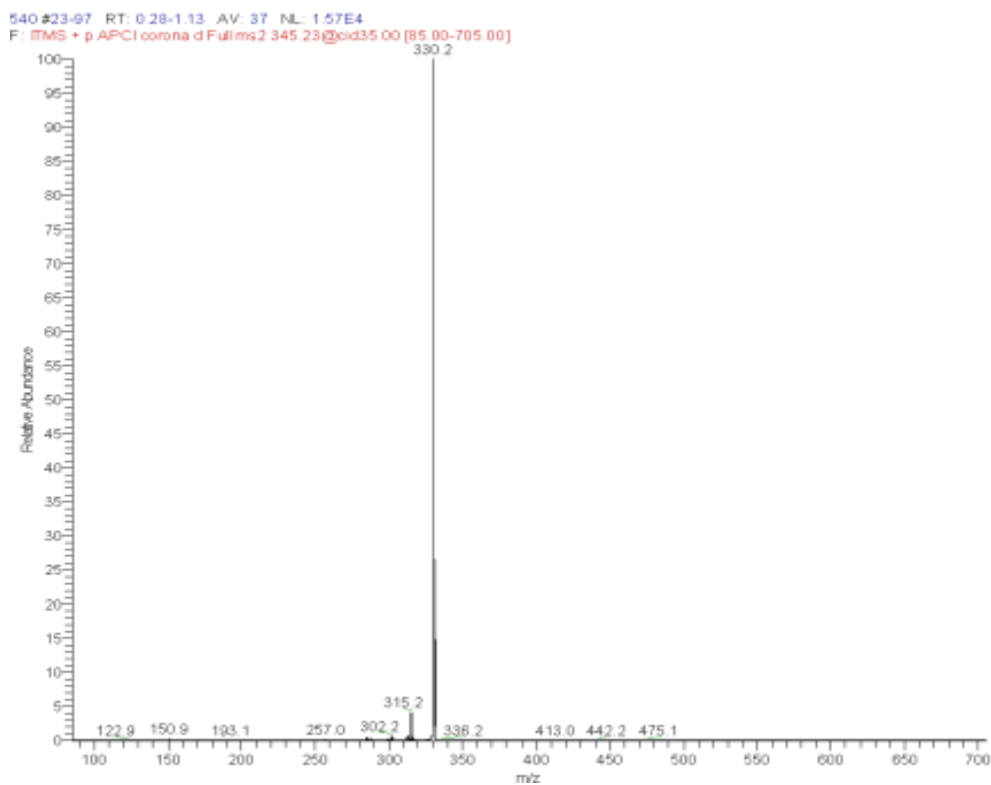


**Fig. S13** Product ion spectrum obtained by CID (35eV) of the precursor ion  $m/z$  345 in **Fr-9** produced by APCI ionization of tri-*O*-methyl-quercetin.

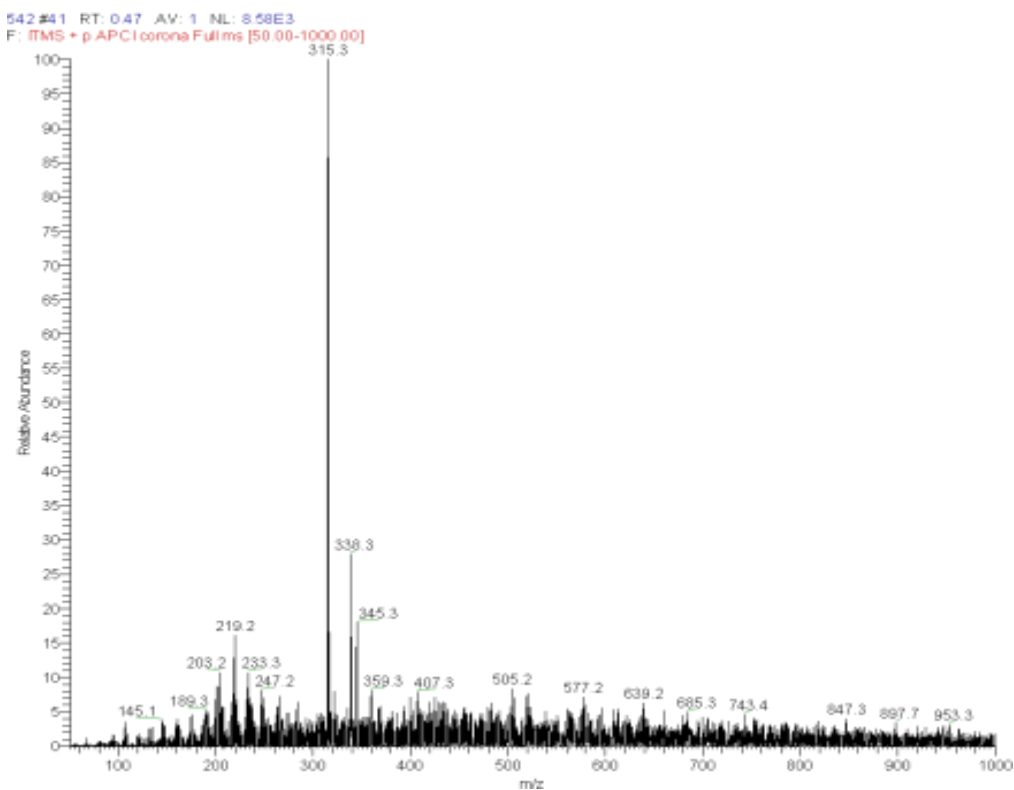


**Fig. S14** MS profile of **Fr-10** ( $R_t = 32.2$  min; 3,7-di-*O*-methyl-kaempferol (kumatakenin), **3**).

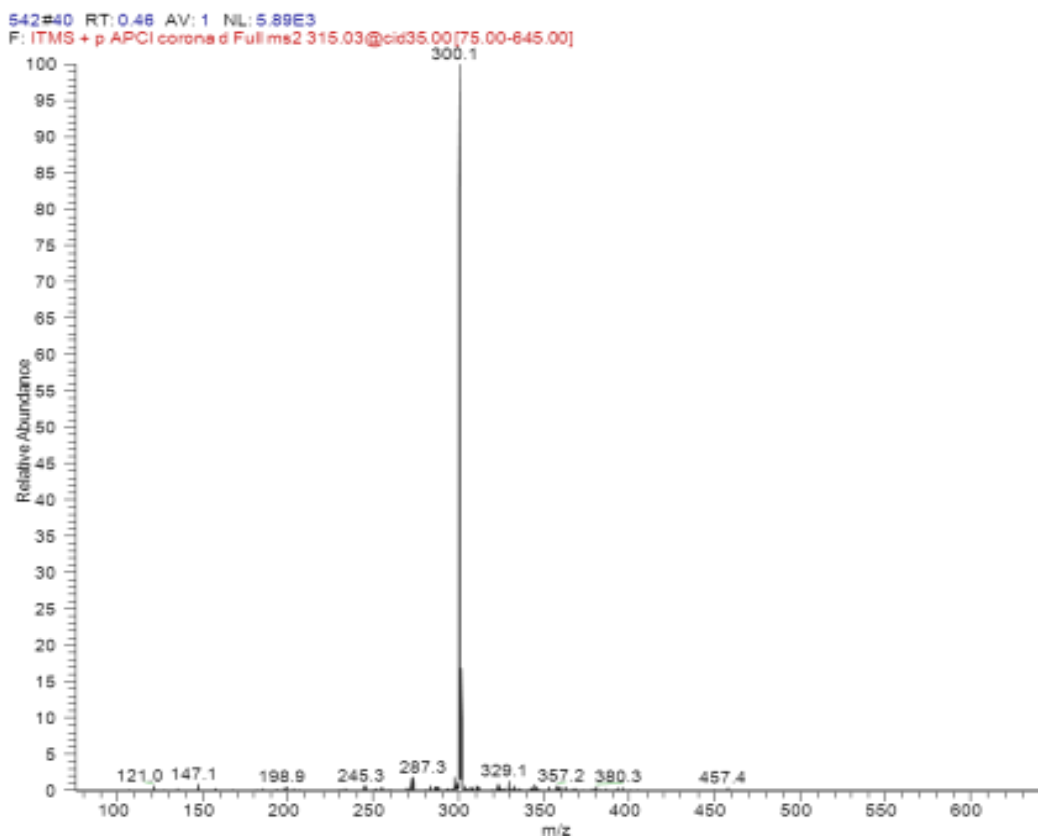


**Fig. S15** Product ion spectrum obtained by CID (35eV) of the precursor ion  $m/z$  315 in **Fr-10** produced by APCI ionization of 3,7-di-*O*-methyl-kaempferol (kumatakenin, **3**).

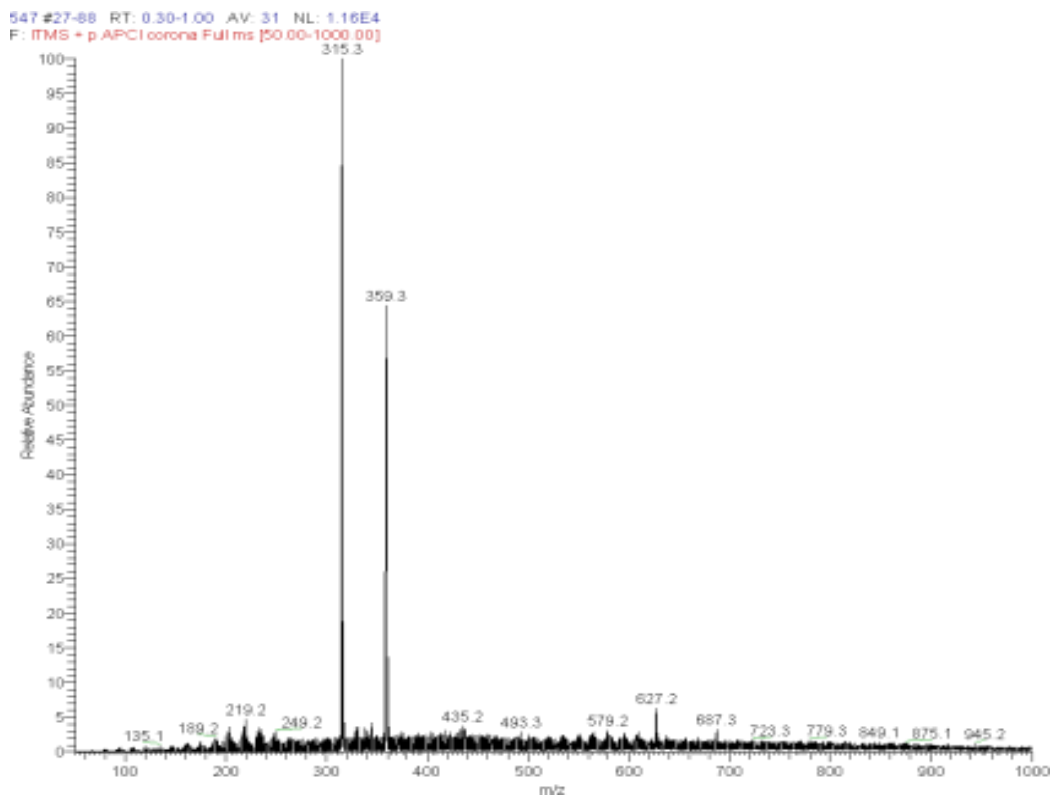


**Fig. S16** MS profile of **Fr-11** ( $R_t = 32.2$  min; 3,7-di-*O*-methyl-kaempferol (kumatakenin), **3** and  $R_t = 36.7$  min; tetra-*O*-methyl-quercetin (retusin), **2**).

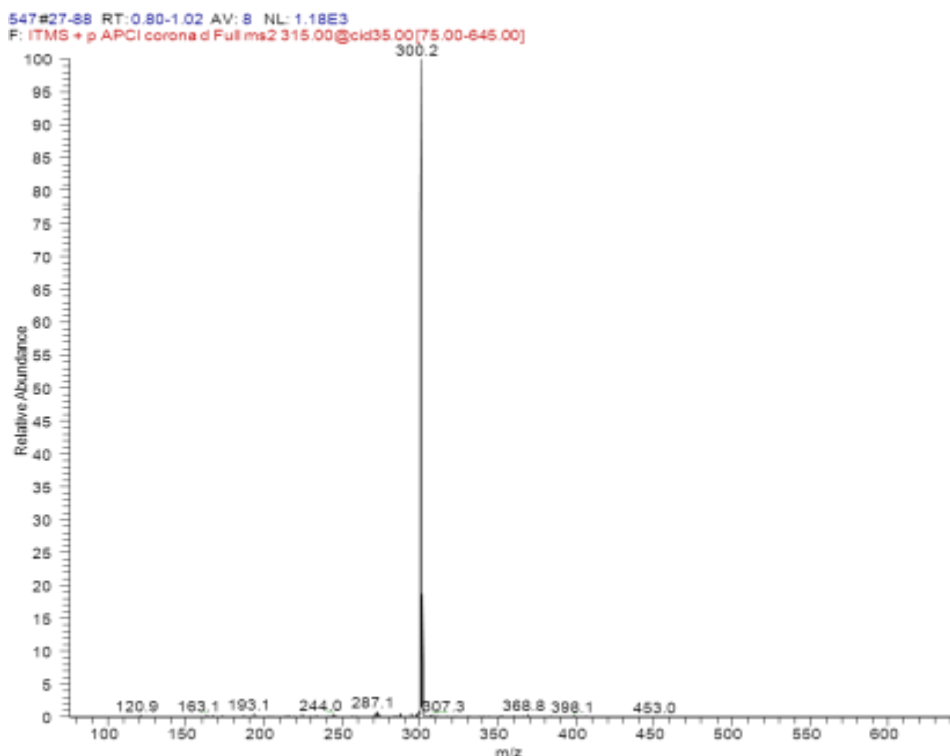


**Fig. S17** Product ion spectrum obtained by CID (35eV) of the precursor ion  $m/z$  315 in **Fr-11** produced by APCI ionization of di-*O*-methyl-kaempferol.

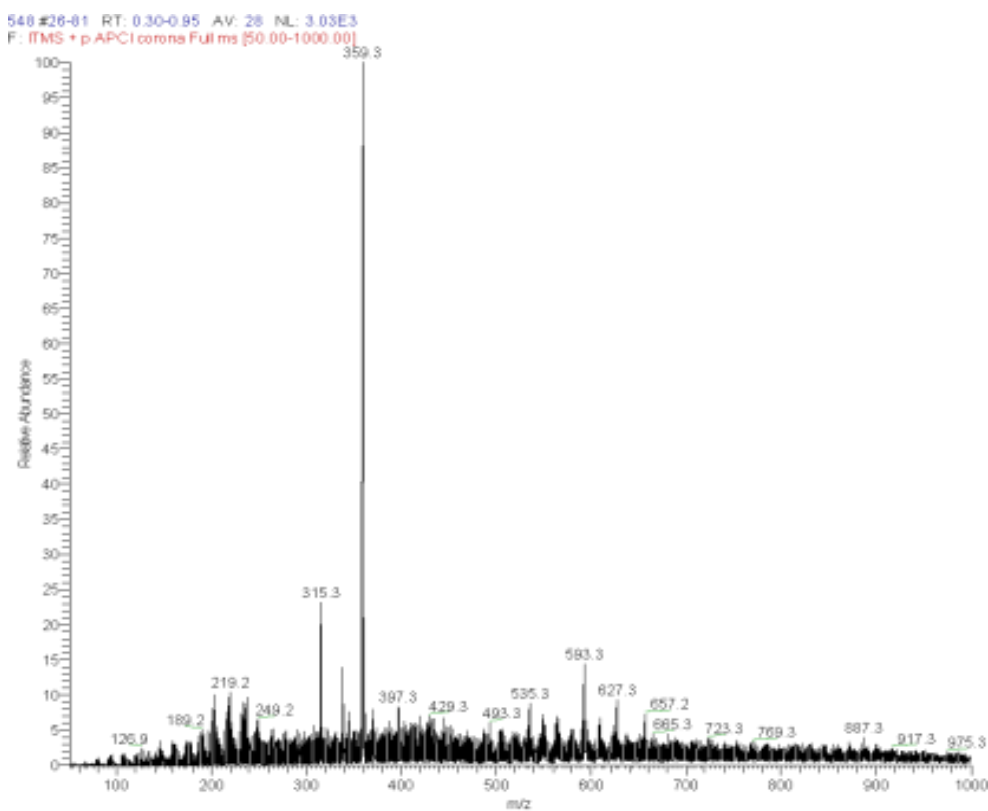


**Fig. S18** MS profile of **Fr-12** ( $R_t = 32.2$  min; di-*O*-methyl-kaempferol and  $R_t = 36.7$  min; tetra-*O*-methyl-quercetin (retusin), **2**).

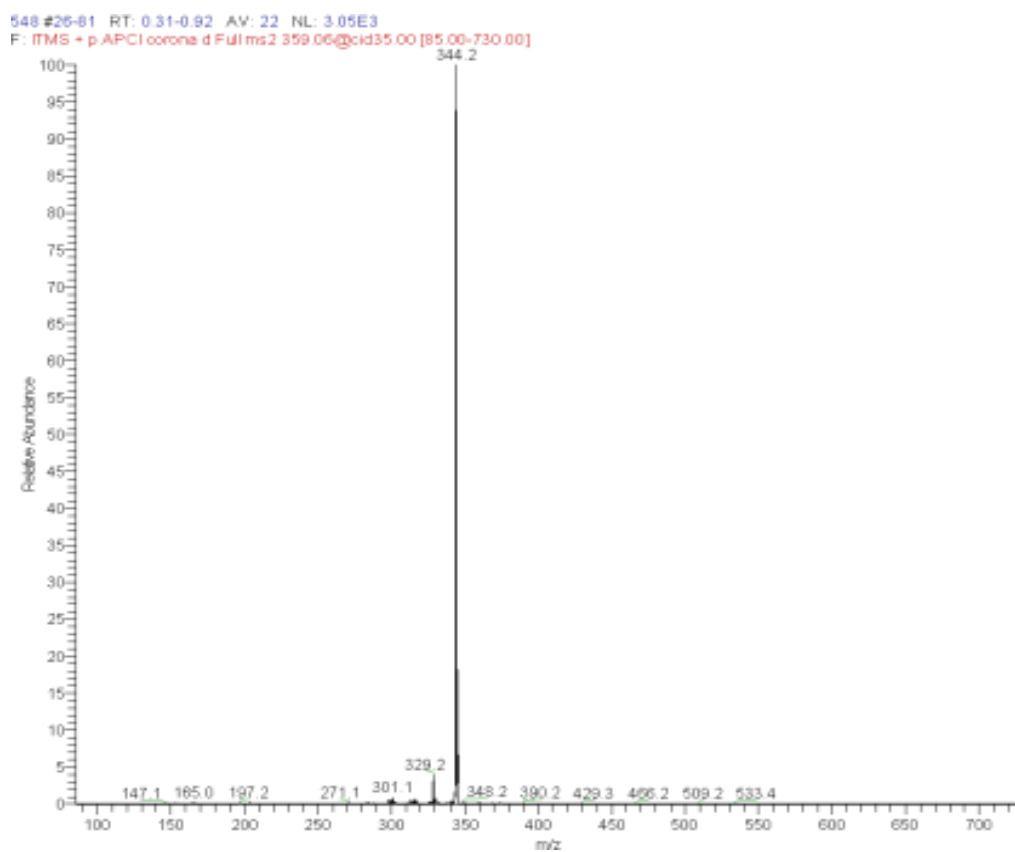


**Fig. S19** Product ion spectrum obtained by CID (35eV) of the precursor ion  $m/z$  359 in **Fr-12** produced by APCI ionization of tetra-*O*-methyl-queretin (retusin), **2**.

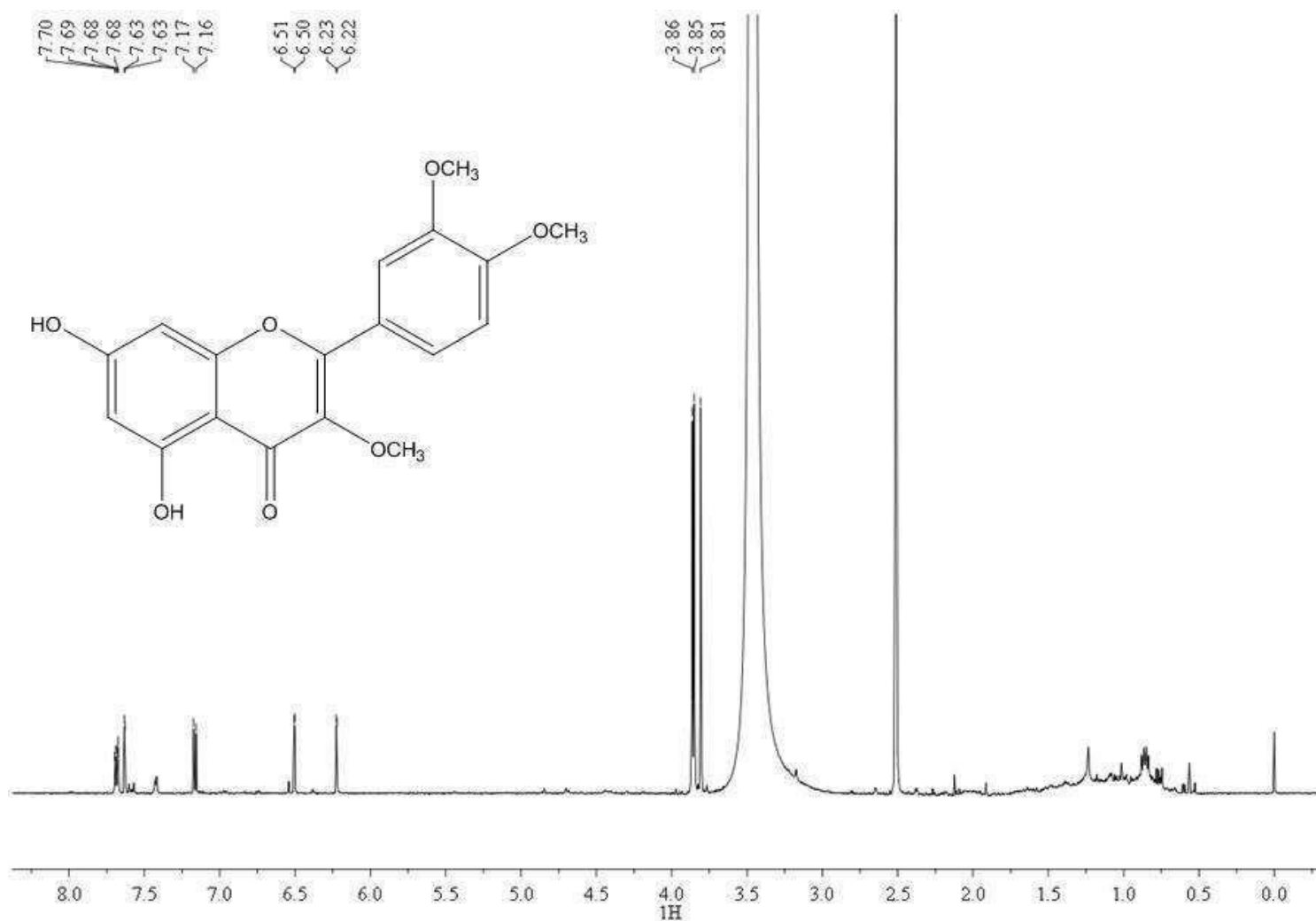
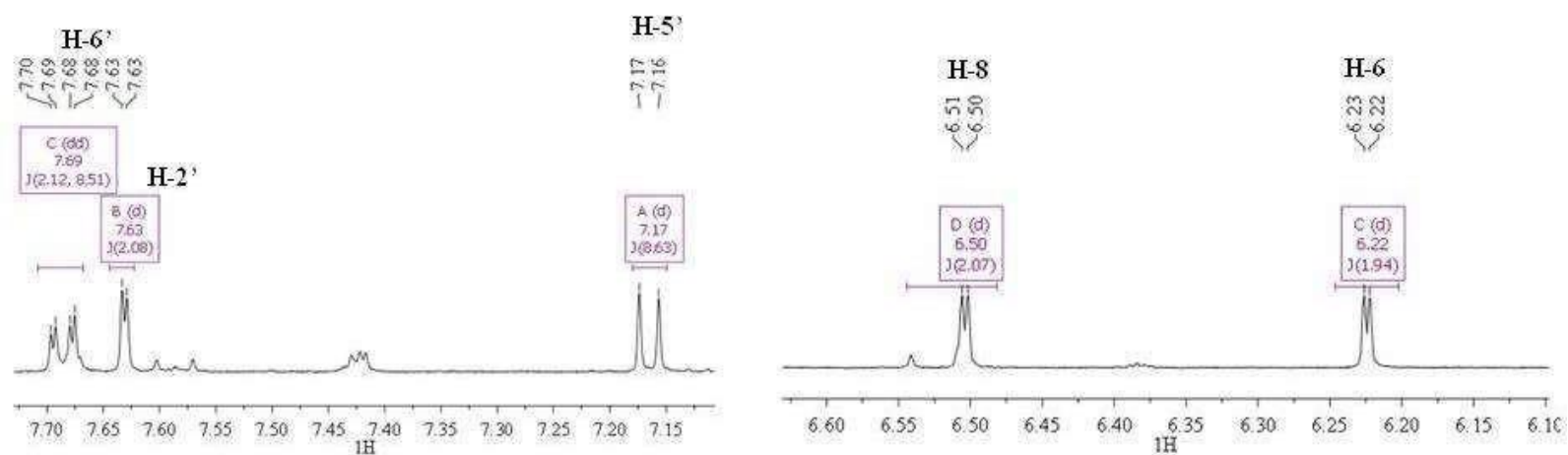
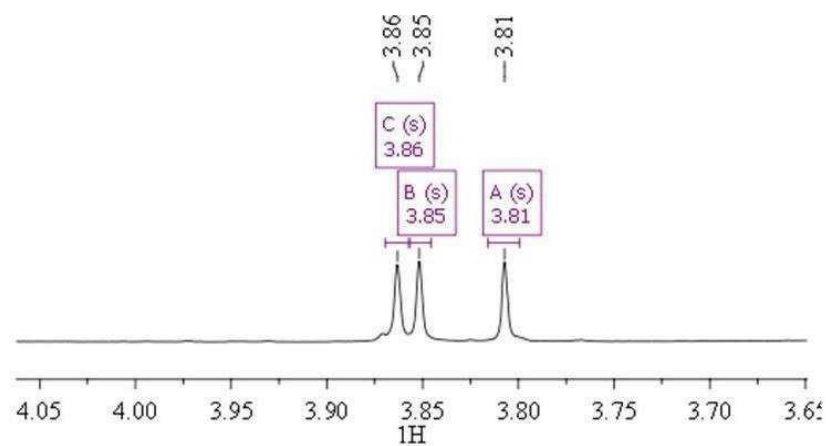


Fig. S20  $^1\text{H}$  NMR spectrum (DMSO- $d_6$ , 500 MHz) of 3,3',4'-tri-*O*-methyl-quercetin, **1** (Fr-7).





**Fig. S21**  $^1\text{H}$  NMR spectrum (DMSO- $d_6$ , 500 MHz) expanded in the aromatic protons region of 3,3',4'- tri-*O*-methyl-quercetin, **1** (Fr-7).



**Fig. S22**  $^1\text{H}$  NMR spectrum (DMSO- $d_6$ , 500 MHz) expanded in the region relative to methoxyl groups of 3,3',4'- tri-*O*-methyl-quercetin, **1** (Fr-7).

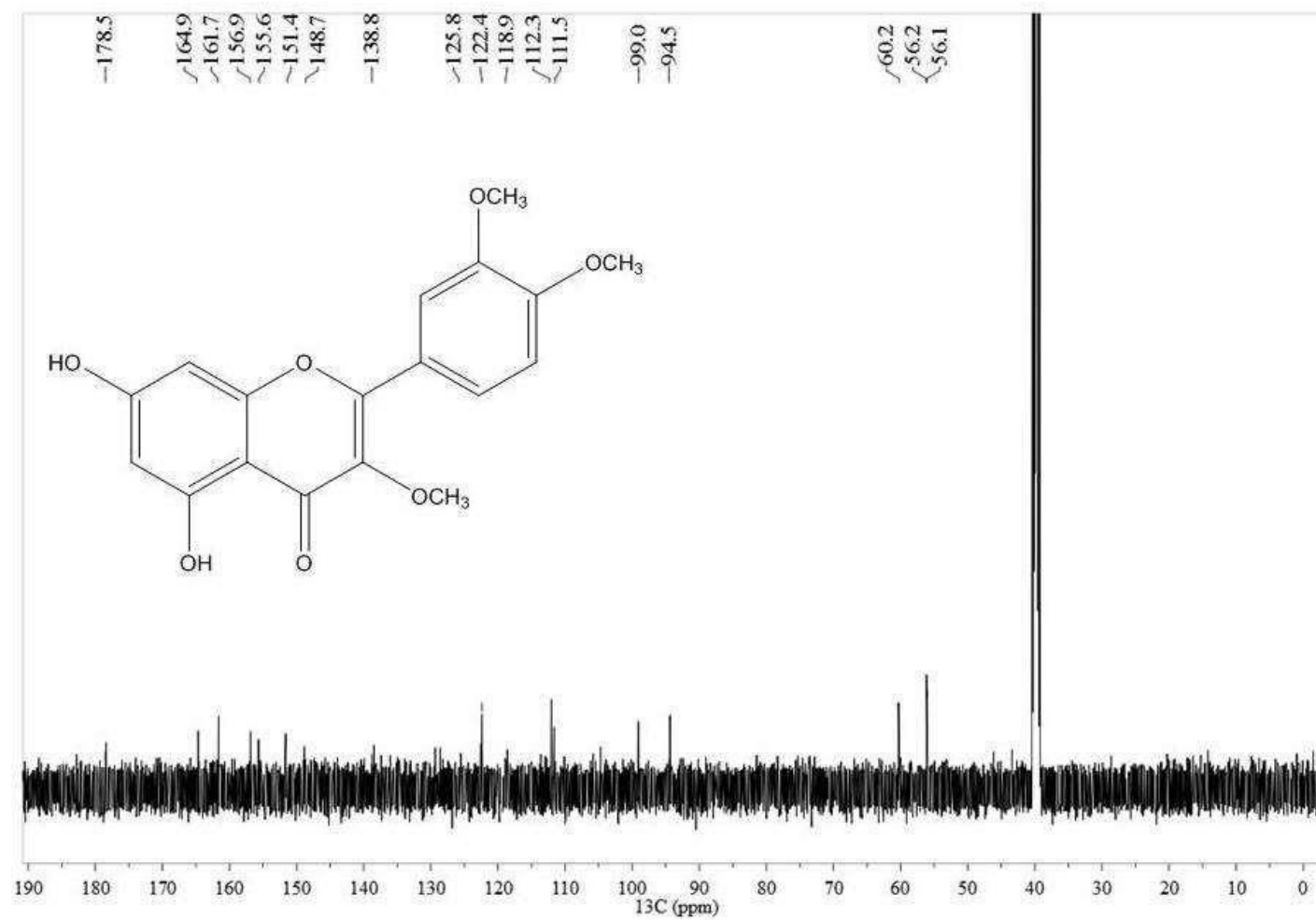


Fig. S23 <sup>13</sup>C NMR spectrum (DMSO-d<sub>6</sub>, 500 MHz) of 3,3',4'-tri-O-methyl-querceetin, **1** (Fr-7).

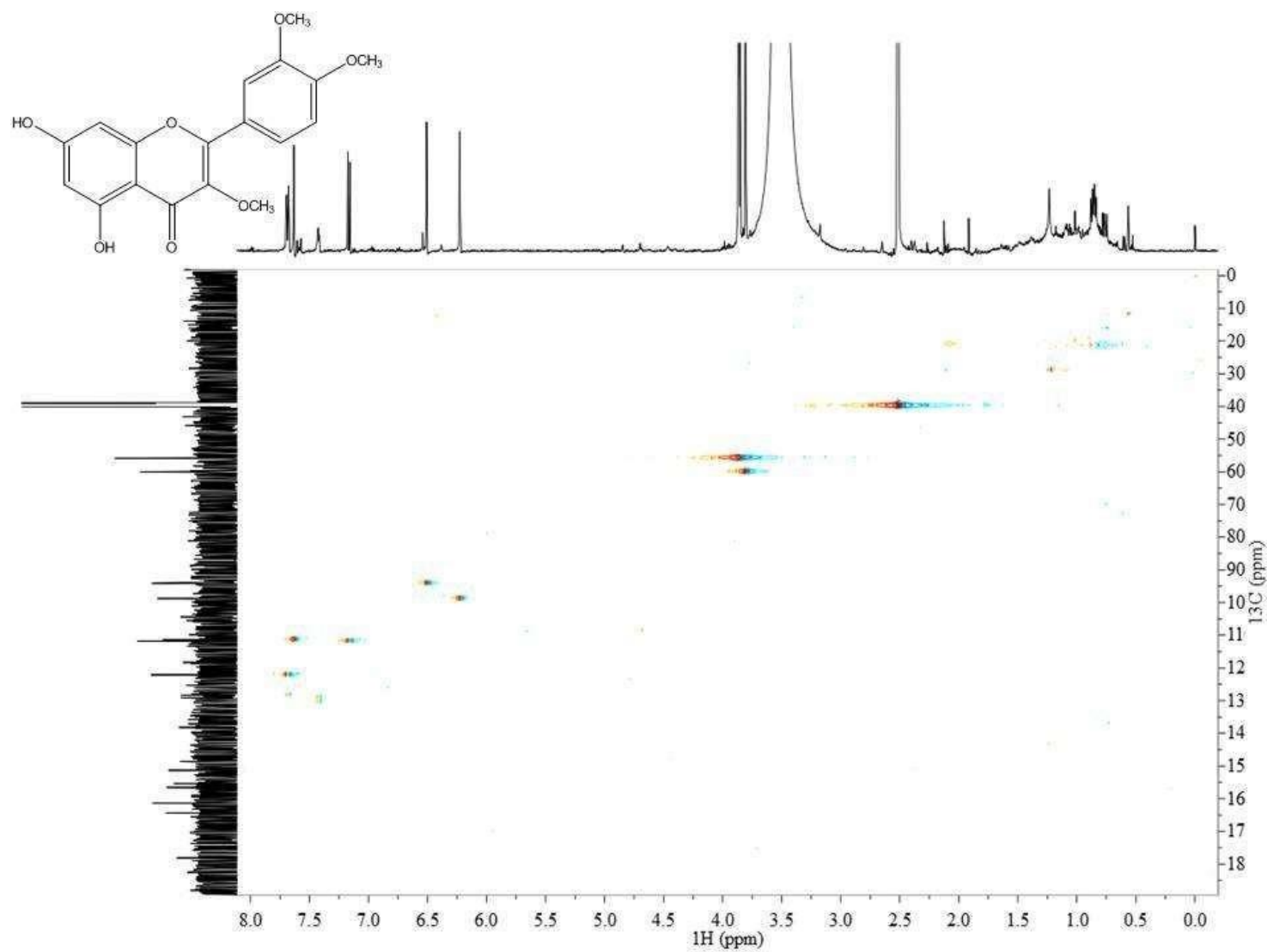
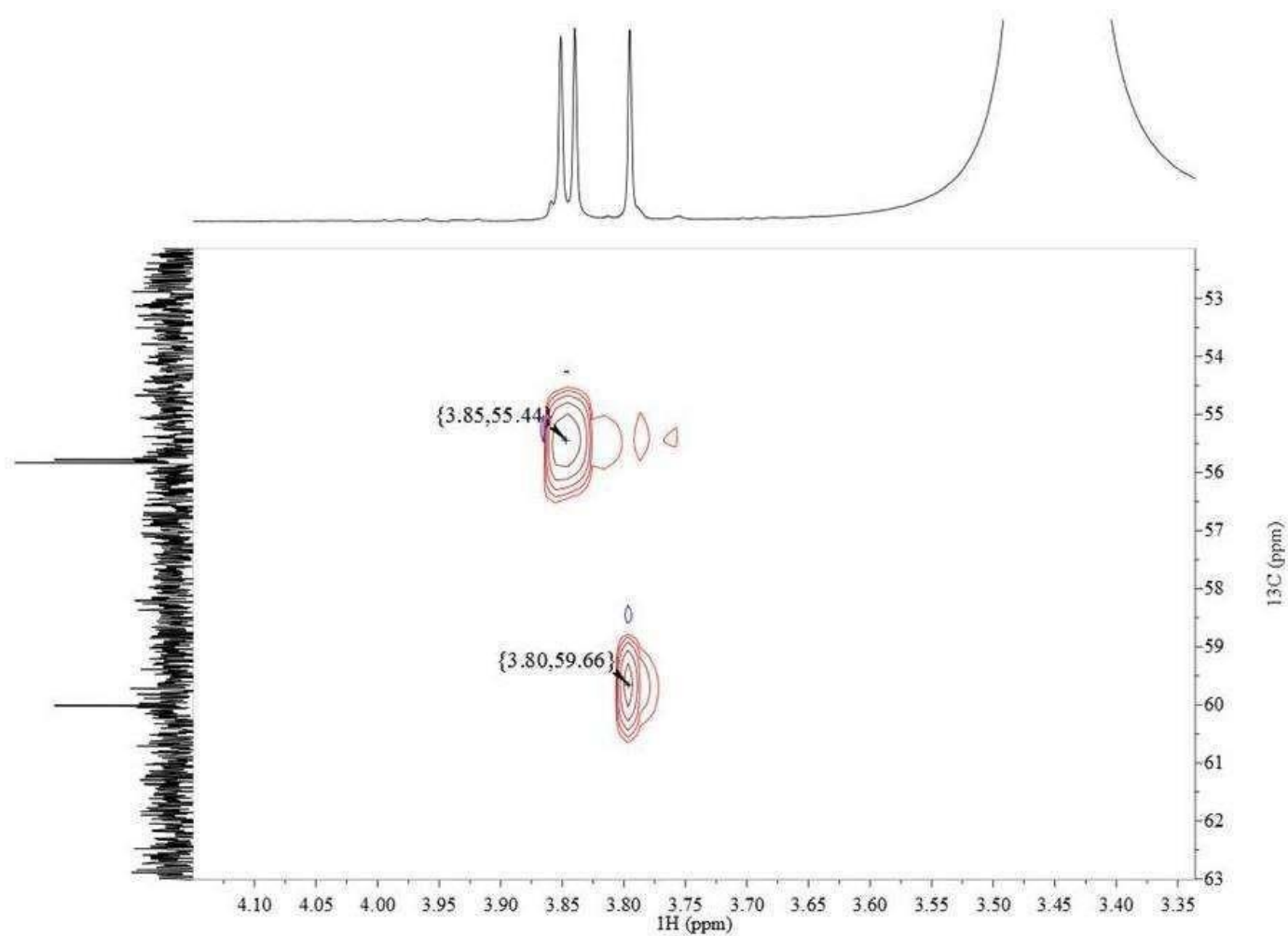


Fig. S24 HSQC  $^1\text{H}$ - $^{13}\text{C}$  NMR spectrum (DMSO- $d_6$ , 500 MHz) of 3,3',4'-tri-*O*-methyl-querceetin, **1** (Fr-7).



**Fig. S25** HSQC  $^1\text{H}$ - $^{13}\text{C}$  NMR spectrum (DMSO- $d_6$ , 500 MHz) expanded in the region relative to methoxyl groups of 3,3',4'-tri-*O*-methyl-quercetin, **1 (Fr-7)**.

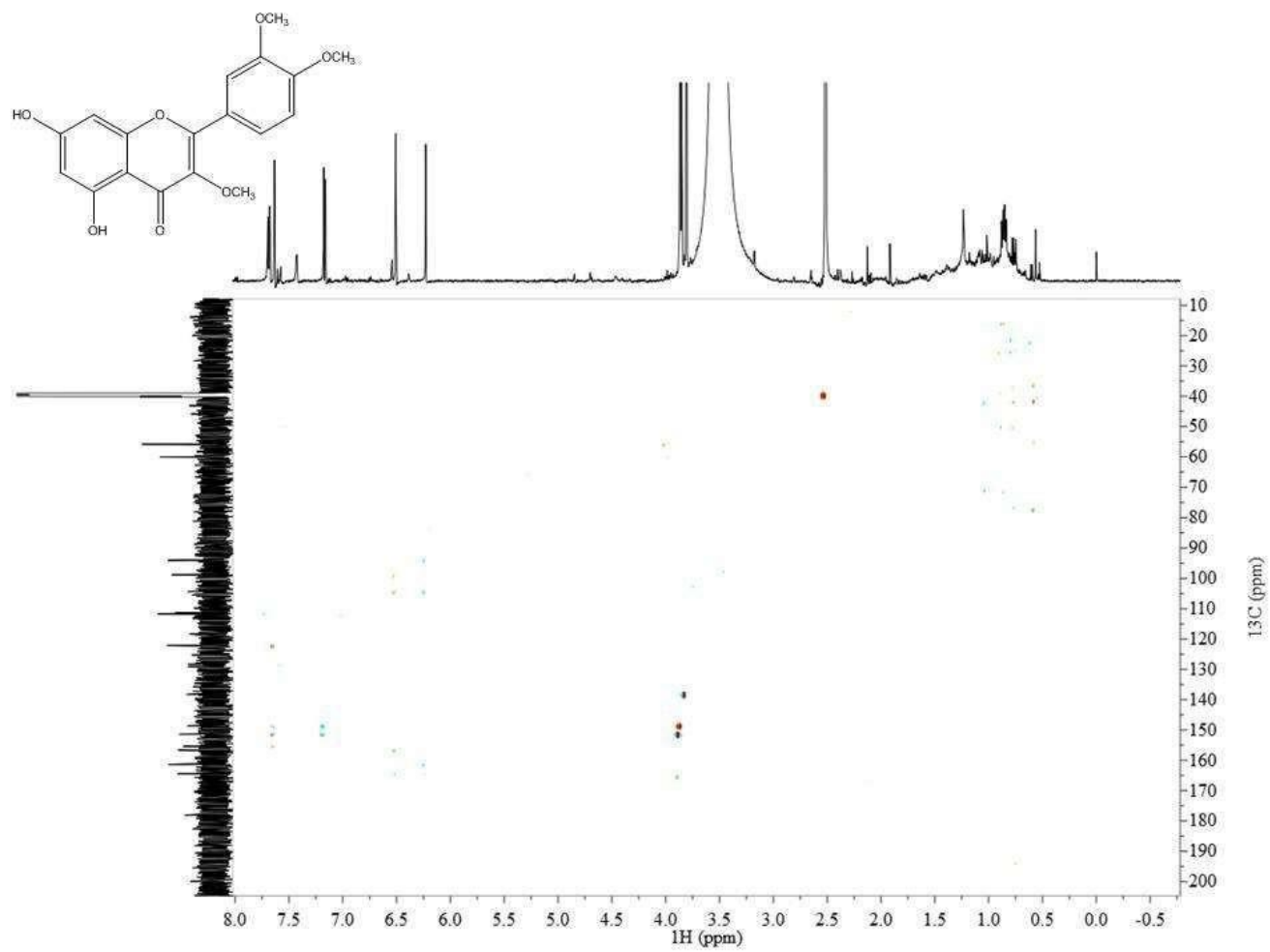
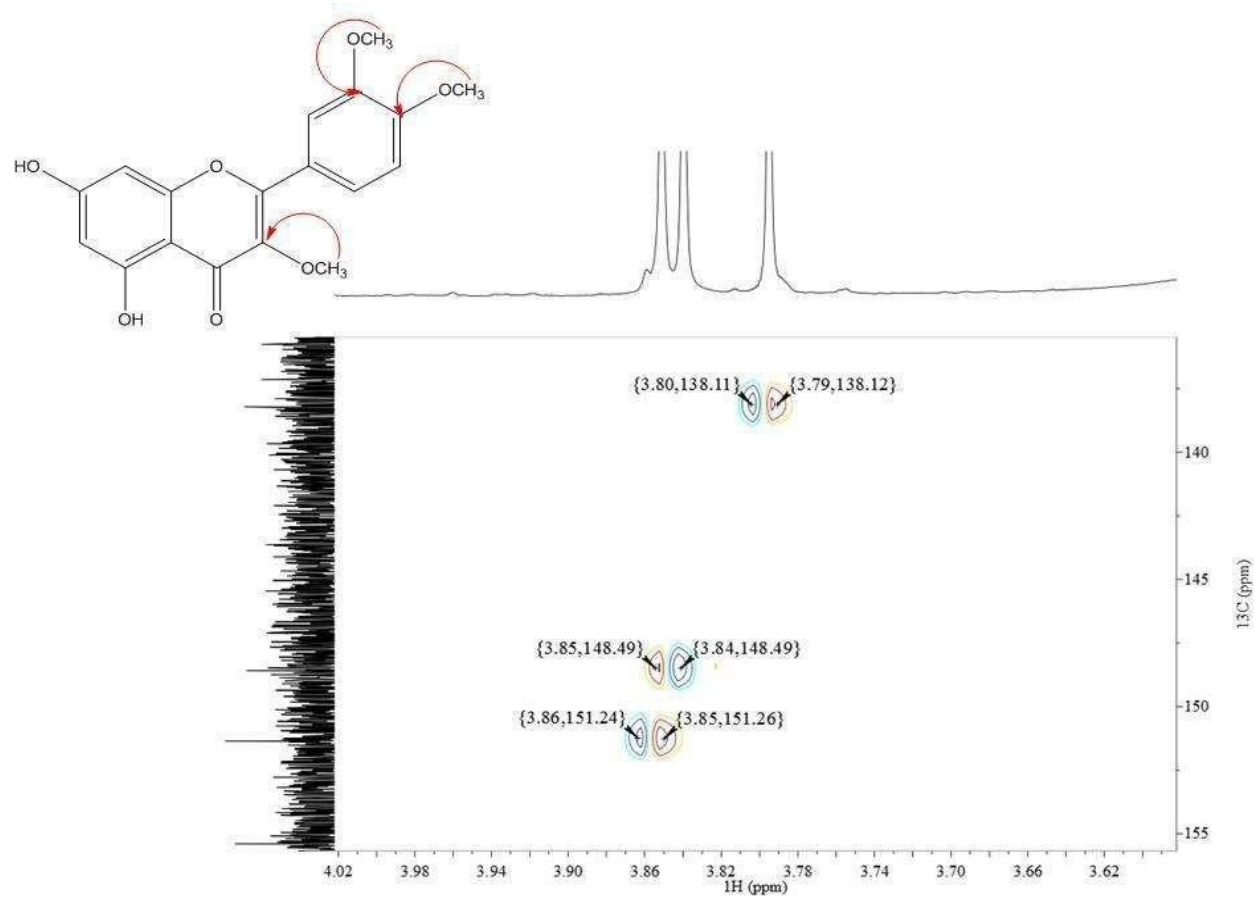


Fig. S26 HMBC  $^1\text{H}$ - $^{13}\text{C}$  NMR spectrum (DMSO- $d_6$ , 500 MHz) of 3,3',4'-tri-*O*-methyl-quercetin, **1** (Fr-7).



**Fig. S27** HMBC <sup>1</sup>H-<sup>13</sup>C NMR spectrum (DMSO-d<sub>6</sub>, 500 MHz) expanded in the region relative to methoxyl groups of 3,3',4'-tri-*O*-methyl-queretin, **1** (Fr-7).



**Table S1.**  $^1\text{H}$  and  $^{13}\text{C}$  NMR spectral data for 3,3',4'-tri-*O*-methyl-quercetin, **1** (DMSO- $d_6$ , 500MHz) compared with the literature.

Quercetin moiety	$^1\text{H}$ $\delta$ (in ppm) mult. ( <i>J</i> in Hz) Compound <b>1</b> in fraction 7	$^1\text{H}$ $\delta$ (in ppm) in CDCl <sub>3</sub> Literature: Awad et al., 2018	$^{13}\text{C}$ $\delta$ (in ppm) Compound <b>1</b> in fraction 7
2			155.6
3			138.8
4			178.5
5			161.7
6	6.22 d (1.9)	6.40 d (2.2)	99.0
7			164.9
8	6.50 d (2.1)	6.47 d (2.2)	94.5
9			156.9
10			111.5
1'			122.4
2'	7.63 d (2.1)	7.78 d (2.0)	112.3
3'			148.7
4'			151.4
5'	7.17 d (8.6)	7.12 d (8.4)	118.9
6'	7.69 dd (8.5, 2.1)	7.66 dd (8.4, 2.2)	125.8

3-OCH <sub>3</sub>	3.81 s	3.84 s	60.2
3'-OCH <sub>3</sub>	3.85 s	3.86 s	56.1
4'-OCH <sub>3</sub>	3.86 s	3.96 s	56.2

---

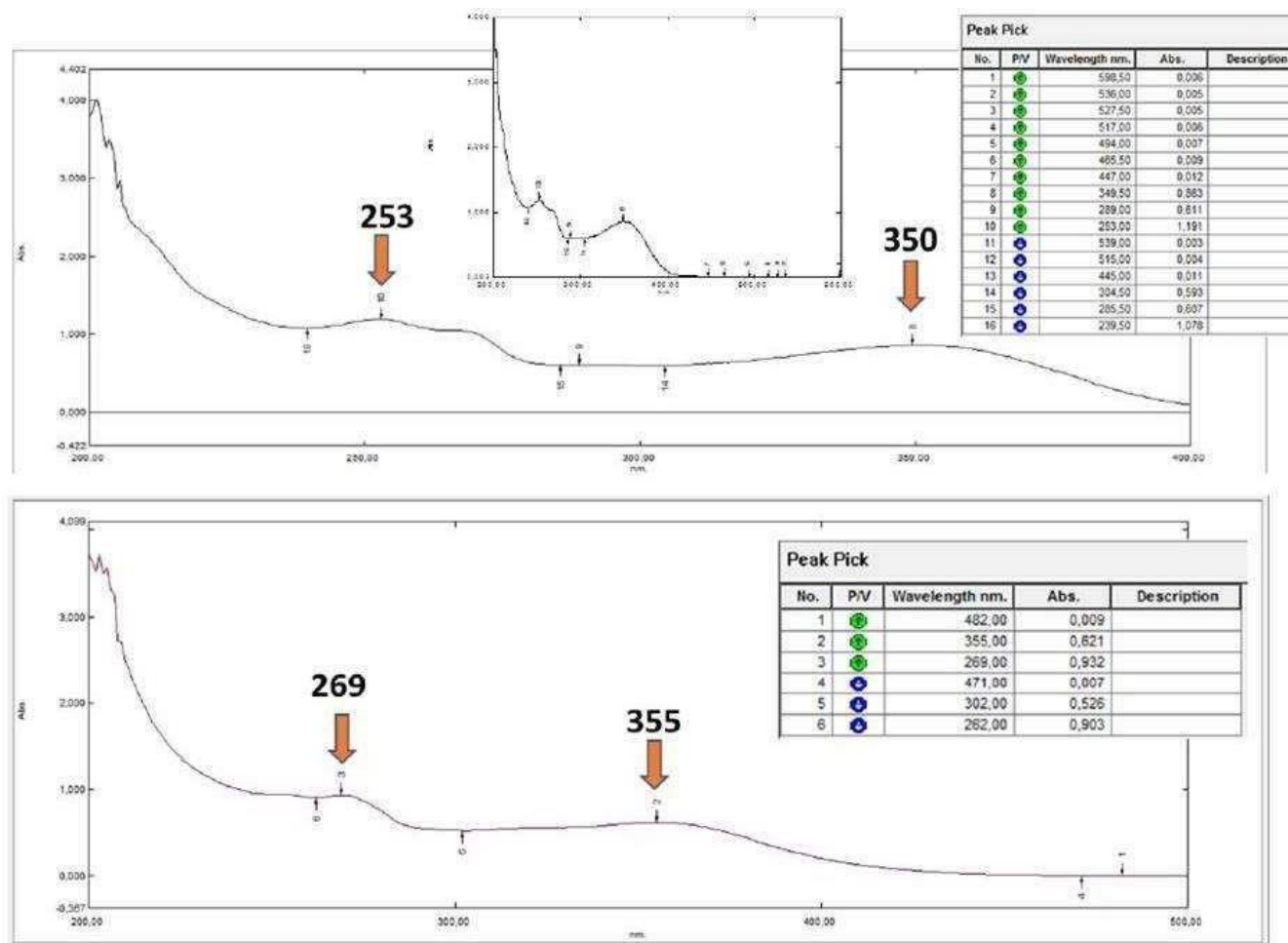
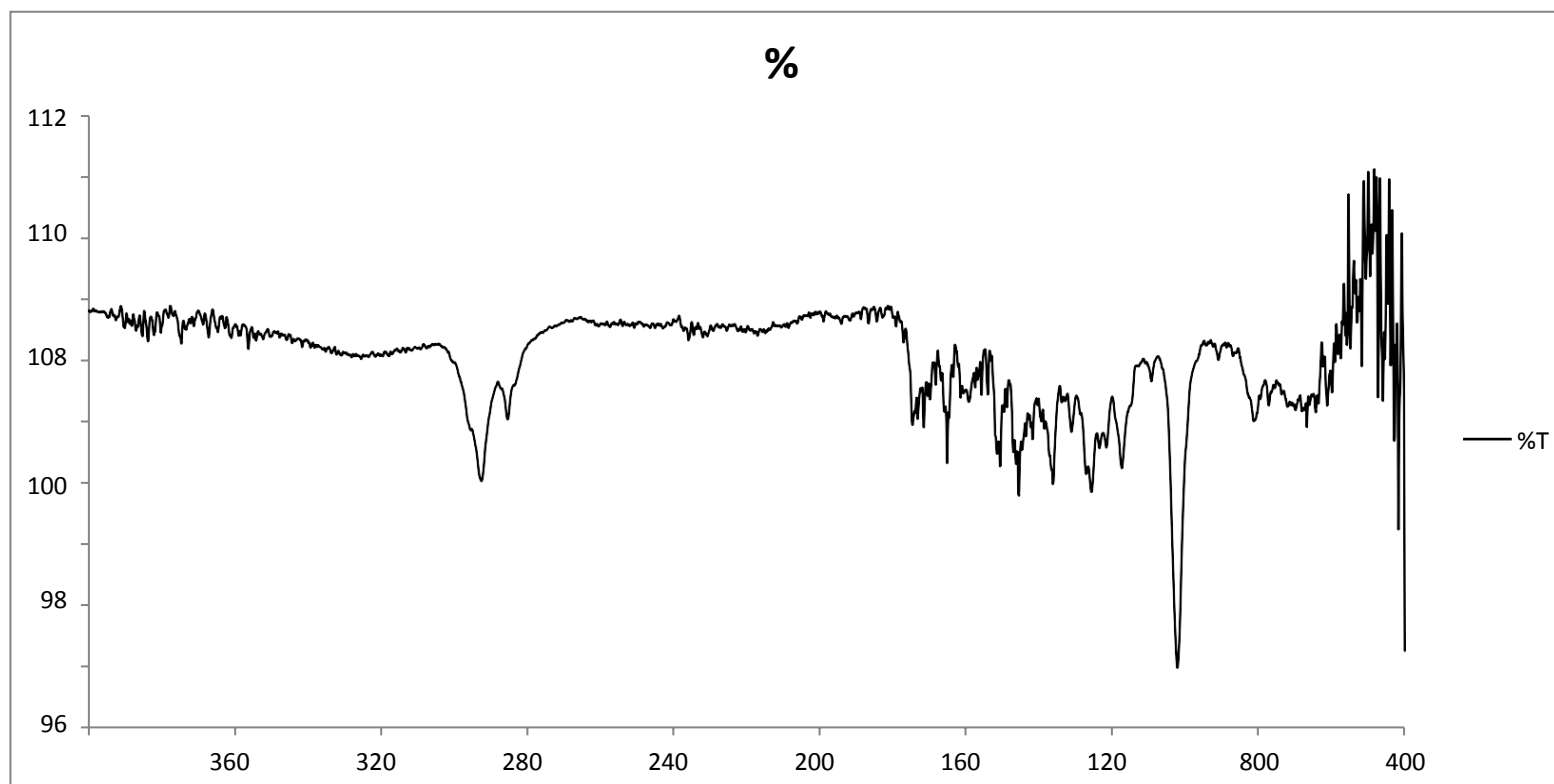
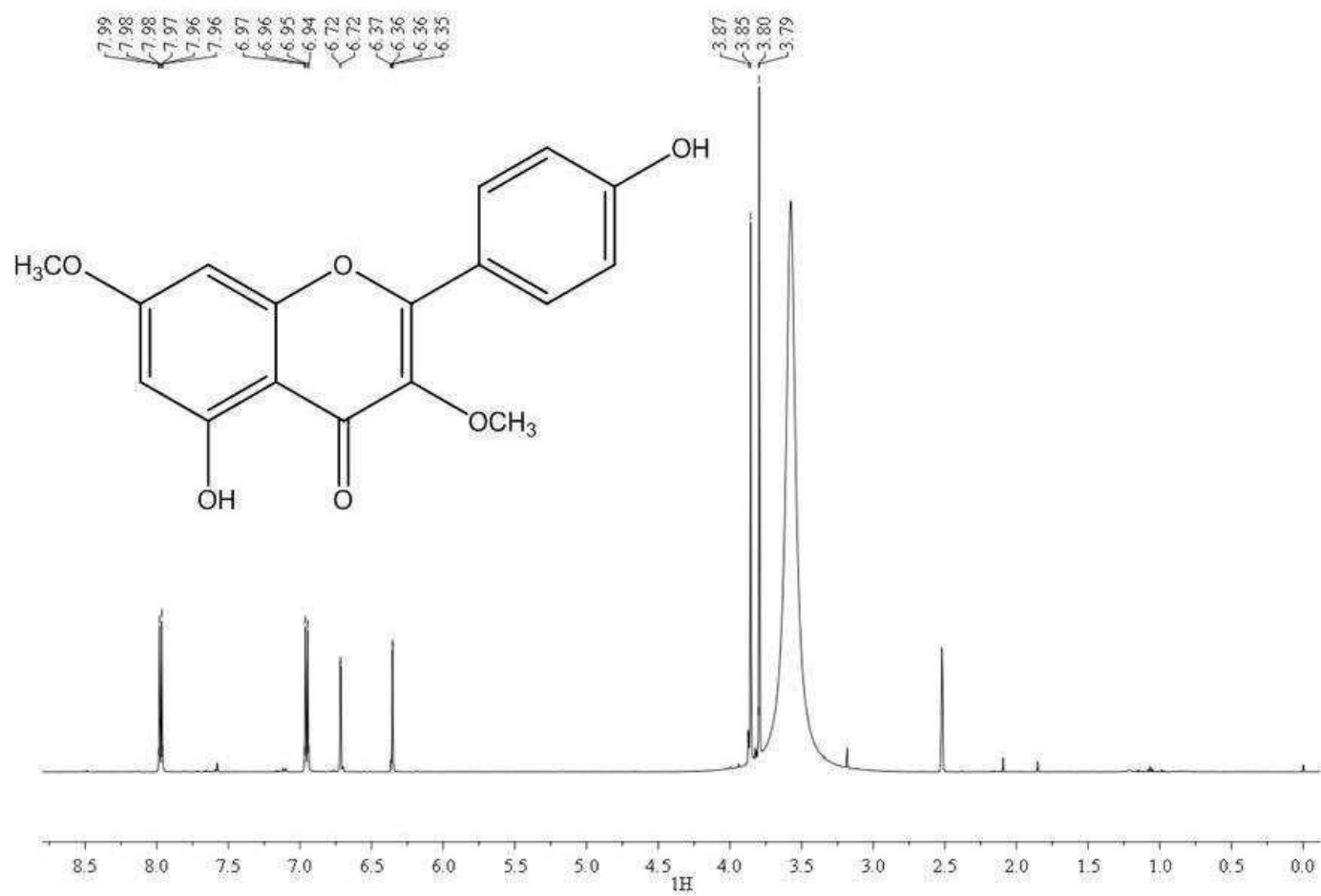


Fig. S28 Ultraviolet spectrum of 3,3',4'-tri-O-methyl-quercetin, 1 (Fr-7).



**Fig. S29** Infrared spectrum (KBr) of 3,3',4'-tri-*O*-methyl-querceetin, **1** (Fr-7).



**Fig. S30**  $^1\text{H}$  NMR spectrum (DMSO- $d_6$ , 500 MHz) of 3,7-di-*O*-methyl-kaempferol (kumatakenin), **3 (Fr-10)**.

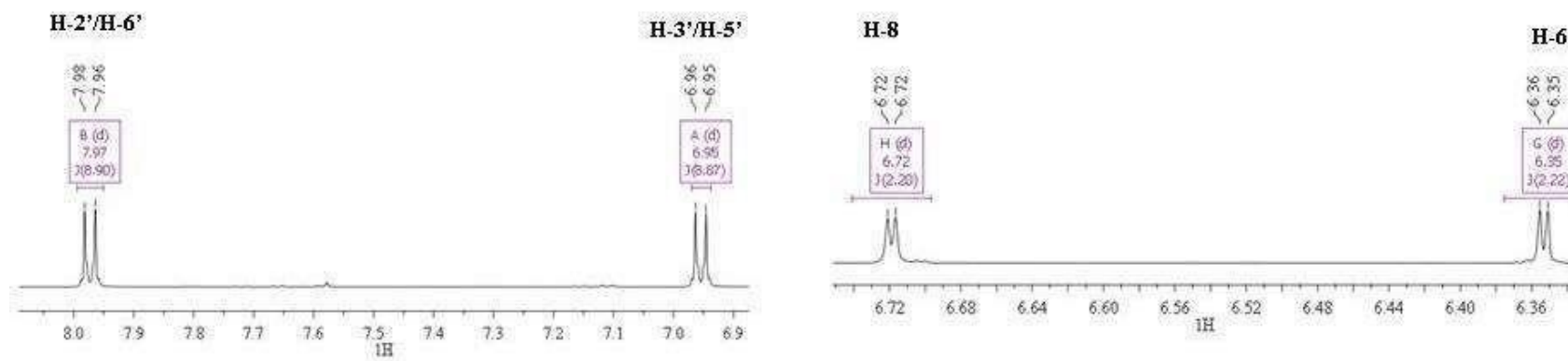


**Fig. S31**  $^1\text{H}$  NMR spectrum (DMSO- $d_6$ , 500 MHz) expanded in the aromatic protons region of 3,7-di-*O*-methyl-kaempferol (kumatakenin), **3** (Fr-10).

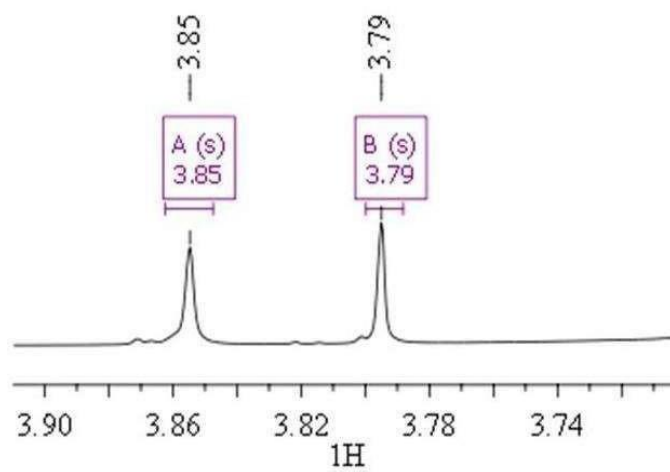


**Fig. S32**  $^1\text{H}$  NMR spectrum (DMSO- $d_6$ , 500 MHz) expanded in the region relative to methoxyl groups of 3,7-di-*O*-methyl-kaempferol(kumatakenin), **3** (Fr-10).



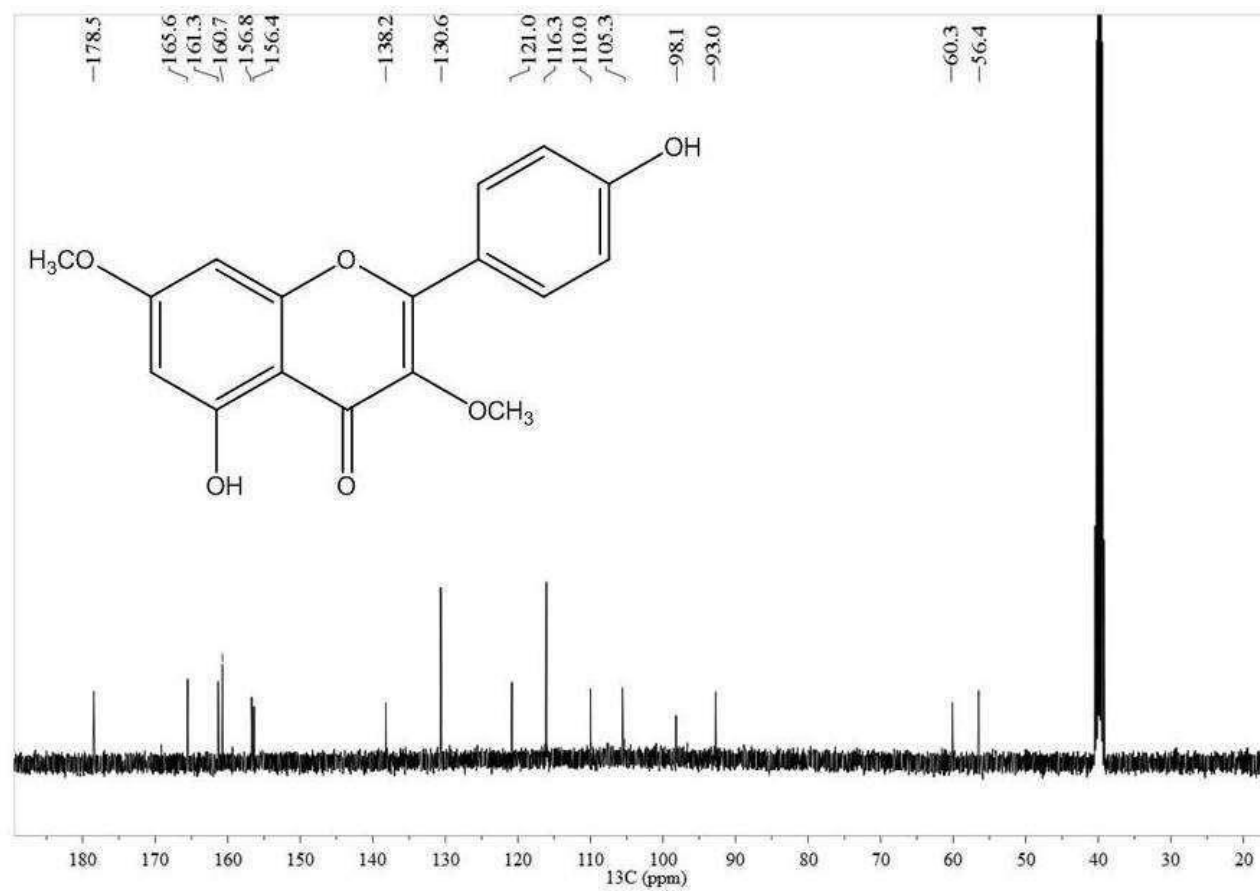


Fig. S33  $^{13}\text{C}$  NMR spectrum (DMSO- $d_6$ , 500 MHz) of 3,7-di-*O*-methyl-kaempferol (kumatakenin), **3** (Fr-10).

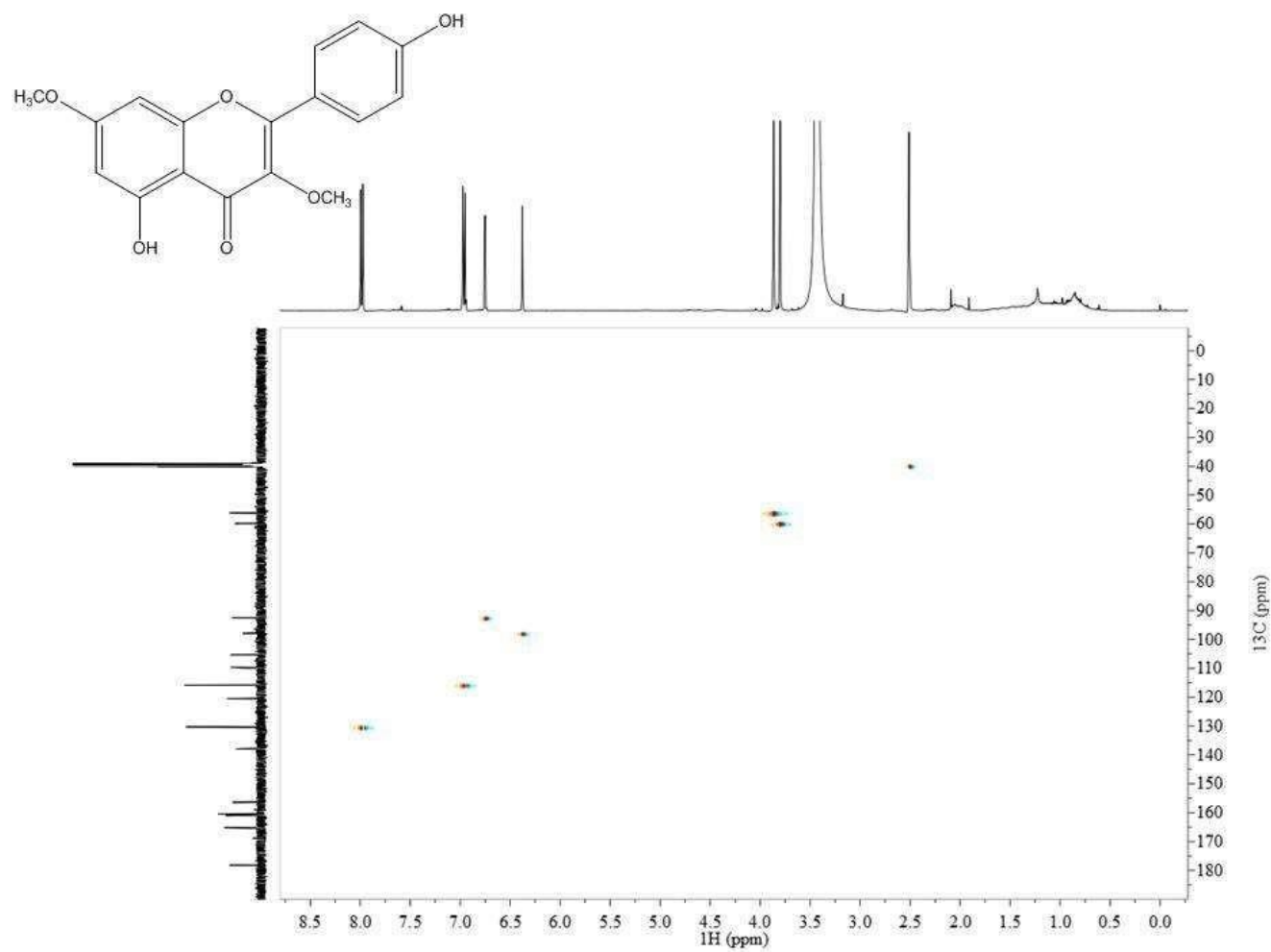
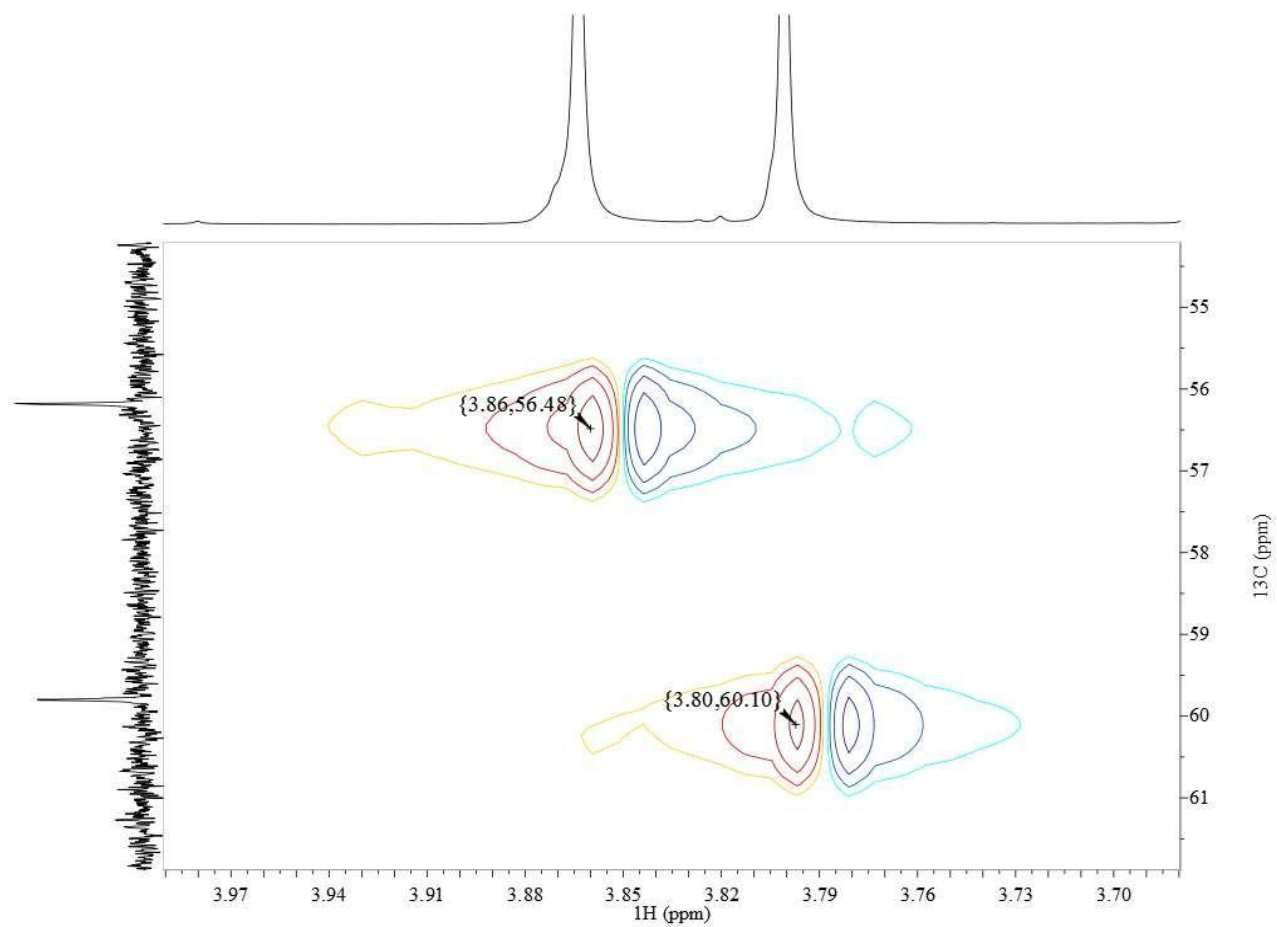


Fig. S34 HSQC  $^1\text{H}$ - $^{13}\text{C}$  NMR spectrum (DMSO- $d_6$ , 500 MHz) of 3,7-di-*O*-methyl-kaempferol (kumatakenin), **3** (Fr-10).



**Fig. S35** HSQC  $^1\text{H}$ - $^{13}\text{C}$  NMR spectrum (DMSO- $d_6$ , 500 MHz) expanded in the region relative to methoxyl groups of 3,7-di-*O*-methyl-kaempferol (kumatakenin), **3 (Fr-10)**.

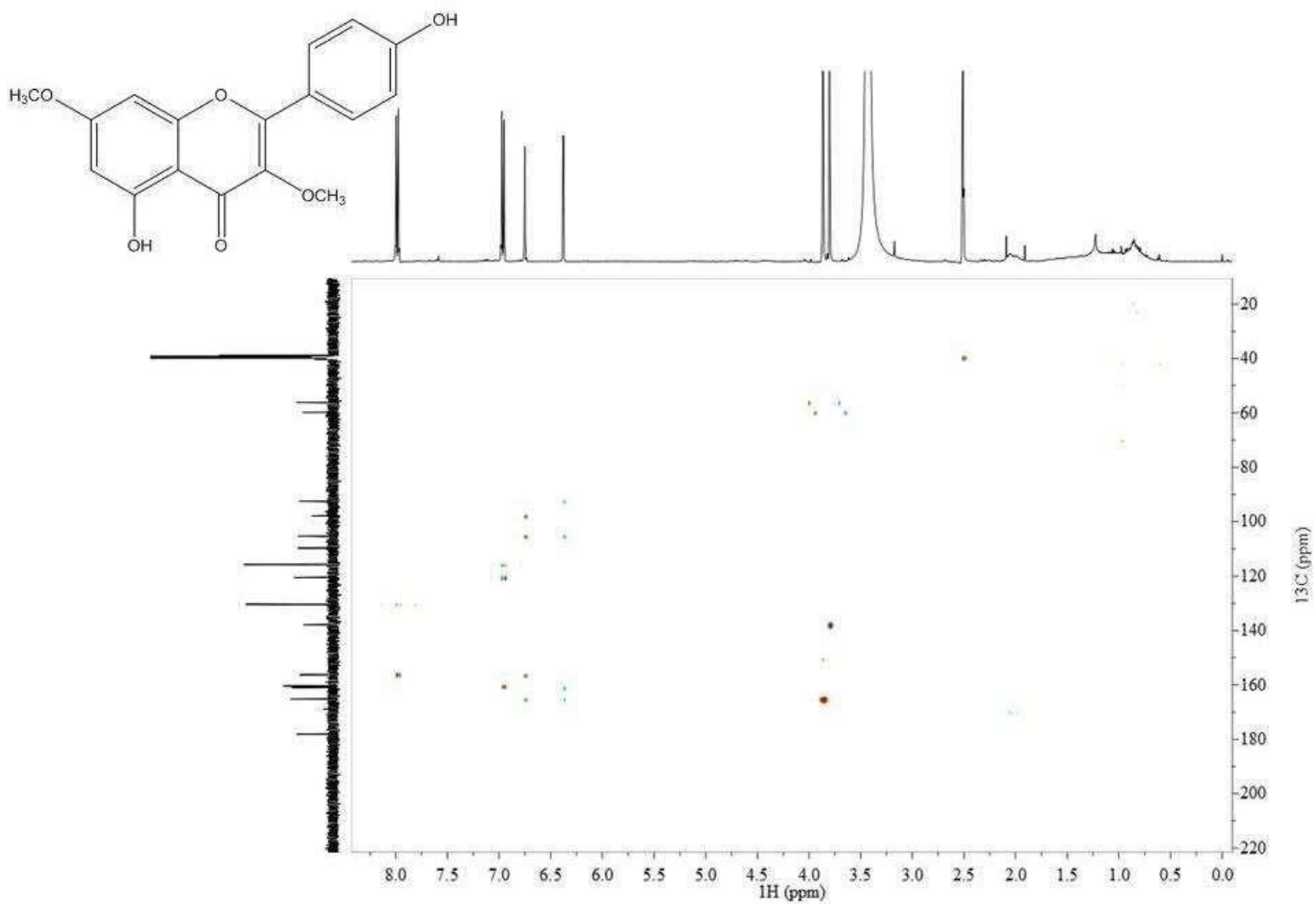
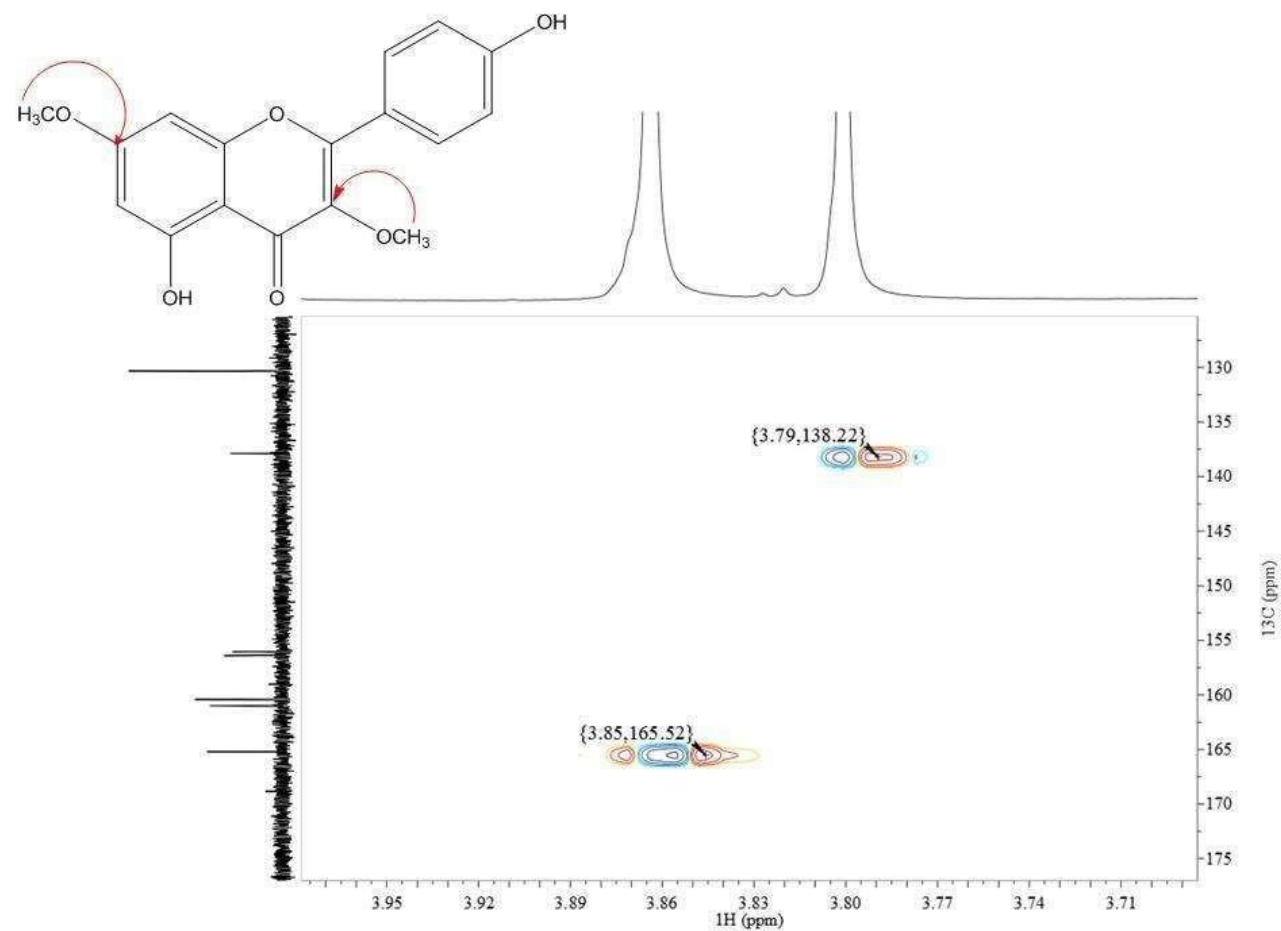


Fig. S36 HMBC <sup>1</sup>H-<sup>13</sup>C NMR spectrum (DMSO-d<sub>6</sub>, 500 MHz) of 3,7-di-*O*-methyl-kaempferol (kumatakenin), **3** (Fr-10)



**Fig. S37** HMBC  $^1\text{H}$ - $^{13}\text{C}$  NMR spectrum (DMSO- $d_6$ , 500 MHz) expanded in the region relative to methoxyl groups of 3,7-di-*O*-methyl-kaempferol (kumatakenin), **3 (Fr-10)**.

**Table S2.**  $^1\text{H}$  and  $^{13}\text{C}$  NMR spectral data for 3,7-di-*O*-methyl-kaempferol (kumatakenin), **3** (DMSO- $d_6$ , 500MHz) compared with the literature.

	$^1\text{H}$ $\delta$ (in ppm) mult. ( <i>J</i> in Hz) Compound <b>3</b> in fraction <b>10</b>	$^1\text{H}$ $\delta$ (in ppm) in DMSO- $d_6$ Literature: Silva et al., 2009	$^{13}\text{C}$ $\delta$ (in ppm) Compound <b>3</b> in fraction <b>10</b>	$^{13}\text{C}$ $\delta$ (in ppm) in DMSO- $d_6$ Literature: Silva et al., 2009
kaempferol moiety				
2			161.3	155.95
3			138.2	137.86
4			178.5	178.09
5			160.7	160.96
6	6.35 d (2.2)	6.35 sl	98.1	97.77
7			165.6	165.13
8	6.72 d (2.2)	6.74 sl	93.0	92.37
9			156.4	156.33
10			105.3	105.21
1'			121.0	120.52
2',6'	7.98 d (8.9)	7.96 d	130.6	130.24
3',5'	6.96 d (8.8)	8.67 d	116.3	115.68
4'			156.8	160.29
3-OCH <sub>3</sub>	3.79 s	3.78 s	60.3	59.72
7-OCH <sub>3</sub>	3.85 s	3.84 s	56.4	56.10



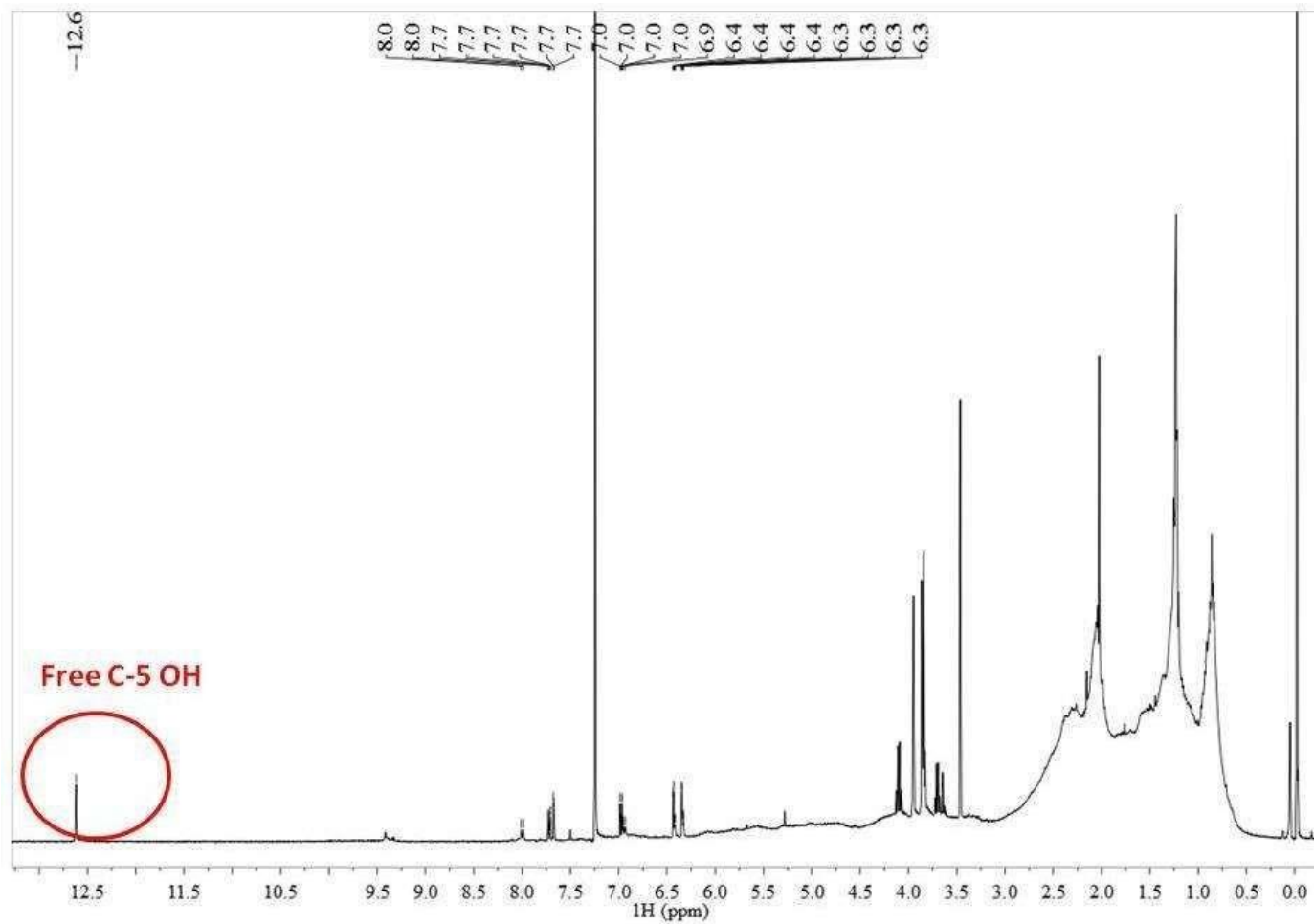


**Fig. S38** <sup>1</sup>H NMR spectrum (CDCl<sub>3</sub>, 500 MHz) of mixture of 3,7-di-*O*-methyl-kaempferol (kumatakenin), (**3**) and tetra-*O*-methyl-queretin (retusin) (**2**) (**Fr-11**).

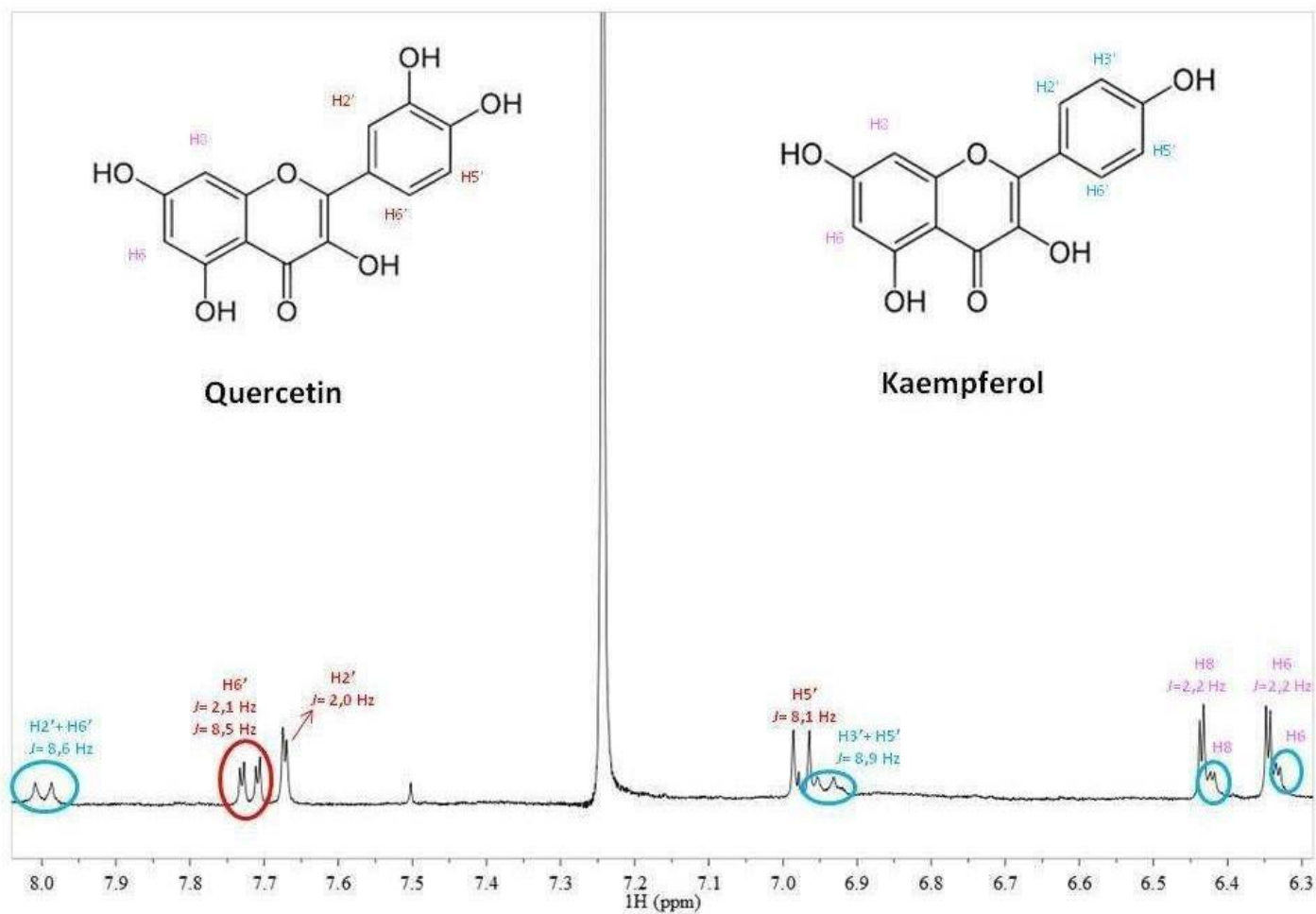


Fig. S39  $^1\text{H}$  NMR spectrum ( $\text{CDCl}_3$ , 500 MHz) expanded in the region relative to the aromatic protons (Fr-11).

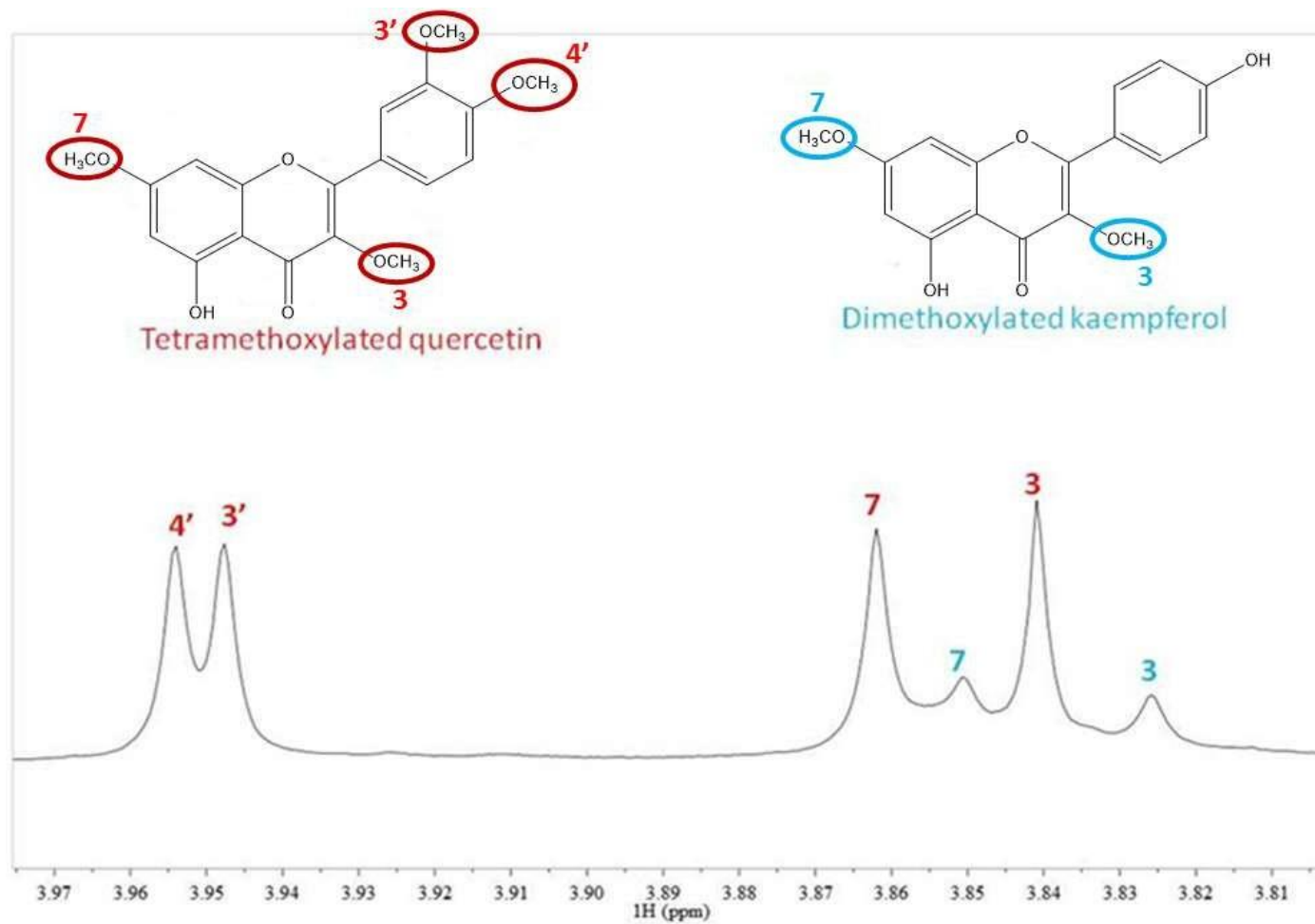
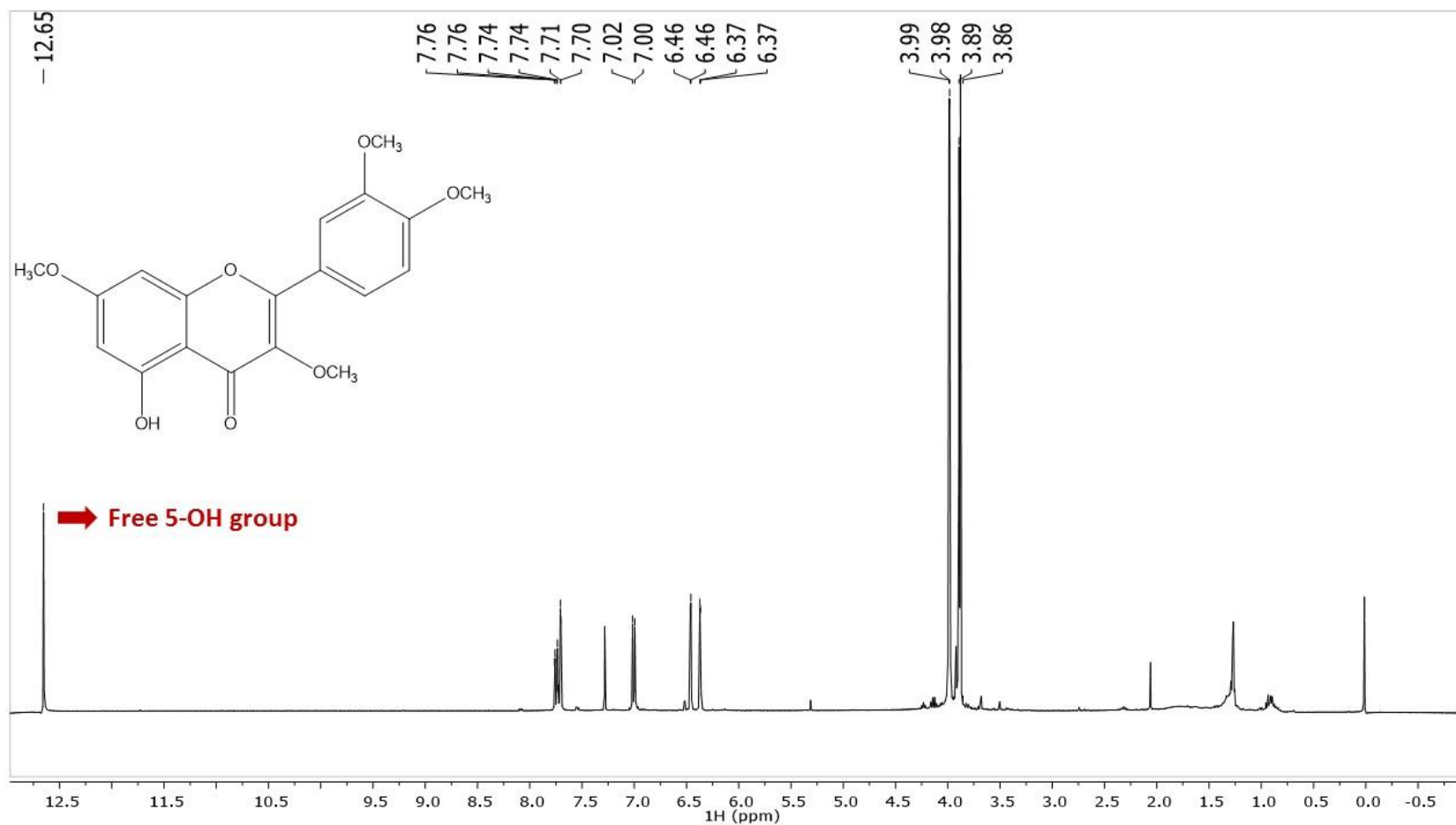
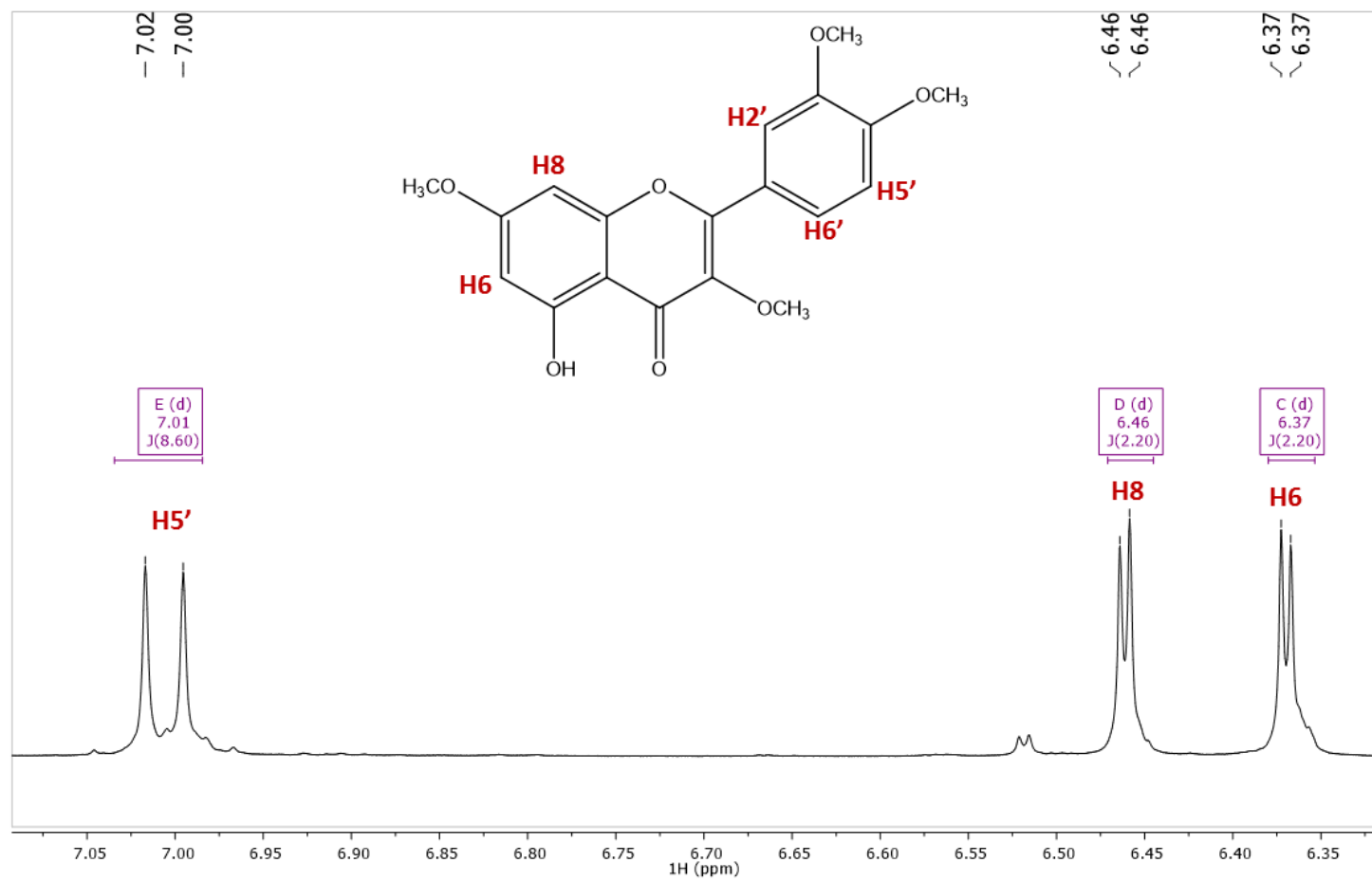


Fig. S40 <sup>1</sup>H NMR spectrum (CDCl<sub>3</sub>, 500 MHz) expanded in the region relative to methoxyl groups (**Fr-11**).



**Fig. S41**  $^1\text{H}$  NMR spectrum (CDCl<sub>3</sub>, 500 MHz) of tetra-*O*-methyl-quercetin (retusin), (2) (**Fr-11A**).



**Fig. S42** <sup>1</sup>H NMR spectrum (CDCl<sub>3</sub>, 500 MHz) expanded in the aromatic protons region of tetra-*O*-methyl-queretin (retusin), (2) (**Fr-11A**).

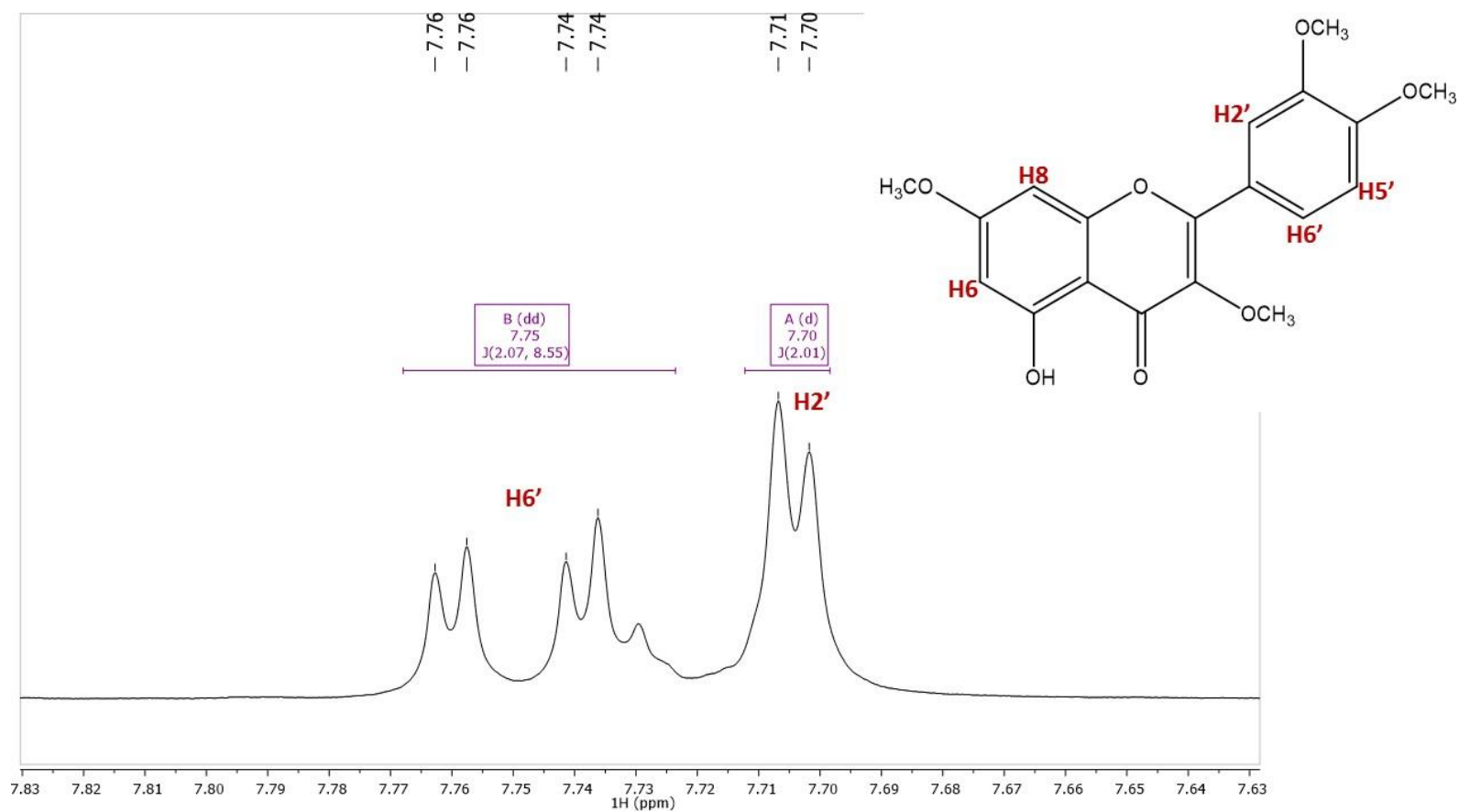


**Fig. S43** <sup>1</sup>H NMR spectrum (CDCl<sub>3</sub>, 500 MHz) expanded in the aromatic protons region of tetra-*O*-methyl-queracetin (retusin), (2) (**Fr-11A**).

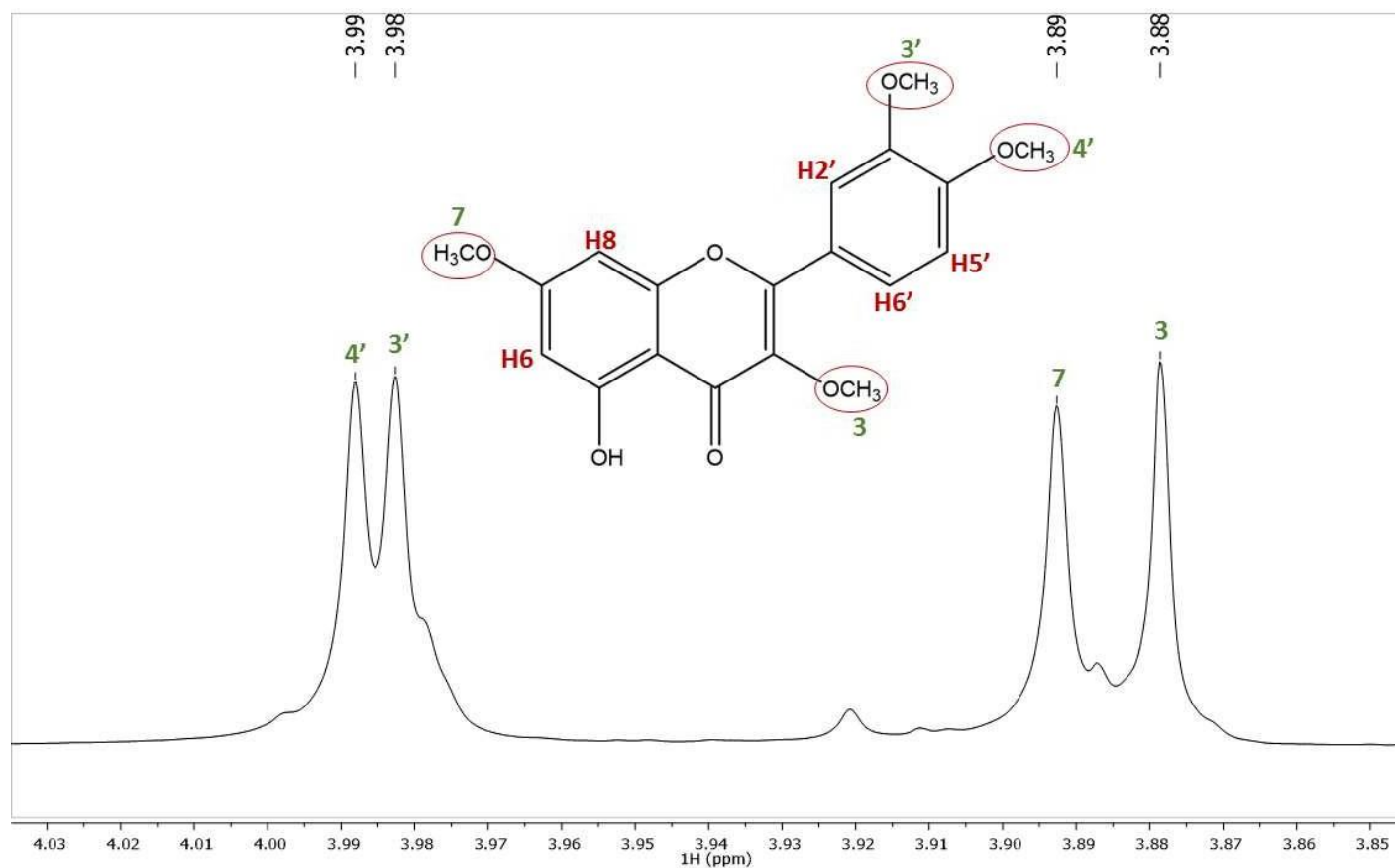


**Fig. S44**  $^1\text{H}$  NMR spectrum ( $\text{CDCl}_3$ , 500 MHz) expanded in the region relative to methoxyl groups of tetra-*O*-methyl-queretin (retusin), (2) (**Fr-11A**).



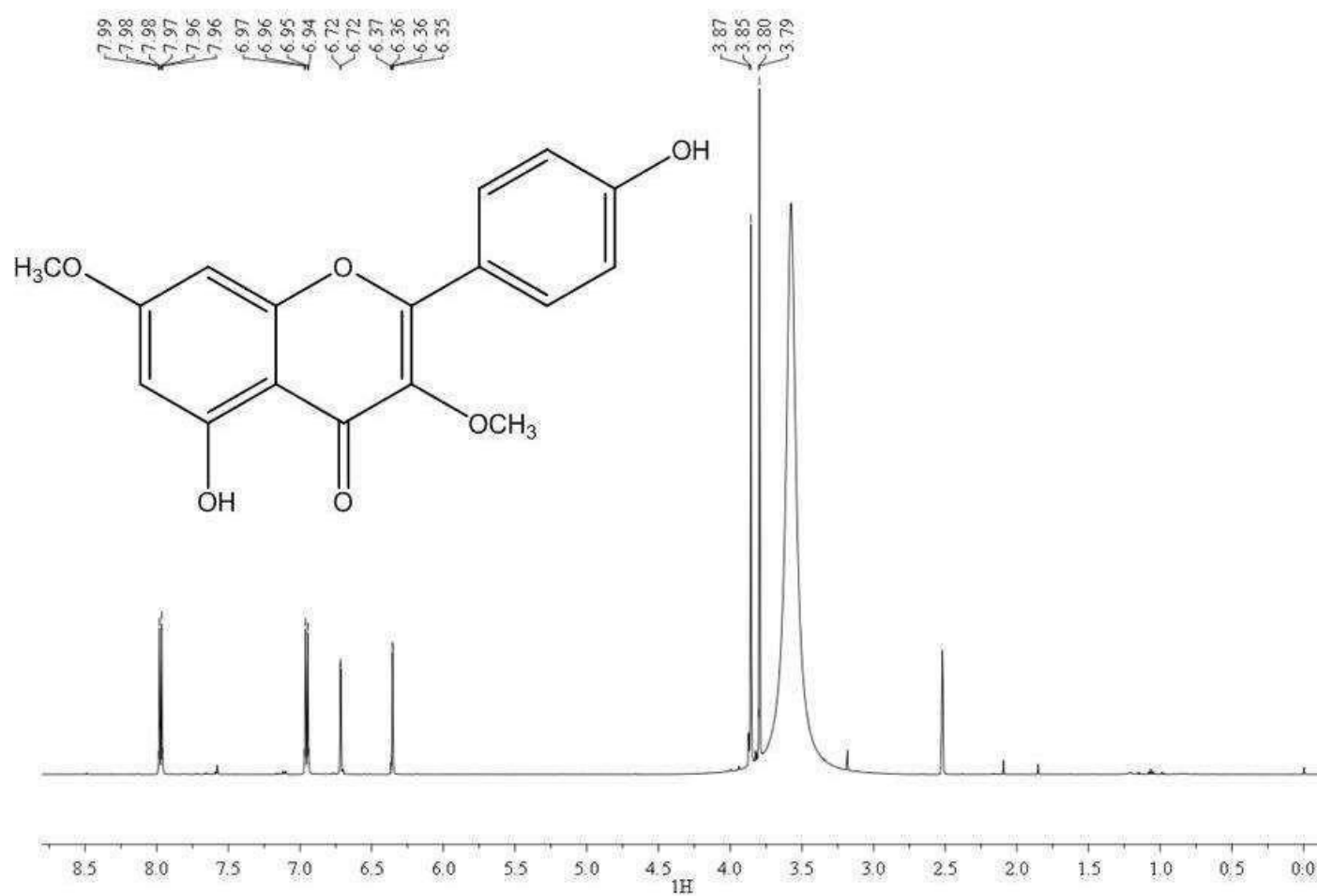
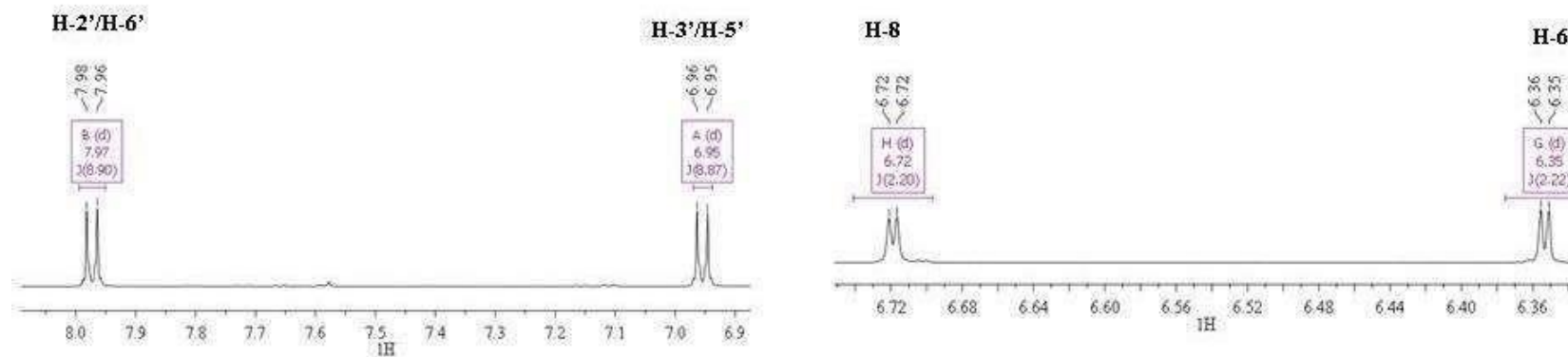
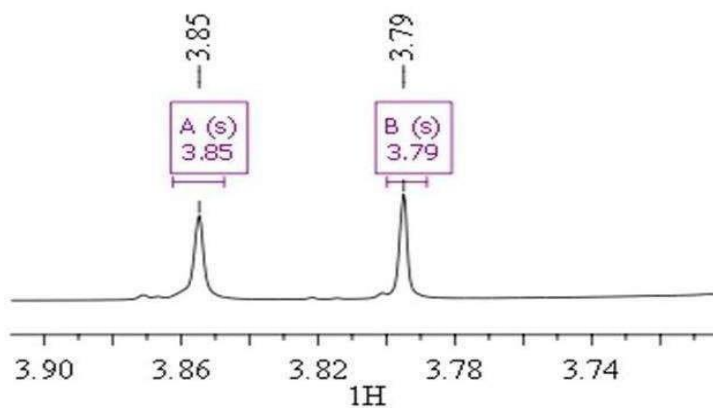


Fig. S45 <sup>1</sup>H NMR spectrum (DMSO-d<sub>6</sub>, 500 MHz) of 3,7-di-O-methyl-kaempferol (kumatakenin), **3** (Fr-11B).



**Fig. S46**  $^1\text{H}$  NMR spectrum (DMSO- $d_6$ , 500 MHz) expanded in the aromatic protons region of 3,7 di-*O*-methyl-kaempferol (kumatakenin), **3** (Fr-11B).



**Fig. S47**  $^1\text{H}$  NMR spectrum (DMSO- $d_6$ , 500 MHz) expanded in the region relative to methoxyl groups of 3,7-di-*O*-methyl-kaempferol (kumatakenin), **3** (Fr-11B).

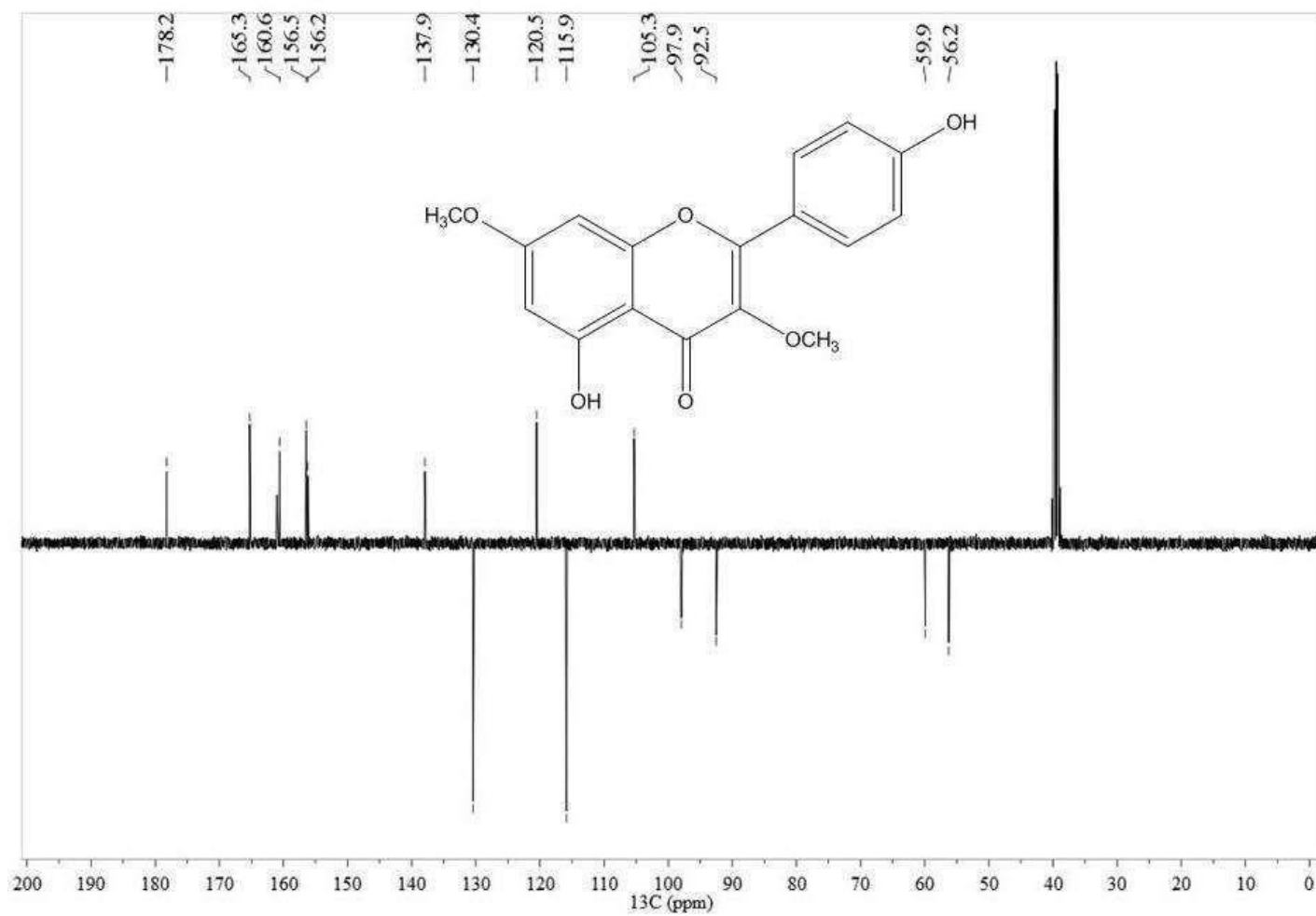


**Fig. S48** APT NMR spectrum (DMSO-d<sub>6</sub>, 500 MHz) of 3,7-di-*O*-methyl-kaempferol (kumatakenin), **3 (Fr-11B)**.

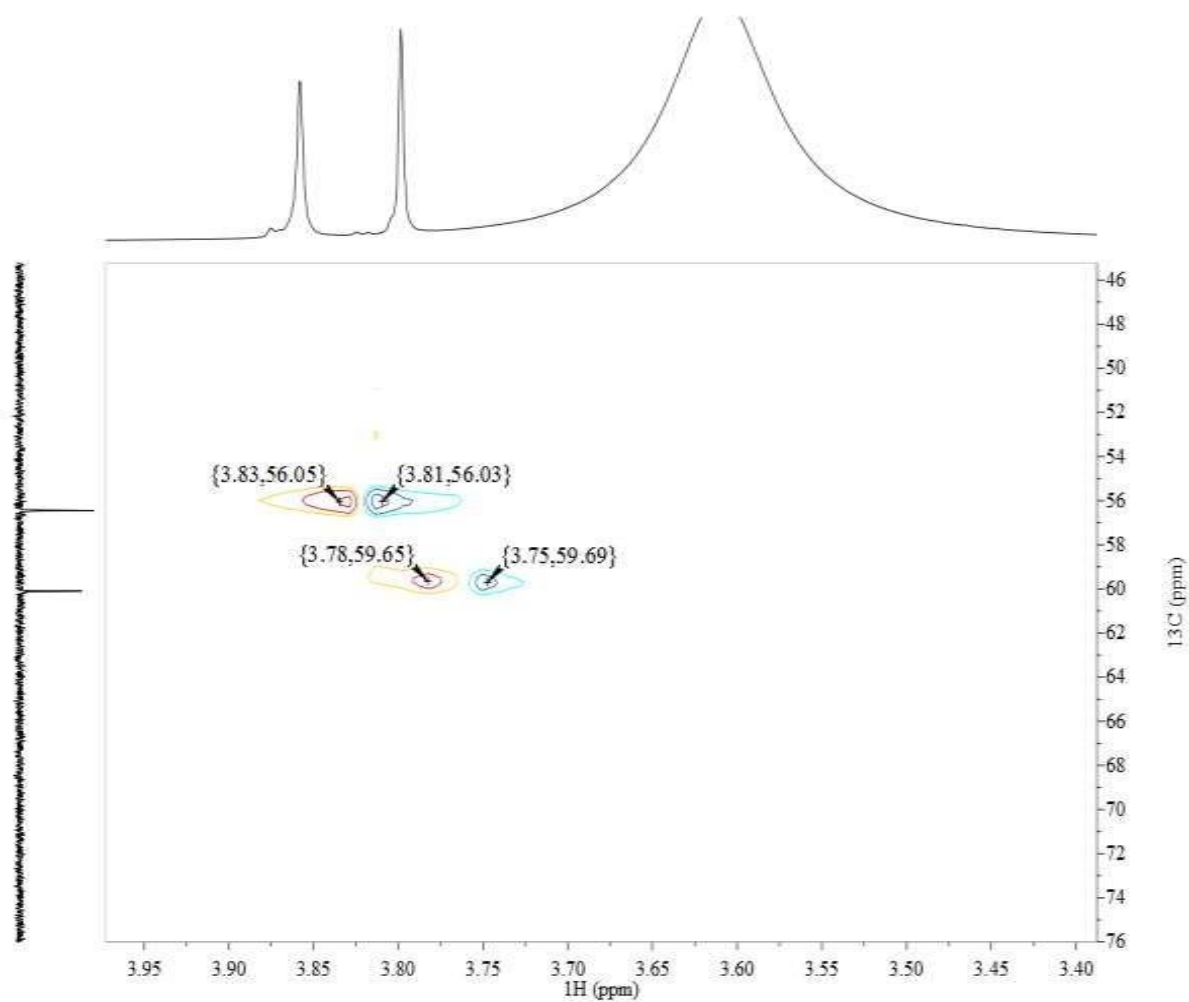


**Fig. S49** HSQC  $^1\text{H}$ - $^{13}\text{C}$  NMR spectrum (DMSO- $d_6$ , 500 MHz) expanded in the region relative to methoxyl groups of 3,7-di-*O*-methyl-kaempferol(kumatakenin), **3 (Fr-11B)**.

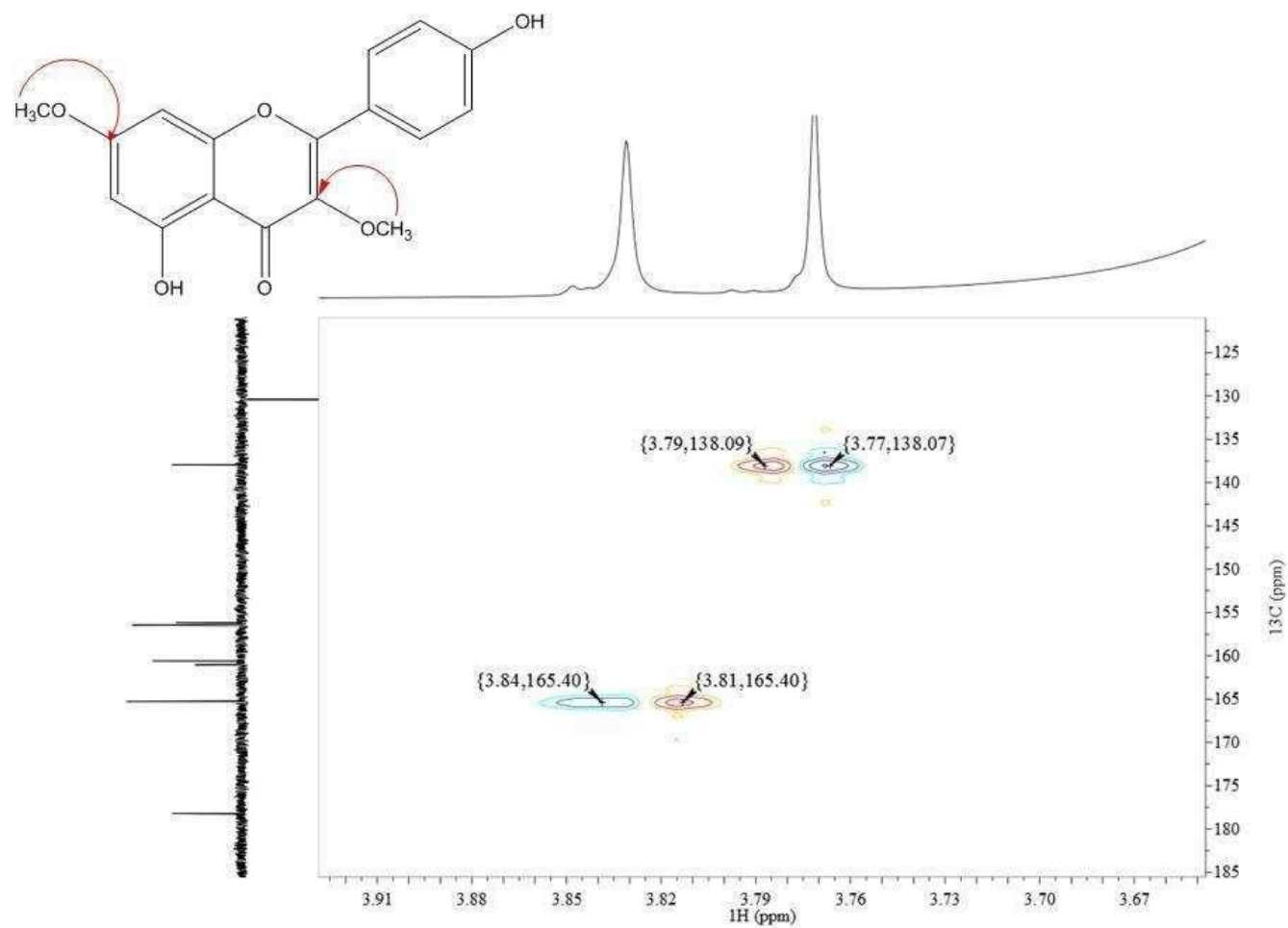


**Fig. S50** HMBC  $^1\text{H}$ - $^{13}\text{C}$  NMR spectrum (DMSO- $d_6$ , 500 MHz) expanded in the region relative to the methoxyl groups of 3,7-di-*O*-methyl-kaempferol(kumatakenin), **3 (Fr-11B)**.

**Table S3** Retention times and UV bands by HPLC-DAD and DI-APCI (+)-MS/MS for the annotated compounds.

<b>ID</b>	<b>R<sub>t</sub> (min) (%)*</b>	<b>UV (λ=280nm)</b>	<b>[M+H]<sup>+</sup> (intensity)</b>	<b>MS<sup>2</sup></b>	<b>Compounds Annotated</b>
<b>Fr-7 (S2;S8;S9)</b>	29.4 (74.8 %)	250; 355	345.2 (100%)	330 (- CH <sub>3</sub> ); 315 (- 2xCH <sub>3</sub> )	3,3',4'-tri- <i>O</i> -methyl- quercetin, <b>1</b>
<b>Fr-8</b>	32.2 (11.3 %)	265; 350	315.2 (8 %)	-	di- <i>O</i> -methyl-kaempferol
<b>(S3;S10;S11)</b>	32.7 (87.6 %)	250; 350	345.2 (100 %)	330 (- CH <sub>3</sub> ); 315 (- 2xCH <sub>3</sub> )	tri- <i>O</i> -methyl-quercetin
<b>Fr-9</b>	32.2 (69.4 %)	255; 355	315.3 (64 %)	300 (- CH <sub>3</sub> ); 287 (Aglycone)	di- <i>O</i> -methyl-kaempferol
<b>(S4;S12;S13)</b>	32.7 (30.1 %)	265; 350	345.3 (100 %)	330 (- CH <sub>3</sub> ); 312 (- CH <sub>3</sub> -H <sub>2</sub> O)	tri- <i>O</i> -methyl-quercetin
<b>Fr-10</b>	32.2 (98.7 %)	265; 345	315.2 (100 %)	300 (- CH <sub>3</sub> ); 287 (Aglycone)	3,7-di- <i>O</i> -methyl-kaempferol (kumatakenin), <b>3</b>
<b>(S5;S14;S15)</b>					
<b>Fr-11</b>	32.2 (79.3 %)	265; 345	315.2 (100 %)	300 (- CH <sub>3</sub> ); 287 (Aglycone)	3,7-di- <i>O</i> -methyl-kaempferol (kumatakenin), <b>3</b>
<b>(S6;S16;S17)</b>					

	36.7 (16.8 %)	250; 350	359.3 (64 %)	344 (- CH <sub>3</sub> )	3,7,3',4'-tetra- <i>O</i> -methyl- quercetin (retusin), <b>2</b>
<b>Fr-12</b> <b>(S7;S18;S19)</b>	32.2 (20.16 %)	265; 345	315.2 (23 %)	300 (- CH <sub>3</sub> )	di - <i>O</i> -methyl-kaempferol
	36.7 (63.64 %)	250; 350	359.3 (100 %)	344 (-CH <sub>3</sub> )	tetra- <i>O</i> -methyl-quercetin

\*These percentages were taken from the area of the HPLC-UV chromatogram at 280 nm.

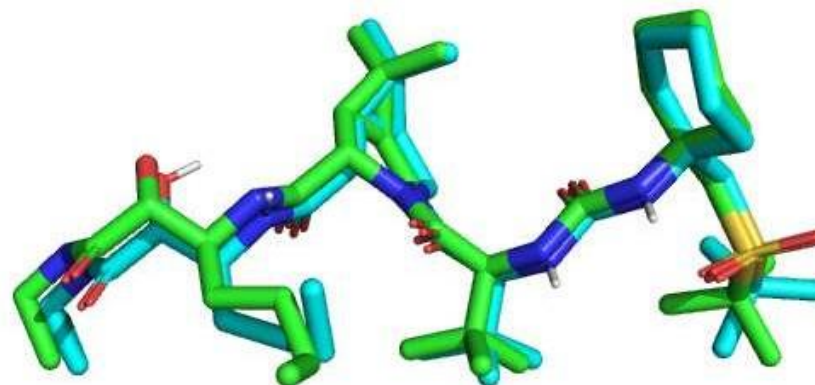


**Fig. S51** Redocking result for 3CLpro crystal (PDBid: 6XQT). In green, the ligand Narlaprevir; in light cyan, pose 1 of the redocking result. Atoms: Dark blue -Nitrogen; Red -Oxygen. RMSD: 0.97 Å.



**Table S4:** Energy redocking values for 3CLpro with Narlaprevir, and PLpro interact with 5-amino-2-methyl-N-[(1R)-1-naphthalen-1-ylethyl]benzamide (GRL0617).

	3CLpro					PLpro		
	Affinity for best distance mode (kcal/mol)	Mode	Distance His41 (Å)	Distance Cys145 (Å)	Distance Glu166 (Å)	Affinity for best distance mode (kcal/mol)	Mode	Distance Tyr268 (Å)
Narlaprevir	-10,4	1	2,2	-	3,11	-	-	-
5-amino-2-methyl-N-[(1R)-1-naphthalen-1-ylethyl]benzamide (GRL0617)	-	-	-	-	-	-9,6	1	2,6

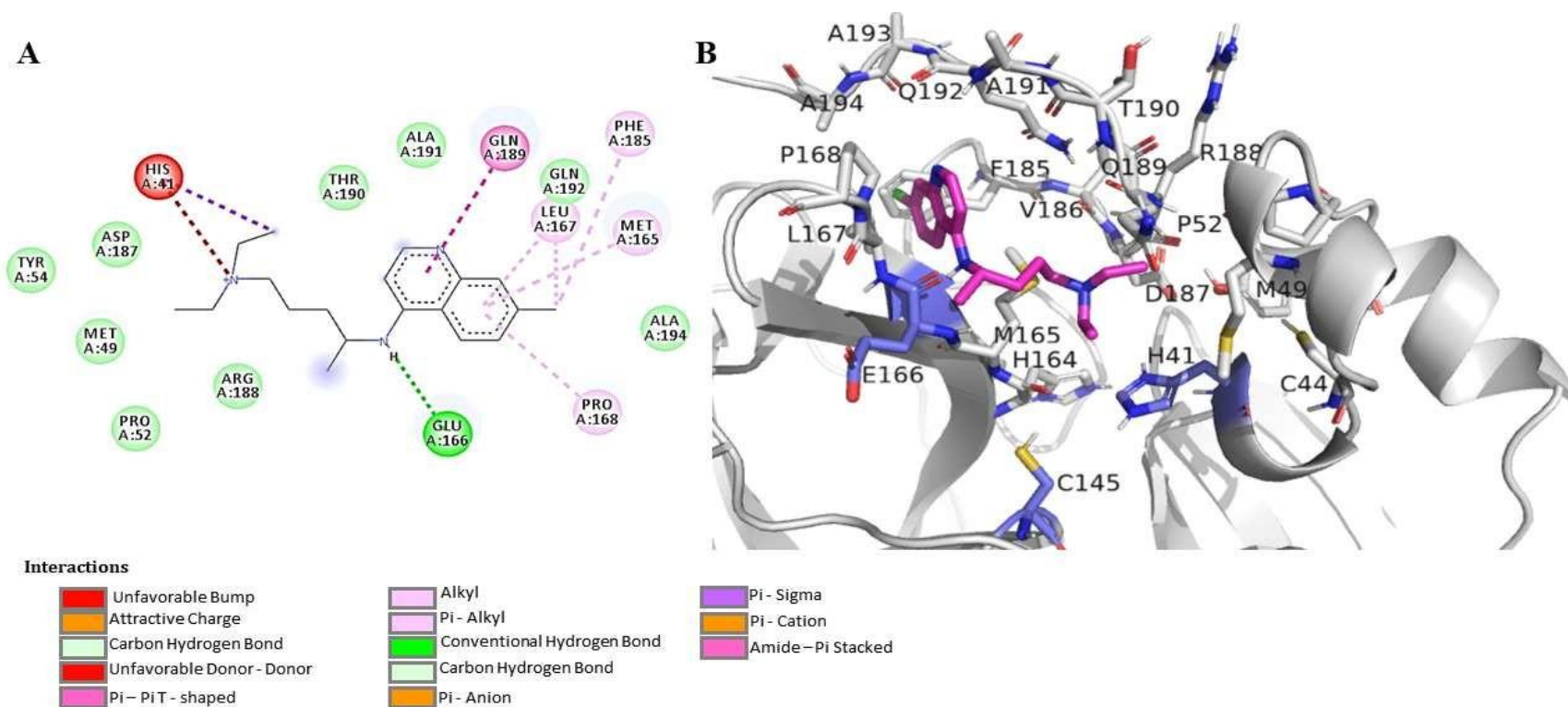


**Fig. S52** Interaction map of the amino acid residues of the 3CLpro (PDBid: 6XQT) with chloroquine. Figure **A** shows the different types of interaction between the protein and the ligand in flat representation. The 3D representation is in Figure **B**, in which the 3CLpro is in gray and residues within a radius of proximity equal to 5 Å of the ligand, represented by sticks, and the ligand is in magenta. In lavender are the residues His41, Cys145 and Glu166.

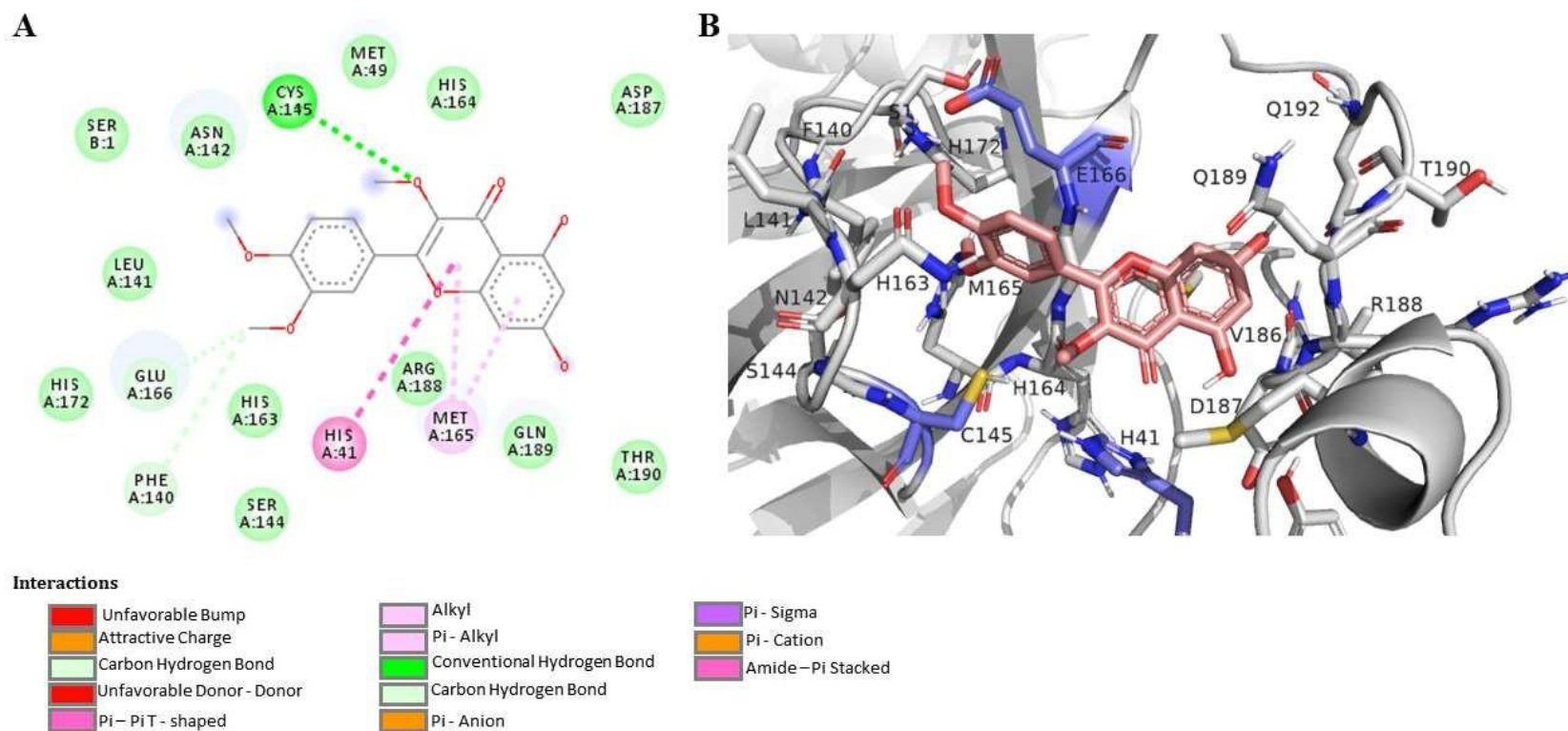


**Fig. S53** Interaction map of the amino acid residues of the 3CLpro (PDBid: 6XQT) with 3,3',4'-tri-*O*-methyl-quercetin (**1**). Figure **A** shows the different types of interaction between the protein and the ligand in flat representation. The 3D representation is in Figure **B**, in which the 3CLpro is in gray and residues within a radius of proximity equal to 5 Å of the ligand, represented by sticks, and the ligand is in light pink. In lavender are the residues His41, Cys145 and Glu166.

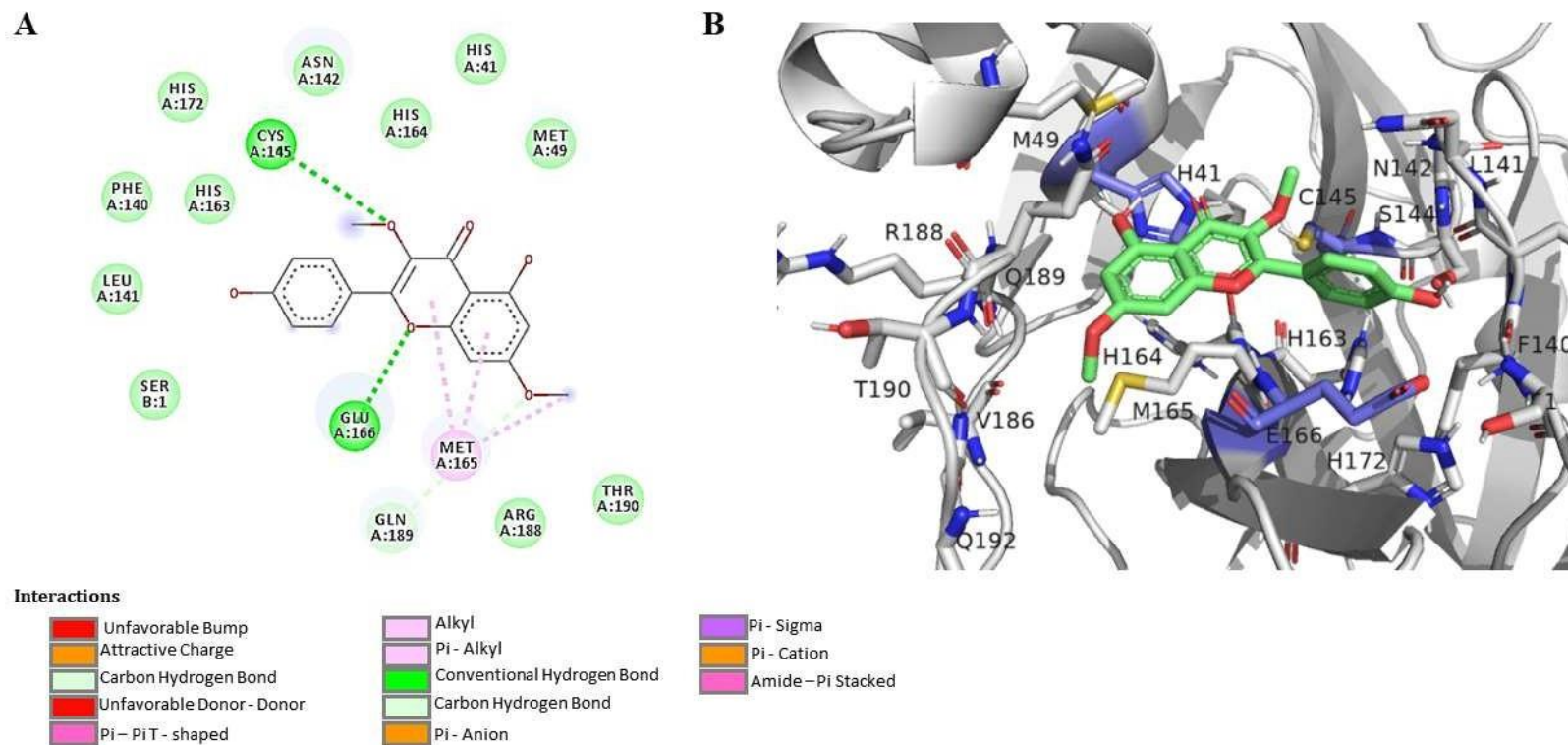


**Fig.S54** Interaction map of the amino acid residues of the 3CLpro (PDBid: 6XQT) with 3,7-di-*O*-methyl-kaempferol (kumatakenin) (**3**). Figure **A** shows the different types of interaction between the protein and the ligand in flat representation. The 3D representation is in Figure **B**, in which the 3CLpro is in gray and residues within a radius of proximity equal to 5 Å of the ligand, represented by sticks, and the ligand is in green. In lavender are the residues His41, Cys145 and Glu166.



**Fig. S55** Redocking result for PLpro crystal (PDBid: 7JRN). In gold, the ligand 5-amino-2-methyl-N - [(1R) -1-naphthalen-1-ylethyl] benzamide(GRL0617); in light blue, pose 1 of the redocking result. Atoms: Dark blue - Nitrogen; White - Hydrogen; Red: Oxygen. RMSD: 0.45356 Å.

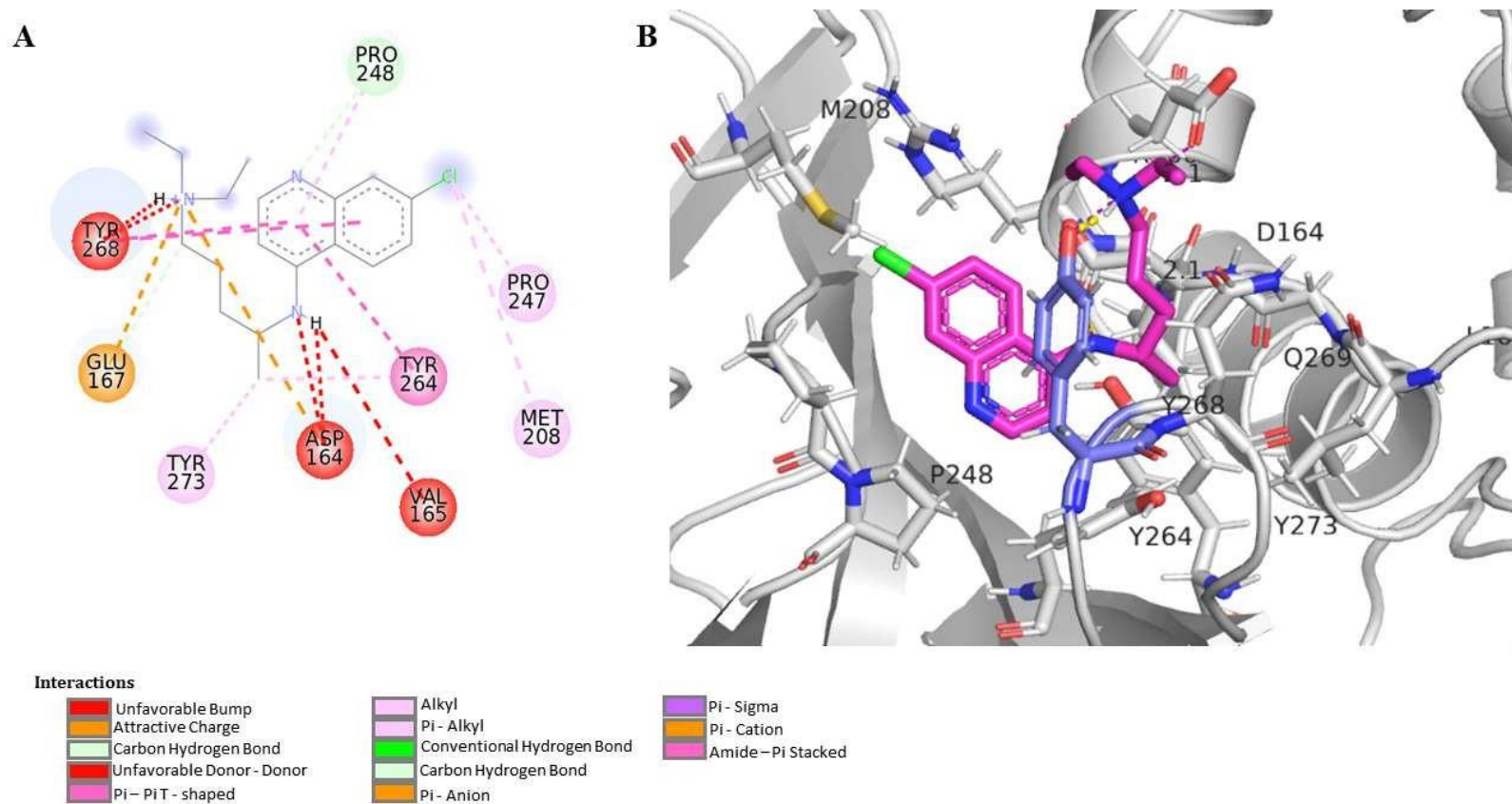


**Fig. S56** Interaction map of the amino acid residues of the PLpro (PDBid: 7JRN) with chloroquine. Figure A shows the different types of interaction between the protein and the ligand in flat representation. The 3D representation is in Figure B, in which the PLpro is in gray and residues within a radius of proximity equal to 5 Å of the ligand, represented by sticks, and the ligand is in magenta. In lavender the residue Tyr268.



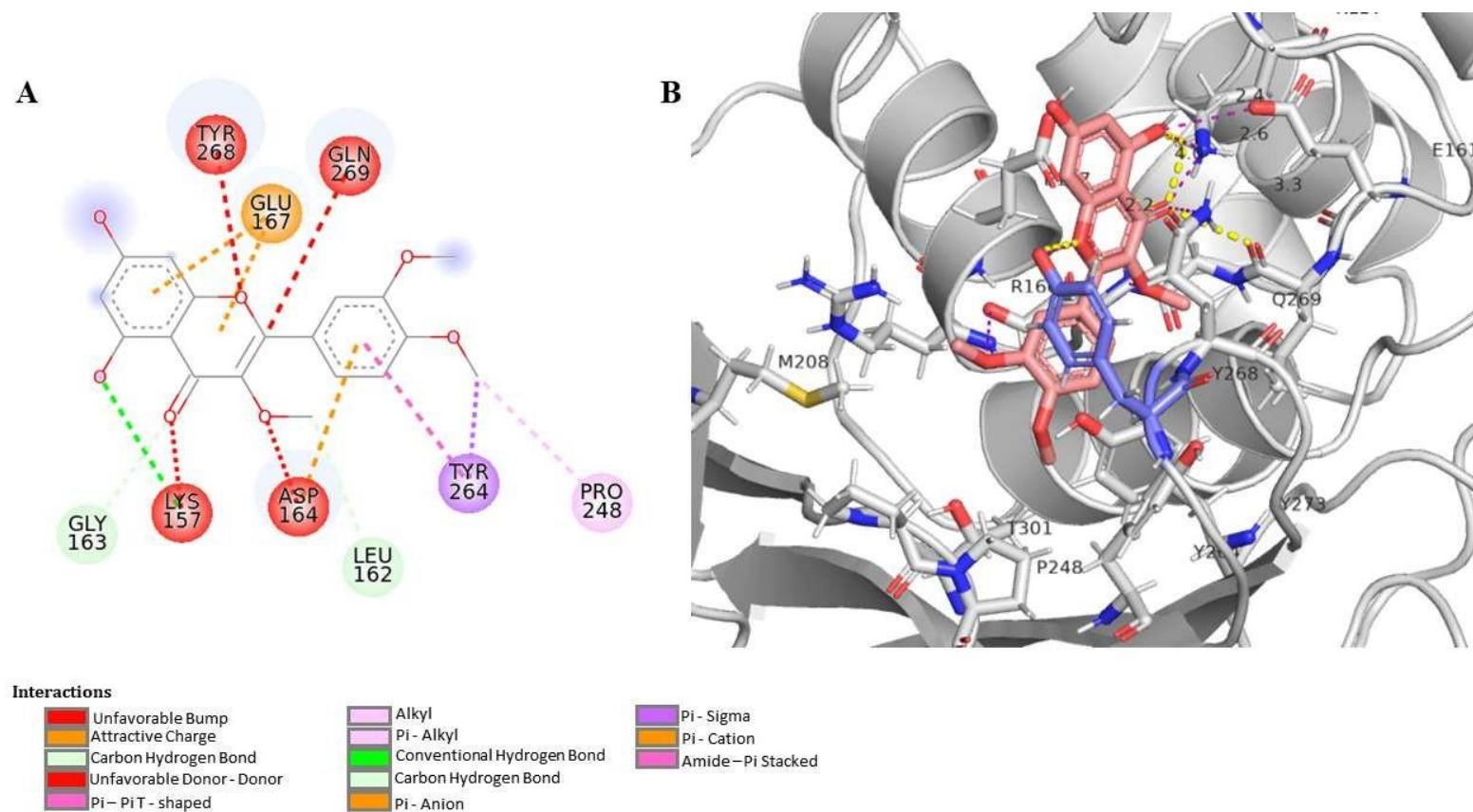


**Fig. S57** Interaction map of the amino acid residues of the PLpro (PDBid: 7JRN) with 3,3',4'-tri-*O*-methyl-quercetin (**1**). Figure **A** shows the different types of interaction between the protein and the ligand in flat representation. The 3D representation is in Figure **B**, in which the PLpro is in gray and residues within a radius of proximity equal to 5 Å of the ligand, represented by sticks, and the ligand is in light pink. In lavender the residue Tyr268.



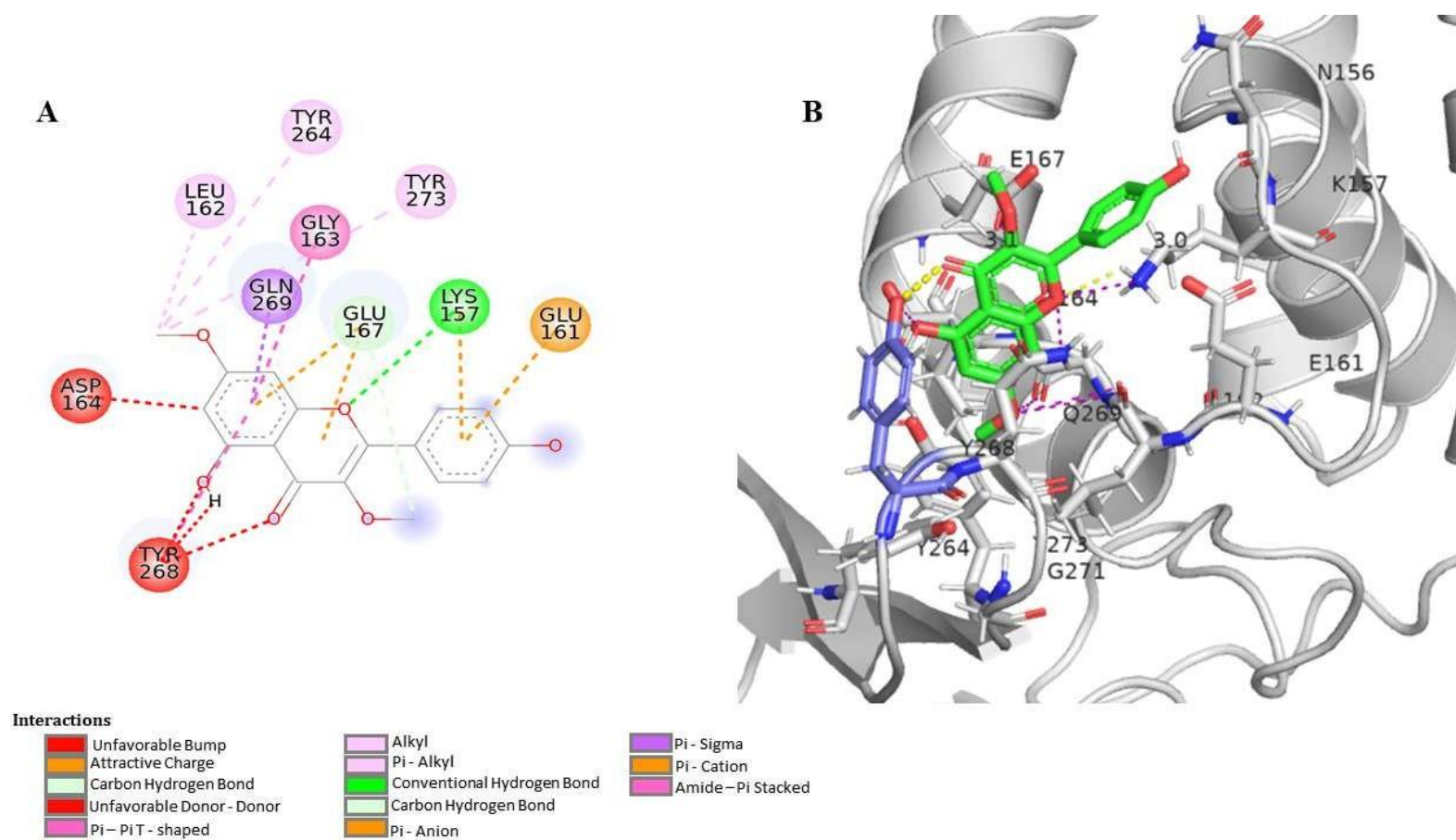


**Fig. S58** Interaction map of the amino acid residues of the PLpro (PDBid: 7JRN) with 3,7-di-*O*-methyl-kaempferol (kumatakenin) (3). Figure **A** shows the different types of interaction between the protein and the ligand in flat representation. The 3D representation is in Figure **B**, in which the PLpro is in gray and residues within a radius of proximity equal to 5 Å of the ligand, represented by sticks, and the ligand is in green. In lavender the residue Tyr 268.

## 5. Conclusões

Este trabalho relata, pela primeira vez, a atividade anti-influenza A(H1N1)pdm09 e anti-SARS-CoV-2 de espécies de *Siparuna* da Amazônia, mostrando o seu potencial para a bioprospecção de agentes antivirais. Os dados corroboram o uso de plantas desse gênero na medicina popular brasileira para o tratamento e profilaxia de resfriados. Os resultados promissores estimularam a investigação química de extratos e frações, assim como a busca de substâncias que poderiam estar relacionadas a essas bioatividades.

As análises por infusão direta em espectrômetro de massas, possibilitaram a rápida investigação dos perfis químicos de 25 extratos das espécies de *Siparuna*. Ademais, os estudos da desreplicação por LC-HR-MS/MS possibilitaram investigar minuciosamente a composição química de diferentes espécies de *Siparuna*, sendo a *S. cristata*, *S. reginae* e *S. sarmentosa*, descritas pela primeira vez neste trabalho, e ampliar o conhecimento químico sobre a *S. glycyarpa*, já descrita pelo grupo de pesquisa, e *S. decipiens*. As ferramentas como o *software* MZmine 2, bancos de dados *online* e a revisão da literatura dos metabólitos descritos para espécies de *Siparuna* auxiliaram na anotação de substâncias conhecidas na família Siparunaceae assim como, outras descritas pela primeira vez no gênero.

Com o uso do equipamento CPC (hidrostático) foi possível realizar o fracionamento bioguiado do extrato *n*-butanol de *S. glycyarpa*, com um sistema de solventes polar (BuMWat), cuja retenção da fase estacionária não ocorreu no equipamento hidrodinâmico. A partir dessa metodologia, foram adquiridas frações que inibiram o vírus influenza e a construção de redes moleculares na plataforma GNPS a partir dos dados LC-HR-MS/MS, auxiliaram na busca e anotação dos metabólitos nessas frações. Além disso, a utilização do equipamento HSCCC (hidrodinâmico) e o sistema de solventes (HEMWat) possibilitou o isolamento dos flavonoides metilados do extrato em diclorometano de *S. cristata*, que apresentaram potencial anti-SARS-CoV-2 *in vitro* e *in silico*.

Portanto, esta pesquisa contribuiu para o conhecimento químico e biológico do gênero *Siparuna*, através da formação de uma Rede colaborativa no estado do Rio de Janeiro para o desenvolvimento e/ou obtenção de novos antivirais de origem natural, ativos contra patógenos de grande importância clínica. Neste contexto, novos estudos estão sendo desenvolvidos a fim de realizar o isolamento e a purificação das substâncias presentes nas frações mais ativas, para serem testadas quanto a atividade antiviral.

## 6. Referências Bibliográficas

ABRAHAM, M. J.; MURTOLA, T.; SCHULZ, R.; PÁLL, S.; SMITH, J. C.; HESS, B.; LINDAHL, E. Gromacs: High performance molecular simulations through multilevel parallelism from laptops to supercomputers. *SoftwareX*, v. 1-2, p. 19-25, 2015.

ADAMSKI, Z.; BLYTHE, L.L.; MILELLA, L.; BUFO, S.A. Biological activities of alkaloids: from toxicology to pharmacology. *Toxins*, v. 12, p. 210, 2020.

AGUIAR, R. W. S.; DOS SANTOS, S. F.; MORGADO, F. S.; ASCENCIO, S. D.; LOPES, M. M.; VIANA, K. F.; DIDONET, J.; RIBEIRO, B. M. Insecticidal and repellent activity of *Siparuna guianensis* Aubl. (Negramina) against *Aedes aegypti* and *Culex quinquefasciatus*. *PlosOne*, v. 10(2), e:0116765, 2015.

AI, W.; ZHANG, J.; ZALLOUM, W. A.; JIA, R.; CHERUKUPALLI, S.; DING, X.; SUN, Z.; SUN, L.; JIANG, X.; MA, X.; LI, Z.; WANG, D.; HUANG, B.; ZHAN, P.; LIU, X. Discovery of novel “Dual-site” binding oseltamivir derivatives as potent influenza virus neuraminidase inhibitors. *European Journal of Medicinal Chemistry*, v. 191, 112147, 2020.

ALLARD, P.M.; PÉRESSE, T.; BISSON, J.; GINDRO, K.; MARCOURT, L.; PHAM, V. C.; ROUSSI, F.; LITAUDON, M.; WOLFENDER, J. L. Integration of molecular networking and in-silico MS/MS fragmentation for natural products desreplication. *Analytical Chemistry*, v.88(6), p. 3317-3323, 2016.

ANDRADE, M. A.; CARDOSO, M. G.; ANDRADE, J.; SILVA, L. F.; TEIXEIRA, M. L.; RESENDE, J. M. V.; FIGUEIREDO, A. C. S.; BARROSO, J. G. Chemical composition and antioxidant activity of essential oils from *Cinnamodendron dinisii* Schwacke and *Siparuna guianensis* Aublet. *Antioxidants*, v. 2, p. 384-397, 2013.

ANTONIO, T. M.; WALLER, G. R.; MUSSINAN, C. J. Composition of essential oil from the leaves of *Siparuna guianensis* (Monimiaceae). *Chemistry & Industry*, v. 14, p. 514-515, 1984.

ARON, A.T.; GENTRY, E.C.; MCPHAIL, K.L.; NOTHIAS, L.F.; NOTHIAS-ESPOSITO, M.; BOUSLIMANI, A.; PETRAS, D.; GAUGLITZ, J.M.; SIKORA, N.; VARGAS, F.; VAN DER HOOFT, J. J. J.; ERNST, M.; KANG, K. B.; ACEVES, C. M.; CARABALLO-RODRÍGUEZ, A. M.; KOESTER, I.; WELDON, K. C.; BERTRAND, S.; ROULLIER, C.; SUN, K.; TEHAN, R. M.; BOYA, C. A.; CHRISTIAN, M. H.; GUTIÉRREZ, M.; ULLOA, A. M.; MORA, J. A. T.; MOJICA-FLORES, R.; LAKEY-BEITIA, J.; VÁSQUEZ-CHAVES, V.; ZHANG, Y.; CALDERÓN, A. I.; TAYLER, N.; KEYZERS, R. A.; TUGIZIMANA, F.; NDLOVU, N.; AKSENOV, A. A.; JARMUSCH, A. K.; SCHIMID, R.; TRUMAN, A. W.; BANDEIRA, N.; WANG, M.; DORRESTEIN, P. C. Reproducible molecular networking of untargeted mass spectrometry data using GNPS. *Nature Protocols*, v. 15, p. 1954-1991, 2020.

ARORA, N.; BANERJEE, A. K. Dereplication in natural product discovery. *Current Topics in Medicinal Chemistry*, v. 19(2), p. 101-102, 2019.

BEN-SHABAT, S.; YARMOLINSKY, L.; PORAT, D.; DAHAN, A. Antiviral effect of phytochemicals from medicinal plants: applications and drug delivery strategies. *Drug Delivery and Translational Research*, v. 10(2), p. 354-367, 2020.

BERTHOD, A.; MARYUTINA, T.; SPIVAKOV, B.; SHPIGUN, O.; SUTHERLAND, I. A. Countercurrent chromatography in analytical chemistry. *Pure and Applied Chemistry*, v. 81(2), p. 355-387, 2009.

BLAZENOVIC, I.; KIND, T.; JI, J.; FIEHN, O. Software tools and approaches for compound identification of LC-MS/MS data in metabolomics. *Metabolites*, v. 8(2), p. 31, 2018.

BOJCZUK, M.; ZYZELEWICZ, D.; HODUREK, P. Centrifugal partition chromatography-a review of recent applications and some classic references. *Journal of Separation Science*, v. 40 (7), p. 1597-1609, 2017.

BOOZARI, M.; HOSSEINZADEH, H. Natural products for COVID-19 prevention and treatment regarding to previous coronavirus infections and novel studies. *Phytotherapy Research*, v. 35(2), p. 864-876, 2021.

BORGES, R. M.; TAUJALE, R.; SOUZA, J.S.; BEZERRA, T.A.; SILVA, E. L.; HERZOG, R.; PONCE, F.V.; WOLFENDER, J.L.; EDISON, A.S. Dereplication of plant phenolics using a mass-spectrometry database independent method. *Phytochemical Analysis*, v. 29(6), p. 601-612, 2018.

BRAZ, R.; GABRIEL, S. J.; GOMES, C. M. R.; GOTTLIEB, O. R.; BICHARA, M. D. G. A.; MAIA, J. G. S. Oxoaporphine alkaloids from *Fusea longifolia* and *Siparuna guianensis*. *Phytochemistry*, v. 15, p. 1187-1188, 1976.

CASTAÑEDA, H. G. T.; DULCEY, A. J. C.; MARTÍNEZ, J. H. I. Flavonoid glycosides from *Siparuna gigantotepala* leaves and their antioxidant activity. *Chemical and Pharmaceutical Bulletin*, v. 64(5), p. 502-506, 2016.

CAVALIERE, C.; FOGLIA, P.; PASTORINI, E.; SAMPERI, R.; LAGANÁ, A. Identification and mass spectrometric characterization of glycosylated flavonoids in *Triticum durum* plants by high-performance liquid chromatography with tandem mass spectrometry. *Rapid Communications in Mass Spectrometry*, v. 19(21), p. 3143-3158, 2005.

CHALECKIS, R.; MEISTER, I.; ZHANG, P.; WHEELOCK, C.E. Challenges, progress and promises of metabolite annotation for LC-MS-based metabolomics. *Current Opinion in Biotechnology*, v. 55, p. 44-50, 2019.

CHIU, S. Y. C.; DOBBERSTEIN, R. H.; FONG, H. H. S.; FARNSWORTH, N. R. Oxoaporphine alkaloids from *Siparuna gilgiana*. *Journal of Natural Products*, v. 45(2), p. 229-230, 1982.

CONWAY, W. D. *Counter-Current Chromatography: Apparatus, Theory and Applications*. VCH Publishers Inc., New York, 1990.

COSTA, F. N.; LEITÃO, G.G. Strategies of solvent system selection for the isolation of flavonoids by countercurrent chromatography. *Journal of Separation Science*, v. 33, p. 336-347, 2010.

COSTA, F. N.; GARRARD, I.; DA SILVA, A. J. R.; LEITÃO, G. G. Changes in the mobile phase composition on a stepwise counter-current chromatography elution for the isolation of

flavonoids from *Siparuna glycyarpa*. Journal of Separation Science, v. 36(14), p. 2253-2259, 2013.

COVID-19 DATA REPOSITORY BY THE CENTER FOR SYSTEMS SCIENCE AND ENGINEERING AT JOHNS HOPKINS UNIVERSITY (JHU CSSE COVID-19), 2022. Disponível em: <https://coronavirus.jhu.edu/>. Acesso: março de 2022.

CUYCKENS, F.; CLAEYS, M. Mass spectrometry in the structural analysis of flavonoids. Journal of Mass Spectrometry, v. 39, p. 1-15, 2004.

DAS, K.; ARAMINI, J. M.; MA, L.C.; KRUG, R.M.; ARNOLD, E. Structures of influenza A proteins and insights into antiviral drug targets. Nature structural & molecular biology, v. 17(5), 530-538, 2010.

DAYEM, A. A.; CHOI, H. Y.; KIM, Y. B.; CHO, S-G. Antiviral Effect of Methylated Flavonol Isorhamnetin against Influenza. Plos One, v. 10, p. 1-21, 2015.

DEBNATH, B.; SINGH, W.S.; DAS, M.; GOSWAMI, S.; SINGH, M.K.; MAITI, D.; MANNA, K. Role of plant alkaloids on human health: A review of biological activities. Materials Today Chemistry, v. 9, 56-72, 2018.

DELANO, W. L. The phyMOL molecular graphics system. Delano Scientific, San Carlos. 2002.

DENARO, M.; SMERIGLIO, A.; BARRECA, D.; FRANCESCO, C.; OCCHIUTO, C.; MILANO, G.; TROMBETTA, D. Antiviral activity of plants and their isolated bioactive compounds: an update. Phytotherapy Research, v. 34(4), p. 742-768, 2019.

DEWICK, P. M. Medicinal Natural Products - A Biosynthetic Approach, Third Edition, John Wiley & Sons Ltd, England, 2009.

DLUDLA, P.V.; JACK, B.; VIRARAGAVAN, A.; PHEIFFER, C.; JOHNSON, R.; LOUW, J.; MULLER, C.J.F. A dose-dependent effect of dimethyl sulfoxide on lipid content, cell viability and oxidative stress in 3T3-L1 adipocytes. Toxicology Reports, v.5, p. 1014-1020, 2018.

DOLINSKY, T. J.; CZODROWSKI, P.; LI, H.; NIELSEN, J. E.; JENSEN, J. H.; KLEBE, G.; BAKER, N. A. PDB2PQR: expanding and upgrading automated preparation of biomolecular structures for molecular simulations. Nucleic Acids Research, v. 35(Suppl. 2), 522-525, 2007.

DOMLING, A.; GAO, L. Chemistry and Biology of SARS-CoV-2. Chem: Cell Press, v. 6(6), 1283-1295, 2020.

EKIERT, H.M.; SZOPA, A. Biological activities of natural products. Molecules, v. 25(23), p. 5769, 2020.

EL-ELIMAT, T.; FIGUEROA, M.; EHRMANN, B.M.; CECH, N. B.; PEARCE, C.J.; OBERLIES, N.H. High-resolution MS, MS/MS, and UV database of fungal secondary metabolites as a dereplication protocol for bioactive natural products. Journal of Natural Products, v. 76(9), p. 1709-1716, 2013.

EL-SEEDI, H.; GHIA, F.; TORSSELL, K. G. B. Cadinane Sesquiterpenes from *Siparuna macrotepala*. *Phytochemistry*, v. 35(6), p. 1495-1497, 1994.

FACUNDO, V. A.; AZEVEDO, M. S.; RODRIGUES, R. V.; NASCIMENTO, L. F.; MILITÃO, J. S. L. T.; SILVA, G. V. J.; BRAZ-FILHO, R. Chemical constituents from three medicinal plants: *Piper renitens*, *Siparuna guianensis* and *Alternanthera brasiliana*. *Revista Brasileira de Farmacognosia*, v. 22(5), p. 1134-1139, 2012.

FERREIRA, T. P.; OLIVEIRA, E. E.; TSCHOEKE, P. H.; PINHEIRO, R. G.; MAIA, A. M. S.; AGUIAR, R. W. S. Potential use of Negramina (*Siparuna guianensis* Aubl.) essential oil to control wax moths and its selectivity in relation to honey bees. *Industrial Crops & Products*, v. 109, p. 151-157, 2017.

FISCHER, D. C. H.; GONÇALVES, M. I.; OLIVEIRA, F.; ALVARENGA, M. A. Phytochemical communication. *Fitoterapia*, v. 70, p. 322-323, 1999.

FOUCAULT, A. P.; CHEVOLOT, L. Counter-current chromatography: instrumentation, solvent selection and some recent applications to natural product purification. *Journal of Chromatography A*, v. 808, p. 3-22, 1998.

FRAIGE, K.; DAMETTO, A.C.; ZERAIK, M.L.; FREITAS, L.; SARAIVA, A.C.; MEDEIROS, A.I.; CASTRO-GAMBOA, I.; CAVALHEIRO, A. J.; SILVA, D.H.S.; LOPES, N.P.; BOLZANI, V.S. Dereplication by HPLC-DAD-ESI-MS/MS and screening for biological activities of *Byrsonima* species (Malpighiaceae). *Phytochemical Analysis*, v. 29(2), p. 196-204, 2018.

FRIESEN, J. B.; McALPINE, J.B.; CHEN, S. N.; PAULI, G.F. Countercurrent separation of natural products: an update. *Journal of Natural Products*, v. 78(7), p. 1765-1796, 2015.

GARCÍA, J.; GILARDONI, G.; CUMBICUS, N.; MOROCHO, V. Chemical analysis of the essential oil from *Siparuna echinata* (Kunth) A. DC. (Siparunaceae) of Ecuador and Isolation of the rare terpenoid Sipaucin A. *Plants*, v. 9(2), p. 187, 2020.

GERARD, R. V.; MACLEAN, D. B.; ANTONIO, T. M. Examination of three *Siparuna* species for alkaloid content. *Phytochemistry*, v. 25(9), p. 2155-2156, 1986.

GNPS DOCUMENTATION, 2021. Disponível em: <https://ccms-ucsd.github.io/GNPSDocumentation/featurebasedmolecularnetworking-with-mzmine2/>.

Acesso: janeiro de 2022.

GONZÁLEZ, G. F. P.; ARCHILA, E. G. Anti-bacterial action of extracts and fractions from *Siparuna sessiliflora* Kunth A. DC. (limoncillo). *Revista Cubana de Plantas Medicinai*, v. 17(1), p. 65-72, 2012.

GRIENKE, U.; SCHMIDTKE, M.; GRAFENSTEIN, S.V.; KIRCHMAIR, J.; LIEDL, K.R.; ROLLINGER, J.M. Influenza neuraminidase: A druggable target for natural products. *Natural Product Reports*, v. 29, p. 11-36, 2012.

HEJAZI, J.; GHANAVATI, M.; HEJAZI, E.; POUSTCHI, H.; SEPANLOU, S. G.; KHOSHNIYA, M.; GHARAVI, A.; SOHRABPOUR, A.A.; SOTOUDEH, M.; DAWSEY, S. M.; BOFFETTA, P.; ABNET, C.C.; KAMANGAR, F.; ETEMADI, A.; POURSHAMS, A.; MALEKSHAH, A.F.; BRENNAN, P.; MALEKZADEH, R.; HEKMATDOOST, A. Habitual dietary intake of flavonoids and all-cause and cause-specific mortality: Golestan cohort study. *Nutrition Journal*, v. 19, 108, 2020.

HOFER, B. Recent developments in the enzymatic *O*-glycosilation of flavonoids. *Applied Microbiology and Biotechnology*, v. 100(10), p. 4269-4281, 2016.

HOLMAN, J. D.; TABB, D. L.; MALLICK, P. Employing ProteoWizard to convert raw mass spectrometry data. *Current Protocols in Bioinformatics*, v. 46, p. 13-24, 2014.

HOSTETTMANN, K.; HOSTETTMANN, M. & MARSTON, A. Isolation of natural products by droplet counter-current chromatography and related methods. *Natural product reports*, v. 1, p. 471-481, 1984.

INTERNATIONAL COMMITTEE ON TAXONOMY OF VIRUSES (ICTV), 2021. Disponível em: [https://talk.ictvonline.org/ictv-reports/ictv\\_9th\\_report/negative-sense-rna-viruses-2011/w/negrna\\_viruses/209/orthomyxoviridae](https://talk.ictvonline.org/ictv-reports/ictv_9th_report/negative-sense-rna-viruses-2011/w/negrna_viruses/209/orthomyxoviridae). Acesso: maio de 2022.

ITO, Y. Origin and Evolution of the coil planet centrifuge: a personal reflection of my 40 years of CCC research and development. *Separation & Purification Reviews*, v. 34, p. 131-154, 2005(a).

ITO, Y. Golden rules and pitfalls in selecting optimum conditions for high-speed counter-current chromatography. *Journal of Chromatography A*, v. 1065, p. 145-168, 2005(b).

JENETT-SIEMS, K.; KRAFT, C.; SIEMS, K.; JAKUPOVIC, J.; SOLIS, P. N.; GUPTA, M. P.; BIENZLE, U. Sipaucins A-C, sesquiterpenoids from *Siparuna pauciflora*. *Phytochemistry*, v. 63, p. 377-381, 2003.

KACHLICKI, P.; PIASECKA, A.; STOBIECKI, M.; MARCZAK, L. Structural characterization of flavonoid glycoconjugates and their derivatives with mass spectrometric techniques. *Molecules*, v. 21, p. 1494, 2016.

KAISER, J. A one-size-fits-all flu vaccine? *Science*, v. 312(5772), p. 380-382, 2006.

KASAL, D. A.; LORENZO, A.; TIBIRIÇÁ, E. COVID-19 and microvascular disease: pathophysiology of SARS-CoV-2 infection with focus on the renin-angiotensin system. *Heart, Lung and Circulation*, v. 11, p. 1596-1602, 2020.

KHAN, B.M.; LIU, Y. High speed counter current chromatography: Overview of solvent-system and elution mode. *Journal of Liquid Chromatography & Related Technologies*, v. 41, p. 629-636, 2018.

KOIRALA, N.; THUAN, N. H.; GHIMIRE, G.P.; THANG, D.V.; SOHNG, J.K. Methylation of flavonoids: Chemical structures, bioactivities, progress and perspectives for biotechnological production. *Enzyme and Microbial Technology*, v. 86, p. 103-116, 2016.

KOLEVA, I.I.; BEEK, T.A.V.; SOFFERS, A.E.M.F.; DUSEMUND, B.; RIETJENS, I.M.C.M. Alkaloids in the human food chain – natural occurrence and possible adverse effects. *Molecular Nutrition & Food Research*, v. 56, p. 30-52, 2012.

KOUZNETSOVA, V. L.; HUANG, D. Z.; TSIGELNY, I. F. Potential SARS-CoV-2 protease M<sup>PRO</sup> inhibitors: repurposing FDA-approved drugs. *Physical Biology*, v. 18(2), 025001, 2021.



- KOZIKOWSKI, B.; BURT, T.M.; TIREY, D.A.; WILLIAMS, L.E.; KUZMAK, B.R.; STANTON, D.T.; MORAND, K.L.; NELSON, S.L. The effect of freeze/thaw cycles on the stability of compounds in DMSO. *Journal of Biomolecular Screening*, v. 8(2), p. 210-215, 2003.
- KUROKAWA, M.; SHIMIZU, T.; WATANABE, W.; SHIRAKI, K. Development of New Antiviral Agents from Natural Products. *The Open Antimicrobial Agents Journal*, v. 2, p. 49-57, 2010.
- LEAL, C. M.; SIMAS, R. C.; MIRANDA, M.; CAMPOS, M. F.; GOMES, B. A.; SIQUEIRA, M. M.; DO VALE, G.; DE ALMEIDA, C. V. G.; LEITÃO, S. G.; LEITÃO, G. G. Amazonian *Siparuna* extracts as potential anti-influenza agentes: Metabolic fingerprinting. *Journal of Ethnopharmacology*, v. 270, 113788, 2021(a).
- LEAL, C. M.; LEITÃO, S. G.; SAUSSET, R.; MENDONÇA, S. C.; NASCIMENTO, P. H. A.; CHEOHEN, C. F. A. R.; ESTEVES, M. E. A.; DA SILVA, M. L.; GONDIM, T. S.; MONTEIRO, M. E. S.; TUCCI, A. R.; FINTELMAN-RODRIGUES, N.; SIQUEIRA, M. M.; MIRANDA, M. D.; COSTA, F. N.; SIMAS, R. C.; LEITÃO, G. G. Flavonoids from *Siparuna cristata* as potential inhibitors of SARS-CoV-2 replication. *Revista Brasileira de Farmacognosia*, v. 31(5), p. 658-666, 2021(b).
- LEAL, C. M.; LEITÃO, S. G.; MELLO, L. L. O.; RANGEL, I. C.; SILVA, C. V. A.; MIRANDA, M. D.; TUCCI, A. R.; ASSIS, C. B.; SACRAMENTO, C. Q.; FINTELMAN-RODRIGUES, N.; KOOLEN, H. H. F.; VAZ, B. G.; SIMAS, R. C.; LEITÃO, G. G. Bioassay-guided fractionation of *Siparuna glycyarpa* n-butanol extract with inhibitory activity against influenza A(H1N1)pdm09 virus by centrifugal partition chromatography (CPC). *Molecules*, v. 27(2), 399, 2022.
- LEITÃO, G. G.; SIMAS, N. K.; SOARES, S. S. V.; DE BRITO, A. P. P.; CLAROS, B. M. G.; BRITO, T. B. M.; MONACHE, F. D. Chemistry and pharmacology of Monimiaceae: a special focus on *Siparuna* and *Mollinedia*. *Journal of Ethnopharmacology*, v. 65, p. 87-102, 1999.
- LEITÃO, G. G.; SOARES, S. S. V.; BRITO, T. B. M.; MONACHE, F. D. Kaempferol glycosides from *Siparuna apiosyce*. *Phytochemistry*, v. 55, p. 679-682, 2000.
- LEITÃO, G. G.; EL-ADJI, S. S.; DE MELO, W. A. L. Separation of free and glycosylated flavonoids from *Siparuna guianensis* by gradient and isocratic CCC. *Journal of Liquid Chromatography & Related Technologies*, v. 28, p. 2041-2051, 2005.
- LEITÃO, G.G.; LEAL, C.M.; MENDONÇA, S.C.; PEREDA-MIRANDA, R. Purification of alkaloids by countercurrent chromatography. *Revista Brasileira de Farmacognosia*, v. 31, p. 625-647, 2021.
- LI, B.; NI, Y.; ZHU, L-J; WU, F-B; YAN, F.; ZHANG, X.; YAO, X-S. Flavonoids from *Matteuccia struthiopteris* and Their Anti-influenza Virus (H1N1) Activity. *Journal of Natural Products*, v. 78, p. 987-995, 2015.
- LI, Z.; LU, Y.; GUO, Y.; CAO, H.; WANG, Q.; SHUI, W. Comprehensive evaluation of untargeted metabolomics data processing software in feature detection, quantification and discriminating marker selection. *Analytica Chimica Acta*, v. 1029, p. 50-57, 2018.
- LIMA, B.R.; SILVA, F.M.A.; SOARES, E.R.; ALMEIDA, R.A.; SILVA-FILHO, F.A.; BARISON, A.; COSTA, E.V.; KOOLEN, H.H.F.; SOUZA, A.D.L.; PINHEIRO, M.L.B. Integrative approach based on leaf spray mass spectrometry, HPLC-DAD-MS/MS, and NMR for comprehensive characterization of isoquinoline-derived alkaloids in leaves of

*Onychopetalum amazonicum* R.E.Fr. Journal of Brazilian Chemical Society, v. 31(1), p. 79-89, 2020.

LINDNER, H. A.; LYTVYN, V.; QI, H.; LACHANCE, P.; ZIOMEK, E.; MÉNARD, R. Archives of Biochemistry and Biophysics, v. 466, p. 8-14, 2007.

LIU, Y.; FRIESEN, J.B.; McALPINE, J.B.; PAULI, G.F. Solvent system selection strategies in countercurrent separation. Planta Medica, v. 81, p. 1582-1591, 2015.

LÓPEZ, D. H. P. Evaluación de la actividad antibacteriana de los alcaloides provenientes de las hojas de *Siparuna sessiliflora*. Facultad de química Bogotá: Pontificia Universidad Javeriana, 2011.

LOURENÇO, A. M.; HADDI, K.; RIBEIRO, B. M.; CORRÊIA, R. F. T.; TOMÉ, H. V. V.; SANTOS-AMAYA, O.; PEREIRA, E. J. G.; GUEDES, R. N. C.; SANTOS, G. R.; OLIVEIRA, E. E.; AGUIAR, R. W. S. Essential oil of *Siparuna guianensis* as an alternative tool for improved lepidopteran control and resistance management practices. Scientific Reports, v. 8, 7215, 2018.

MAHASE, E. Covid-19: Pfizer's paxlovid is 89% effective in patients at risk of serious illness, company reports. British Medical Journal, v. 375:n2713, 2021.

MANI, J. S.; JOHNSON, J. B.; STEEL, J. C.; BROSZCZAK, D. A.; NEILSEN, P. M.; WALSH, K. B.; NAIKER, M. Natural product-derived phytochemicals as potential agents against coronaviruses: a review. Virus Research, v. 284, 197989, 2020.

MARSTON, A.; HOSTETTMANN, K. Developments in the application of counter-current chromatography to plant analysis. Journal of Chromatography A, v. 1112, p. 181-194, 2006.

MARTI, G.; EPARVIER, V.; MORLEO, B.; LE VEN, J.; APEL, C.; BODO, B.; AMAND, S.; DUMONTET, V.; LOZACH, O.; MEIJER, L.; GUÉRITTE, F.; LITAUDON, M. Natural aristolactams and aporphine alkaloids as inhibitors of CDK1/Cyclin B and DYRK1A. Molecules, v. 18, p. 3018-3027, 2013.

MARTIN, R.; LI, J.; PARVANGADA, A.; PERRY, J.; CIHLAR, T.; MO, H.; PORTER, D.; SVAROVSKAIA, E. Genetic conservation of SARS-CoV-2 RNA replication complex in globally circulating isolates and recently emerged variants from humans and minks suggests minimal pre-existing resistance to remdesivir. Antiviral Research, v. 188, 105033, 2021.

MELO, D. C.; MIRANDA, M. L. D.; JÚNIOR, W. G. F.; ANDRADE, P. M.; ALCOBA, A. E. T.; SILVA, T. S.; CAZAL, C. M.; MARTINS, C. H. G. Anticariogenic and antimycobacterial activities of the essential oil of *Siparuna guianensis* Aublet (Siparunaceae). Orbital: The Electronic Journal of Chemistry, v. 9(1), p. 55-60, 2017.

MOLAVI, Z.; RAZI, S.; MIRMOTALEBISOHI, S. A.; ADIBI, A.; SAMENI, M.; KARAMI, F.; NIAZI, V.; NIKNAM, Z.; ALIASHRAFI, M.; TAHERI, M.; GHAFOURI-FARD, S.; JEIBOUEI, S.; MAHDIAN, S.; ZALI, H.; RANJBAR, M. M.; YAZDANI, M. Identification of FDA approved drugs against SARS-CoV-2 RNA dependent RNA polymerase (RdRp) and 3-chymotrypsin-like protease (3CLpro), drug repurposing approach. Biomedicine & Pharmacotherapy, v. 138, 111544, 2021.

MORADI, M.T.; KARIMI, A.; LORIGOOINI, Z. Alkaloids as the natural anti-influenza virus agents: a systematic review. Toxin Reviews, v. 1-8, 2017.

MORRIS, G. M.; HUEY, R.; LINDSTROM, W.; SANNER, M. F.; BELEW, R. K.; GOODSELL, D. S.; OLSON, A. J. AutoDock4 and AutoDockTools4: Automated docking with selective receptor flexibility. *Journal of Computational Chemistry*, v. 30(16), p. 2785-2791, 2009.

MUSARRA-PIZZO, M.; PENNISI, R.; BEN-AMOR, I.; MANDALARI, G.; SCIORTINO, M. T. Antiviral activity exerted by natural products against human viroses. *Viruses*, v. 13, p. 828, 2021.

MZMINE, FEATURES, 2015. Disponível em: <http://mzmine.github.io/features.html>. Acesso: janeiro de 2022.

NEGRI, G.; SANTI, D.; TABACH, R. Chemical composition of hydroethanolic extracts from *Siparuna guianensis*, medicinal plant used as anxiolytics in Amazon region. *Revista Brasileira de Farmacognosia*, v. 22(5), p. 1024-1034, 2012.

NEWMAN, D.J.; CRAGG, G. Natural products as sources of new drugs over the nearly four decades from 01/1981 to 09/2019. *Journal of Natural Products*, v. 83, p. 770-803, 2020.

NGUYEN, S.T.; NGUYEN, H.T.L.; TRUONG, K.D. Comparative cytotoxic effects of methanol, ethanol and DMSO on human cancer cell lines. *Biomedical Research and Therapy*, v. 7, n.7, 3855-3859, 2020.

NIELSEN, K.F.; MANSSON, M.; RANK, C.; FRISVAD, J.C.; LARSEN, T.O. Dereplication of microbial natural products by LC-DAD-TOFMS. *Journal of Natural Products*, v. 74, p. 2338-2348, 2011.

NORIEGA, P.; GUERRINI, A.; SACCHETTI, G.; GRANDINI, A.; ANKUASH, E.; MANFREDINI, S. Chemical composition and biological activity of five essential oils from the Ecuadorian Amazon rain forest. *Molecules*, v. 24, 1637, 2019.

OLIVEIRA, G.B.; NETO, F.C.; DEMARQUE, D.P.; PEREIRA-JUNIOR, J.A.S.; FILHO, R.C.S.P.; MELO, S.J.; ALMEIDA, J.R.G.S.; LOPES, J.L.C.; LOPES, N.P. Dereplication of flavonoid glycoconjugates from *Adenocalymma imperatoris-maximiliani* by untargeted tandem mass-spectrometry-based molecular networking. *Planta Medica*, v. 83, p. 636-646, 2017.

OLIVEIRA, M. S.; CRUZ, J. N.; COSTA, W. A.; SILVA, S. G.; BRITO, M. P.; MENEZES, S. A. F.; NETO, A. M. J. C.; ANDRADE, E. H. A.; JUNIOR, R. N. C. Chemical composition, antimicrobial properties of *Siparuna guianensis* essential oil and a molecular docking and dynamics molecular study of its major chemical constituent. *Molecules*, v. 25, p. 3852, 2020.

PANCHE, A.N.; DIWAN, A.D.; CHANDRA, S.R. Flavonoids: an overview. *Journal of Nutrition Science*, v. 5, p. 1-15, 2016.

PAULI, G. F.; PRO, S. M.; FRIESEN, J. B. Countercurrent separation of natural products. *Journal of Natural Products*, v. 71, p. 1489-1508, 2008.

PEIXOTO, A.L.; LIRIO, E.J.; PIGNAL, M., 2020. *Siparunaceae in Flora do Brasil 2020*. Jardim Botânico do Rio de Janeiro. Disponível em: <http://floradobrasil.jbrj.gov.br/reflora/floradobrasil/FB223>. Acesso: novembro de 2021.

- PETTERSEN, E. F.; GODDARD, T. D.; HUANG, C. C.; COUCH, G. S.; GREENBLATT, D. M.; MENG E. C.; FERRIN, T. E. UCSF Chimera- a visualization system for exploratory research and analysis. *Journal of Computational Chemistry*, v. 25 (13), p. 1605-1612, 2004.
- PILON, A.C.; SELEGATO, D.M.; FERNANDES, R.P.; BUENO, P.C.P.; PINHO, D.R.; NETO, F.C.; FREIRE, R.T.; CASTRO-GAMBOA, I.; BOLZANI, V.S.; LOPES, N.P. Metabolômica de plantas: métodos e desafios. *Química Nova*, v. 43(3), p. 329-354, 2020.
- PILON, A.C.; VIEIRA, N.C.; AMARAL, J.G.; MONTEIRO, A.F.; SILVA, R.R.; SPÍNDOLA, L.S.; CASTRO-GAMBOA, I.; LOPES, N. P. Redes moleculares: uma análise sobre anotações e descoberta de novos ativos. *Química Nova*, v. 44(9), p. 1168-1179, 2021.
- PLUSKAL, T.; CASTILLO, S.; VILLAR-BRIONES, A.; ORESIC, M. MZmine 2: modular framework for processing, visualizing, and analyzing mass spectrometry-based molecular profile data. *BMC Bioinformatics*, v. 11, p. 395, 2010.
- PORTET, B.; FABRE, N.; ROZENBERG, R.; HABIB-JIWAN, J.L.; MOULIS, C.; QUETIN-LECLERCQ, J. Analysis of minor flavonoids in *Piper hostmannianum* var. *berbicense* using liquid chromatography coupled with atmospheric pressure chemical ionization mass spectrometry. *Journal of Chromatography A*, v. 1210, p. 45-54, 2008.
- QAMAR, M. T. U.; ALQAHTANI, S. M.; ALAMRI, M. A.; CHEN, L. L. Structural basics of SARS-CoV-2 3CL<sup>pro</sup> and anti-COVID-19 drug discovery from medicinal plants. *Journal of Pharmaceutical Analysis*, v. 10, p. 313-319, 2020.
- RATHAHAO-PARIS, E.; ALVES, S.; JUNOT, C.; TABET, J.C. High resolution mass spectrometry for structural identification of metabolites in metabolomics. *Metabolomics*, v. 12, p. 10-15, 2016.
- REED, J.; MOUNCH, M. An endpoint assay to evaluate the 50% tissue cytopathic effect. *Journal of General Virology*, v. 5, p. 25-29, 1938.
- RENNER SS, HAUSNER G. Siparunaceae *In: Flora Neotropica, Monograph 95*, The New York Botanical Garden, 2005.
- RIVERA, P. F. N.; GUERRINI, A.; TSAMARAINT, E. A. Chemical composition of leaf essential oil of *Siparuna schimpffii* Diels (limoncillo). *Revista Cubana de Plantas Mediciniais*, v. 19(2), p. 128-137, 2014.
- RUIZ, S.; MALAGÓN, O.; ZARAGOZA, T.; VALAREZO, E. Composition of the essential oils of *Artemisia sodiroi* Hieron, *Siparuna eggersii* Hieron, *Tagetes filifolia* Lag. and *Clinopodium nubigenum* (Kunth) from Loja Ecuador. *Journal of Essential Oil Bearing Plants*, v. 13(6), p. 676-691, 2010.
- SALTOS, M. B. V.; PUENTE, B. F. N.; MALAFRONTA, N.; BRACA, A. A new monoterpene glycoside from *Siparuna thecaphora*. *Natural Product Research*, v. 28(1), p. 57-60, 2014.
- SETZER, W. N. Essential oils as complementary and alternative medicines for the treatment of influenza. *American Journal of Essential Oils and Natural Products*, v. 4, p. 16-22, 2016.
- SIMAS, N. K.; FERRARI, S. F.; PEREIRA, S. N.; LEITÃO, G. G. Chemical ecological characteristics of herbivory of *Siparuna guianensis* seeds by buffy-headed marmosets (*Callithrix flaviceps*) in the Atlantic forest of southeastern Brazil. *Journal of Chemical Ecology*, v. 27(1), p. 93-107, 2001.

SOUZA, L. V.; ALMEIDA, M. P. O.; SILVA, N. M.; MIRANDA, N. C.; NEBO, L.; SILVA, C. A.; MORAES, D.; RODRIGUES, R. M. *Siparuna guianensis* controls *Toxoplasma gondii* infection *in vitro*. *Revista Brasileira de Farmacognosia*, 2021.

SOVANN, L.Y.; SAR, B.; KAB, V.; YANN, S.; KINZER, M.; RAFTERY, P.; ALBALAK, R.; PATEL, S.; HAY, P.L.; SENG, H.; UM, S.; CHIN, S.; CHAU, D.; KHALAKDINA, A.; KARLSSON, E.; OLSEN, S.J.; MOTT, J.A. An influenza A(H3N2) virus outbreak in the Kingdom of Cambodia during the COVID-19 pandemic of 2020. *International Journal of Infectious Diseases*, v. 103, p. 352-357, 2021

STÉVIGNY, C.; JIWAN, J.L.H.; ROZENBERG, R.; HOFFMANN, E.; QUETIN-LECLERCQ, J. Key fragmentation patterns of aporphine alkaloids by electrospray ionization with multistage mass spectrometry. *Rapid Communications in Mass Spectrometry*, v. 18, p. 523-528, 2004.

STÉVIGNY, C.; BAILLY, C.; QUETIN-LECLERCQ, J. Cytotoxic and antitumor potentialities of aporphinoid alkaloids. *Current Medicinal Chemistry-Anticancer Agents*, v. 5, p. 173-182, 2005.

THEISEN, L.L.; ERDELMEIER, C.A.J.; SPODEN, G.A.; BOUKHALLOUK, F.; SAUSY, A.; FLORIN, L.; MULLER, C.P. Tannins from *Hamamelis virginiana* bark extract: characterization and improvement of the antiviral efficacy against influenza A virus and human papillomavirus. *PloS One*, v. 9(1), e88062, 2014.

TROTT, O.; OLSON, A. J. AutoDock Vina: improving the speed and accuracy of docking with a new scoring function, efficient optimization and multithreading. *Journal of Computational Chemistry*, v. 31(2), p. 455-461, 2009.

ULLRICH, S.; NITSCHKE, C. The SARS-CoV-2 main protease as drug target. *Bioorganic & Medicinal Chemistry Letters*, v. 17, 127377, 2020.

VALLI, M.; RUSSO, H. M.; BOLZANI, V. S. The potential contribution of the natural products from Brazilian biodiversity to bioeconomy. *Anais da Academia Brasileira de Ciências*, v. 90(1), p. 763-778, 2018.

VILLIERS, A., VENTER, P.; PASCH, H. Recent advances and trends in the liquid-chromatography –mass spectrometry analysis of flavonoids. *Journal of Chromatography A*, v. 1430, p. 16-78, 2016.

VRIES, E.; DU, W.; GUO, H.; HAAN, C.A.M. Influenza A virus hemagglutinin-neuraminidase-receptor balance: preserving virus motility. *Trends in Microbiology*, v. 28(1), p. 57-67, 2020.

WANG, P.; ZHANG, J.Z.H. Selective binding of antiinfluenza drugs and their analogues to ‘open’ and ‘closed’ conformations of H5N1 neuraminidase. *The Journal of Physical Chemistry B*, v.114, p. 12958-12964, 2010.

WANG, M. et al. Sharing and community curation of mass spectrometry data with Global Natural Products Social Molecular Networking. *Nature Biotechnology*, v. 34, p. 828-837, 2016.

WANG, T. Y.; LI, Q.; BI, K.S. Bioactive flavonoids in medicinal plants: Structure, activity and biological fate. *Asian Journal of Pharmaceutical Sciences*, v. 13, p. 12-23, 2018.

WANG, D.; KHAN, M.S.; CUI, L.; SONG, X.; ZHU, H.; MA, T.; LI, X.; SUN, R. A novel method for the highly efficient biotransformation of genistein from genistin using a high-speed-counter-current chromatography bioreactor. *RSC Advances*, v. 9, p. 4892, 2019.

WORLD HEALTH ORGANIZATION (WHO), 2011. Manual for the laboratory diagnosis and virological surveillance of influenza. World Health Organization. Disponível em: [http://www.who.int/influenza/gisrs\\_laboratory/manual\\_diagnosis\\_surveillance\\_influenza/en/](http://www.who.int/influenza/gisrs_laboratory/manual_diagnosis_surveillance_influenza/en/).

WORLD HEALTH ORGANIZATION (WHO), 2018. Influenza (seasonal). Disponível em: <http://www.who.int/mediacentre/factsheets/fs211/en/>.

XU, Y.; CHEN, K.; PAN, J.; LEI, Y.; ZHANG, D.; FANG, L.; TANG, J.; CHEN, X.; MA, Y.; ZHENG, Y.; ZHANG, B.; ZHOU, Y.; ZHAN, J.; XU, W. *International Journal of Biological Macromolecules*, v. 188, p. 137-146, 2021.

YANG, J.Y.; SANCHEZ, L.M.; RATH, C.M.; LIU, X.; BOUDREAU, P.D.; BRUNS, N.; GLUKHOV, E.; WODTKE, A.; FELICIO, R.; FENNER, A.; WONG, W. R.; LININGTON, R.G.; ZHANG, L.; DEBONSI, H.M.; GERWICK, W. H.; DORRESTEIN, P.C. *Molecular Networking as a dereplication strategy. Journal of Natural Products*, v. 76, p. 1686-1699, 2013.

ZANI, C.L.; CARROLL, A.R. Database for rapid dereplication of known natural products using data from MS and fast NMR experiments. *Journal of Natural Products*, v. 80, p. 1758-1766, 2017.

ZHOU, B.; XIAO, J.F.; TULI, L.; RESSOM, H.W. LC-MS-based metabolomics. *Molecular BioSystems*, v. 8, p. 470-481, 2012.

ZOGHBI, M. G. B.; ANDRADE, E. H. A.; SANTOS, A. S.; SILVA, M. H. L.; MAIA, J. G. S. Essential oils of *Siparuna guianensis* Aubl. *Journal of Essential Oil Research*, v.10, p. 543-546, 1998.

## ANEXOS

Tabela 1. Substâncias isoladas e/ou anotadas das espécies do gênero *Siparuna*.

Substância	Parte da planta	Fórmula molecular	Massa monoisotópica (Da)	Referências bibliográficas
<i>Siparuna aspera</i>				
<b>Terpenoides</b>				
$\alpha$ -Pineno	Folhas	C <sub>10</sub> H <sub>16</sub>	136,12520	Noriega <i>et al.</i> , 2019
$\beta$ -Pineno	Folhas	C <sub>10</sub> H <sub>16</sub>	136,12520	Noriega <i>et al.</i> , 2019
Canfeno	Folhas	C <sub>10</sub> H <sub>16</sub>	136,12520	Noriega <i>et al.</i> , 2019
Mirceno	Folhas	C <sub>10</sub> H <sub>16</sub>	136,12520	Noriega <i>et al.</i> , 2019
Limoneno	Folhas	C <sub>10</sub> H <sub>16</sub>	136,12520	Noriega <i>et al.</i> , 2019
1,8-Cineol	Folhas	C <sub>10</sub> H <sub>18</sub> O	154,13577	Noriega <i>et al.</i> , 2019
(Z)- $\beta$ -Ocimeno	Folhas	C <sub>10</sub> H <sub>16</sub>	136,12520	Noriega <i>et al.</i> , 2019
$\alpha$ -Terpineol	Folhas	C <sub>10</sub> H <sub>18</sub> O	154,13577	Noriega <i>et al.</i> , 2019
$\beta$ -Elemeno	Folhas	C <sub>15</sub> H <sub>24</sub>	204,18780	Noriega <i>et al.</i> , 2019
$\delta$ -Elemeno	Folhas	C <sub>15</sub> H <sub>24</sub>	204,18780	Noriega <i>et al.</i> , 2019
$\alpha$ -Cubebeno	Folhas	C <sub>15</sub> H <sub>24</sub>	204,18780	Noriega <i>et al.</i> , 2019
$\beta$ -Cubebeno	Folhas	C <sub>15</sub> H <sub>24</sub>	204,18780	Noriega <i>et al.</i> , 2019
$\alpha$ -Ilangeno	Folhas	C <sub>15</sub> H <sub>24</sub>	204,18780	Noriega <i>et al.</i> , 2019
$\alpha$ -Copaeno	Folhas	C <sub>15</sub> H <sub>24</sub>	204,18780	Noriega <i>et al.</i> , 2019
$\beta$ -Bourboneno	Folhas	C <sub>15</sub> H <sub>24</sub>	204,18780	Noriega <i>et al.</i> , 2019
Ciclosativeno	Folhas	C <sub>15</sub> H <sub>24</sub>	204,18780	Noriega <i>et al.</i> , 2019
Isolongifoleno	Folhas	C <sub>15</sub> H <sub>24</sub>	204,18780	Noriega <i>et al.</i> , 2019
E- $\beta$ -Cariofileno	Folhas	C <sub>15</sub> H <sub>24</sub>	204,18780	Noriega <i>et al.</i> , 2019
$\beta$ -Copaeno	Folhas	C <sub>15</sub> H <sub>24</sub>	204,18780	Noriega <i>et al.</i> , 2019
$\beta$ -Gurjuneno	Folhas	C <sub>15</sub> H <sub>24</sub>	204,18780	Noriega <i>et al.</i> , 2019
$\gamma$ -Gurjuneno	Folhas	C <sub>15</sub> H <sub>24</sub>	204,18780	Noriega <i>et al.</i> , 2019



$\alpha$ -Guaieno	Folhas	C <sub>15</sub> H <sub>24</sub>	204,18780	Noriega <i>et al.</i> , 2019
Aristoleno	Folhas	C <sub>15</sub> H <sub>24</sub>	204,18780	Noriega <i>et al.</i> , 2019
cis-Muurolo-3,5-dieno	Folhas	C <sub>15</sub> H <sub>24</sub>	204,18780	Noriega <i>et al.</i> , 2019
$\alpha$ -Humuleno	Folhas	C <sub>15</sub> H <sub>24</sub>	204,18780	Noriega <i>et al.</i> , 2019
Allo-Aromandendreno	Folhas	C <sub>15</sub> H <sub>24</sub>	204,18780	Noriega <i>et al.</i> , 2019
cis-Cadina-1(6),4-dieno	Folhas	C <sub>15</sub> H <sub>24</sub>	204,18780	Noriega <i>et al.</i> , 2019
trans-Cadina-1(2),4 dieno	Folhas	C <sub>15</sub> H <sub>24</sub>	204,18780	Noriega <i>et al.</i> , 2019
9-epi-Cariofileno	Folhas	C <sub>15</sub> H <sub>24</sub>	204,18780	Noriega <i>et al.</i> , 2019
$\alpha$ -Muurolo	Folhas	C <sub>15</sub> H <sub>24</sub>	204,18780	Noriega <i>et al.</i> , 2019
$\gamma$ -Muurolo	Folhas	C <sub>15</sub> H <sub>24</sub>	204,18780	Noriega <i>et al.</i> , 2019
Biciclogermacrano	Folhas	C <sub>15</sub> H <sub>24</sub>	204,18780	Noriega <i>et al.</i> , 2019
Germacreno A	Folhas	C <sub>15</sub> H <sub>24</sub>	204,18780	Noriega <i>et al.</i> , 2019
Germacreno B	Folhas	C <sub>15</sub> H <sub>24</sub>	204,18780	Noriega <i>et al.</i> , 2019
Germacreno D	Folhas	C <sub>15</sub> H <sub>24</sub>	204,18780	Noriega <i>et al.</i> , 2019
$\beta$ -Selineno	Folhas	C <sub>15</sub> H <sub>24</sub>	204,18780	Noriega <i>et al.</i> , 2019
Valenceno	Folhas	C <sub>15</sub> H <sub>24</sub>	204,18780	Noriega <i>et al.</i> , 2019
$\beta$ -Himachaleno	Folhas	C <sub>15</sub> H <sub>24</sub>	204,18780	Noriega <i>et al.</i> , 2019
$\alpha$ -Cadineno	Folhas	C <sub>15</sub> H <sub>24</sub>	204,18780	Noriega <i>et al.</i> , 2019
$\gamma$ -Cadineno	Folhas	C <sub>15</sub> H <sub>24</sub>	204,18780	Noriega <i>et al.</i> , 2019
$\delta$ -Cadineno	Folhas	C <sub>15</sub> H <sub>24</sub>	204,18780	Noriega <i>et al.</i> , 2019
$\alpha$ -Calacoreno	Folhas	C <sub>15</sub> H <sub>20</sub>	200,15650	Noriega <i>et al.</i> , 2019
Espatuleno	Folhas	C <sub>15</sub> H <sub>24</sub> O	220,18272	Noriega <i>et al.</i> , 2019
Óxido de cariofileno	Folhas	C <sub>15</sub> H <sub>24</sub> O	220,18272	Noriega <i>et al.</i> , 2019
Viridiflorol	Folhas	C <sub>15</sub> H <sub>26</sub> O	222,19837	Noriega <i>et al.</i> , 2019
Guaiol	Folhas	C <sub>15</sub> H <sub>26</sub> O	222,19837	Noriega <i>et al.</i> , 2019
$\beta$ -Oplopenona	Folhas	C <sub>15</sub> H <sub>24</sub> O	220,18272	Noriega <i>et al.</i> , 2019
1,10-di-epi-Cubenol	Folhas	C <sub>15</sub> H <sub>26</sub> O	222,19837	Noriega <i>et al.</i> , 2019
1-epi-Cubenol	Folhas	C <sub>15</sub> H <sub>26</sub> O	222,19837	Noriega <i>et al.</i> , 2019

epi- $\alpha$ -Cadinol	Folhas	C <sub>15</sub> H <sub>26</sub> O	222,19837	Noriega <i>et al.</i> , 2019
$\alpha$ -Cadinol	Folhas	C <sub>15</sub> H <sub>26</sub> O	222,19837	Noriega <i>et al.</i> , 2019
epi- $\alpha$ -Muurolol	Folhas	C <sub>15</sub> H <sub>26</sub> O	222,19837	Noriega <i>et al.</i> , 2019
$\alpha$ -Muurolol	Folhas	C <sub>15</sub> H <sub>26</sub> O	222,19837	Noriega <i>et al.</i> , 2019
Khusinol	Folhas	C <sub>15</sub> H <sub>24</sub> O	220,18272	Noriega <i>et al.</i> , 2019
Eudesma-4(15),7-dien-1- $\beta$ -ol	Folhas	C <sub>15</sub> H <sub>24</sub> O	220,18272	Noriega <i>et al.</i> , 2019
<b><i>Siparuna brasiliensis</i></b>				
<b>Flavonoides</b>				
3,7,4'-tri- <i>O</i> -metil-kaempferol	Folhas e casca do caule	C <sub>18</sub> H <sub>16</sub> O <sub>6</sub>	328,09469	Leitão <i>et al.</i> , 1999; Leitão <i>et al.</i> , 2000
Siparunosídeo	Folhas	C <sub>29</sub> H <sub>34</sub> O <sub>15</sub>	622,18977	Leitão <i>et al.</i> , 2000
Tilirosídeo	Folhas	C <sub>30</sub> H <sub>26</sub> O <sub>13</sub>	594,13734	Leitão <i>et al.</i> , 1999; Leitão <i>et al.</i> , 2000
<b>Alcaloides</b>				
Assimilobina	Partes aéreas	C <sub>17</sub> H <sub>17</sub> NO <sub>2</sub>	267,12593	Fischer <i>et al.</i> , 1999
Liriodenina	Folhas e casca do caule	C <sub>17</sub> H <sub>9</sub> NO <sub>3</sub>	275,05824	Leitão <i>et al.</i> , 1999; Leitão <i>et al.</i> , 2000
Reticulina	Folhas e casca do caule	C <sub>19</sub> H <sub>23</sub> NO <sub>4</sub>	329,16271	Leitão <i>et al.</i> , 1999; Leitão <i>et al.</i> , 2000
<i>N</i> -Metil-laurotetanina	Casca do caule	C <sub>20</sub> H <sub>23</sub> NO <sub>4</sub>	341,16271	Leitão <i>et al.</i> , 1999; Leitão <i>et al.</i> , 2000
Laurotetanina	Casca do caule	C <sub>19</sub> H <sub>21</sub> NO <sub>4</sub>	327,14706	Leitão <i>et al.</i> , 1999; Leitão <i>et al.</i> , 2000
<b>Amidas</b>				
<i>cis-N</i> -feruloiltiramina	Casca do caule	C <sub>18</sub> H <sub>19</sub> NO <sub>4</sub>	313,13141	Leitão <i>et al.</i> , 2000
<i>trans-N</i> -feruloiltiramina	Casca do caule	C <sub>18</sub> H <sub>19</sub> NO <sub>4</sub>	313,13141	Leitão <i>et al.</i> , 2000
<b>Terpenoides</b>				
Glicosídeo de sitosterol	Folhas	C <sub>35</sub> H <sub>60</sub> O <sub>6</sub>	576,43899	Leitão <i>et al.</i> , 1999
Sitosterol	Folhas	C <sub>29</sub> H <sub>50</sub> O	414,38617	Leitão <i>et al.</i> , 1999
Estigmasterol	Folhas	C <sub>29</sub> H <sub>48</sub> O	412,37052	Leitão <i>et al.</i> , 1999
<b><i>Siparuna cristata</i></b>				
<b>Alcaloides</b>				
<i>N</i> -Metil-laurotetanina	Folhas	C <sub>20</sub> H <sub>23</sub> NO <sub>4</sub>	341,16271	Leal <i>et al.</i> , 2021(a)
Reticulina	Folhas	C <sub>19</sub> H <sub>23</sub> NO <sub>4</sub>	329,16271	Leal <i>et al.</i> , 2021(a)

Boldina	Folhas	C <sub>19</sub> H <sub>21</sub> NO <sub>4</sub>	327,14706	Leal <i>et al.</i> , 2021(a)
Dicentrina	Folhas	C <sub>20</sub> H <sub>21</sub> NO <sub>4</sub>	339,14706	Leal <i>et al.</i> , 2021(a)
Nantenina	Folhas	C <sub>20</sub> H <sub>21</sub> NO <sub>4</sub>	339,14706	Leal <i>et al.</i> , 2021(a)
<b>Flavonoides</b>				
Kumatakenina	Folhas	C <sub>17</sub> H <sub>14</sub> O <sub>6</sub>	314,07904	Leal <i>et al.</i> , 2021(a); Leal <i>et al.</i> , 2021(b)
3,3',4'- tri- <i>O</i> -metil quercetina	Folhas	C <sub>18</sub> H <sub>16</sub> O <sub>7</sub>	344,08960	Leal <i>et al.</i> , 2021(b)
Retusina	Folhas	C <sub>19</sub> H <sub>18</sub> O <sub>7</sub>	358,10525	Leal <i>et al.</i> , 2021(b)
<b><i>Siparuna decipiens</i></b>				
<b>Alcaloides</b>				
Boldina	Folhas	C <sub>19</sub> H <sub>21</sub> NO <sub>4</sub>	327,14706	Marti <i>et al.</i> , 2013; Leal <i>et al.</i> , 2021(a)
<i>N</i> -Nornuciferina	Folhas	C <sub>18</sub> H <sub>19</sub> NO <sub>2</sub>	281,14158	Marti <i>et al.</i> , 2013
Coclaurina	Folhas	C <sub>17</sub> H <sub>19</sub> NO <sub>3</sub>	285,13649	Leal <i>et al.</i> , 2021(a)
Reticulina	Folhas	C <sub>19</sub> H <sub>23</sub> NO <sub>4</sub>	329,16271	Leal <i>et al.</i> , 2021(a)
Actinodafinina	Folhas	C <sub>18</sub> H <sub>17</sub> NO <sub>4</sub>	311,11576	Leal <i>et al.</i> , 2021(a)
Norglaucina	Folhas	C <sub>20</sub> H <sub>23</sub> NO <sub>4</sub>	341,16271	Resultado para publicação
Glaucina	Folhas	C <sub>21</sub> H <sub>25</sub> NO <sub>4</sub>	355,17836	Resultado para publicação
<b>Feofitina</b>				
Feofitina A	Folhas	C <sub>55</sub> H <sub>74</sub> N <sub>4</sub> O <sub>5</sub>	870,56592	Resultado para publicação
<b><i>Siparuna dresslerana</i></b>				
<b>Alcaloides</b>				
<i>O</i> -Metilflavinantina	Folhas	C <sub>20</sub> H <sub>23</sub> NO <sub>4</sub>	341,16271	Gerard <i>et al.</i> , 1986; Leitão <i>et al.</i> , 1999
Flavinantina	Folhas	C <sub>19</sub> H <sub>21</sub> NO <sub>4</sub>	327,14706	Gerard <i>et al.</i> , 1986; Leitão <i>et al.</i> , 1999
<b><i>Siparuna echinata</i></b>				
<b>Terpenoides</b>				
$\alpha$ -Pineno	Partes aéreas	C <sub>10</sub> H <sub>16</sub>	136,12520	García <i>et al.</i> , 2020
$\beta$ -Pineno	Partes aéreas	C <sub>10</sub> H <sub>16</sub>	136,12520	García <i>et al.</i> , 2020
$\beta$ -Elemeno	Partes aéreas	C <sub>15</sub> H <sub>24</sub>	204,18780	García <i>et al.</i> , 2020
Germacreno A	Partes aéreas	C <sub>15</sub> H <sub>24</sub>	204,18780	García <i>et al.</i> , 2020

Germacreno B	Partes aéreas	C <sub>15</sub> H <sub>24</sub>	204,18780	García <i>et al.</i> , 2020
Germacreno D	Partes aéreas	C <sub>15</sub> H <sub>24</sub>	204,18780	García <i>et al.</i> , 2020
α-Humuleno	Partes aéreas	C <sub>15</sub> H <sub>24</sub>	204,18780	García <i>et al.</i> , 2020
β-Eudesmol	Partes aéreas	C <sub>15</sub> H <sub>26</sub> O	222,19837	García <i>et al.</i> , 2020
β-Selineno	Partes aéreas	C <sub>15</sub> H <sub>24</sub>	204,18780	García <i>et al.</i> , 2020
<i>trans</i> -Cariofileno	Partes aéreas	C <sub>15</sub> H <sub>24</sub>	204,18780	García <i>et al.</i> , 2020
Canfeno	Partes aéreas	C <sub>10</sub> H <sub>16</sub>	136,12520	García <i>et al.</i> , 2020
Sabineno	Partes aéreas	C <sub>10</sub> H <sub>16</sub>	136,12520	García <i>et al.</i> , 2020
β-Mirceno	Partes aéreas	C <sub>10</sub> H <sub>16</sub>	136,12520	García <i>et al.</i> , 2020
Limoneno	Partes aéreas	C <sub>10</sub> H <sub>16</sub>	136,12520	García <i>et al.</i> , 2020
<i>cis</i> -Ocimeno	Partes aéreas	C <sub>10</sub> H <sub>16</sub>	136,12520	García <i>et al.</i> , 2020
<i>trans</i> -Ocimeno	Partes aéreas	C <sub>10</sub> H <sub>16</sub>	136,12520	García <i>et al.</i> , 2020
Perilleno	Partes aéreas	C <sub>10</sub> H <sub>14</sub> O	150,10447	García <i>et al.</i> , 2020
Óxido de cariofileno	Partes aéreas	C <sub>15</sub> H <sub>24</sub> O	220,18272	García <i>et al.</i> , 2020
Linalol	Partes aéreas	C <sub>10</sub> H <sub>18</sub> O	154,13577	García <i>et al.</i> , 2020
<i>trans</i> -pinocarveol	Partes aéreas	C <sub>10</sub> H <sub>16</sub> O	152,12012	García <i>et al.</i> , 2020
<i>cis</i> -Verbenol	Partes aéreas	C <sub>10</sub> H <sub>16</sub> O	152,12012	García <i>et al.</i> , 2020
Sipaucina A	Partes aéreas	C <sub>19</sub> H <sub>26</sub> O <sub>7</sub>	366,16785	García <i>et al.</i> , 2020
Nopinona	Partes aéreas	C <sub>9</sub> H <sub>14</sub> O	138,10447	García <i>et al.</i> , 2020
Mirtenol	Partes aéreas	C <sub>10</sub> H <sub>16</sub> O	152,12012	García <i>et al.</i> , 2020
<b>Álcool</b>				
6-undecanol	Partes aéreas	C <sub>11</sub> H <sub>24</sub> O	172,18272	García <i>et al.</i> , 2020
<b>Metilcetonas</b>				
2-Tridecanona	Partes aéreas	C <sub>13</sub> H <sub>26</sub> O	198,19837	García <i>et al.</i> , 2020
2-Undecanona	Partes aéreas	C <sub>11</sub> H <sub>22</sub> O	170,16707	García <i>et al.</i> , 2020
<b>Ácido graxo</b>				
Ácido decanóico	Partes aéreas	C <sub>10</sub> H <sub>20</sub> O <sub>2</sub>	172,14633	García <i>et al.</i> , 2020
<i>Siparuna eggersii</i>				

<b>Terpenoides</b>				
$\alpha$ -Pineno	Folhas	C <sub>10</sub> H <sub>16</sub>	136,12520	Ruiz <i>et al.</i> , 2010
$\beta$ -Pineno	Folhas	C <sub>10</sub> H <sub>16</sub>	136,12520	Ruiz <i>et al.</i> , 2010
$\beta$ -Elemeno	Folhas	C <sub>15</sub> H <sub>24</sub>	204,18780	Ruiz <i>et al.</i> , 2010
$\gamma$ -Elemeno	Folhas	C <sub>15</sub> H <sub>24</sub>	204,18780	Ruiz <i>et al.</i> , 2010
$\delta$ -Elemeno	Folhas	C <sub>15</sub> H <sub>24</sub>	204,18780	Ruiz <i>et al.</i> , 2010
Canfeno	Folhas	C <sub>10</sub> H <sub>16</sub>	136,12520	Ruiz <i>et al.</i> , 2010
$\alpha$ -Cubebeno	Folhas	C <sub>15</sub> H <sub>24</sub>	204,18780	Ruiz <i>et al.</i> , 2010
$\beta$ -Cubebeno	Folhas	C <sub>15</sub> H <sub>24</sub>	204,18780	Ruiz <i>et al.</i> , 2010
Sabineno	Folhas	C <sub>10</sub> H <sub>16</sub>	136,12520	Ruiz <i>et al.</i> , 2010
Mirceno	Folhas	C <sub>10</sub> H <sub>16</sub>	136,12520	Ruiz <i>et al.</i> , 2010
$\alpha$ -Felandreno	Folhas	C <sub>10</sub> H <sub>16</sub>	136,12520	Ruiz <i>et al.</i> , 2010
$\beta$ -Felandreno	Folhas	C <sub>10</sub> H <sub>16</sub>	136,12520	Ruiz <i>et al.</i> , 2010
Limoneno	Folhas	C <sub>10</sub> H <sub>16</sub>	136,12520	Ruiz <i>et al.</i> , 2010
<i>cis</i> - $\beta$ -Ocimeno	Folhas	C <sub>10</sub> H <sub>16</sub>	136,12520	Ruiz <i>et al.</i> , 2010
<i>trans</i> - $\beta$ -Ocimeno	Folhas	C <sub>10</sub> H <sub>16</sub>	136,12520	Ruiz <i>et al.</i> , 2010
Linalol	Folhas	C <sub>10</sub> H <sub>18</sub> O	154,13577	Ruiz <i>et al.</i> , 2010
Elemol	Folhas	C <sub>15</sub> H <sub>26</sub> O	222,19837	Ruiz <i>et al.</i> , 2010
$\alpha$ -Copaeno	Folhas	C <sub>15</sub> H <sub>24</sub>	204,18780	Ruiz <i>et al.</i> , 2010
Alloocimeno	Folhas	C <sub>10</sub> H <sub>16</sub>	136,12520	Ruiz <i>et al.</i> , 2010
<i>trans</i> -Cariofileno	Folhas	C <sub>15</sub> H <sub>24</sub>	204,18780	Ruiz <i>et al.</i> , 2010
$\alpha$ -Guaieno	Folhas	C <sub>15</sub> H <sub>24</sub>	204,18780	Ruiz <i>et al.</i> , 2010
Aromadendreno	Folhas	C <sub>15</sub> H <sub>24</sub>	204,18780	Ruiz <i>et al.</i> , 2010
<i>trans</i> - $\beta$ -Farneseno	Folhas	C <sub>15</sub> H <sub>24</sub>	204,18780	Ruiz <i>et al.</i> , 2010
$\alpha$ -Humuleno	Folhas	C <sub>15</sub> H <sub>24</sub>	204,18780	Ruiz <i>et al.</i> , 2010
$\gamma$ -Muuroleno	Folhas	C <sub>15</sub> H <sub>24</sub>	204,18780	Ruiz <i>et al.</i> , 2010
$\beta$ -Selineno	Folhas	C <sub>15</sub> H <sub>24</sub>	204,18780	Ruiz <i>et al.</i> , 2010
Germacreno A	Folhas	C <sub>15</sub> H <sub>24</sub>	204,18780	Ruiz <i>et al.</i> , 2010

Germacreno B	Folhas	C <sub>15</sub> H <sub>24</sub>	204,18780	Ruiz <i>et al.</i> , 2010
Germacreno D	Folhas	C <sub>15</sub> H <sub>24</sub>	204,18780	Ruiz <i>et al.</i> , 2010
Germacreno D-4-ol	Folhas	C <sub>15</sub> H <sub>26</sub> O	222,19837	Ruiz <i>et al.</i> , 2010
Biciclogermacreno	Folhas	C <sub>15</sub> H <sub>24</sub>	204,18780	Ruiz <i>et al.</i> , 2010
Germacrona	Folhas	C <sub>15</sub> H <sub>22</sub> O	218,16707	Ruiz <i>et al.</i> , 2010
$\alpha$ -Farneseno	Folhas	C <sub>15</sub> H <sub>24</sub>	204,18780	Ruiz <i>et al.</i> , 2010
$\beta$ -Bourboneno	Folhas	C <sub>15</sub> H <sub>24</sub>	204,18780	Ruiz <i>et al.</i> , 2010
Espatulanol	Folhas	C <sub>15</sub> H <sub>24</sub> O	220,18272	Ruiz <i>et al.</i> , 2010
Óxido de cariofileno	Folhas	C <sub>15</sub> H <sub>24</sub> O	220,18272	Ruiz <i>et al.</i> , 2010
$\delta$ -Cadineno	Folhas	C <sub>15</sub> H <sub>24</sub>	204,18780	Ruiz <i>et al.</i> , 2010
Curzerenona	Folhas	C <sub>15</sub> H <sub>18</sub> O <sub>2</sub>	230,13068	Ruiz <i>et al.</i> , 2010
Epicurzerenona	Folhas	C <sub>15</sub> H <sub>18</sub> O <sub>2</sub>	230,13068	Ruiz <i>et al.</i> , 2010
$\alpha$ -Cadinol	Folhas	C <sub>15</sub> H <sub>26</sub> O	222,19837	Ruiz <i>et al.</i> , 2010
Muurolol	Folhas	C <sub>15</sub> H <sub>26</sub> O	222,19837	Ruiz <i>et al.</i> , 2010
Acetato de sabinilo	Folhas	C <sub>12</sub> H <sub>18</sub> O <sub>2</sub>	194,13068	Ruiz <i>et al.</i> , 2010
Viridiflorol	Folhas	C <sub>15</sub> H <sub>26</sub> O	222,19837	Ruiz <i>et al.</i> , 2010
<b>Aldeído</b>				
Decanal	Folhas	C <sub>10</sub> H <sub>20</sub> O	156,15142	Ruiz <i>et al.</i> , 2010
<b>Metilcetona</b>				
2-Tridecanona	Folhas	C <sub>13</sub> H <sub>26</sub> O	198,19837	Ruiz <i>et al.</i> , 2010
<i>Siparuna gesnerioides</i>				
<b>Alcaloides</b>				
Isocoridina	Hastes	C <sub>20</sub> H <sub>23</sub> NO <sub>4</sub>	341,16271	Leitão <i>et al.</i> , 1999
Assimilobina	Hastes, casca do caule e raízes	C <sub>17</sub> H <sub>17</sub> NO <sub>2</sub>	267,12593	Leitão <i>et al.</i> , 1999
N-Metil-laurotetanina	Hastes, casca do caule e raízes	C <sub>20</sub> H <sub>23</sub> NO <sub>4</sub>	341,16271	Leitão <i>et al.</i> , 1999
Nantenina	Hastes, casca do caule e raízes	C <sub>20</sub> H <sub>21</sub> NO <sub>4</sub>	339,14706	Leitão <i>et al.</i> , 1999
<i>Siparuna gigantotepala</i>				
<b>Flavonoides</b>				

Kaempferol 3- <i>O</i> -β-xilopiranosil-(1→2)-α-arabinofuranosídeo	Folhas	C <sub>25</sub> H <sub>25</sub> O <sub>14</sub>	549,12443	Castañeda <i>et al.</i> , 2016
Kaempferol 3,7-di- <i>O</i> -metil-4'- <i>O</i> -α-rhamnopyranosil-(1→2)-β-glicopiranosídeo	Folhas	C <sub>29</sub> H <sub>33</sub> O <sub>15</sub>	621,18195	Castañeda <i>et al.</i> , 2016
Rutina	Folhas	C <sub>27</sub> H <sub>30</sub> O <sub>16</sub>	610,15338	Castañeda <i>et al.</i> , 2016
Kaempferol 3- <i>O</i> -rutinosídeo	Folhas	C <sub>27</sub> H <sub>30</sub> O <sub>15</sub>	594,15847	Castañeda <i>et al.</i> , 2016
Kaempferol 3,7-di- <i>O</i> -metil-4'- <i>O</i> -rutinosídeo	Folhas	C <sub>29</sub> H <sub>34</sub> O <sub>15</sub>	622,18977	Castañeda <i>et al.</i> , 2016
Quercetina	Folhas	C <sub>15</sub> H <sub>10</sub> O <sub>7</sub>	302,04265	Castañeda <i>et al.</i> , 2016
Kaempferol 3,7-dimetileter	Folhas	C <sub>17</sub> H <sub>14</sub> O <sub>6</sub>	314,07904	Castañeda <i>et al.</i> , 2016
Kaempferol 3,7,4'-trimetileter	Folhas	C <sub>18</sub> H <sub>16</sub> O <sub>6</sub>	328,09469	Castañeda <i>et al.</i> , 2016

***Siparuna glycyarpa***

**Flavonoides**

Rutina	Folhas	C <sub>27</sub> H <sub>30</sub> O <sub>16</sub>	610,15338	Costa <i>et al.</i> , 2013; Leal <i>et al.</i> , 2021(a); Leal <i>et al.</i> , 2022
Kaempferol 3- <i>O</i> -rutinosídeo	Folhas	C <sub>27</sub> H <sub>30</sub> O <sub>15</sub>	594,15847	Leal <i>et al.</i> , 2022
Quercetina 7- <i>O</i> -rutinosídeo	Folhas	C <sub>27</sub> H <sub>30</sub> O <sub>16</sub>	610,15338	Costa <i>et al.</i> , 2013
Kaempferol 3- <i>O</i> -β-glicopiranosídeo	Folhas	C <sub>21</sub> H <sub>20</sub> O <sub>11</sub>	448,10056	Costa <i>et al.</i> , 2013; Leal <i>et al.</i> , 2022
Kaempferol 3- <i>O</i> -β-rhamnopyranosídeo	Folhas	C <sub>21</sub> H <sub>20</sub> O <sub>10</sub>	432,10565	Costa <i>et al.</i> , 2013
Kaempferol 3- <i>O</i> -glucosídeo-7- <i>O</i> -rhamnosídeo	Folhas	C <sub>27</sub> H <sub>30</sub> O <sub>15</sub>	594,15847	Leal <i>et al.</i> , 2021(a); Leal <i>et al.</i> , 2022
Kaempferol 3- <i>O</i> -β-6''(p-coumaroil)glicopiranosídeo	Folhas	C <sub>30</sub> H <sub>26</sub> O <sub>13</sub>	594,13734	Costa <i>et al.</i> , 2013
Quercetina 3- <i>O</i> -[β-D-xilosil-(1→2)-β-D-glucosídeo]	Folhas	C <sub>26</sub> H <sub>28</sub> O <sub>16</sub>	596,13773	Leal <i>et al.</i> , 2021(a)
Quercetina 3- <i>O</i> -glucosídeo-7- <i>O</i> -rhamnosídeo	Folhas	C <sub>27</sub> H <sub>30</sub> O <sub>16</sub>	610,15338	Leal <i>et al.</i> , 2021(a); Leal <i>et al.</i> , 2022
Quercetina 3- <i>O</i> -rhamnosídeo-7- <i>O</i> -glucosídeo	Folhas	C <sub>27</sub> H <sub>30</sub> O <sub>16</sub>	610,15338	Leal <i>et al.</i> , 2021(a); Leal <i>et al.</i> , 2022
Quercetina 3- <i>O</i> -β-glicopiranosídeo	Folhas	C <sub>21</sub> H <sub>19</sub> O <sub>12</sub>	463,08765	Costa <i>et al.</i> , 2013
Kaempferol 3- <i>O</i> -hexosídeo- <i>O</i> -desoxihexosídeo- <i>O</i> -pentosídeo	Folhas	C <sub>32</sub> H <sub>38</sub> O <sub>19</sub>	726,20073	Leal <i>et al.</i> , 2022



Quercetina 3- <i>O</i> -(2''- <i>O</i> -galoil)-pentosídeo	Folhas	C <sub>27</sub> H <sub>22</sub> O <sub>15</sub>	586,09587	Leal <i>et al.</i> , 2022
Quercetina 3- <i>O</i> -(6''- <i>O</i> -galoil)-β-galactopiranosídeo	Folhas	C <sub>28</sub> H <sub>24</sub> O <sub>16</sub>	616,10643	Leal <i>et al.</i> , 2022
2',6'-Dihidroxi-4,4'-dimetoxidihidrochalcona	Folhas	C <sub>17</sub> H <sub>18</sub> O <sub>5</sub>	302,11542	Costa <i>et al.</i> , 2013; Leal <i>et al.</i> , 2021(a); Leal <i>et al.</i> , 2022
2',6'-Dihidroxi-4'-metoxidihidrochalcona	Folhas	C <sub>16</sub> H <sub>16</sub> O <sub>4</sub>	272,10486	Leal <i>et al.</i> , 2021(a); Leal <i>et al.</i> , 2022
<b>Ácido fenólico</b>				
Ácido protocatecuico	Folhas	C <sub>7</sub> H <sub>6</sub> O <sub>4</sub>	154,02661	Costa <i>et al.</i> , 2013
<b>Alcaloides</b>				
Norcoclaurina	Folhas	C <sub>16</sub> H <sub>17</sub> NO <sub>3</sub>	271,12084	Leal <i>et al.</i> , 2021(a)
<i>N</i> -Metilcoclaurina	Folhas	C <sub>18</sub> H <sub>21</sub> NO <sub>3</sub>	299,15214	Leal <i>et al.</i> , 2021(a); Leal <i>et al.</i> , 2022
Apoglaziovina	Folhas	C <sub>18</sub> H <sub>19</sub> NO <sub>3</sub>	297,13649	Leal <i>et al.</i> , 2021(a)
Reticulina	Folhas	C <sub>19</sub> H <sub>23</sub> NO <sub>4</sub>	329,16271	Leal <i>et al.</i> , 2021(a); Leal <i>et al.</i> , 2022
Annonaina	Folhas	C <sub>17</sub> H <sub>15</sub> NO <sub>2</sub>	265,11028	Leal <i>et al.</i> , 2021(a)
Cocclaurina	Folhas	C <sub>17</sub> H <sub>19</sub> NO <sub>3</sub>	285,13649	Leal <i>et al.</i> , 2021(a); Leal <i>et al.</i> , 2022
Demetil-cocclaurina	Folhas	C <sub>16</sub> H <sub>17</sub> NO <sub>3</sub>	271,12084	Leal <i>et al.</i> , 2022
<i>N</i> -óxido de reticulina	Folhas	C <sub>19</sub> H <sub>23</sub> NO <sub>5</sub>	345,15762	Leal <i>et al.</i> , 2022
Normuciferina	Folhas	C <sub>18</sub> H <sub>19</sub> NO <sub>2</sub>	281,14158	Leal <i>et al.</i> , 2022
Isopilina	Folhas	C <sub>18</sub> H <sub>19</sub> NO <sub>3</sub>	297,13649	Leal <i>et al.</i> , 2022
<i>O</i> -Metilisopilina	Folhas	C <sub>19</sub> H <sub>21</sub> NO <sub>3</sub>	311,15214	Leal <i>et al.</i> , 2022
Estefolidina	Folhas	C <sub>19</sub> H <sub>21</sub> NO <sub>4</sub>	327,14706	Leal <i>et al.</i> , 2022
Isocoripalmina	Folhas	C <sub>20</sub> H <sub>23</sub> NO <sub>4</sub>	341,16271	Leal <i>et al.</i> , 2022
Magnocurarina	Folhas	C <sub>19</sub> H <sub>24</sub> NO <sub>3</sub> <sup>+</sup>	314,17562	Leal <i>et al.</i> , 2022
<b><i>Siparuna grandiflora</i></b>				
<b>Alcaloides</b>				
Assimilobina	Hastes, casca do caule e raízes	C <sub>17</sub> H <sub>17</sub> NO <sub>2</sub>	267,12593	Leitão <i>et al.</i> , 1999
<i>N</i> -Metil-laurotetanina	Hastes, casca do caule e raízes	C <sub>20</sub> H <sub>23</sub> NO <sub>4</sub>	341,16271	Leitão <i>et al.</i> , 1999
Nantenina	Hastes, casca do caule e raízes	C <sub>20</sub> H <sub>21</sub> NO <sub>4</sub>	339,14706	Leitão <i>et al.</i> , 1999
Oxonantenina	Casca do caule e raízes	C <sub>19</sub> H <sub>13</sub> NO <sub>5</sub>	335,07937	Leitão <i>et al.</i> , 1999

Liriodenina	Casca do caule e raízes	C <sub>17</sub> H <sub>9</sub> NO <sub>3</sub>	275,05824	Leitão <i>et al.</i> , 1999
Laurotetanina	Casca do caule e raízes	C <sub>19</sub> H <sub>21</sub> NO <sub>4</sub>	327,14706	Leitão <i>et al.</i> , 1999
Anonaina	Casca do caule e raízes	C <sub>17</sub> H <sub>15</sub> NO <sub>2</sub>	265,11028	Leitão <i>et al.</i> , 1999
Reticulina	Casca do caule e raízes	C <sub>19</sub> H <sub>23</sub> NO <sub>4</sub>	329,16271	Leitão <i>et al.</i> , 1999
Normantenina	Casca do caule e raízes	C <sub>19</sub> H <sub>19</sub> NO <sub>4</sub>	325,13141	Leitão <i>et al.</i> , 1999
<b><i>Siparuna guianensis</i></b>				
<b>Flavonoides</b>				
Quercetina	Folhas	C <sub>15</sub> H <sub>10</sub> O <sub>7</sub>	302,04265	Leitão <i>et al.</i> , 2005
Rutina	Folhas	C <sub>27</sub> H <sub>30</sub> O <sub>16</sub>	610,15338	Leitão <i>et al.</i> , 2005
Quercetina 7- <i>O</i> -rutinosídeo	Folhas	C <sub>27</sub> H <sub>30</sub> O <sub>16</sub>	610,15338	Leitão <i>et al.</i> , 2005
Kaempferol	Folhas	C <sub>15</sub> H <sub>10</sub> O <sub>6</sub>	286,04774	Leitão <i>et al.</i> , 2005
Kaempferol 3,7,4'-trimetileter	Folhas	C <sub>18</sub> H <sub>16</sub> O <sub>6</sub>	328,09469	Facundo <i>et al.</i> , 2012
Kumatakenina	Folhas	C <sub>17</sub> H <sub>14</sub> O <sub>6</sub>	314,07904	Facundo <i>et al.</i> , 2012
Vicenina-2	Folhas	C <sub>27</sub> H <sub>30</sub> O <sub>15</sub>	594,15847	Negri <i>et al.</i> , 2012
Quercetina 3,7-di- <i>O</i> -rhamnosídeo	Folhas	C <sub>27</sub> H <sub>30</sub> O <sub>15</sub>	594,15847	Negri <i>et al.</i> , 2012
Kaempferol 3,7-di- <i>O</i> -rhamnosídeo	Folhas	C <sub>27</sub> H <sub>30</sub> O <sub>14</sub>	578,16356	Negri <i>et al.</i> , 2012
Quercetina 3- <i>O</i> -rutinosídeo-7- <i>O</i> -rhamnosídeo	Folhas	C <sub>33</sub> H <sub>40</sub> O <sub>20</sub>	756,21129	Negri <i>et al.</i> , 2012
Quercetina 3- <i>O</i> -pentosil-pentosídeo-7- <i>O</i> -rhamnosídeo	Folhas	C <sub>31</sub> H <sub>36</sub> O <sub>19</sub>	712,18508	Negri <i>et al.</i> , 2012
Kaempferol 3- <i>O</i> -pentosil-pentosídeo-7- <i>O</i> -rhamnosídeo	Folhas	C <sub>31</sub> H <sub>36</sub> O <sub>18</sub>	696,19016	Negri <i>et al.</i> , 2012
Dímero de procianidina B1	Folhas	C <sub>30</sub> H <sub>26</sub> O <sub>12</sub>	578,14243	Negri <i>et al.</i> , 2012
Lucenina-2	Folhas	C <sub>27</sub> H <sub>30</sub> O <sub>16</sub>	610,15338	Negri <i>et al.</i> , 2012
Quercetina 3- <i>O</i> -pentosil-rhamnosídeo-7- <i>O</i> -rhamnosídeo	Folhas	C <sub>32</sub> H <sub>38</sub> O <sub>19</sub>	726,20073	Negri <i>et al.</i> , 2012
<b>Alcaloides</b>				
Fuseina	Madeira do caule	C <sub>17</sub> H <sub>13</sub> NO <sub>3</sub>	279,08954	Braz <i>et al.</i> , 1976
Liriodenina	Madeira do caule, folhas e fruto	C <sub>17</sub> H <sub>9</sub> NO <sub>3</sub>	275,05824	Braz <i>et al.</i> , 1976; Leitão <i>et al.</i> , 1999; Simas <i>et al.</i> , 2001; Marti <i>et al.</i> , 2013

Cassamedina	Madeira do caule	$C_{19}H_{11}NO_6$	349,05864	Braz <i>et al.</i> , 1976; Leitão <i>et al.</i> , 1999
Anonaina	Madeira do caule e fruto	$C_{17}H_{15}NO_2$	265,11028	Braz <i>et al.</i> , 1976; Simas <i>et al.</i> , 2001
Bulbocapnina	Folhas	$C_{19}H_{19}NO_4$	325,13141	Marti <i>et al.</i> , 2013
N-metil-lindcarpina	Folhas	$C_{19}H_{21}NO_4$	327,14706	Marti <i>et al.</i> , 2013
Actinodafinina	Folhas	$C_{18}H_{17}NO_4$	311,11576	Marti <i>et al.</i> , 2013
Nantenina	Fruto	$C_{20}H_{21}NO_4$	339,14706	Simas <i>et al.</i> , 2001
N-Metil-laurotetanina	Fruto	$C_{20}H_{23}NO_4$	341,16271	Simas <i>et al.</i> , 2001
Norglaucina	Fruto	$C_{20}H_{23}NO_4$	341,16271	Simas <i>et al.</i> , 2001
Assimilobina	Fruto	$C_{17}H_{17}NO_2$	267,12593	Simas <i>et al.</i> , 2001
(+)-11-metoxi-nomeolistina	Folhas	$C_{19}H_{19}NO_5$	341,12632	Marti <i>et al.</i> , 2013
Nornantenina	Fruto	$C_{19}H_{19}NO_4$	325,13141	Simas <i>et al.</i> , 2001
<b>Terpenoides</b>				
$\beta$ -Elemeno	Folhas	$C_{15}H_{24}$	204,18780	Antônio <i>et al.</i> , 1984; Leitão <i>et al.</i> , 1999; Oliveira <i>et al.</i> , 2020
$\gamma$ -Elemeno	Folhas	$C_{15}H_{24}$	204,18780	Zoghbi <i>et al.</i> , 1998; Andrade <i>et al.</i> , 2013; Aguiar <i>et al.</i> , 2015; De Melo <i>et al.</i> , 2017; Lourenço <i>et al.</i> , 2018
$\delta$ -Elemeno	Folhas e caule	$C_{15}H_{24}$	204,18780	Antonio <i>et al.</i> , 1984; Zoghbi <i>et al.</i> , 1998; Leitão <i>et al.</i> , 1999; Andrade <i>et al.</i> , 2013; Aguiar <i>et al.</i> , 2015; De Melo <i>et al.</i> , 2017; Ferreira <i>et al.</i> , 2017; Oliveira <i>et al.</i> , 2020
$\alpha$ -Pineno	Folhas e fruto	$C_{10}H_{16}$	136,12520	Zoghbi <i>et al.</i> , 1998; Andrade <i>et al.</i> , 2013; Aguiar <i>et al.</i> , 2015; De Melo <i>et al.</i> , 2017; Ferreira <i>et al.</i> , 2017; Lourenço <i>et al.</i> , 2018; Oliveira <i>et al.</i> , 2020
$\beta$ -Pineno	Folhas	$C_{10}H_{16}$	136,12520	Zoghbi <i>et al.</i> , 1998; Andrade <i>et al.</i> , 2013; Aguiar <i>et al.</i> , 2015; De Melo <i>et al.</i> , 2017; Ferreira <i>et al.</i> , 2017; Lourenço <i>et al.</i> , 2018; Oliveira <i>et al.</i> , 2020
Germacrona	Folhas	$C_{15}H_{22}O$	218,16707	Antonio <i>et al.</i> , 1984; Zoghbi <i>et al.</i> , 1998; Leitão <i>et al.</i> , 1999; Oliveira <i>et al.</i> , 2020
Canfeno	Folhas	$C_{10}H_{16}$	136,12520	Zoghbi <i>et al.</i> , 1998; Andrade <i>et al.</i> , 2013; Aguiar <i>et al.</i> , 2015; De Melo <i>et al.</i> , 2017;

				Ferreira <i>et al.</i> , 2017; Lourenço <i>et al.</i> , 2018
Germacreno A	Folhas	C <sub>15</sub> H <sub>24</sub>	204,18780	Zoghbi <i>et al.</i> , 1998; Aguiar <i>et al.</i> , 2015; Lourenço <i>et al.</i> , 2018; Oliveira <i>et al.</i> , 2020
Germacreno B	Folhas	C <sub>15</sub> H <sub>24</sub>	204,18780	Zoghbi <i>et al.</i> , 1998; Andrade <i>et al.</i> , 2013; Aguiar <i>et al.</i> , 2015; De Melo <i>et al.</i> , 2017; Lourenço <i>et al.</i> , 2018; Oliveira <i>et al.</i> , 2020
Germacreno D	Folhas e caule	C <sub>15</sub> H <sub>24</sub>	204,18780	Zoghbi <i>et al.</i> , 1998; Andrade <i>et al.</i> , 2013; Aguiar <i>et al.</i> , 2015; De Melo <i>et al.</i> , 2017; Lourenço <i>et al.</i> , 2018; Oliveira <i>et al.</i> , 2020
Biciclogermacreno	Folhas e caule	C <sub>15</sub> H <sub>24</sub>	204,18780	Zoghbi <i>et al.</i> , 1998; Andrade <i>et al.</i> , 2013; Aguiar <i>et al.</i> , 2015; Lourenço <i>et al.</i> , 2018
Curzerenona	Folhas	C <sub>15</sub> H <sub>18</sub> O <sub>2</sub>	230,13068	Antonio <i>et al.</i> , 1984; Leitão <i>et al.</i> , 1999
$\alpha$ -Bisabolol	Folhas	C <sub>15</sub> H <sub>26</sub> O	222,19837	Andrade <i>et al.</i> , 2013; De Melo <i>et al.</i> , 2017; Carvalho <i>et al.</i> , 2019; Souza <i>et al.</i> , 2021
Santolina trieno	Folhas	C <sub>10</sub> H <sub>16</sub>	136,12520	Aguiar <i>et al.</i> , 2015; Lourenço <i>et al.</i> , 2018
$\beta$ -Mirceno	Folhas, caule e fruto	C <sub>10</sub> H <sub>16</sub>	136,12520	Zoghbi <i>et al.</i> , 1998; Andrade <i>et al.</i> , 2013; Aguiar <i>et al.</i> , 2015; De Melo <i>et al.</i> , 2017; Ferreira <i>et al.</i> , 2017; Lourenço <i>et al.</i> , 2018; Oliveira <i>et al.</i> , 2020
$\alpha$ -Limoneno	Caule	C <sub>10</sub> H <sub>16</sub>	136,12520	Aguiar <i>et al.</i> , 2015
D-Limoneno	Folhas e fruto	C <sub>10</sub> H <sub>16</sub>	136,12520	Aguiar <i>et al.</i> , 2015; De Melo <i>et al.</i> , 2017; Lourenço <i>et al.</i> , 2018
(E)- $\beta$ -Ocimeno	Folhas	C <sub>10</sub> H <sub>16</sub>	136,12520	Oliveira <i>et al.</i> , 2020
(Z)- $\beta$ -Ocimeno	Folhas	C <sub>10</sub> H <sub>16</sub>	136,12520	Zoghbi <i>et al.</i> , 1998
Terpinoleno	Folhas	C <sub>10</sub> H <sub>16</sub>	136,12520	Andrade <i>et al.</i> , 2013; Aguiar <i>et al.</i> , 2015; Ferreira <i>et al.</i> , 2017; Lourenço <i>et al.</i> , 2018
$\alpha$ -Cariofileno	Caule	C <sub>15</sub> H <sub>24</sub>	204,18780	Aguiar <i>et al.</i> , 2015

$\beta$ -Cariofileno	Folhas	$C_{15}H_{24}$	204,18780	Zoghbi <i>et al.</i> , 1998; Andrade <i>et al.</i> , 2013; Aguiar <i>et al.</i> , 2015; Ferreira <i>et al.</i> , 2017; Lourenço <i>et al.</i> , 2018
<i>E</i> -Cariofileno	Folhas	$C_{15}H_{24}$	204,18780	De Melo <i>et al.</i> , 2017; Oliveira <i>et al.</i> , 2020
Óxido de $\beta$ -cariofileno	Folhas	$C_{15}H_{24}O$	220,18272	Zoghbi <i>et al.</i> , 1998; Andrade <i>et al.</i> , 2013; De Melo <i>et al.</i> , 2017
$\alpha$ -Amorfeno	Folhas	$C_{15}H_{24}$	204,18780	Oliveira <i>et al.</i> , 2020
$\gamma$ -Cadineno	Folhas	$C_{15}H_{24}$	204,18780	Andrade <i>et al.</i> , 2013; Aguiar <i>et al.</i> , 2015; De Melo <i>et al.</i> , 2017; Lourenço <i>et al.</i> , 2018; Oliveira <i>et al.</i> , 2020
$\delta$ -Cadineno	Folhas	$C_{15}H_{24}$	204,18780	Zoghbi <i>et al.</i> , 1998; Andrade <i>et al.</i> , 2013; De Melo <i>et al.</i> , 2017; Ferreira <i>et al.</i> , 2017; Oliveira <i>et al.</i> , 2020
Espatuleno	Folhas e caule	$C_{15}H_{24}O$	220,18272	Zoghbi <i>et al.</i> , 1998; Andrade <i>et al.</i> , 2013; Aguiar <i>et al.</i> , 2015; Ferreira <i>et al.</i> , 2017; Lourenço <i>et al.</i> , 2018
epi- $\alpha$ -Cadinol	Folhas	$C_{15}H_{26}O$	222,19837	Aguiar <i>et al.</i> , 2015; Lourenço <i>et al.</i> , 2018
$\alpha$ -Cadinol	Folhas, caule e fruto	$C_{15}H_{26}O$	222,19837	Andrade <i>et al.</i> , 2013; Aguiar <i>et al.</i> , 2015; De Melo <i>et al.</i> , 2017; Ferreira <i>et al.</i> , 2017; Lourenço <i>et al.</i> , 2018
$\delta$ -Cadinol	Folhas	$C_{15}H_{26}O$	222,19837	Ferreira <i>et al.</i> , 2017
T-Cadinol	Folhas	$C_{15}H_{26}O$	222,19837	Andrade <i>et al.</i> , 2013; De Melo <i>et al.</i> , 2017
$\alpha$ -Copaeno	Folhas	$C_{15}H_{24}$	204,18780	Zoghbi <i>et al.</i> , 1998; Andrade <i>et al.</i> , 2013; Aguiar <i>et al.</i> , 2015; De Melo <i>et al.</i> , 2017; Lourenço <i>et al.</i> , 2018; Oliveira <i>et al.</i> , 2020
$\beta$ -Copaeno	Folhas	$C_{15}H_{24}$	204,18780	Zoghbi <i>et al.</i> , 1998; Andrade <i>et al.</i> , 2013; De Melo <i>et al.</i> , 2017; Oliveira <i>et al.</i> , 2020
<i>E,E</i> -Farnesol	Folhas	$C_{15}H_{26}O$	222,19837	De Melo <i>et al.</i> , 2017
Siparunona	Folhas	$C_{15}H_{22}O$	218,16707	De Melo <i>et al.</i> , 2017
$\alpha$ -Felandreno	Folhas	$C_{10}H_{16}$	136,12520	Zoghbi <i>et al.</i> , 1998; Andrade <i>et al.</i> , 2013; De Melo <i>et al.</i> , 2017; Oliveira <i>et al.</i> , 2020
$\beta$ -Felandreno	Folhas	$C_{10}H_{16}$	136,12520	Andrade <i>et al.</i> , 2013; De Melo <i>et al.</i> , 2017

$\delta$ -3-Careno	Folhas e caule	C <sub>10</sub> H <sub>16</sub>	136,12520	Zoghbi <i>et al.</i> , 1998; Andrade <i>et al.</i> , 2013; Aguiar <i>et al.</i> , 2015; De Melo <i>et al.</i> , 2017
<i>p</i> -Cimeno	Folhas	C <sub>10</sub> H <sub>14</sub>	134,10955	Andrade <i>et al.</i> , 2013; De Melo <i>et al.</i> , 2017
$\beta$ -Bourboneno	Folhas	C <sub>15</sub> H <sub>24</sub>	204,18780	Zoghbi <i>et al.</i> , 1998; Andrade <i>et al.</i> , 2013; De Melo <i>et al.</i> , 2017; Oliveira <i>et al.</i> , 2020
$\alpha$ -Cubebeno	Folhas	C <sub>15</sub> H <sub>24</sub>	204,18780	Oliveira <i>et al.</i> , 2020
$\beta$ -Cubebeno	Folhas	C <sub>15</sub> H <sub>24</sub>	204,18780	Zoghbi <i>et al.</i> , 1998; Andrade <i>et al.</i> , 2013; Ferreira <i>et al.</i> , 2017; De Melo <i>et al.</i> , 2017; Oliveira <i>et al.</i> , 2020
Aromadendreno	Folhas	C <sub>15</sub> H <sub>24</sub>	204,18780	Andrade <i>et al.</i> , 2013; De Melo <i>et al.</i> , 2017; Oliveira <i>et al.</i> , 2020
$\alpha$ -Humuleno	Folhas	C <sub>15</sub> H <sub>24</sub>	204,18780	Zoghbi <i>et al.</i> , 1998; Andrade <i>et al.</i> , 2013; Ferreira <i>et al.</i> , 2017; De Melo <i>et al.</i> , 2017; Oliveira <i>et al.</i> , 2020
Allo-Aromadendreno	Folhas	C <sub>15</sub> H <sub>24</sub>	204,18780	Zoghbi <i>et al.</i> , 1998; Andrade <i>et al.</i> , 2013; De Melo <i>et al.</i> , 2017; Oliveira <i>et al.</i> , 2020
$\beta$ -Selineno	Folhas	C <sub>15</sub> H <sub>24</sub>	204,18780	Zoghbi <i>et al.</i> , 1998; Andrade <i>et al.</i> , 2013; De Melo <i>et al.</i> , 2017; Oliveira <i>et al.</i> , 2020
Ledol	Folhas	C <sub>15</sub> H <sub>26</sub> O	222,19837	Zoghbi <i>et al.</i> , 1998; De Melo <i>et al.</i> , 2017
$\alpha$ -Muuroleno	Folhas	C <sub>15</sub> H <sub>24</sub>	204,18780	Zoghbi <i>et al.</i> , 1998; Andrade <i>et al.</i> , 2013; Ferreira <i>et al.</i> , 2017; De Melo <i>et al.</i> , 2017; Oliveira <i>et al.</i> , 2020
$\gamma$ -Muuroleno	Folhas	C <sub>15</sub> H <sub>24</sub>	204,18780	Zoghbi <i>et al.</i> , 1998; Andrade <i>et al.</i> , 2013; Ferreira <i>et al.</i> , 2017; Oliveira <i>et al.</i> , 2020
<i>trans</i> -Calameno	Folhas	C <sub>15</sub> H <sub>22</sub>	202,17215	Andrade <i>et al.</i> , 2013; De Melo <i>et al.</i> , 2017
Globulol	Folhas	C <sub>15</sub> H <sub>26</sub> O	222,19837	Andrade <i>et al.</i> , 2013; Ferreira <i>et al.</i> , 2017; De Melo <i>et al.</i> , 2017
Viridiflorol	Folhas	C <sub>15</sub> H <sub>26</sub> O	222,19837	Andrade <i>et al.</i> , 2013; De Melo <i>et al.</i> , 2017
Cubenol	Folhas	C <sub>15</sub> H <sub>26</sub> O	222,19837	Zoghbi <i>et al.</i> , 1998
1- <i>epi</i> -Cubenol	Folhas	C <sub>15</sub> H <sub>26</sub> O	222,19837	Zoghbi <i>et al.</i> , 1998; Andrade <i>et al.</i> , 2013; De Melo <i>et al.</i> , 2017
$\beta$ -Eudesmol	Folhas	C <sub>15</sub> H <sub>26</sub> O	222,19837	Zoghbi <i>et al.</i> , 1998; Andrade <i>et al.</i> , 2013; De Melo <i>et al.</i> , 2017

$\gamma$ -Eudesmol	Folhas	C <sub>15</sub> H <sub>26</sub> O	222,19837	Zoghbi <i>et al.</i> , 1998
Agarospinol	Fruto	C <sub>15</sub> H <sub>26</sub> O	222,19837	Aguiar <i>et al.</i> , 2015
Triciclono	Folhas	C <sub>10</sub> H <sub>16</sub>	136,12520	Andrade <i>et al.</i> , 2013
$\alpha$ -Tujeno	Folhas	C <sub>10</sub> H <sub>16</sub>	136,12520	Andrade <i>et al.</i> , 2013
Sabineno	Folhas	C <sub>10</sub> H <sub>16</sub>	136,12520	Andrade <i>et al.</i> , 2013
Curzereno	Folhas	C <sub>15</sub> H <sub>20</sub> O	216,15142	Andrade <i>et al.</i> , 2013; Oliveira <i>et al.</i> , 2020
Epóxido de humuleno II	Folhas	C <sub>15</sub> H <sub>24</sub> O	220,18272	Zoghbi <i>et al.</i> , 1998; Andrade <i>et al.</i> , 2013
Ipsdienol	Folhas	C <sub>10</sub> H <sub>16</sub> O	152,12012	Ferreira <i>et al.</i> , 2017
Terpineol	Folhas	C <sub>10</sub> H <sub>18</sub> O	154,13577	Ferreira <i>et al.</i> , 2017
Elixeno	Folhas	C <sub>15</sub> H <sub>24</sub>	204,18780	Ferreira <i>et al.</i> , 2017
Elemol	Folhas	C <sub>15</sub> H <sub>26</sub> O	222,19837	Zoghbi <i>et al.</i> , 1998; Ferreira <i>et al.</i> , 2017
Linalol	Folhas	C <sub>10</sub> H <sub>18</sub> O	154,13577	Zoghbi <i>et al.</i> , 1998
Ciclosativeno	Folhas	C <sub>15</sub> H <sub>24</sub>	204,18780	Zoghbi <i>et al.</i> , 1998
$\alpha$ -Ilangeno	Folhas	C <sub>15</sub> H <sub>24</sub>	204,18780	Zoghbi <i>et al.</i> , 1998; Oliveira <i>et al.</i> , 2020
$\beta$ -Ilangeno	Folhas	C <sub>15</sub> H <sub>24</sub>	204,18780	Oliveira <i>et al.</i> , 2020
$\alpha$ -Gurjuneno	Folhas	C <sub>15</sub> H <sub>24</sub>	204,18780	Oliveira <i>et al.</i> , 2020
$\beta$ -Gurjuneno	Folhas	C <sub>15</sub> H <sub>24</sub>	204,18780	Zoghbi <i>et al.</i> , 1998
$\gamma$ -Gurjuneno	Folhas	C <sub>15</sub> H <sub>24</sub>	204,18780	Oliveira <i>et al.</i> , 2020
<i>trans</i> - $\alpha$ -Bergamoteno	Folhas	C <sub>15</sub> H <sub>24</sub>	204,18780	Zoghbi <i>et al.</i> , 1998
(Z)- $\beta$ -Farneseno	Folhas	C <sub>15</sub> H <sub>24</sub>	204,18780	Zoghbi <i>et al.</i> , 1998
$\alpha$ -Curcumeno	Folhas	C <sub>15</sub> H <sub>22</sub>	202,17215	Zoghbi <i>et al.</i> , 1998
Cubebol	Folhas	C <sub>15</sub> H <sub>26</sub> O	222,19837	Zoghbi <i>et al.</i> , 1998
epi-Cubebol	Folhas	C <sub>15</sub> H <sub>24</sub> O	220,18272	Zoghbi <i>et al.</i> , 1998
Valenceno	Folhas	C <sub>15</sub> H <sub>24</sub>	204,18780	Zoghbi <i>et al.</i> , 1998
$\beta$ -Bisaboleno	Folhas	C <sub>15</sub> H <sub>24</sub>	204,18780	Zoghbi <i>et al.</i> , 1998
$\alpha$ -Calacoreno	Folhas	C <sub>15</sub> H <sub>20</sub>	200,15650	Zoghbi <i>et al.</i> , 1998
Hidrato de <i>cis</i> -sesquisabineno	Folhas	C <sub>15</sub> H <sub>26</sub> O	222,19837	Zoghbi <i>et al.</i> , 1998
Guaiol	Folhas	C <sub>15</sub> H <sub>26</sub> O	222,19837	Zoghbi <i>et al.</i> , 1998



<i>cis</i> - $\beta$ -Elemenona	Folhas	C <sub>15</sub> H <sub>22</sub> O	218,16707	Oliveira <i>et al.</i> , 2020
<i>trans</i> - $\beta$ -Elemenona	Folhas	C <sub>15</sub> H <sub>22</sub> O	218,16707	Oliveira <i>et al.</i> , 2020
$\alpha$ -Muurolol	Folhas	C <sub>15</sub> H <sub>26</sub> O	222,19837	Zoghbi <i>et al.</i> , 1998
Atractilona	Folhas	C <sub>15</sub> H <sub>20</sub> O	216,15142	Zoghbi <i>et al.</i> , 1998; Oliveira <i>et al.</i> , 2020
Selin-11-en-4 $\alpha$ -ol	Folhas	C <sub>15</sub> H <sub>26</sub> O	222,19837	Zoghbi <i>et al.</i> , 1998
Cadaleno	Folhas	C <sub>15</sub> H <sub>18</sub>	198,14085	Zoghbi <i>et al.</i> , 1998
epi- $\alpha$ -Bisabolol	Folhas	C <sub>15</sub> H <sub>26</sub> O	222,19837	Zoghbi <i>et al.</i> , 1998
Silvestreno	Folhas	C <sub>10</sub> H <sub>16</sub>	136,12520	Oliveira <i>et al.</i> , 2020
$\alpha$ -Funebreno	Folhas	C <sub>15</sub> H <sub>24</sub>	204,18780	Oliveira <i>et al.</i> , 2020
$\alpha$ -Guaieno	Folhas	C <sub>15</sub> H <sub>24</sub>	204,18780	Oliveira <i>et al.</i> , 2020
Guaia-6,9-dieno	Folhas	C <sub>15</sub> H <sub>24</sub>	204,18780	Oliveira <i>et al.</i> , 2020
<i>trans</i> -Muurolo-4(14),5-dieno	Folhas	C <sub>15</sub> H <sub>24</sub>	204,18780	Oliveira <i>et al.</i> , 2020
<i>cis</i> -Muurolo-3,5-dieno	Folhas	C <sub>15</sub> H <sub>24</sub>	204,18780	Oliveira <i>et al.</i> , 2020
<i>cis</i> -Cadina-1(6),4-dieno	Folhas	C <sub>15</sub> H <sub>24</sub>	204,18780	Oliveira <i>et al.</i> , 2020
<i>trans</i> -Cadina-1,4-dieno	Folhas	C <sub>15</sub> H <sub>24</sub>	204,18780	Oliveira <i>et al.</i> , 2020
9-epi-(E)-Cariofileno	Folhas	C <sub>15</sub> H <sub>24</sub>	204,18780	Oliveira <i>et al.</i> , 2020
Zonareno	Folhas	C <sub>15</sub> H <sub>24</sub>	204,18780	Oliveira <i>et al.</i> , 2020
Selina-4(14),7(11)-dieno	Folhas	C <sub>15</sub> H <sub>24</sub>	204,18780	Oliveira <i>et al.</i> , 2020
Selina-3,7(11)-dieno	Folhas	C <sub>15</sub> H <sub>24</sub>	204,18780	Oliveira <i>et al.</i> , 2020
Allohediacariol	Folhas	C <sub>15</sub> H <sub>26</sub> O	222,19837	Oliveira <i>et al.</i> , 2020
<i>trans</i> -Óxido de linalol (furanóide)	Folhas	C <sub>10</sub> H <sub>18</sub> O <sub>2</sub>	170,13068	Zoghbi <i>et al.</i> , 1998
<i>cis</i> - $\beta$ -Di-hidroterpineol	Folhas	C <sub>10</sub> H <sub>20</sub> O	156,15142	Zoghbi <i>et al.</i> , 1998
10,11-oxidocalameneno	Folhas	C <sub>15</sub> H <sub>20</sub> O	216,15142	Zoghbi <i>et al.</i> , 1998
Naftaleno	Folhas	C <sub>10</sub> H <sub>8</sub>	128,06260	Zoghbi <i>et al.</i> , 1998
Glicosídeo de sitosterol	Fruto	C <sub>35</sub> H <sub>60</sub> O <sub>6</sub>	576,43899	Simas <i>et al.</i> , 2001
Estigmasterol	Madeira do caule	C <sub>29</sub> H <sub>48</sub> O	412,37052	Braz <i>et al.</i> , 1976; Chiu <i>et al.</i> , 1981
$\beta$ -Sitosterol	Fruto	C <sub>29</sub> H <sub>50</sub> O	414,38617	Braz <i>et al.</i> , 1976; Chiu <i>et al.</i> , 1981
<b>Metilcetonas</b>				

2-Tridecanona	Fruto	C <sub>13</sub> H <sub>26</sub> O	198,19837	Aguiar <i>et al.</i> , 2015 Zoghbi <i>et al.</i> , 1998; Andrade <i>et al.</i> , 2013; Aguiar <i>et al.</i> , 2015; De Melo <i>et al.</i> , 2017; Ferreira <i>et al.</i> , 2017; Lourenço <i>et al.</i> , 2018
2-Undecanona	Folhas, caule e fruto	C <sub>11</sub> H <sub>22</sub> O	170,16707	
6-metil-5-hepten-2-ona	Folhas	C <sub>8</sub> H <sub>14</sub> O	126,10447	Zoghbi <i>et al.</i> , 1998
<b>Ácidos graxos</b>				
Ácido palmítico	Fruto	C <sub>16</sub> H <sub>32</sub> O <sub>2</sub>	256,24023	Simas <i>et al.</i> , 2001
Ácido linoleico	Fruto	C <sub>18</sub> H <sub>32</sub> O <sub>2</sub>	280,24023	Simas <i>et al.</i> , 2001
Ácido oleico	Fruto	C <sub>18</sub> H <sub>34</sub> O <sub>2</sub>	282,25588	Simas <i>et al.</i> , 2001
Ácido esteárico	Fruto	C <sub>18</sub> H <sub>36</sub> O <sub>2</sub>	284,27153	Simas <i>et al.</i> , 2001
<b>Álcool</b>				
Nonanol	Fruto e folhas	C <sub>9</sub> H <sub>20</sub> O	144,15142	Zoghbi <i>et al.</i> , 1998; Aguiar <i>et al.</i> , 2015; Ferreira <i>et al.</i> , 2017
Undecanol	Folhas	C <sub>11</sub> H <sub>24</sub> O	172,18272	Zoghbi <i>et al.</i> , 1998
Decanol	Folhas	C <sub>10</sub> H <sub>22</sub> O	158,16707	Zoghbi <i>et al.</i> , 1998
<b>Fenilpropanóides</b>				
Safrol	Folhas	C <sub>10</sub> H <sub>10</sub> O <sub>2</sub>	162,06808	Zoghbi <i>et al.</i> , 1998
Dillapiole	Folhas	C <sub>12</sub> H <sub>14</sub> O <sub>4</sub>	222,08921	Zoghbi <i>et al.</i> , 1998
<b><i>Siparuna macrotrepala</i></b>				
<b>Terpenoides</b>				
Cadaleno	Galhos e folhas	C <sub>15</sub> H <sub>18</sub>	198,14085	El-Seedi <i>et al.</i> , 1994; Leitão <i>et al.</i> , 1999
Calameneno	Galhos e folhas	C <sub>15</sub> H <sub>22</sub>	202,17215	El-Seedi <i>et al.</i> , 1994; Leitão <i>et al.</i> , 1999
7-Hidróxi-calameneno	Galhos e folhas	C <sub>15</sub> H <sub>22</sub> O	218,16707	El-Seedi <i>et al.</i> , 1994; Leitão <i>et al.</i> , 1999
Dímero de 7-hidróxi-calameneno	Galhos e folhas	C <sub>30</sub> H <sub>42</sub> O <sub>2</sub>	434,31848	El-Seedi <i>et al.</i> , 1994; Leitão <i>et al.</i> , 1999
1-Hidróxi-calameneno	Galhos e folhas	C <sub>15</sub> H <sub>22</sub> O	218,16707	El-Seedi <i>et al.</i> , 1994; Leitão <i>et al.</i> , 1999
1,6-Dimetiltetra-hidronaftalenona-4	Galhos e folhas	C <sub>12</sub> H <sub>14</sub> O	174,10447	El-Seedi <i>et al.</i> , 1994; Leitão <i>et al.</i> , 1999 El-Seedi <i>et al.</i> , 1994; Leitão <i>et al.</i> , 1999;
Espatuleno	Galhos e folhas	C <sub>15</sub> H <sub>24</sub> O	220,18272	Noriega <i>et al.</i> , 2019
α-Pineno	Folhas	C <sub>10</sub> H <sub>16</sub>	136,12520	Noriega <i>et al.</i> , 2019

$\beta$ -Pineno	Folhas	C <sub>10</sub> H <sub>16</sub>	136,12520	Noriega <i>et al.</i> , 2019
Canfeno	Folhas	C <sub>10</sub> H <sub>16</sub>	136,12520	Noriega <i>et al.</i> , 2019
Mirceno	Folhas	C <sub>10</sub> H <sub>16</sub>	136,12520	Noriega <i>et al.</i> , 2019
Limoneno	Folhas	C <sub>10</sub> H <sub>16</sub>	136,12520	Noriega <i>et al.</i> , 2019
$\alpha$ -Cubebeno	Folhas	C <sub>15</sub> H <sub>24</sub>	204,18780	Noriega <i>et al.</i> , 2019
$\beta$ -Cubebeno	Folhas	C <sub>15</sub> H <sub>24</sub>	204,18780	Noriega <i>et al.</i> , 2019
Ciclosativeno	Folhas	C <sub>15</sub> H <sub>24</sub>	204,18780	Noriega <i>et al.</i> , 2019
$\alpha$ -Ilangeno	Folhas	C <sub>15</sub> H <sub>24</sub>	204,18780	Noriega <i>et al.</i> , 2019
$\alpha$ -Copaeno	Folhas	C <sub>15</sub> H <sub>24</sub>	204,18780	Noriega <i>et al.</i> , 2019
$\beta$ -Copaeno	Folhas	C <sub>15</sub> H <sub>24</sub>	204,18780	Noriega <i>et al.</i> , 2019
$\beta$ -Bourboneno	Folhas	C <sub>15</sub> H <sub>24</sub>	204,18780	Noriega <i>et al.</i> , 2019
$\beta$ -Elemeno	Folhas	C <sub>15</sub> H <sub>24</sub>	204,18780	Noriega <i>et al.</i> , 2019
$\beta$ -Cariofileno	Folhas	C <sub>15</sub> H <sub>24</sub>	204,18780	Noriega <i>et al.</i> , 2019
Óxido de cariofileno	Folhas	C <sub>15</sub> H <sub>24</sub> O	220,18272	Noriega <i>et al.</i> , 2019
$\alpha$ -Guaieno	Folhas	C <sub>15</sub> H <sub>24</sub>	204,18780	Noriega <i>et al.</i> , 2019
<i>cis</i> -Muuro-la-3,5-dieno	Folhas	C <sub>15</sub> H <sub>24</sub>	204,18780	Noriega <i>et al.</i> , 2019
<i>trans</i> -Muuro-la-3,5-dieno	Folhas	C <sub>15</sub> H <sub>24</sub>	204,18780	Noriega <i>et al.</i> , 2019
<i>cis</i> -Muuro-la-4(14),5-dieno	Folhas	C <sub>15</sub> H <sub>24</sub>	204,18780	Noriega <i>et al.</i> , 2019
<i>trans</i> -Muuro-la-4(14),5-dieno	Folhas	C <sub>15</sub> H <sub>24</sub>	204,18780	Noriega <i>et al.</i> , 2019
$\alpha$ -Humuleno	Folhas	C <sub>15</sub> H <sub>24</sub>	204,18780	Noriega <i>et al.</i> , 2019
Allo-Aromadendreno	Folhas	C <sub>15</sub> H <sub>24</sub>	204,18780	Noriega <i>et al.</i> , 2019
$\alpha$ -Muuro-leno	Folhas	C <sub>15</sub> H <sub>24</sub>	204,18780	Noriega <i>et al.</i> , 2019
$\gamma$ -Muuro-leno	Folhas	C <sub>15</sub> H <sub>24</sub>	204,18780	Noriega <i>et al.</i> , 2019
Germacreno B	Folhas	C <sub>15</sub> H <sub>24</sub>	204,18780	Noriega <i>et al.</i> , 2019
Germacreno D	Folhas	C <sub>15</sub> H <sub>24</sub>	204,18780	Noriega <i>et al.</i> , 2019
Biciclogermacreno	Folhas	C <sub>15</sub> H <sub>24</sub>	204,18780	Noriega <i>et al.</i> , 2019
Globulol	Folhas	C <sub>15</sub> H <sub>26</sub> O	222,19837	Noriega <i>et al.</i> , 2019
Viridiflorol	Folhas	C <sub>15</sub> H <sub>26</sub> O	222,19837	Noriega <i>et al.</i> , 2019

Guaiol	Folhas	C <sub>15</sub> H <sub>26</sub> O	222,19837	Noriega <i>et al.</i> , 2019
β-Selineno	Folhas	C <sub>15</sub> H <sub>24</sub>	204,18780	Noriega <i>et al.</i> , 2019
( <i>E,E</i> )-α-Farneseno	Folhas	C <sub>15</sub> H <sub>24</sub>	204,18780	Noriega <i>et al.</i> , 2019
α-Muurolol	Folhas	C <sub>15</sub> H <sub>26</sub> O	222,19837	Noriega <i>et al.</i> , 2019
<i>epi</i> -α-Muurolol	Folhas	C <sub>15</sub> H <sub>26</sub> O	222,19837	Noriega <i>et al.</i> , 2019
α-Cadinol	Folhas	C <sub>15</sub> H <sub>26</sub> O	222,19837	Noriega <i>et al.</i> , 2019
<i>epi</i> -α-Cadinol	Folhas	C <sub>15</sub> H <sub>26</sub> O	222,19837	Noriega <i>et al.</i> , 2019
α-Cadineno	Folhas	C <sub>15</sub> H <sub>24</sub>	204,18780	Noriega <i>et al.</i> , 2019
γ-Cadineno	Folhas	C <sub>15</sub> H <sub>24</sub>	204,18780	Noriega <i>et al.</i> , 2019
δ-Cadineno	Folhas	C <sub>15</sub> H <sub>24</sub>	204,18780	Noriega <i>et al.</i> , 2019
<i>trans</i> -Cadina-1(2),4 dieno	Folhas	C <sub>15</sub> H <sub>24</sub>	204,18780	Noriega <i>et al.</i> , 2019
Cubebol	Folhas	C <sub>15</sub> H <sub>26</sub> O	222,19837	Noriega <i>et al.</i> , 2019
Zonareno	Folhas	C <sub>15</sub> H <sub>24</sub>	204,18780	Noriega <i>et al.</i> , 2019
α-Calacoreno	Folhas	C <sub>15</sub> H <sub>20</sub>	200,15650	Noriega <i>et al.</i> , 2019
1- <i>epi</i> -Cubenol	Folhas	C <sub>15</sub> H <sub>26</sub> O	222,19837	Noriega <i>et al.</i> , 2019
1,10-di- <i>epi</i> -Cubenol	Folhas	C <sub>15</sub> H <sub>26</sub> O	222,19837	Noriega <i>et al.</i> , 2019
β-Oplopenona	Folhas	C <sub>15</sub> H <sub>24</sub> O	220,18272	Noriega <i>et al.</i> , 2019
<b>Metilcetona</b>				
2-Undecanona	Folhas	C <sub>11</sub> H <sub>22</sub> O	170,16707	Noriega <i>et al.</i> , 2019
<i>Siparuna pachyantha</i>				
<b>Alcaloides</b>				
Coridina	Folhas	C <sub>20</sub> H <sub>23</sub> NO <sub>4</sub>	341,16271	Marti <i>et al.</i> , 2013
Roemerina	Folhas	C <sub>18</sub> H <sub>17</sub> NO <sub>2</sub>	279,12593	Marti <i>et al.</i> , 2013
Liriodenina	Folhas	C <sub>17</sub> H <sub>9</sub> NO <sub>3</sub>	275,05824	Marti <i>et al.</i> , 2013
<i>Siparuna pauciflora</i>				
<b>Alcaloides</b>				
Nantenina	Hastes	C <sub>20</sub> H <sub>21</sub> NO <sub>4</sub>	339,14706	Leitão <i>et al.</i> , 1999
<i>N</i> -Metillaurotetanina	Hastes	C <sub>20</sub> H <sub>23</sub> NO <sub>4</sub>	341,16271	Leitão <i>et al.</i> , 1999; Jenett-Siems <i>et al.</i> , 2003

Boldina	Folhas	C <sub>19</sub> H <sub>21</sub> NO <sub>4</sub>	327,14706	Jenett-Siems <i>et al.</i> , 2003
Noroliverolina	Hastes	C <sub>17</sub> H <sub>15</sub> NO <sub>3</sub>	281,10519	Leitão <i>et al.</i> , 1999
Laurotetanina	Folhas	C <sub>19</sub> H <sub>21</sub> NO <sub>4</sub>	327,14706	Jenett-Siems <i>et al.</i> , 2003
Norboldina=Laurokitsina	Folhas	C <sub>18</sub> H <sub>19</sub> NO <sub>4</sub>	313,13141	Jenett-Siems <i>et al.</i> , 2003
<b>Terpenoides</b>				
Sipaucina A	Folhas	C <sub>19</sub> H <sub>26</sub> O <sub>7</sub>	366,16785	Jenett-Siems <i>et al.</i> , 2003
Sipaucina B	Folhas	C <sub>19</sub> H <sub>26</sub> O <sub>6</sub>	350,17294	Jenett-Siems <i>et al.</i> , 2003
Sipaucina C	Folhas	C <sub>19</sub> H <sub>26</sub> O <sub>7</sub>	366,16785	Jenett-Siems <i>et al.</i> , 2003
<i>Siparuna poeppigii</i>				
<b>Alcaloides</b>				
Lisicamina	Folhas	C <sub>18</sub> H <sub>13</sub> NO <sub>3</sub>	291,08954	Marti <i>et al.</i> , 2013
O-Metilisopilina	Folhas	C <sub>19</sub> H <sub>21</sub> NO <sub>3</sub>	311,15214	Marti <i>et al.</i> , 2013
N-Nornuciferina	Folhas	C <sub>18</sub> H <sub>19</sub> NO <sub>2</sub>	281,14158	Marti <i>et al.</i> , 2013
Liriodenina	Folhas	C <sub>17</sub> H <sub>9</sub> NO <sub>3</sub>	275,05824	Marti <i>et al.</i> , 2013
<i>Siparuna reginae</i>				
<b>Alcaloides</b>				
Coclaurine	Folhas	C <sub>17</sub> H <sub>19</sub> NO <sub>3</sub>	285,13649	Leal <i>et al.</i> , 2021(a)
Laurokitsine	Folhas	C <sub>18</sub> H <sub>19</sub> NO <sub>4</sub>	313,13141	Leal <i>et al.</i> , 2021(a)
Reticuline	Folhas	C <sub>19</sub> H <sub>23</sub> NO <sub>4</sub>	329,16271	Leal <i>et al.</i> , 2021(a)
Norneolitsine	Folhas	C <sub>18</sub> H <sub>15</sub> NO <sub>4</sub>	309,10011	Leal <i>et al.</i> , 2021(a)
<i>Siparuna sarmentosa</i>				
<b>Alcaloides</b>				
Norcoclaurina	Folhas	C <sub>16</sub> H <sub>17</sub> NO <sub>3</sub>	271,12084	Leal <i>et al.</i> , 2021(a)
Laurokitsina	Folhas	C <sub>18</sub> H <sub>19</sub> NO <sub>4</sub>	313,13141	Leal <i>et al.</i> , 2021(a)
Boldina	Folhas	C <sub>19</sub> H <sub>21</sub> NO <sub>4</sub>	327,14706	Leal <i>et al.</i> , 2021(a)
Coclaurina	Folhas	C <sub>17</sub> H <sub>19</sub> NO <sub>3</sub>	285,13649	Leal <i>et al.</i> , 2021(a)
Bulbocapnina	Folhas	C <sub>19</sub> H <sub>19</sub> NO <sub>4</sub>	325,13141	Leal <i>et al.</i> , 2021(a)
Caaverina	Folhas	C <sub>17</sub> H <sub>17</sub> NO <sub>2</sub>	267,12593	Leal <i>et al.</i> , 2021(a)

Xilopina	Folhas	C <sub>18</sub> H <sub>17</sub> NO <sub>3</sub>	295,12084	Leal <i>et al.</i> , 2021(a)
Cassitina	Folhas	C <sub>19</sub> H <sub>19</sub> NO <sub>5</sub>	341,12632	Leal <i>et al.</i> , 2021(a)
<b>Flavonoides</b>				
Quercetina 3- <i>O</i> -rhamnosídeo-7- <i>O</i> -glucosídeo	Folhas	C <sub>27</sub> H <sub>30</sub> O <sub>16</sub>	610,15338	Leal <i>et al.</i> , 2021(a)
Quercetina 3- <i>O</i> -glucosídeo-7- <i>O</i> -rhamnosídeo	Folhas	C <sub>27</sub> H <sub>30</sub> O <sub>16</sub>	610,15338	Leal <i>et al.</i> , 2021(a)
Rutina	Folhas	C <sub>27</sub> H <sub>30</sub> O <sub>16</sub>	610,15338	Leal <i>et al.</i> , 2021(a)
Dímero de procianidina (B1, B2, B3, B4, B5, B6, B7 ou B8)	Folhas	C <sub>30</sub> H <sub>26</sub> O <sub>12</sub>	578,14243	Leal <i>et al.</i> , 2021(a)
Vicenina-2	Folhas	C <sub>27</sub> H <sub>30</sub> O <sub>15</sub>	594,15847	Leal <i>et al.</i> , 2021(a)
<b>Feofitina</b>				
Feofitina A	Folhas	C <sub>55</sub> H <sub>74</sub> N <sub>4</sub> O <sub>5</sub>	870,56592	Leal <i>et al.</i> , 2021(a)
<i>Siparuna schimpffii</i>				
<b>Terpenoides</b>				
Tujeno	Folhas	C <sub>10</sub> H <sub>16</sub>	136,12520	Rivera <i>et al.</i> , 2014
$\alpha$ -Pineno	Folhas	C <sub>10</sub> H <sub>16</sub>	136,12520	Rivera <i>et al.</i> , 2014
$\beta$ -Pineno	Folhas	C <sub>10</sub> H <sub>16</sub>	136,12520	Rivera <i>et al.</i> , 2014
$\beta$ -Elemeno	Folhas	C <sub>15</sub> H <sub>24</sub>	204,18780	Rivera <i>et al.</i> , 2014
$\delta$ -Elemeno	Folhas	C <sub>15</sub> H <sub>24</sub>	204,18780	Rivera <i>et al.</i> , 2014
$\alpha$ -Cubebeno	Folhas	C <sub>15</sub> H <sub>24</sub>	204,18780	Rivera <i>et al.</i> , 2014
$\beta$ -Cubebeno	Folhas	C <sub>15</sub> H <sub>24</sub>	204,18780	Rivera <i>et al.</i> , 2014
$\alpha$ -Ylangeno	Folhas	C <sub>15</sub> H <sub>24</sub>	204,18780	Rivera <i>et al.</i> , 2014
Ciclosativeno	Folhas	C <sub>15</sub> H <sub>24</sub>	204,18780	Rivera <i>et al.</i> , 2014
Copaeno	Folhas	C <sub>15</sub> H <sub>24</sub>	204,18780	Rivera <i>et al.</i> , 2014
$\beta$ -Bourboneno	Folhas	C <sub>15</sub> H <sub>24</sub>	204,18780	Rivera <i>et al.</i> , 2014
Isolongilofoleno	Folhas	C <sub>15</sub> H <sub>24</sub>	204,18780	Rivera <i>et al.</i> , 2014
$\beta$ -Cariofileno	Folhas	C <sub>15</sub> H <sub>24</sub>	204,18780	Rivera <i>et al.</i> , 2014
$\alpha$ -Guaieno	Folhas	C <sub>15</sub> H <sub>24</sub>	204,18780	Rivera <i>et al.</i> , 2014
$\alpha$ -Humuleno	Folhas	C <sub>15</sub> H <sub>24</sub>	204,18780	Rivera <i>et al.</i> , 2014

cis-Muurolo-4(14),5-dieno	Folhas	C <sub>15</sub> H <sub>24</sub>	204,18780	Rivera <i>et al.</i> , 2014
cis-Muurolo-3,5-dieno	Folhas	C <sub>15</sub> H <sub>24</sub>	204,18780	Rivera <i>et al.</i> , 2014
Germacreno B	Folhas	C <sub>15</sub> H <sub>24</sub>	204,18780	Rivera <i>et al.</i> , 2014
Germacreno D	Folhas	C <sub>15</sub> H <sub>24</sub>	204,18780	Rivera <i>et al.</i> , 2014
Biciclogermacreno	Folhas	C <sub>15</sub> H <sub>24</sub>	204,18780	Rivera <i>et al.</i> , 2014
β-Selineno	Folhas	C <sub>15</sub> H <sub>24</sub>	204,18780	Rivera <i>et al.</i> , 2014
α-Muurolo	Folhas	C <sub>15</sub> H <sub>24</sub>	204,18780	Rivera <i>et al.</i> , 2014
γ-Muurolo	Folhas	C <sub>15</sub> H <sub>24</sub>	204,18780	Rivera <i>et al.</i> , 2014
γ-Amorfeno	Folhas	C <sub>15</sub> H <sub>24</sub>	204,18780	Rivera <i>et al.</i> , 2014
α-Cadineno	Folhas	C <sub>15</sub> H <sub>24</sub>	204,18780	Rivera <i>et al.</i> , 2014
γ-Cadineno	Folhas	C <sub>15</sub> H <sub>24</sub>	204,18780	Rivera <i>et al.</i> , 2014
Nootkatona	Folhas	C <sub>15</sub> H <sub>22</sub> O	218,16707	Rivera <i>et al.</i> , 2014
α-Calcoreno	Folhas	C <sub>15</sub> H <sub>20</sub>	200,15650	Rivera <i>et al.</i> , 2014
Viridiflorol	Folhas	C <sub>15</sub> H <sub>26</sub> O	222,19837	Rivera <i>et al.</i> , 2014
Espatuleno	Folhas	C <sub>15</sub> H <sub>24</sub> O	220,18272	Rivera <i>et al.</i> , 2014
Guaiol	Folhas	C <sub>15</sub> H <sub>26</sub> O	222,19837	Rivera <i>et al.</i> , 2014
1,10-di-epicubenol	Folhas	C <sub>15</sub> H <sub>26</sub> O	222,19837	Rivera <i>et al.</i> , 2014
1-epi-Cubenol	Folhas	C <sub>15</sub> H <sub>26</sub> O	222,19837	Rivera <i>et al.</i> , 2014
Cedrelanol	Folhas	C <sub>15</sub> H <sub>26</sub> O	222,19837	Rivera <i>et al.</i> , 2014
tau-Muurolol	Folhas	C <sub>15</sub> H <sub>26</sub> O	222,19837	Rivera <i>et al.</i> , 2014
α-Muurolol	Folhas	C <sub>15</sub> H <sub>26</sub> O	222,19837	Rivera <i>et al.</i> , 2014
α-Cadinol	Folhas	C <sub>15</sub> H <sub>26</sub> O	222,19837	Rivera <i>et al.</i> , 2014
Mirceno	Folhas	C <sub>10</sub> H <sub>16</sub>	136,12520	Rivera <i>et al.</i> , 2014
<b>Metilcetona</b>				
2-Undecanona	Folhas	C <sub>11</sub> H <sub>22</sub> O	170,16707	Rivera <i>et al.</i> , 2014
<i>Siparuna sessiliflora</i>				
<b>Alcaloides</b>				
Talicarpina	Folhas	C <sub>41</sub> H <sub>48</sub> N <sub>2</sub> O <sub>8</sub>	696,34107	López, 2011



Ajmalina	Folhas	$C_{20}H_{26}N_2O_2$	326,19943	López, 2011
Corlumina	Folhas	$C_{21}H_{21}NO_6$	383,13689	González <i>et al.</i> , 2012
Assimilobina	Folhas	$C_{17}H_{17}NO_2$	267,12593	González <i>et al.</i> , 2012
<b>Derivados do ácido cinâmico</b>				
Ácido 4-metoxi-2-metilcinâmico	Folhas	$C_{11}H_{12}O_3$	192,07864	González <i>et al.</i> , 2012
<i>Siparuna thecaphora</i>				
<b>Alcaloides</b>				
Liriodenina	Raízes e galhos	$C_{17}H_9NO_3$	275,05824	Chiu <i>et al.</i> , 1982; Gerard <i>et al.</i> , 1986; Leitão <i>et al.</i> , 1999
Oxonantenina	Raízes	$C_{19}H_{13}NO_5$	335,07937	Chiu <i>et al.</i> , 1982; Gerard <i>et al.</i> , 1986; Leitão <i>et al.</i> , 1999
<b>Flavonoides</b>				
Rutina	Folhas	$C_{27}H_{30}O_{16}$	610,15338	Saltos <i>et al.</i> , 2014
Quercetina 3- <i>O</i> - $\beta$ -D-glicopiranosídeo	Folhas	$C_{21}H_{20}O_{12}$	464,09548	Saltos <i>et al.</i> , 2014
<b>Aldeído fenólico</b>				
3,4-di-hidroxibenzaldeído	Folhas	$C_7H_6O_3$	138,03169	Saltos <i>et al.</i> , 2014
<b>Terpenoide</b>				
<i>trans</i> -Thujane-1 $\alpha$ ,7-diol 1- <i>O</i> - $\beta$ -D-glicopiranosídeo	Folhas	$C_{16}H_{28}O_7$	332,18350	Saltos <i>et al.</i> , 2014